Defense Nuclear Agency
Alexandria, VA 22310-3398

DNA-TR-94-59

Thermoreactive Aircraft Coatings (TRAC) Program

Kurt E. Jechel
Deborah E. Bielecka
PDA Engineering
P.O. Box 11491
Costa Mesa, CA 92627

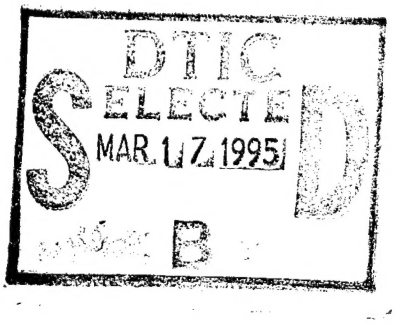

March 1995

Technical Report

CONTRACT No. DNA 001-89-C-0066

Approved for public release;
distribution is unlimited.

Destroy this report when it is no longer needed. Do not return to sender.

PLEASE NOTIFY THE DEFENSE NUCLEAR AGENCY, ATTN: CSTI, 6801 TELEGRAPH ROAD, ALEXANDRIA, VA 22310-3398, IF YOUR ADDRESS IS INCORRECT, IF YOU WISH IT DELETED FROM THE DISTRIBUTION LIST, OR IF THE ADDRESSEE IS NO LONGER EMPLOYED BY YOUR ORGANIZATION.

DISTRIBUTION LIST UPDATE

This mailer is provided to enable DNA to maintain current distribution lists for reports. (We would appreciate your providing the requested information.)

NOTE:
Please return the mailing label from the document so that any additions, changes, corrections or deletions can be made easily. For distribution cancellation or more information call DNA/IMAS (703) 325-1036.

☐ Add the individual listed to your distribution list.

☐ Delete the cited organization/individual.

☐ Change of address.

NAME: _____

ORGANIZATION: _____

OLD ADDRESS	CURRENT ADDRESS
_____	_____
_____	_____
_____	_____

TELEPHONE NUMBER: ( ) _____

DNA PUBLICATION NUMBER/TITLE	CHANGES/DELETIONS/ADDITIONS, etc.) *(Attach Sheet if more Space is Required)*
_____	_____
_____	_____
_____	_____

DNA OR OTHER GOVERNMENT CONTRACT NUMBER: _____

CERTIFICATION OF NEED-TO-KNOW BY GOVERNMENT SPONSOR (if other than DNA):

SPONSORING ORGANIZATION: _____

CONTRACTING OFFICER OR REPRESENTATIVE: _____

SIGNATURE: _____

CUT HERE AND RETURN

REPORT DOCUMENTATION PAGE

Form Approved OMB No. 0704-0188

1. AGENCY USE ONLY (Leave blank)	2. REPORT DATE	3. REPORT TYPE AND DATES COVERED
	950301	Technical 890901 – 940415

4. TITLE AND SUBTITLE

Thermoreactive Aircraft Coatings (TRAC) Program

5. FUNDING NUMBERS

C - DNA 001-89-C-0066
PE - 62715H
PR - RA
TA - RJ
WU - DH091090

6. AUTHOR(S)

Kurt E. Jechel and Deborah E. Bielecka

7. PERFORMING ORGANIZATION NAME(S) AND ADDRESS(ES)

PDA Engineering
P.O. Box 11491
Costa Mesa, CA 92627

8. PERFORMING ORGANIZATION REPORT NUMBER

PDA TR-94-1161-54-13

9. SPONSORING/MONITORING AGENCY NAME(S) AND ADDRESS(ES)

Defense Nuclear Agency
6801 Telegraph Road
Alexandria, VA 22310-3398
SPWE/DiNova

10. SPONSORING/MONITORING AGENCY REPORT NUMBER

DNA-TR-94-59

11. SUPPLEMENTARY NOTES

This work was sponsored by the Defense Nuclear Agency under RDT&E RMC Code B4662D RA RJ 00181 SPWE 4400A 25904D.

12a. DISTRIBUTION/AVAILABILITY STATEMENT

Approved for public release; distribution is unlimited.

12b. DISTRIBUTION CODE

13. ABSTRACT *(Maximum 200 words)*

A Thermoreactive Aircraft Coatings (TRAC) system has been developed which, when used in place of conventional paint, provides aircraft or other weapon systems with the thermal hardness benefits of a white coating while retaining a dark camouflage color under benign conditions. The TRAC system, which can be applied by conventional spray techniques, consists of a white, heat reflective primer top-coated with a passively reactive, thermally activated coating which reversibly changes from dark grey to white upon exposure to radiant thermal flux. The effectiveness of the TRAC system was demonstrated through tests of white, grey, black and TRAC coated test samples constructed from composite/honeycomb sandwich material, simulating aircraft skin, which were subjected to combined radiant thermal energy exposure and simultaneous mechanical loading. Test results indicated that, compared to comparably painted grey samples, TRAC provided up to a 443% improvement in thermal hardness, and was up to 98% as effective as gloss white paint in protecting the composite substrate from damage induced by radiant thermal energy exposure.

14. SUBJECT TERMS			15. NUMBER OF PAGES
Thermal Hardness Aircraft Vulnerability	Nuclear Protection Thermoreactive Coating	External Surfaces Composite Materials	248
			16. PRICE CODE

17. SECURITY CLASSIFICATION OF REPORT	18. SECURITY CLASSIFICATION OF THIS PAGE	19. SECURITY CLASSIFICATION OF ABSTRACT	20. LIMITATION OF ABSTRACT
UNCLASSIFIED	UNCLASSIFIED	UNCLASSIFIED	SAR

CLASSIFIED BY:

N/A since Unclassified.

DECLASSIFY ON:

N/A since Unclassified..

PREFACE

This report summarizes the results of a technical effort conducted by PDA Engineering for the development and limited evaluation of a Thermoreactive Aircraft Coating (TRAC) system for passive thermal protection of the external composite surfaces of military aircraft. All tasks were conducted under Defense Nuclear Agency (DNA) Contract DNA001-89-C-0066. The DNA Contract Technical Monitors were Lt. Col. Vayl Oxford and Lt. Col. Gerald Miatech, both assigned to the Shock Physics Weapons Effects (SPWE) branch of DNA. Their technical contributions and other assistance are gratefully acknowledged.

The technical effort for this contract was conducted by the Systems Engineering department of PDA Engineering. The PDA Program Manager was Mr. J. David Theis. The Principal Investigators included Ms. Deborah E. Bielecka, Mr. William Perkins, and Mr. Tyler L. Housel. Demonstration testing of coated composite/honeycomb structural test samples was performed by Mr. Kurt Jechel with the assistance of Messrs. Ken Shaw and Ross Hoecker. Mr. J. C. Schutzler was responsible for the conception of the combined thermal-mechanical testing technique as well as design of the test sample configuration and specialized apparatus used in support of this testing. The assistance provided by Messrs. Al Lewandowski, Carl Bingham and Kent Scholl of the National Renewable Energy Laboratory High Flux Solar Furnace is also gratefully acknowledged.

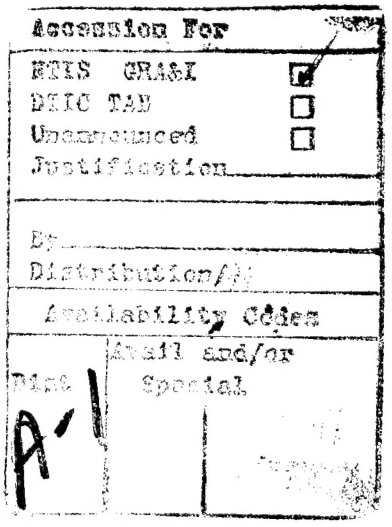

Conversion factors for U. S. customary to metric (SI) units of measurement.

To Convert From	To	Multiply By
angstrom	meters (m)	1.000 000 X E -10
atmosphere (normal)	kilo pascal (kPa)	1.013 25 X E +2
bar	kilo pascal (kPa)	1.000 000 X E +2
barn	meter^2 (m^2)	1.000 000 X E -28
British thermal unit (thermochemical)	joule (J)	1.054 350 X E +3
calorie (thermochemical)	joule (J)	4.184 000
cal (thermochemical)/cm^2	mega joule/m^2 (MJ/m^2)	4.184 000 X E -2
curie	giga becquerel (GBq)*	3.700 000 X E +1
degree (angle)	radian (rad)	1.745 329 X E -2
degree Fahrenheit	degree kelvin (K)	$T_K = (t^o f + 459.67)/1.8$
electron volt	joule (J)	1.602 19 X E -19
erg	joule (J)	1.000 000 X E -7
erg/second	watt (W)	1.000 000 X E -7
foot	meter (m)	3.048 000 X E -1
foot-pound-force	joule (J)	1.355 818
gallon (U. S. liquid)	meter^3 (m^3)	3.785 412 X E -3
inch	meter (m)	2.540 000 X E -2
jerk	joule (J)	1.000 000 X E +9
joule/kilogram (J/kg) (radiation dose absorbed)	Gray (Gy)**	1.000 000
kilotons	terajoules	4.183
kip (1000 lbf)	newton (N)	4.448 222 X E +3
kip/inch^2 (ksi)	kilo pascal (kPa)	6.894 757 X E +3
ktap	newton-second/m^2 ($N-s/m^2$)	1.000 000 X E +2
micron	meter (m)	1.000 000 X E -6
mil	meter (m)	2.540 000 X E -5
mile (international)	meter (m)	1.609 344 X E +3
ounce	kilogram (kg)	2.834 952 X E -2
pound-force (lbf avoirdupois)	newton (N)	4.448 222
pound-force inch	newton-meter (N·m)	1.129 848 X E -1
pound-force/inch	newton/meter (N/m)	1.751 268 X E +2
pound-force/foot^2	kilo pascal (kPa)	4.788 026 X E -2
pound-force/inch^2 (psi)	kilo pascal (kPa)	6.894 757
pound-mass (lbm avoirdupois)	kilogram (kg)	4.535 924 X E -1
pound-mass-foot^2 (moment of inertia)	kilogram-meter^2 ($kg \cdot m^2$)	4.214 011 X E -2
pound-mass/foot^3	kilogram/meter^3 (kg/m^3)	1.601 846 X E +1
rad (radiation dose absorbed)	Gray (Gy)**	1.000 000 X E -2
roentgen	coulomb/kilogram (C/kg)	2.579 760 X E -4
shake	second (s)	1.000 000 X E -8
slug	kilogram (kg)	1.459 390 X E +1
torr (mm Hg, 0° C)	kilo pascal (kPa)	1.333 22 X E -1

*The becquerel (Bq) is the SI unit of radioactivity; 1 Bq = 1 event/s.
**The Gray (Gy) is the SI unit of absorbed radiation.

A more complete listing of conversions may be found in "Metric Practice Guide E 380-74," American Society for Testing and Materials.

TABLE OF CONTENTS

TABLE OF CONTENTS (Continued)

FIGURES

FIGURES (Continued)

FIGURES (Continued)

FIGURES (Continued)

FIGURES (Continued)

TABLES

SECTION 1
INTRODUCTION

Aircraft exterior surfaces fabricated from composite materials, particularly laminates of honeycomb or foam-core with thin face sheets, are vulnerable to the effects of fireball radiation. A fireball produced by a nuclear burst within the atmosphere radiates thermal energy at a blackbody temperature of approximately 6000°K. When radiant thermal energy is intercepted by an aircraft in the vicinity of such a burst, the energy which is absorbed by the aircraft's exterior coatings is conducted to the thin face sheet (skin) which is effectively back-face insulated by the honeycomb or foam core. The resulting rapid temperature rise in the face sheet material can cause thermochemical degradation which may result in various failure modes involving face sheet wrinkling and local fiber bundle failure, as well as face sheet to core adhesive failure.

The state of stress of a composite material under conditions of rapid heating by thermal radiation depends to a great extent on the emissivity of the exposed surface, as well as the magnitude of any simultaneously imposed mechanical loads. The rate of radiant energy (heat) absorption of a surface is principally determined by its emissivity, which for aircraft exterior surface coatings is typically high because of the requirement to utilize dark camouflage colors. Thus, the vulnerability of dark colored composite structures (i.e. aircraft) operating in a nuclear thermal environment results from both the reduction in strength caused by increased skin surface temperature, and the additional stress caused by thermal expansions resulting from the absorbed radiation, which further adds to stress from mechanical loads already sustained by the airframe at the time of exposure to the thermal pulse.

The Thermoreactive Aircraft Coating (TRAC) as conceived and developed by PDA Engineering has a temperature dependent surface emissivity which transitions to a low emissivity when exposed to 6000°K blackbody radiation. Through the application of this coating to an aircraft's exterior surfaces, the fraction of thermal energy absorbed by an airframe's composite materials can be reduced significantly, while maintaining dark, high emissivity colors in the benign state.

Proof of principal was demonstrated for a coating which appears dark in the visible range under benign conditions and transitions to a highly reflective white color upon exposure to intense radiant thermal energy. The coating system utilizes thermoreactive materials dispersed in a clear binder and applied over a white undercoat to achieve the desired color changes. Preliminary instrumented tests were conducted at the White Sands Solar Facility (WSSF) and with PDA's Xenon Light Test Bench (XLTB). Results from these tests effectively demonstrated that the coating, while dark gray under benign conditions, protected the composite substrate from intense thermal radiation nearly as effectively as white paint.

The proof of concept for thermoreactive coatings was demonstrated by PDA under a small Boeing subcontract to an ASD program GU 7898, "The Application of Photochromic Technology to Camouflage Coatings". The reactive dyes were developed by PDA under IRAD sponsorship. The TRAC program was proposed to expand this technology to meet the requirements for military aircraft coatings.

The effort to develop the TRAC coating to meet the specifications for military aircraft coatings is discussed in this report. The principal technical challenges involved in developing TRAC for this application included the formulation of a pigment which transitions at temperatures in excess of the operating skin temperatures of the candidate aircraft, development of a process for pigment microencapsulation which is resistant to the solvent base of the aircraft coating, environmental stabilization of the thermochromic pigments, and integration of the pigment into a suitable Mil-Spec qualifiable binder material. The final result was production of a pigmented binder that could be manufactured at reasonable cost by a government qualified manufacturer.

This report includes a technical discussion of the background and preliminary research conducted during the development of the TRAC coating and the rationale for the approach taken. The test methods and test facilities used for this program are described, and the test results for TRAC development are presented and discussed. A new test methodology combining the simultaneous application of mechanical and radiant thermal energy loading on composite material samples is discussed, and the results of testing using this method, which illustrate the effectiveness of the TRAC coating are presented. The final sections document conclusions, recommendations and significant references.

SECTION 2
TRAC CONCEPT

2.1 BACKGROUND.

PDA Engineering has been extensively engaged in the research, development and manufacture of Passive Thermal Protective Systems (PTPS). Initial systems were designed to protect crew members, their flight gear, life support systems and other materials within cockpits of strategic aircraft by reducing the transmission of incident radiant thermal energy through the cockpit transparencies. PTPS concepts focused on the development and application of photochromic materials, infra-red (IR) absorbing dyes, and reflective coatings incorporated into transparent panels which were designed to be installed inside existing cockpit transparencies. Using this concept, transparency-transmitted thermal energy was successfully reduced to the 3.5 cal/cm^2 level established in Reference 1 as the accepted safe level for an aircraft operating in a nuclear thermal threat environment.

PTPS panels, composed of IR reflective glass plies laminated together with a photochromic dye-doped interlayer, were designed, fabricated, fully ground qualified and flight tested in a U.S. Air Force Strategic Air Command B-52G aircraft. This work was conducted under DNA contract DNA001-81-C-0083 (Reference 2). Similar work was performed under DNA contract DNA001-86-C0033 for the B-1B aircraft (Reference 3). Under both contracts the PTPS designs were successfully qualified to shock, vibration, optical and environmental specifications in full-scale ground tests. Air Force flight testing confirmed that PTPS transparencies provided a highly effective method of reducing the threat thermal radiation to acceptable levels in the cockpit while retaining critical aircrew vision requirements.

Application of this technology to compound-curved tactical aircraft cockpit canopies was conducted under DNA contract DNA001-87-C-0115. The effort involved the necessity of protecting photochromic dyes from atmospheric oxygen due to the high permeability of the polycarbonate/polyurethane/acrylic cross-section, and the development of IR-reflective coatings suitable for deposition on rigid plastic substrates. The Integrated PTPS (IPTPS) concept and materials were demonstrated by the production and testing of full-scale F-111 canopies. Tests conducted at the National Solar Thermal Test Facility (NSTTF) and at White Sands Solar Facility (WSSF) demonstrated the ability of the IPTPS design to protect a tactical aircraft's cockpit in a nuclear thermal threat environment.

Boeing subcontract BU-7879 explored the potential for using photochromic dyes incorporated into aircraft coatings for the purpose of reducing an aircraft's vulnerability to nuclear thermal flash. Preliminary tests had indicated that the intense ultraviolet exposure caused bleaching of the opacity of photochromic pigments due to chemical fatigue. This technology quickly evolved into the investigation of thermochromic materials which would absorb visible radiation under benign conditions, but become highly reflective in a high flux environment.

Color block dyes and polymer dispersed liquid crystals were identified as early candidate materials for their thermochromic behavior. Aging tests, thermal response tests performed at WSSF and on the PDA Xenon Light Test Bench (XLTB), compatibility with paint binders, and thermal stability of compatible paint binders indicated the superiority of the color block reverse type thermochromics over liquid crystals. PDA identified the refinement of thermochromic technology for military applications as compatible with PDA expertise.

2.2 THERMAL RESPONSE.

Earlier work performed by Boeing illustrated the dependence of thermal hardness of aircraft coatings to the effects of nuclear flash on the coating system. The response characteristics of an ideal thermoreactive coating are best explained by first examining the thermal response of a surface coated with a conventional paint.

2.2.1 Conventional Coating.

A conventional paint coating may consist of one or more discrete layers (total thickness of approximately 0.005-inch or less) covering a substrate of either metallic or composite material. When the surface is exposed to radiant energy from a nuclear fireball, radiant energy is reflected by and/or absorbed within the coating. The fraction of incident flux that is absorbed causes the temperature of the paint coating to increase. As the coating temperature rises, heat is conducted into the substrate, reradiated from the coating surface, and convectively transferred to a surface air flow.

In addition to the incident thermal pulse characteristics, the coating and adjacent surface temperatures are affected by the absorptivity (or emissivity) of the coating as well as the thermal conductivity of the coating and the substrate. Surface temperatures for coated high conductivity materials (i.e. metals) are significantly lower than for low conductivity composite substrates under identical conditions. Convective cooling and reradiation at the coating surface will also tend to

reduce the coating temperature. However, if the absorbed thermal flux cannot be efficiently transferred to the substrate or external environment, coating and adjacent substrate surface temperatures may reach levels sufficient to cause permanent degradation to the aircraft skin. Thermal decomposition within the coating may create vapor bubbles, appearing as blisters within the coating which may be sheared off the surface by aerodynamic forces. High temperatures within a composite substrate may lead to delamination or other forms of material degradation affecting the structural integrity of the aircraft.

2.2.2 Thermoreactive Coating.

Since the substrate and external environments are fixed by the aircraft and the mission, the surface coating or paint is the most obvious candidate for affecting improved thermal performance. However, a dark camouflage coating with an associated high absorptivity is required for tactical reasons and a reflective (e.g. white) paint cannot be used. Thermoreactive coatings change color and, therefore, reflectivity when heated to a critical temperature, called the transition temperature ($T_{transition}$). These coatings maintain their camouflage color scheme at standard operational temperature. Above the transition temperature the color changes to one of high reflectivity, approaching the emissivity characteristics of white paint. The reflectance characteristics as a function of coating surface temperature for an ideal thermoreactive coating are illustrated in Figure 2-1.

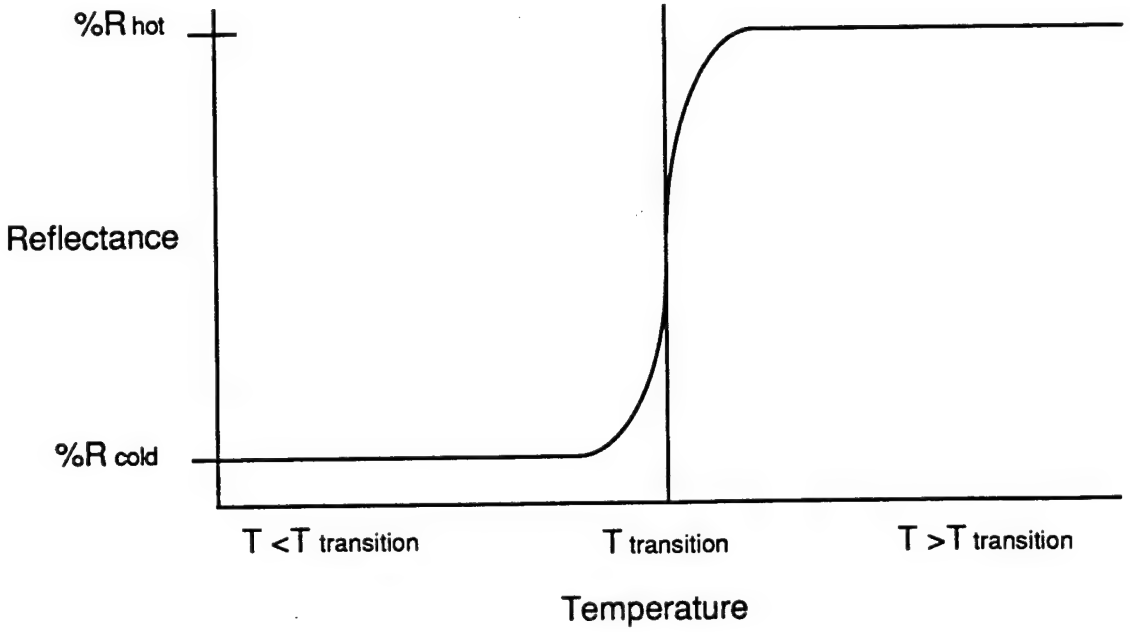

Figure 2-1. Ideal thermoreactive coating response.

A thermoreactive coating conceptually consists of two layers. The primer coating (i.e. undercoat) is typically a highly reflective titanium dioxide (TiO_2) pigmented epoxy. The topcoat is a thermoreactive coating which matches the dark camouflage color required under benign conditions. When heated to the predetermined transition temperature, the topcoat increases in transparency, allowing the incident radiant energy to be transmitted through to the undercoat where it is reflected. Little heat is, therefore, retained in the coating where it could be absorbed by the substrate. Ideally, the temperature rise in the composite substrate remains below the critical levels which cause degradation. Following thermal exposure, the coating cools back down to below its transition temperature and reassumes its original camouflage color.

The theoretical temperature response for a conventional and a thermoreactive coated substrate exposed to an arbitrary radiant thermal energy pulse is compared in Figure 2-2. The conventional camouflage paint coated substrate's temperature rises rapidly to levels at which thermal decomposition of the composite structure may occur. The thermoreactive coating scheme retains its camouflage color until the transition temperature is reached at which point the coating becomes reflective (white), reflecting away most of the additional incident radiant energy, thus allowing the substrate temperature to remain below degradation levels.

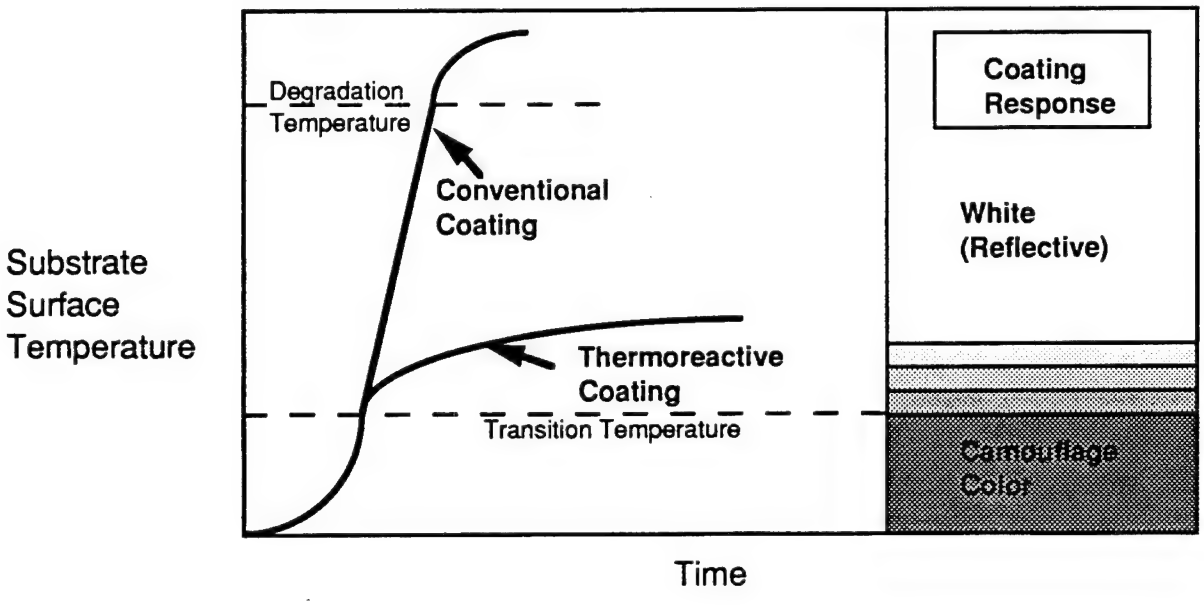

Figure 2-2. Temperature response of thermoreactive and conventionally coated substrates.

2.3 THERMOREACTIVE COATING COMPONENTS.

The color block reversible thermochromic pigment which was identified for optimum performance for this application is a multiple component system in which the transition temperature, color, and reflectivity can all be varied independently. Therefore, paints can be custom designed to meet the requirements of different applications by making only minor changes in materials. Prototype systems have demonstrated that reflectivity can be varied from 12 to 80 percent upon heating and that the transition temperature can be varied from 30° to 70°C and above. Green, blue, red, and gray pigments have been developed; any combination of these can be used to broaden the available range of colors.

As the basic thermoreactive pigment is composed of multiple components, it cannot be simply dissolved into a paint binder. The sensitivity of the component equilibrium requires that the dye must first be encapsulated prior to dispersion into a binder system in order to isolate it from unwanted dilution or reaction with the paint binder and solvent components. It has been shown that the pigment can be microencapsulated in a polymeric shell and still retain its excellent thermochromic properties. The capsules can then be dispersed into a transparent binder and applied by conventional spray coating techniques.

SECTION 3
TRAC DEVELOPMENT

3.1 INTRODUCTION.

A comprehensive program was undertaken to conduct the research, development, and testing activities leading to the evaluation of a sub-scale coating system as a passive thermal protective system. The program was divided into a series of tasks, which were intended to logically address each step in the development of the TRAC coating system. Each task, its purpose, and outcome are described.

3.2 REQUIREMENTS DEFINITION.

The objective of this task was to generate a preliminary Product Function Specification, otherwise referred to as a "system specification" for thermoreactive aircraft coatings which addresses the requirements of a wide variety of candidate military end-users and their potential applications. Definition of the system specification for thermoreactive aircraft coatings came as a result of compilation of general and specific requirements for paint color, gloss, durability, hardness, compatibility with low observables, anti-static coatings, and substrate materials which were solicited from various end-user agencies. While several of the end-users had different specific coating color requirements, a composite was drawn up which would satisfy most of the specified requirements for each given application, with the intention of encompassing the broadest possible range of advanced program objectives. These requirements were then compared with those of commonly used Mil-Spec aircraft exterior coatings to ensure that the proposed required properties were appropriate and achievable. This task resulted in a draft system specification, presented in Appendix A, which was used as a guideline for development and evaluation of the thermoreactive coating system.

Copies of the draft specification were sent on June 14, 1990 to the following candidate end-user representatives:

William F. Anspach, Materials Research Engineer, Wright Patterson AFB
Maj. Louis Cipriani Jr., HMX-1 Plans, Quantico, VA
Mr. Greg Curry, Northrop Corporation, B-2 Division, Pico Rivera, CA
Maj. Thomas E. Dayton, HQ SAC-XRFS, Offut AFB, NE
Mr. Richard Foulkroud, VH-3D Program Manager, Sikorsky Aircraft, Stratford, CT
Mr. Christopher Fulton, McDonnell Aircraft Company, St. Louis, MO
Mr. Dale Henning, General Dynamics-Fort Worth Division, TX
Mr. Richard McBride, VH-60 Program, Sikorsky Aircraft, Stratford, CT
Lt. Col. Gary Simpson, Naval Air Systems Command, Washington D.C.
Maj. George T. Simpson, NAVAIR, Washington D.C.
Dr. Richard D. Stolk, McDonnell Aircraft Company, St. Louis, MO
LCDR John S. Rosa, Dept. of the Navy, Naval Air Systems Command, Washington, D.C.

3.3 COATING COMPONENT DEVELOPMENT.

This major task, which encompassed all development aspects of each of the thermoreactive coating components (thermoreactive pigment, paint binder, and reflective undercoat), was divided into a series of sub-tasks, reflecting the complexity of this overall development effort. Included in these sub-tasks are all phases of the chemistry employed to formulate and microencapsulate the PDA thermoreactive pigment, development of a compatible transparent binder system for the pigment, evaluation of reflective undercoat materials, and formulation of a protective top-coat. All tasks utilized preliminary tests for screening of candidate materials and processes. The following sub-tasks describe each stage of the TRAC component development.

3.3.1 Thermoreactive Pigment Development.

This task comprises the heart of the overall thermoreactive coating system development. Development of the thermoreactive pigment, which is the key (active) ingredient in the coating was the primary objective of this task. In addition to formulation of the pigment to satisfy the coating performance requirements outlined in the system specification, any alterations in the chemistry to accommodate the requirements of ultraviolet (UV) stabilization had to be identified and carried out. The pigment, formulated in bulk, had to be reduced to a particle size compatible with the gloss requirements of the finished coating. The evaluation of color, thermal performance and durability, and UV stability had to be performed simultaneously with this task to guide the formulation.

Color for this task was limited to a dark camouflage grey. Specimens were tested for transmissivity, reflectivity, and color characterization in both the colored (benign) and uncolored (heated) states. Thermal performance and stability was determined from tests conducted on PDA's Xenon Light Test Bench (XLTB) and at the White Sands Solar Facility (WSSF). Weathering tests were performed using a QUV accelerated weathering chamber, and outdoors on the roof of PDA's laboratory facility in order to evaluate environmental durability.

3.3.1.1 Thermoreactive Pigment Formulation. A basic thermoreactive pigment formulation was developed as a result of a PDA funded IR&D effort conducted prior to contract award, for the purposes of proof of concept. The TRAC system specification requirements, however, deviate from the original formulation's properties in one important parameter: transition temperature. Other thermochromic materials possessing chemistry similar to the TRAC pigment are widely available in the marketplace with transition temperatures ranging from -10°C to +55°C. Several manufacturers claimed that an 80°C transition temperature material was available, but none of them could deliver such a product once an order was placed. Discussions with experts in the field verified that thermochromic materials which transition at temperatures beyond 60°C did not exist in the marketplace at that time. Therefore, it was determined that it was necessary to develop new thermochromic technology which extends beyond the current state of the art.

Development of a higher transition temperature thermochromic pigment requires an understanding of the mechanism of decolorization. The thermochromic mechanism is governed by three basic components: an electron-donating chromatic compound (commonly referred to as the "dye"), a compound containing a phenolic hydroxyl group (called the "activator"), and the "carrier", which is a blend of compounds selected from the higher aliphatic monovalent alcohols and the higher aliphatic monovalent acid alcohol esters.

The melting point of the monovalent alcohol defines the transition temperature, and the monovalent acid alcohol ester sharpens the transition from the colored to uncolored state. By carefully formulating the carrier with a combination of monovalent aliphatic alcohols and esters, the desired temperature range for color transition (also referred to as "metachromism") can be obtained.

The dye determines the color of the thermochromic pigment. Dyes are available for the colors red, blue, yellow, green, orange, violet, and black, and can be used in combination to form nearly any other desired color. The activator is the source of metachromism, reacting reversibly with the dye upon heating or cooling of the compound. From a combination of these compounds it is possible to formulate a pigment which changes from the desired color to colorless or nearly transparent above the desired transition temperature.

The thermochromicity of the pigment is due to the acid strength of the phenolic compound (activator). The phenol reacts with the dye to form an acid-dye complex and a phenolate ion upon the application of heat. Upon cooling, it retains the molecular geometry established, due to the extreme stability of the triphenyl cation formed. This triphenyl cation is an extensively conjugated molecule, which absorbs energy in the visible range which accounts for its color. The reapplication of heat to a temperature beyond the melting point of the waxy carrier (the transition temperature) causes bond formation between the phenolate ion and the cation, interrupting the extended conjugation of the triphenyl cation, such that it no longer absorbs visible light. The energy levels absorbed increase dramatically, shifting the wavelength of absorption to shorter wavelengths, that have no visible color. The result is conversion of the thermochromic pigment to the colorless state. Upon removal of applied heat, the equilibrium between the colored and uncolored states shifts back to the colored form, the more stable triphenyl cation. This equilibrium is infinitely reversible, unless this thermochemical reaction is disturbed by the presence of contaminants. Contaminants may take the form of solvents, degradation products of any of the organic components, oxygen, etc.

The reaction between the dye and the activator, as previously described, is a combination of thermal activation and solvation effects. Depending upon the formulation, the transition temperature can be adjusted to fall anywhere from 50°C below to 50°C above the melting point of the carrier. If the dye-activator ratio is adjusted to cause transition at the melting point of the carrier, then thermochromism is controlled by the melting point of the carrier. The primary consideration, therefore, in the development of a higher transition temperature thermochromic material, is the proper choice of carrier materials. Since the transition temperature of a well modulated pigment falls 7 to 10°C below the melting point of the carrier, the ideal carrier material for this application was determined to have a melting point of between 100° and 140°C. A wide variety of long chain hydrocarbons which melt in this temperature range are available in the form of polyethylene, perhalogenated polyethylenes, and shorter chain hydrocarbons (commonly referred to as "waxes"). They are available with a variety of functional groups that may be used to optimize the solubility of the other pigment components. As a group, they offer a wide range of advantages: high melting points to 200°C, high heat capacity, UV stability, insolubility in common solvents, and excellent transparency in the molten state.

A broad range of polyethylenic materials were investigated in an effort to optimize the thermochromicity of the system. Polyethylenes with functional groups including pyrollidone, carboxylic acid, acrylic, acetate, and alcohol were evaluated. The high temperature requirement for the system made these materials very desirable, but their inherently low polarity decreased compatibility with the system tremendously. The ionic dye-activator complex had very low solubility in these non-polar carriers. Several acidified waxes were also investigated. The high acidity resulted in activation of the dye without additional activator, but the heated state contained unacceptably high residual color.

Other problems which were encountered in the use of polyethylenes were associated with the broad melting temperature range of polyethylene due to the diversity of molecular weights in these polymeric materials. Sharper melting temperature range waxes produce sharper transition temperatures in the final pigment. However, thermoplastic materials have a glass transition temperature that extends from 30% to 100% below the melting point. In the glass transition range, the specific volume increases rapidly with temperature, allowing greater chain mobility and increased movement of molecules within the polymeric matrix. These parameters result in a tendency for the transition temperature to drop, causing the color to change gradually over a very broad range.

To optimize all necessary parameters, a blending of waxes was then investigated. Polymers, because of their large size and high viscosity, can be blended to form solids consisting of combinations of different polymers. Due to the small particle size desired in the end product, the blend required a high degree of compatibility. The addition of an esterified wax with lower molecular weight and higher polarity was chosen to increase the solubility of the system and sharpen the transition temperature. The resulting product had a higher dye concentration, which increased the color intensity of the pigment, and a heated state with greater transparency than that of the polyethylene alone. In addition, a dramatic drop in the melt viscosity of the carrier blend served to expedite particle formation, an advantage which will be obvious when pigment particle formation methods are discussed later in Section 3.3.1.2.

The incorporation of UV stabilizers was evaluated extensively as an integral part of the formulation process. The thermochromic system is an extremely sensitive mechanism. The addition of any chemical requires complete readjustment of component concentrations. The results of stabilization are discussed in Section 3.3.1.4.

3.3.1.2 Pigment Particle Formation Methods. The proposed processing sequence for the production of a pigment for incorporation into a thermoreactive aircraft coating was to reduce the bulk thermoreactive pigment material down into discrete particles with a size in the range of 5 to 25 microns, microencapsulate the particles in a solvent-resistant polymeric coating, and then disperse the microencapsulated material in a solvent-based paint binder. To optimize the solvent resistance of the microcapsules, spherical shaped particles were required. To facilitate the microencapsulation process, a dry powder or aqueous suspension was desired. Much difficulty was encountered in achieving these objectives. The choice of polyethylene as a carrier for the thermoreactive dye system allowed for several methods of particle formation to be tried: emulsification, solvent dispersion, grinding, and atomization. The results of those experiments are described below.

Most of the early particle formation experimentation was performed with oxidized (acidified) polyethylene waxes. These materials were selected for their inherent compatibility with the thermoreactive dye system and their high emulsifiability. Emulsification of acidified waxes is typically accomplished by subjecting the material to a strong base, thereby neutralizing the acid functionalities. Very little surfactant is required due to the negative charges on the polymer backbone. The degree of functionality (represented by the acid number) is indicative of the ease of emulsification.

Problems were immediately encountered in the processing of the pigment material by this method. The most critical problem involved interference with the thermochromic chemistry. The thermochromic system is an acid-base reaction and the base used in emulsification deactivated the system.

The addition of surfactants to the system negated the requirement for strongly alkaline dispersion media in the emulsification system. Experimentation was performed with the cationic emulsifiers Ethomeen C12 and Ethoquad 18/12, products of Akzo Chemicals. Both of these surfactants produced excellent emulsions with particle sizes in the range of 1 to 15 microns when used with the plain polyethylene copolymer. However, the addition of dye and activator to the polyethylene inhibited emulsification. It appeared that the dye was easily extracted into the aqueous emulsion medium by the highly polar surfactants. By reacting with the surfactant molecules, the dye neutralized the surfactant,

inhibiting emulsification of the wax. Evidence of this mechanism was observed in the darkening of the aqueous phase and loss of color in the polymer.

Emulsification in suspending agents was also investigated. Three suspending agents were investigated: solutions of polyvinyl alcohol, gelatin, and polyacrylic acid. Removal of these suspending agents is necessary prior to encapsulation, however, which imposed limits on the feasibility of two of these processes.

Aqueous solutions of polyvinyl alcohol (PVA) with an average molecular weight of 100,000 were evaluated at concentrations of 3%, 6%, and 9%. A very nice emulsion was formed at each concentration, the particle size decreasing with an increasing PVA concentration. The drawback to utilizing PVA as a suspending medium for particle formation was its incompatibility with the subsequent microencapsulation process. Filtration or resuspension in water would be required to make this a workable system, and in practice PVA is very difficult to filter. Similar results were obtained with solutions of 50% gelatin, which yielded an average particle size of 35 microns. Gelatin, however, leaves a sticky aggregated mass of particles upon filtration.

Emulsification in solutions of polyacrylic acid was extensively investigated, since this is the suspending medium used in many microencapsulation processes. A 5% solution of polyacrylic acid with a molecular weight of 250,000 showed some promise, forming 5 to 50 micron sized particles; however the system exhibited poor repeatability.

Solvent dispersion of polyethylene was extensively investigated. This process is very attractive due to its simplicity, and is used extensively in the paint industry to produce gloss reduction and surface roughening additives. For our application the processing procedure entails finding a solvent in which the polyethylene has minimal solubility at room temperature, but goes into solution readily at temperatures above 80°C. Slow cooling of the hot solution then causes precipitation of particles with sizes in the range of 2 to 5 microns.

Extensive solubility tests were run on the dye and activator in various solvents which were recommended by the polyethylene manufacturer. In theory, if the dye and activator are less soluble in the solvent than in the polyethylene, the probability that the dye will precipitate out into the polyethylene (the desired result) increases. The

following solvents showed negligible solvation of the dye and activator: mineral oil, heptane, 2,2,4-trimethylpentane, kerosene, mineral spirits, naptha, Isopar H (a high-boiling hydrocarbon mixture from Exxon), and halocarbon oil (a chloro-flouro-hydrocarbon solvent). The results from experiments using these solvents were very similar, producing particles in the size range of 2 to 5 microns; however, the particles produced by this process were generally of low color density. Allowing the particles to sit in the solvent for a longer period of time revealed a gradual settling of black dye on the bottom with clear polyethylene beads on top. Microscopic analysis revealed that the dye/activator complex and polyethylene precipitated out randomly, with only a fraction of the dye/activator complex in the polyethylene, and with the largest portion of it on the surface of the beads, which was unacceptable.

From the previously described experiments it became apparent that mechanical methods for the production of small pigment particles would most likely be successful in maintaining the integrity of the pigment composition. In practice, particle size reduction by mechanical methods was most successfully performed cryogenically by either grinding or using fluid energy techniques. However, grinding produced irregularly shaped particles that made solvent-resistant microencapsulation, the subsequent step, difficult. The encapsulating polymer tended to sphericize the particle, which produced particles with thick walls on the flat sides and very thin (and thereby easily permeated) walls over the sharper edges. Sphericization of ground particles by heating to 90°C in a suspending agent was also investigated, as a pre-encapsulation process. Some rounding of the particles occurred at the expense of heavy particle agglomeration. A noteworthy advantage however, to grinding techniques was a narrow particle size distribution, which yields a more uniform wall thickness in the subsequent encapsulation process.

In July of 1991, Yamato Scientific was contacted regarding the possibility of atomizing the pigment in its molten state at 140°C. Their response was that this was not possible using standard spray drying equipment, which is designed for spraying liquids at room temperature into a chamber heated to 100° C for the purpose of dehydration. While the heated chamber could easily be converted for use at room temperature conditions, heating the transfer hoses from the sample reservoir to the atomizer was difficult due to the peristaltic pumping system that was employed in their atomizer. They proposed building a prototype atomizer

with a heated reservoir utilizing gravity feed to the atomizing nozzle. The transfer pipes and nozzle would be heated to 195°C. The cooling chamber would require no heating or cooling, so a 55 gallon drum would suffice. A standard cyclone based collection system could be fed from either the top or the bottom of the hopper positioned at the base of the 55 gallon drum. PDA agreed to purchase the proposed system, contingent on the demonstrated ability to produce good yields of particles in an acceptable size range. A diagram of the prototype system is shown below.

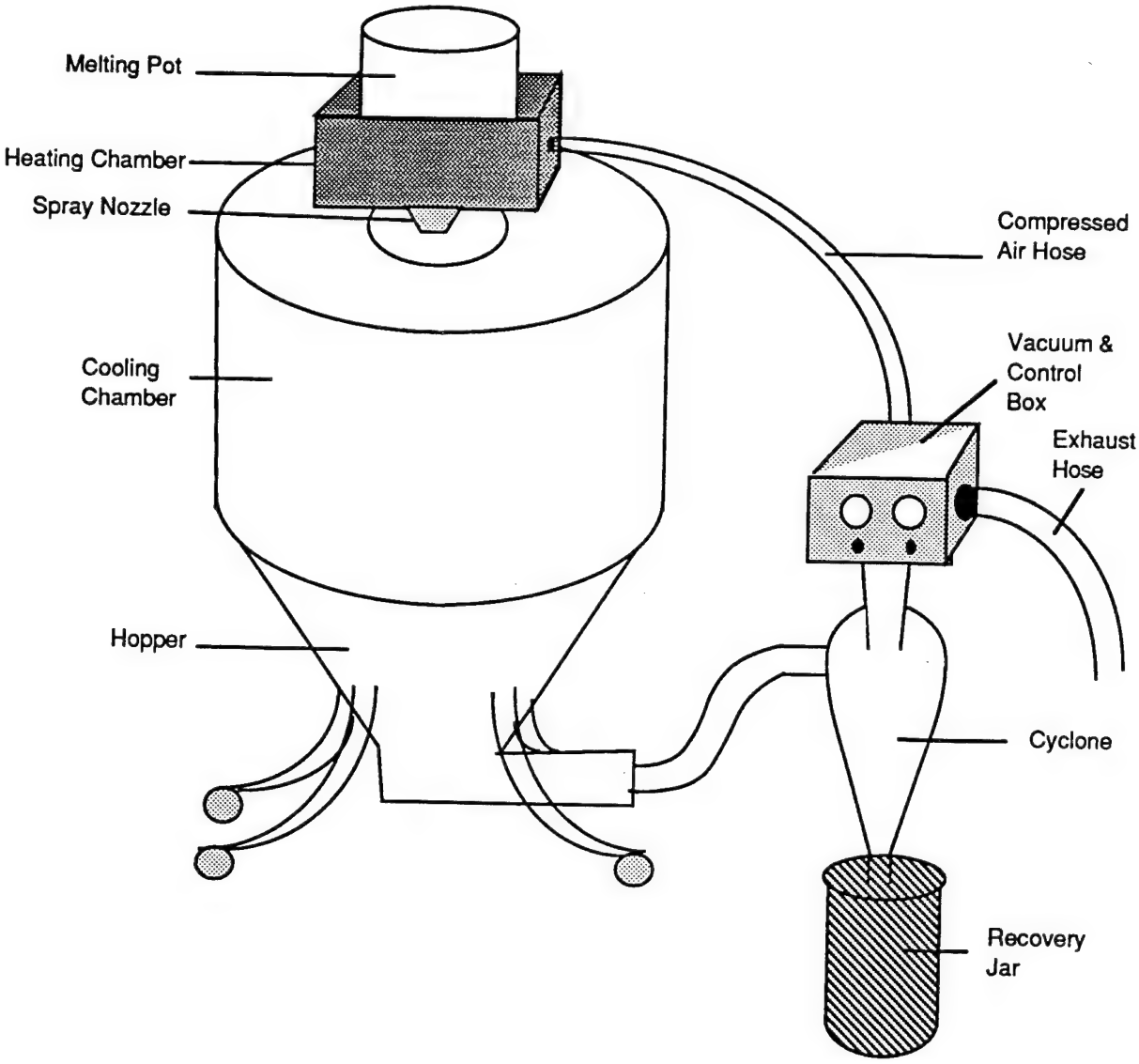

Figure 3-1. PDA hot atomizer.

Optimization of the pigment carrier composition was performed as a cooperative effort with Yamato during the time the spray dryer was being built. Initial experimentation with this process was performed with the polyethylene-based pigment. The viscosity was found to be too high for spraying. The processed material contained, in addition to powder, spherical particles possessing 'tails'. Spraying of a second wax having a very low viscosity (less than 50 centipoises) resulted in acceptable micronization. The compatibility of these two waxes was examined and their miscibility determined. An appropriate blend resulted in a material with a sprayable viscosity which produced a thermochromic pigment with improved color intensity due to increased solubility of the dye component. The increased polarity of the blended carrier as compared to 100% polyethylene, however, dropped the transition temperature to 85°C to 105°C from 100°C to 120°C. But this temperature range was still beyond the ambient operating skin temperatures of most candidate applications, so the process was approved at this stage of development.

Analysis of the particle size distribution from the hot atomization process was performed using a Horiba LA-700 laser diffraction particle size distribution analyzer. Final approval on the hot atomizer purchase was made when analysis (results shown in Appendix B) showed that 57% of the particles by volume collected through the cyclone were in the size range of 5 to 25 microns (15 micron median size). Yamato assured us that the powder collected in the bottom of the hopper, median size 60 microns, could be remelted and cycled back through the atomizer to produce an overall yield of at least 50% of usable material.

Following the delivery, setup, and a preliminary system checkout of the system in September of 1992, some minor modifications such as replacement of all rubber hoses with plastic, enclosing and insulating of the heating chamber, and grounding of the cyclone were performed. A liner was also added to the cooling chamber to prevent contamination of the pigment powder from the interior of the 55 gallon drum.

After modifications were completed, further experimentation was performed to optimize the operating parameters in order to obtain the desired particle size distribution. It was found that particle size is primarily determined by the viscosity of the molten material, the rate of flow of the molten material through the atomizing nozzle, and the air pressure through the nozzle. Particle size can be indirectly controlled by the temperature of the molten material, due to the temperature-viscosity relationship of the thermoplastic material.

The optimum batch size was determined to be 750 grams of molten pigment. Yield under these conditions was approximately 400 grams of powder, of which all of the collected material could be used without fractionation. The particle size range was approximately 2 to 25 microns, as determined using an Olympus OM2 microscope.

3.3.1.3 Pigment Properties Characterization. The most important properties which characterize the thermochromic pigment are its color in the benign and heated states, and its transition temperature. While this project was limited in the scope of colors to be developed, information was accumulated to evaluate the potential for additional colors.

The dyes for five basic colors were formulated, from which any desired color can be created for future TRAC applications requiring specifically defined colors. Due to the slight differences in shade produced by small changes in the extended conjugation of the dye-activator complexes, two different activators were tested. Thin coatings of the resultant pigments were prepared on glass slides by a draw-down technique and absorbance spectra were obtained using a Beckman Acta MIV UV-Visible Spectrophotometer. Absorbance as a function of wavelength for the five pigments, for the carrier alone, and for the carrier in combination with each of the two activators are shown in the following spectral plots.

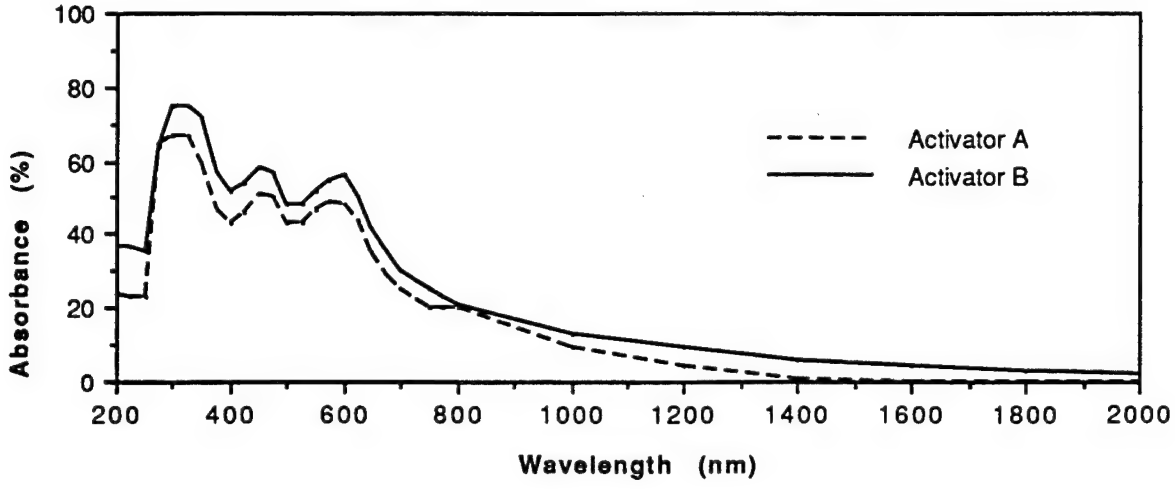

Figure 3-2. Absorbance spectrum of black pigment.

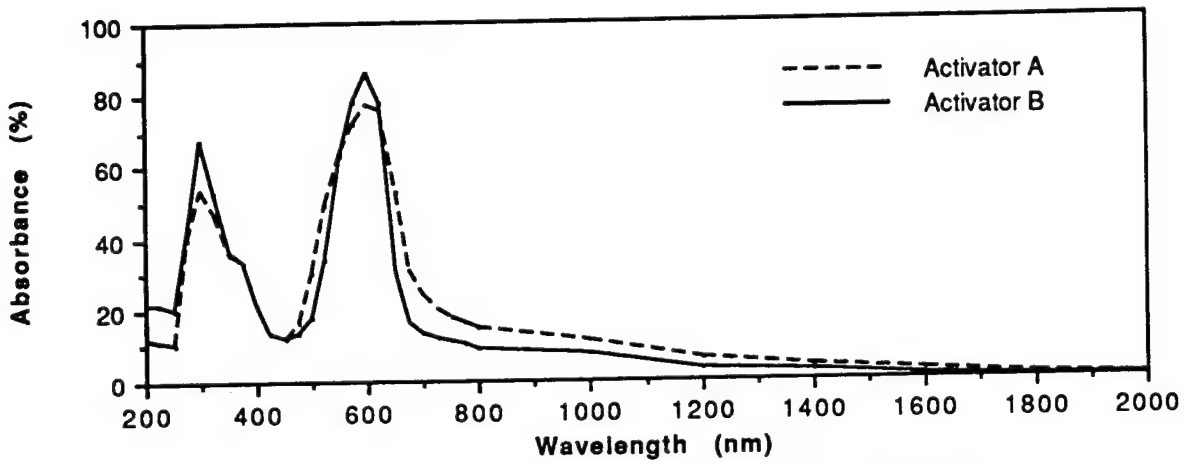

Figure 3-3. Absorbance spectrum of blue pigment.

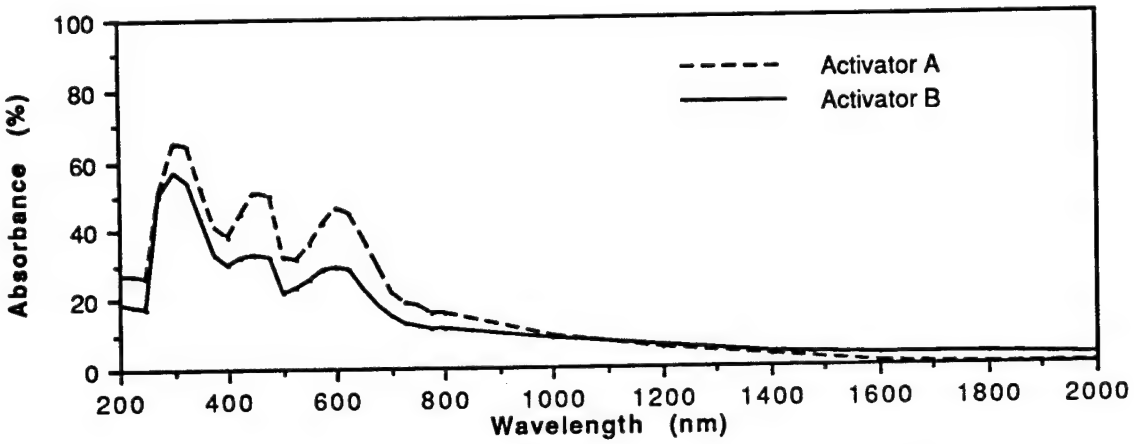

Figure 3-4. Absorbance spectrum of green pigment.

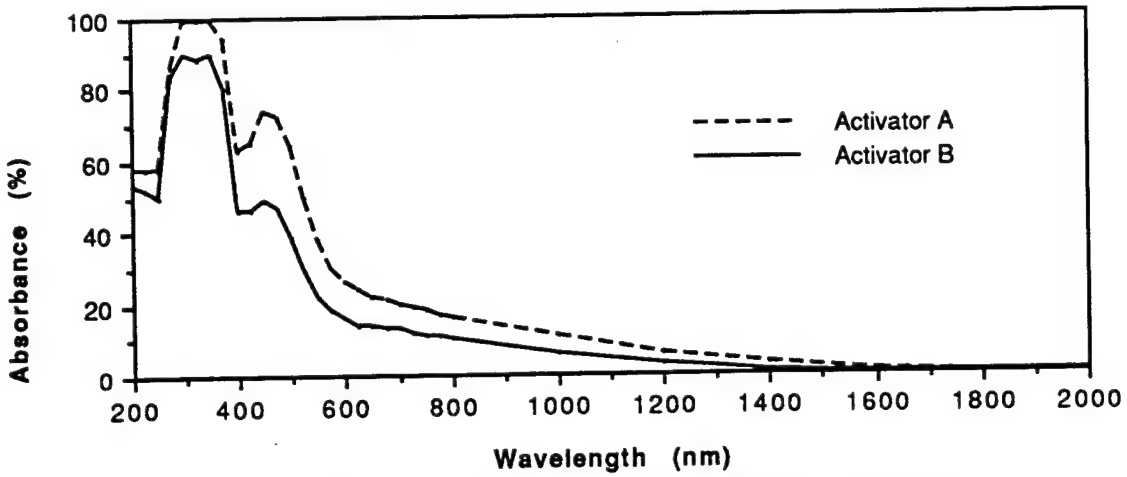

Figure 3-5. Absorbance spectrum of orange pigment.

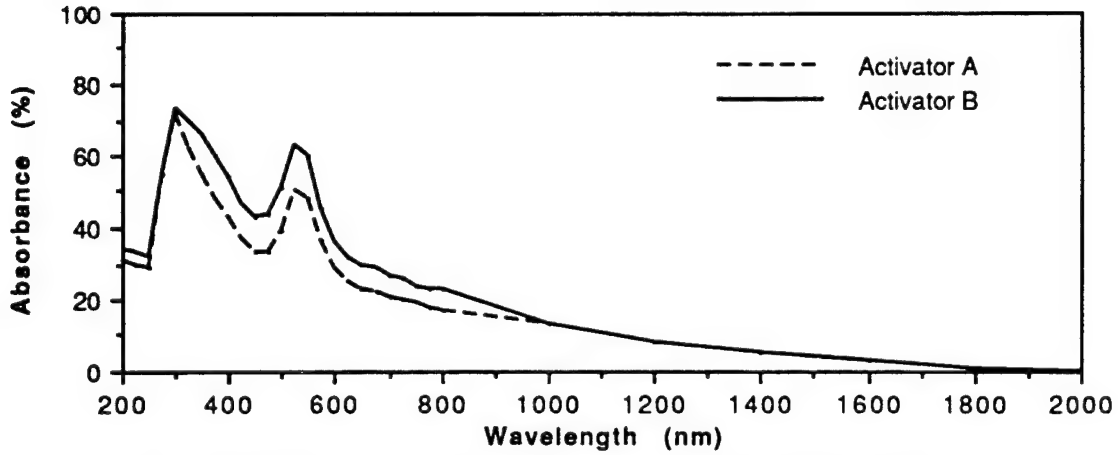

Figure 3-6. Absorbance spectrum of red pigment.

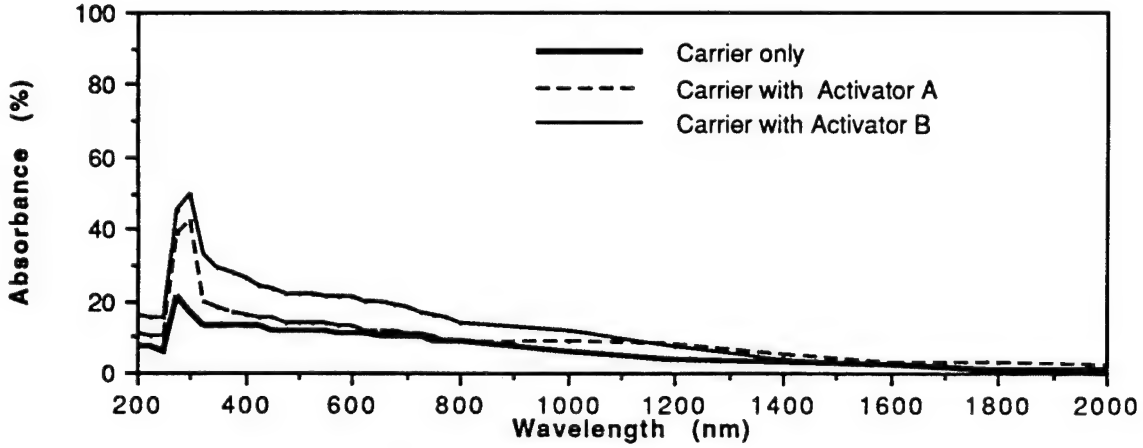

Figure 3-7. Absorbance spectra of carrier and activators.

Visually, the pigments transition according to the table below:

Table 3-1. Pigment colors in the benign and heated states.

PIGMENT COLOR AT AMBIENT TEMPERATURE (Benign State)	PIGMENT COLOR ABOVE TRANSITION TEMPERATURE (Heated State)
Black	Pale beige transparent
Blue	Pale yellow transparent
Green	Transparent gold
Orange	Pale yellow transparent
Red	Pale pink transparent

From user inputs collected in the requirements definition phase of this program it was determined that an "ideal" pigment should transition from the colored state to clear (colorless) at a temperature in excess of 125°C. However, a material that transitions at a temperature greater than 80°C will effectively protect approximately 80% of the primary candidate vehicles for this coating. Materials transitioning at temperatures in excess of 140° to 150°C require processing temperatures in the range of 175°C, and at this high temperature, thermal degradation of the dye occurs rapidly. Thus, these considerations bracket the possible transition temperature for thermochromic pigments.

The transition temperatures were determined for a wide range of candidate pigment formulations. The final formulation was the result of meshing many different variables, of which the transition temperature is one component. These included the solubility of the dye components in the carrier, the processability for the formation of small particles, the color intensity and hue of the benign state, the transparency of the heated state, solubility of the pigment components in the microencapsulating slurry, and environmental aging characteristics.

Ultimately, the transition temperature proved to be a balance of carrier polarity and the ratio of the dye to activator concentrations. For any given pigment formulation, the transition temperature could be varied by as much as 60°C by changing the dye/activator ratio. It was demonstrated experimentally that for pigments using carrier materials with a given constant melting point temperature and activator concentration, the transition temperature decreases with increasing polarity of the carrier. The list of candidate carrier materials shown in Table 3-2 are presented from top to bottom in order of increasing polarity and decreasing transition temperature.

Table 3-2. Carrier material properties.

CARRIER MATERIAL	MELTING POINT (°C)	DYE/ACTIVATOR MOLAR RATIO	TRANSITION TEMPERATURE (°C)
Homopolymer	102	4/1	160+ (incomplete)
Ethylene-2-ethylhexyl Acrylate	91	4/1	100-110
Ethylene Vinyl Proprionate	97	4/1	100-130
Ethylene Ethyl Acrylate	103	4/1	105-120
Ethylene-methyl Acrylate	92	4/1	105-120
PE/Vinyl Acetate	95	4/1	85-120
Ethylene Vinyl Alcohol	90	3/1	60-70
Ethylene Vinyl Pyrollidone	95	4/1	65-85
Ethylene Acrylic Acid	95	72/1	65-85

The final pigment, a result of considerable experimentation and the balancing of all relevant variables, transitions from the colored to clear state within a temperature range between 85°C and 105°C.

Optimal performance of the TRAC coating requires that incident radiant thermal energy be efficiently transmitted through the TRAC pigmented binder to the reflective undercoat, where it can be reflected away from the coating's substrate. The radiant thermal energy transmittance and thermal hardness of candidate TRAC formulations was determined from tests performed at the White Sands Solar Facility (described in Section 3.3). Test samples were prepared by applying the candidate paint formulations to one side of 3-inch by 3-inch squares of clear polycarbonate. Samples were exposed to constant 15 cal/cm^2-sec flux level radiant thermal energy pulses of one and four second timed durations. Thermal energy transmitted through each sample was measured using a blackbody calorimeter and is expressed as a percentage of the incident thermal energy using the notation "%T_{bb}".

Following the one second exposures (15 cal/cm^2 total incident fluence), nearly all formulations transitioned to clear and returned back to their original benign state color. Four second exposures (60 cal/cm^2 total incident fluence) caused deterioration in several formulations, primarily in the form of blistering. The baseline formulation exhibited excellent thermal hardness, or the ability to withstand exposure without evidence of degradation, up to a total fluence of approximately 50 cal/cm^2. The thermal energy transmittance (%T_{bb}) of these samples averaged 67 to 70% for one second pulses and 84 to 87% for the four second duration pulse condition.

This series of tests served as an excellent indicator of candidate coating formulation thermal hardness. Figure 3-8 shows a comparison of the transmitted energy as a function of time for two different sample formulations. The upper plot is a typical example of a coating with high thermal hardness, indicated by the nearly constant level of transmittance throughout the entire pulse duration. The lower plot, by comparison, shows a sharp decrease in thermal energy transmittance occurring during the last one second of exposure. This decrease is indicative of coating deterioration in the form of smoke generation during exposure, verified by blistering and permanent bleaching (failure to return to the benign state color) observed after completion of the test.

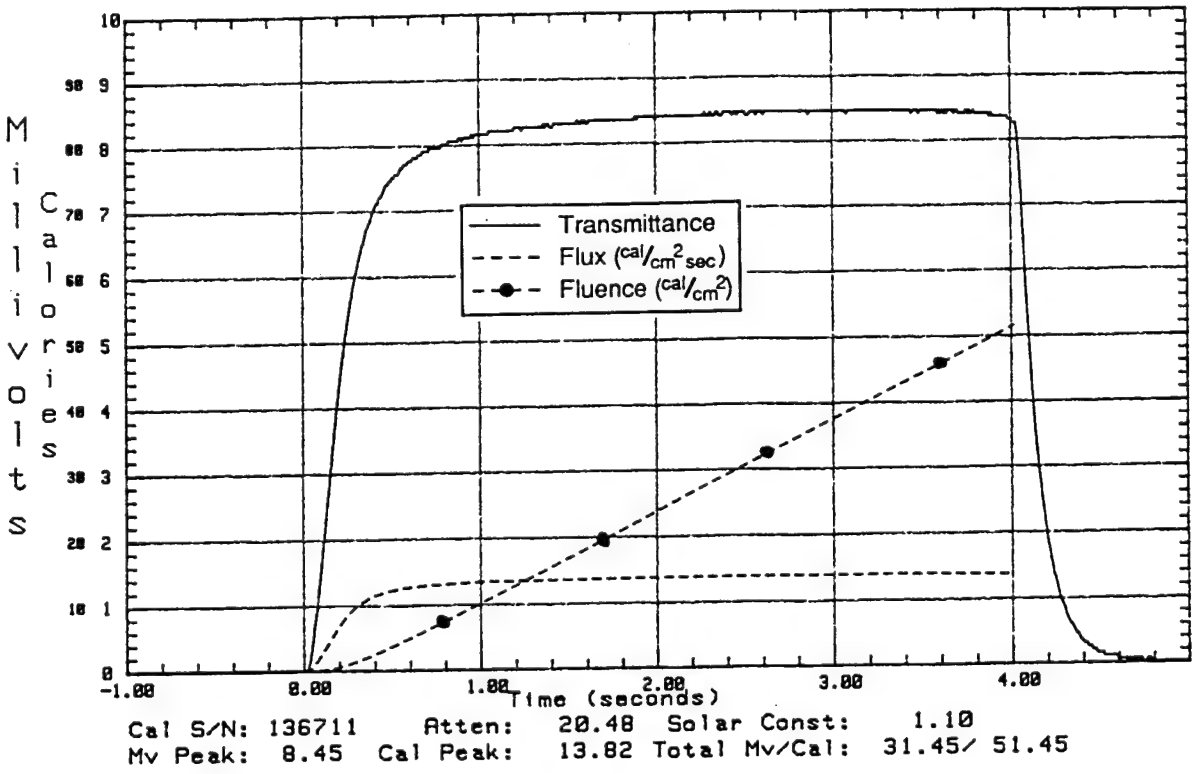

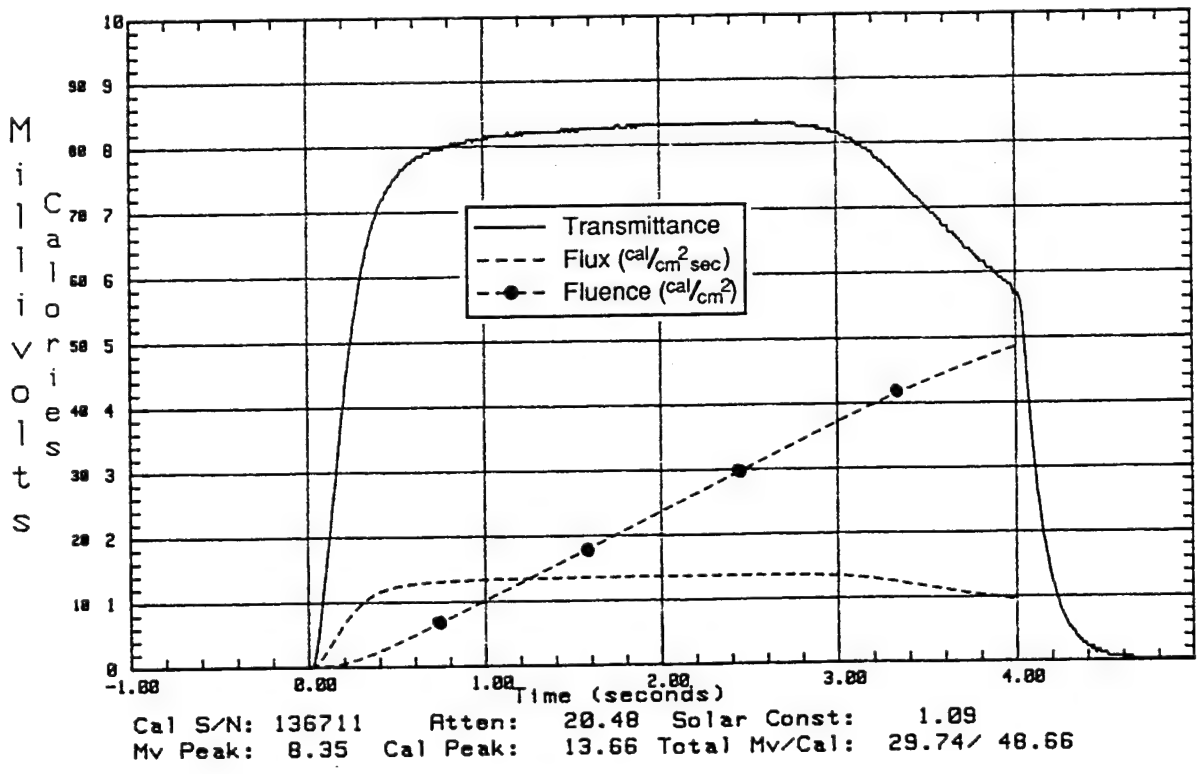

Figure 3-8. Thermal energy transmittance of two sample formulations.

A spectral scan of the baseline black pigment obtained from testing at the White Sands Solar Facility is shown in Figure 3-9 below. The pigment was coated on a 3 by 3-inch square of polycarbonate and exposed to a one second duration 15 cal/cm^2-sec thermal pulse. The transmittance was recorded as a function of wavelength while exposed using the PDA Spectral Analyzer (high flux spectrophotometer) equipped with narrow bandpass filters for transmittance measurements at 16 discrete wavelengths between 400 and 850 nm.

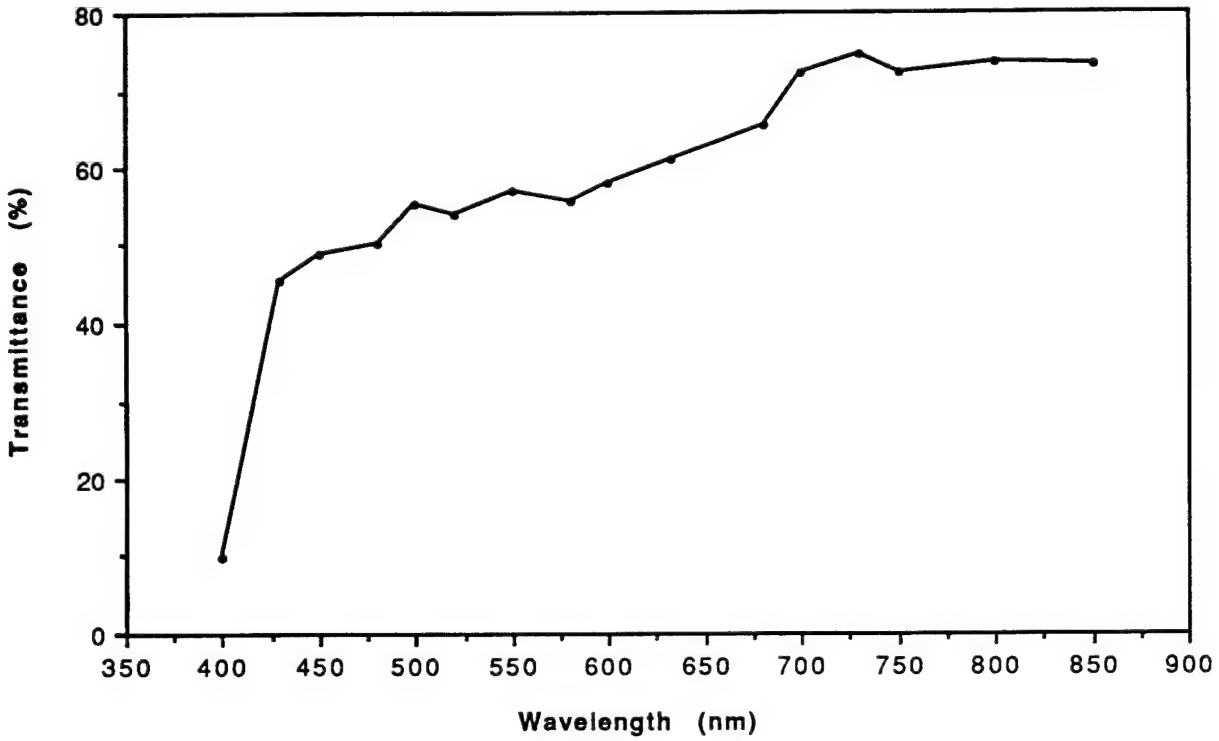

Figure 3-9. Spectral transmittance of TRAC pigment under thermal flux.

Spectral scans were used during pigment formulation development mainly as a diagnostic tool to analyze the effects of component variations on heated state residual "color". By comparing spectral transmittance curves for various candidate formulations in the heated state, particular wavebands where the transmittance of energy was less than optimum could be identified. This in turn provided for a better understanding of how individual component changes affect overall thermal energy transmittance and resulting overall coating system heat rejection efficiency.

3.3.1.4 UV Stabilization. Stabilization of the TRAC pigment is critically important to the long term durability and usefulness of the entire coating system. Stabilization was approached conceptually with recognition of the fact that degradation in any one organic component accelerates degradation of all other organic components, and that all components are required in their original concentrations for the TRAC pigment to perform properly. The dye and activator must remain molecularly stable and the carrier must maintain its integrity and solvent properties in the molten state to facilitate thermoreactivity. Triarylmethyl lactone dyes of the type used in the TRAC pigment are structurally analogous to the spiropyran dyes with which PDA has considerable experience in stabilizing.

The photodegradation of the leuco-dye cation, the colored form of the triarylmethyl lactone dye molecule, has been studied extensively in the dye and textile industries. These studies demonstrate the tremendous impact of oxygen on pigment degradation as illustrated by the degradative mechanism shown below.

D^+(dye molecule) + U.V. energy ---> $^1D^+$ ---> $^3D^+$ (excited dye molecule)
$^3D^+$ + solvent ----> $D\cdot^{++}$(dye free radical cation) + e^-(solvated)
D^+ + e^-(solvated) ----> $D\cdot$ (dye free radical) + solvent
e^-(solvated) + O_2 ----> $O_2\cdot^-$(peroxygen radical) + solvent
$O_2\cdot^-$ + H_20 ----> $HO_2\cdot$(peroxide radical) + OH^-
$2HO_2\cdot$ ----> H_2O_2 + O_2 (Peroxide formation)
D^+ + H_2O_2 ----> Oxidized products (Primarily ketones)

These reactions show the mechanism by which oxygen reacts with a dye molecule, excited by UV energy, to form degradation products of the dye molecule. UV stabilization therefore, is designed to inhibit the formation of free radicals and peroxides. There are four basic categories of stabilizers which have the potential to inhibit these reactions:

1. UV absorbers (UVA's) are designed to absorb incident radiation, thereby screening it from the pigment. Using a process known as tautomerism, they convert UV energy into harmless levels of heat energy, which are dissipated through the coating.

2. Benztriazoles act as energy transfer agents, converting photo-excited molecules back to their ground state.

3. Hindered Amine Light Stabilizers (HALS) are regenerative in their stabilizing mechanism and, therefore, can often be used in surprisingly low concentrations. Their mechanisms include energy transfer, free radical termination, and peroxide decomposition. They are known as free radical scavengers.

4. Hindered Phenolic Antioxidants (AO's) also function as free radical scavengers, specifically of peroxy radicals, but are more generally used to retard degradation due to heat exposure. Antioxidants are consumed in the stabilization process.

Combinations of UVA's and HALS are known to act synergistically. For coating systems that include a clear topcoat, it is generally recommended that the topcoat include concentrations of 1 to 3% UVA, and that the binder coat include a 1 to 2% concentration of HALS in addition to the 1 to 3% UVA. Antioxidants are recommended for high temperature processing, generally in the range of 0.1 to 1% concentration.

Considerable effort has been expended in working with the pigment in bulk form (before microencapsulation) as well as in the microencapsulated form, in a solvent-based binder with combinations of UV absorbers, hindered amine type free radical scavengers and antioxidants. This section of the report focuses on those efforts directed toward stabilization of the TRAC pigment only.

From a practical standpoint, the environmental factors affecting the durability of the TRAC system are known to be ultraviolet energy, oxygen, and thermal energy. An initial series of tests was targeted at identifying the effects of these factors in order to optimize the approach to stabilization. In these tests, unstabilized microencapsulated pigment was dispersed in MIL-C-85285 solvent-based clear polyurethane binder and coated on glass slides.

The purpose of this study was to evaluate the effects of heat and oxygen on the stability of the pigment in the absence of UV energy. The relative degree of pigment degradation at the termination of exposure was determined by the amount of increase in luminous reflectance, visual assessment of color change, and the quality of transition to the heated state at 130°C

Six samples were prepared for this study. Two of the test samples were wrapped in 0.015 inch thick EVAL-XL film, purged with nitrogen, and sealed. EVAL is the trade name for an ethylene vinyl alcohol

copolymer film known for its low oxygen permeability. Samples were shielded from U.V. light and placed in a convection oven at a temperature of either 23°C (room temperature), 50°C, 70°C, or 100°C for a period of 207 hours. The luminous reflectance of all samples measured before exposure ranged from 1.6 to 1.8%. The post-exposure test results are given in Table 3-3 below.

Table 3-3. Thermal/oxygen pigment stability test results.

SOAK TEMPERATURE	REFLECTANCE (%)	VISUAL ASSESSMENT
23°C (room temperature)	1.6	Black
50°C	3.0	Almost Black
70°C w/EVAL film	4.0	Brown
70°C	4.4	Brown
100°C	6.9	Light Brown
100°C w/EVAL film	8.1	Light Brown

After exposure, all samples transitioned well, however, irreversible darkening was noticed upon cooling, corresponding to the degree of fading (increase in reflectance) which was observed in the benign state.

The results of this test suggest that degradation of the pigment is caused by elevated temperature exposure in addition to other known factors, such as oxygen and ultraviolet radiation. The effect of the oxygen barrier seemed inconsistent, having some beneficial effect at 70°C, but none at 100°C. It should be noted that the glass transition temperature of the barrier material is approximately 70°C. It is quite possible that at 100°C, the polymeric free volume (permeability) was sufficiently increased to render the barrier film ineffective.

This test was intended to investigate the effect of UV light in both the presence and absence of oxygen on the weatherability of the TRAC system. Samples were evaluated according to the previously described procedures.

These samples were prepared in the same manner as those prepared for the thermal test. They were then wrapped in the films designated in Table 3-4, sealed around the edges, and placed outdoors in a rooftop aging fixture for natural sunlight exposure. The UVA film, a product of American Cyanamid, contained a 3% concentration of UV 24

dispersed in a 12 mil thick sheet of cellulose acetate. It was determined that one thickness of this film blocked 100% of all UV radiation from 200 to 280 nm., and that two thicknesses blocked 100% of all UV radiation from 200 to 400 nm. The oxygen barrier film was the same EVAL-XL film as that used in the thermal test, again sealed following a nitrogen purge.

All samples turned to a brown color after nine days exposure in natural sunlight, exhibiting decreased levels of activation and darkening upon cooling. However, the degree of degradation varied with the level of protection, indicated by the change in luminous reflectance, ΔR, shown in Table 3-4 below.

Table 3-4. UV/Oxygen Pigment Stability Test Results.

PROTECTIVE FILM CROSS-SECTION	ΔR (%)
O2 barrier film only	0.8
2 layers of UVA (200-400 nm.)	1.0
O2 barrier film/2 layers UVA (200-400 nm.)	1.7
O2 barrier film/ I layer UVA (200-280 nm.)	2.2
1 layer of UVA (200-280 nm.)	2.9
No barrier films	3.1

The UV absorption peaks for the activators and the carrier lie within the 250 to 350 nm. wavelength range. Therefore, it is not surprising that the blocking of energy between 200 and 280 nm. decreased degradation only slightly as compared to the control, since absorption between 280 nm. and 400 nm. has the most deleterious effects on the pigment. The addition of a second layer of UVA film, which increased the blocked energy waveband out to 400 nm. did reduce pigment degradation as expected. However, the addition of the oxygen barrier did not consistently provide additional reductions in degradation, as expected. It is possible that the paint film samples may have themselves contained absorbed oxygen, causing anomalies in the result of the use of oxygen barrier films. Carrying this test on for a longer period of time might have reversed the order of some of the trends, assuming that retarding the oxygen penetration actually does have a significant beneficial long term effect.

The results of the previous test were verified in an aging test designed to isolate the UV wavelengths which have the greatest effect on the degradation process. Specimens prepared on glass slides were covered with narrow bandpass filters which blocked out all incident radiation (light) except for a 20 nanometer wide band of energy at selected discrete

wavelengths. Care was taken to assure normal oxygen exposure and avoid light reflected from the sides of the samples. The test was terminated after 38 days of outdoor exposure. Post-test degradation evaluations were performed visually, and the increase in luminous reflectance of each sample was measured and recorded.

The degradative sensitivity to wavelength was apparent within the first six days of exposure. A slight increase in reflectance (fading) was noticed at all wavelengths. Samples exposed to radiation between 310 nm. and 375 nm. turned brown, and continued to darken with continued exposure.

The absorption spectrum of the black pigment between 200 and 400 nm., shown in Figure 3-10, illustrates the correlation between the test results presented above and the absorption characteristics of the pigment. There is strong overlap between the wavelengths exhibiting maximum degradation and the UV wavelengths of maximum absorption in the pigment. A control specimen, exposed to the full sunlight spectrum with no filtration had both browned and bleached with much greater severity than the filtered specimens. While the intensity of radiation impinging on this sample was much higher than in the filtered samples, there is a strong indication that significant absorption in the visible range of the solar spectrum may accelerate the degradation process. Based on these test results, it was concluded that no single approach to UV stabilization could be defined.

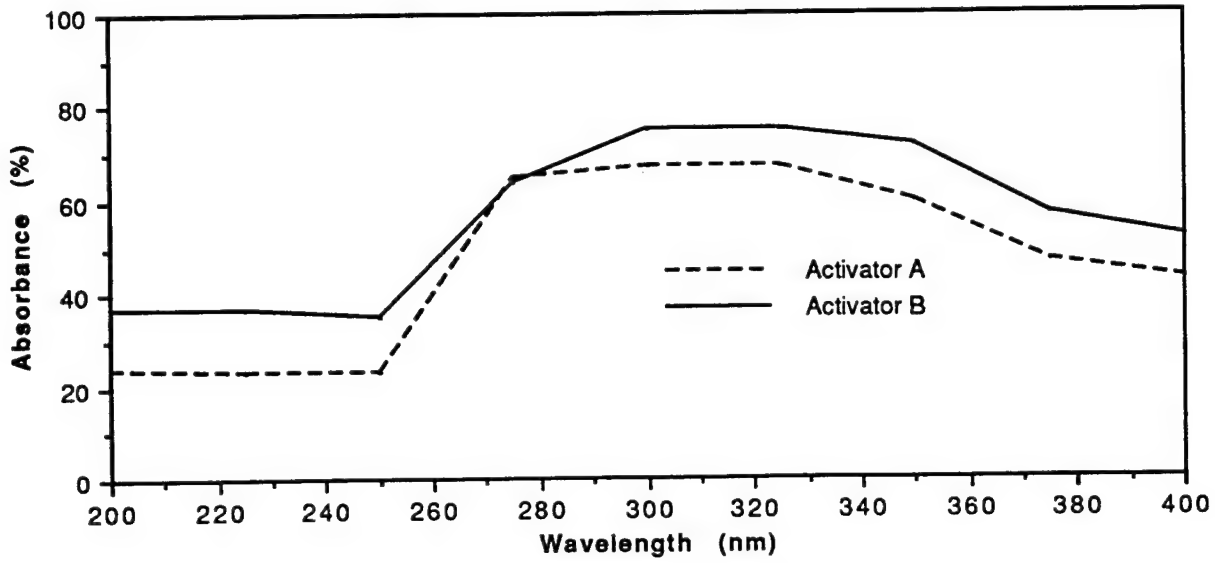

Figure 3-10. Absorption spectrum of black thermochromic pigment.

The weatherability of commercially available thermochromic pigments known to have chemistry similar to the TRAC pigment was evaluated in order to provide a point for comparison with the results of PDA's pigment stabilization efforts. A sample kit of black thermochromic paint was obtained from the Matsui Shikiso Chemical Company. This kit contained a sample quantity of paint composed of a black microencapsulated thermochromic pigment dispersed in a mineral spirits-based alkyd binder, along with a separate yellowish colored translucent material intended for use as a UV absorbing topcoat. The Matsui pigment was known to be stabilized with a phenolic stabilizer, and the UV absorbing topcoat material was determined, from spectral analysis, to absorb in excess of 75% of all UV energy between 260 and 310 nm., with complete (100%) absorption within the 275 to 300 nm. wavelength range.

Environmental aging test samples were prepared by spraying the Matsui thermochromic paint onto both bare aluminum and white painted (primed) aluminum panels. Samples were prepared both with and without the UV absorbing topcoat material provided in the sample kit. Half of each sample was covered with aluminum foil to provide an unexposed control area for post-test comparative purposes. Samples were placed outdoors in a rooftop aging fixture for natural sunlight exposure.

The outdoor aging test results can best be viewed graphically, as shown in Figure 3-11 below.

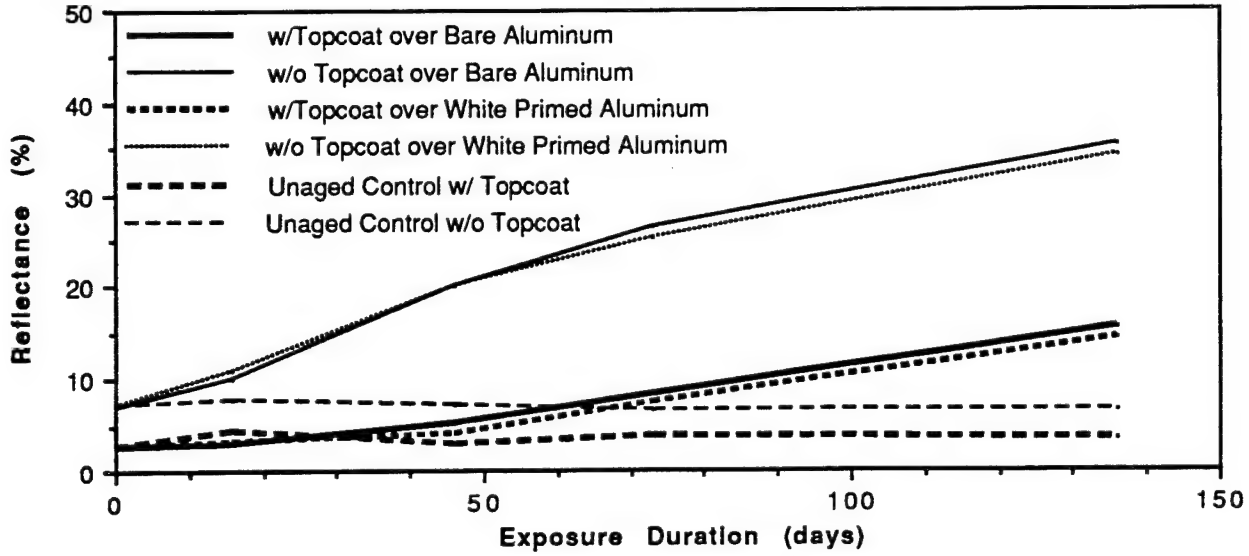

Figure 3-11. Environmental aging response of matsui thermochromic paint.

Matsui had informed us that three months was the maximum allowable outdoor exposure period for this material. This material would not meet Mil-Spec qualifications for allowable color fading after only two weeks of outdoor exposure. After 136 days of outdoor exposure, the samples were completely devoid of color and had luminous reflectance values in the range of 35%.

Preliminary tests were run to determine the relative UV stability of candidate pigment components. Where there was a choice to be made in the formulation, the more stable component was chosen, although due to the complexity of the pigment chemistry, other parameters often prevented that selection. An example is offered here which illustrates the degree to which U.V. stability was considered in the formulation process.

Many studies on the stability of organic pigments indicated that their degradation rate is dependant on pigment concentration. Theoretically, the pigment molecules, possessing extended conjugation, can transfer absorbed UV energy between themselves if they are in close proximity to each other. This effectively decreases the energy available for molecular degradation. As shown in Figure 3-12, tests of pigments which were prepared with dye concentrations in the range of 10 to 50% indicated that the U.V. stability improved dramatically as the dye concentration increased.

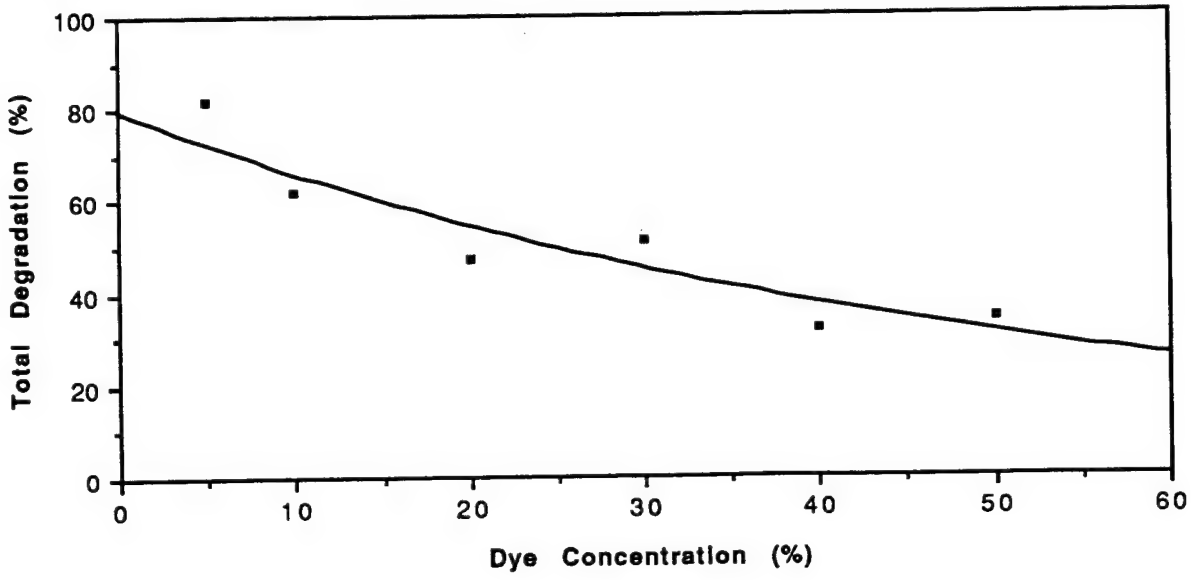

Figure 3-12. Pigment degradation rate as a function of dye concentration.

The percentage of total degradation decreased from 80% with a 5% dye loading in the pigment to 30% with a 50% dye loading in the pigment after 10 days of accelerated aging. However, when the pigment was loaded to 50% dye concentration, the luminous transmittance of the pigment in its heated state decreased to 35%. The transmittance of a pigment with 5% dye loading was measured at 60%. Since high transmittance, a result of solubility of the dye in the carrier, is necessary for proper thermal performance of the TRAC system, the dye load was limited to a maximum of 12%, which is the limit of dye solubility in the carrier. At higher dye loadings the pigment's heated state becomes unacceptably cloudy.

The results of the preliminary tests performed on unstabilized pigmented coatings and testing of individual components indicated that degradation of the pigment could not be controlled by any one method that could feasibly be incorporated into an aircraft coating. The pigment degraded in the absence of light at a rate that was dependent on temperature. While pigment exposure to U.V. energy can be attenuated significantly with UV absorbers, it would not be possible to eliminate all oxygen or all U.V. and visible light exposure to the pigment. Stabilization is therefore entirely dependent on the ability of added chemicals (stabilizers) to scavenge free radicals produced in the coating.

Unfortunately, there are no easy formulas to determine the optimum combination of stabilizers for any given organic system. Stabilization must be approached empirically for each system encountered, and is limited by the chemical compatibility of the components. Stabilization of the pigment thus became an integral part of the pigment formulation.

The various types of UV stabilizers were grouped in categories as defined earlier in Section 3.3.1.4. Hindered amines, due to their regenerative free radical scavenging ability were determined to be of primary importance. The stabilization process was begun by screening hindered amine stabilizers for compatibility and performance. UV absorbers are known to act synergistically with hindered amines. Having incorporated the optimum hindered amine stabilizer into the pigment formulation, screening of UV absorbers, both phenolics and benzotriazoles, was begun using the same evaluation criteria. Finally, antioxidants were added, using the same screening techniques. For each test sample, good compatibility, evidenced by solubility and lack of migration of individual

components, was required before the specimen was subjected to environmental aging testing. Due to the large number of stabilizers available, the test sample matrices were often quite large. Only the most significant tests and their results are reported herein.

Initial evaluations of UV light stability were performed using accelerated aging methodology. Two types of accelerated aging equipment, described in more detail in Section 5.2, have been utilized during the TRAC development program. Early aging tests were performed in a Sunlighter Model 50 ultraviolet aging chamber which uses a General Electric RS-4 bulb to age specimens at a rate approximately 50 times faster than natural sunlight exposure. A QUV accelerated weathering chamber, which utilizes 48 inch fluorescent lamps as the ultraviolet light source, was later acquired to facilitate accelerated aging in the laboratory.

A wide variety of specialty lamps are available for use in the QUV chamber, which allows the user to select the spectral energy distribution of light inside the chamber which best duplicates the effects of natural outdoor exposure on the particular type of sample being tested. However, the most commonly available lamps have spectral energy distributions heavily weighted in the short wavelength ultraviolet regions, which are inappropriate for aging of organic pigments with strong absorption curves in the visible range of the spectrum, such as the TRAC pigment, which are highly susceptible to excitation by the longer wavelength photons. Unfortunately, lamps with the proper spectral energy distribution required for reproducing the degradational effects of natural sunlight are not widely available. Therefore, most UV stabilization tests were conducted in an unaccelerated manner under natural sunlight in a fixture on the roof of PDA's Santa Ana laboratory facility. Samples were positioned in the fixture facing south at a 34° inclination angle to maximize solar exposure at this latitude, providing a worst case aging environment.

Pigment degradation was typically characterized visually in the benign state by fading of the pigment's color, and the tendency for the original dark grey color to take on a somewhat brownish hue. These effects were quantified by a measured increase in luminous reflectance (fading) and in luminous transmittance (reduced hiding power) in the benign state. Evaluation of the heated state was performed by heating samples on a hot plate to a temperature above the transition temperature (130°C) for 20 to 30 seconds. Most evaluations performed in the heated state were visual, but the high heat capacity of the glass slides allowed measurement of reflectance when desired. Degradative fatigue was also

evidenced upon cooling of the transitioned samples. In many instances the degraded pigment samples transitioned to a clear or milky white color as expected, but upon cooling, turned to a permanent color darker than the original benign state color, and failed to act thermochromically thereafter.

Hindered amine light stabilizers (HALS) fall into a class of light stabilizers known as free radical scavengers. Within this class, those compounds that were oligomeric (low molecular weight polymers) and in liquid form were favored for their compatibility and low migration within the carrier. A broad spectrum of candidate HALS were screened for optimum stabilization performance under accelerated aging conditions with identical samples exposed outdoors for verification. Stabilizers included in the screening tests were AM 806 (Ferro Chemicals), Chimasorb 944 (Ciba Geigy), Tinuvin 144 (Ciba Geigy), Tinuvin 292 (Ciba Geigy), Tinuvin 765 (Ciba Geigy), Tinuvin 123 (Ciba Geigy), Luchem HA-R100 (Penwalt Corp.), Cyasorb UV 2908 (American Cyanamid), Cyasorb UV 3581(American Cyanamid), Cyasorb UV3668 (American Cyanamid), and Cyasorb UV3346 (American Cyanamid). Tinuvin 123, a low basicity, oligomeric HALS supplied in liquid form consistently provided optimum stabilization for the black pigment, as formulated. Stabilizer concentrations in the range of 0.5 to 1.0% concentration were recommended for most applications. Concentrations in the range of 3 to 5% however, were required to stabilize this pigment system.

While the primary objective of this program was to develop a grey (or black) pigment, a preliminary screening of candidate colored pigments was also performed. A very large matrix of samples was subjected to natural sunlight exposure for 77 days for an empirical determination of the optimum HALS for each color, with the understanding that each pigment molecule has different stabilization requirements. The following table includes those HALS that most effectively stabilized the colored pigments.

Table 3-5. Optimum hindered amine stabilizers for colored pigments.

PIGMENT COLOR	OPTIMUM HINDERED AMINE (at 5% concentration)
Blue	Tinuvin 765, AM 806, Tinuvin 123
Red	UV 3581
Yellow	UV 3346
Black (Grey)	Tinuvin 123
Orange	UV 3581, UV 3604, UV 3346, and Tinuvin 144

The optimum UV absorber would theoretically absorb 100% of the energy in the entire ultraviolet spectrum. Initial screening of candidate UVA's included spectral analysis of the wavelength dependant absorption characteristics of each candidate at a concentration of 2.5%. The following table identifies the "absorption waveband", defined here as the wavelength range in which the absorption was measured to be 75% or greater, for each candidate UVA. It should be noted that a slight increase in UVA concentration would result in 100% absorption over the absorption waveband.

Table 3-6. Absorption wavebands for various candidate UV absorbers.

UV ABSORBER	ABSORPTION WAVEBAND (nm.)	MANUFACTURER
UV531	250-380	American Cyanamid
UV2300	280-350	American Cyanamid
AM340	280-350	Ferro Corporation
UV24	275-415	American Cyanamid
CHIM944	200-350	Ciba Geigy
AM300	275-400	Ferro Corporation
AM205	200-440	Ferro Corporation
AM806	275-375	Ferro Corporation
MIXXUM BB50	280-405	Fairmont Chemical
UV5411	275-400	American Cyanamid
UV2126	250-360	American Cyanamid
TIN 328	275-410	Ciba Geigy

The primary objective of this stabilization activity was to determine which of the candidate UVA's worked synergistically with 5% Tinuvin 123, in addition to blocking UV energy over the wavelengths of pigment absorption, 280 to 350 nm. Samples were formulated in a polyethylene based pigment with a 5% concentration of Tinuvin 123 and a 5% concentration of each candidate UV absorber, coated on glass slides, and exposed outdoors in natural sunlight.

This screening test was terminated after 13 days, at which time a rating of relative effectiveness of each candidate, judged according to previously described parameters, could be made. Among the UVA's tested, UV24 and UV531, both benzophenone type UV absorbers, were most effective when used in combination with Tinuvin 123. These were followed in effectiveness by Mixxum BB100 and UV5411, both benzotriazoles, and UV2126, a benzophenone.

A broad spectrum of antioxidants were screened for compatibility and effectiveness in protecting the pigment during thermal processing. Samples of the pigment were prepared and placed in a convection oven at 165°C for six hours and observed for signs of discoloration. Of the nineteen antioxidants tested, the most effective are presented in the table below.

Table 3-7. Most effective antioxidants.

ANTIOXIDANT	CHEMICAL FAMILY	MANUFACTURER
Naugard XL-1	Phenolic/Proprionate	Uniroyal
Irganox 1010	Hindered Phenolic	Ciba Geigy
Irganox 1098	Hindered Phenolic	Ciba Geigy
Irganox 1330	Hindered Phenolic	Ciba Geigy
Cyanox STDP	Thioproprionate	American Cyanamid
Cyanox 425	Hindered Phenolic	American Cyanamid
Cyanox 1790	Hindered Phenolic	American Cyanamid
Toponol CA	Hindered Phenolic	ICI Polymer Additives

These antioxidants were then tested in a matrix which combined them with either 5% Tinuvin 123 + 5% UV24 or 5% Tinuvin 123 + 5% UV 531 to determine the optimum stabilization system. Samples were prepared as in the previous tests and placed outdoors in natural sunlight for 30 days. Benign state color and transition were evaluated at 7, 14, and 30 days.

UV24 and UV531 worked well with Cyanox 1790, Naugard XL-1, or Cyanox 425. In general, benzophenone-type UV absorbers combined with phenolic-type antioxidants seem to be most effective.

The following tests were performed with an alternate carrier material which was waxy in nature, but not polymeric. It was chosen for its high surface tension, which promoted the formation of spherical particles when using the hot atomization process described above. Since this material did not coat a glass slide as easily as the polyethylenes, a film was formed by sandwiching the carrier between two slides. This enhanced the environmental stability of the pigment components

significantly due to the 100% UV absorption between 200 and 300 nm, and sharply decreased oxygen permeation provided by the glass slides. Some indication of the potential effect of the glass cladding can be seen by reviewing the results of the UVA/O_2 barrier test, where one layer of UVA film and O_2 barrier retarded the pigment aging rate by 50% during the first 10 days of outdoor exposure. Therefore, the additional protection afforded by the glass cladding of the sample materials must be considered when evaluating the test results presented in the following section.

Sample materials for this aging test were prepared with a 5% concentration of Tinuvin 123 (HALS). The relative effectiveness of a 5% concentration of each of candidate UVA's and AO's was determined in this study. Samples were evaluated under ambient conditions using the previously described criteria. Heated state properties were evaluated periodically, and testing was discontinued if a sample's heated state developed a cloudy or dark appearance, regardless of its benign state color.

UV 24 and UV531 were again the most effective UVA's. In general, the choice of antioxidant appeared to be less critical, as several of them in combination with Tinuvin 123 and UV24 or UV531 were effective. In addition to good light stability, the combination of UV24 with Irganox 1098, and UV 531 with Topanol CA resulted in the least darkening with cooling after transition at the completion of the test, a measure of the degree of degradation. The solubility of the antioxidants in this carrier was very much lower than the solubility of the HALS (most of them liquid) and the UVA's (which have low melting points), and in most applications could be used only in low concentrations.

The test results, plotted as transmittance through each sample as a function of natural sunlight exposure duration, are illustrated in Figure 3-13. The unstabilized pigment exhibited acceptable performance for the first 169 days, with good heated state properties. The optimized stabilization systems effectively doubled the expected lifetime of the pigment.

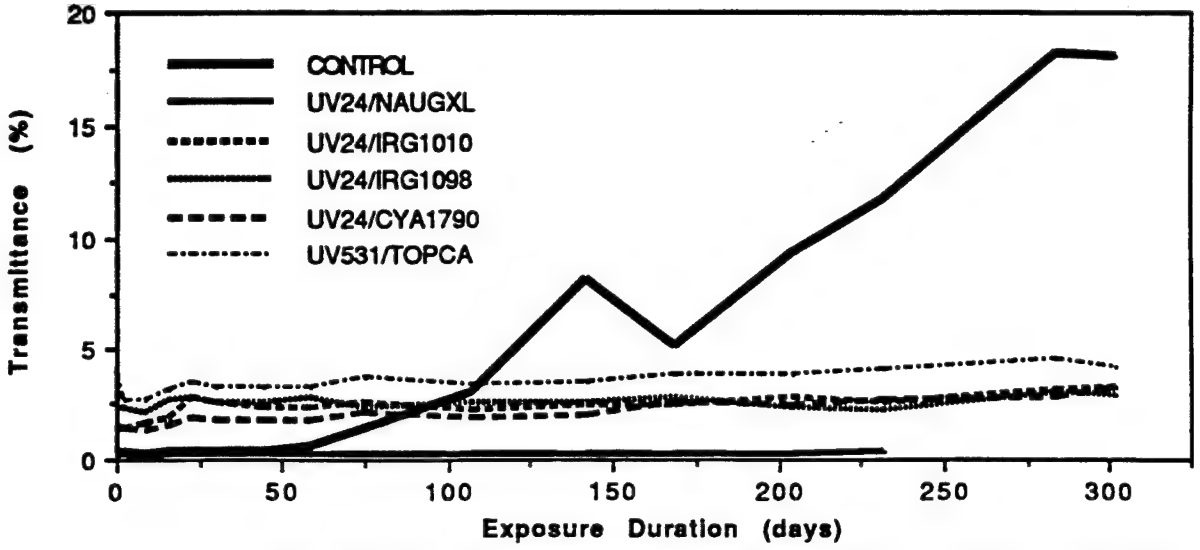

Figure 3-13. Environmental aging response of alternate carrier material.

Due to residual color in the heated state, mixtures of the polyethylene derivative and the alternate carrier were evaluated and showed excellent compatibility in all mixture ratios. A preliminary outdoor aging test of the inherent stability of this thermochromic formulation was performed, again between glass slides. After 80 days, a considerable difference in stability among the different samples was noted. A plot of transmittance versus the percentage of the alternate carrier in the mixture, shown in Figure 3-14, exhibits a nearly linear correlation between stability improvement and increasing concentration of the alternate carrier material. Hot atomization properties and solubility of the pigment components in the carrier also improved, which provided guidance towards optimization of the carrier formulation.

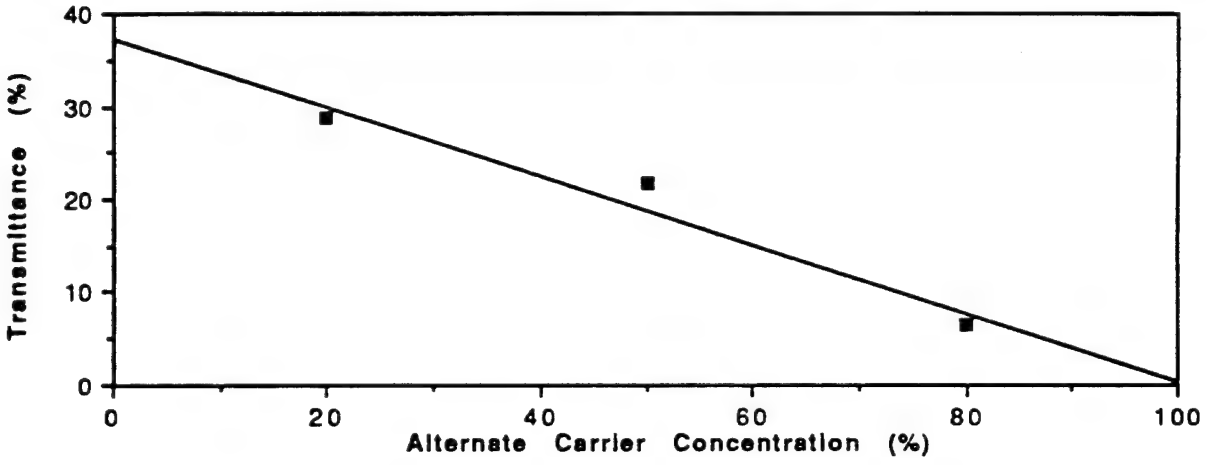

Figure 3-14. Transmittance as a function of alternate carrie concentration.

The next study examined the effect of varying carrier mixture ratios on stabilization. Three different carrier blends were tested: 20% Alternate Carrier/80% Polyethylene (20/80), 50% Alternate Carrier/50% Polyethylene (50/50), and 80% Alternate Carrier/20% Polyethylene (80/20). Samples were placed outdoors under natural sunlight exposure, again between glass slides, for a period of 344 days. Samples were evaluated periodically for transmittance, fading, and the clarity of the heated state at 130°C. Samples were removed from the study when they had deteriorated significantly in any parameter.

The testing of the stabilized 50/50 blends was terminated on day 183, due to cloudiness and browning exhibited in the heated state. Among the set of 20/80 blend samples, the only sample that retained acceptable properties was stabilized with Tinuvin 123, UV 24, and Irganox 1010. The heated state of this sample began to show deterioration at about 183 days of exposure. Most of the 80/20 blends remained in the study until the end. Of these, the samples stabilized with Tinuvin 123, UV 24 and Irganox 1010 or Cyanox 1790 exhibited the least degradation in the heated state, and had good benign state color. Test results from all three carrier blends are plotted in the figures below.

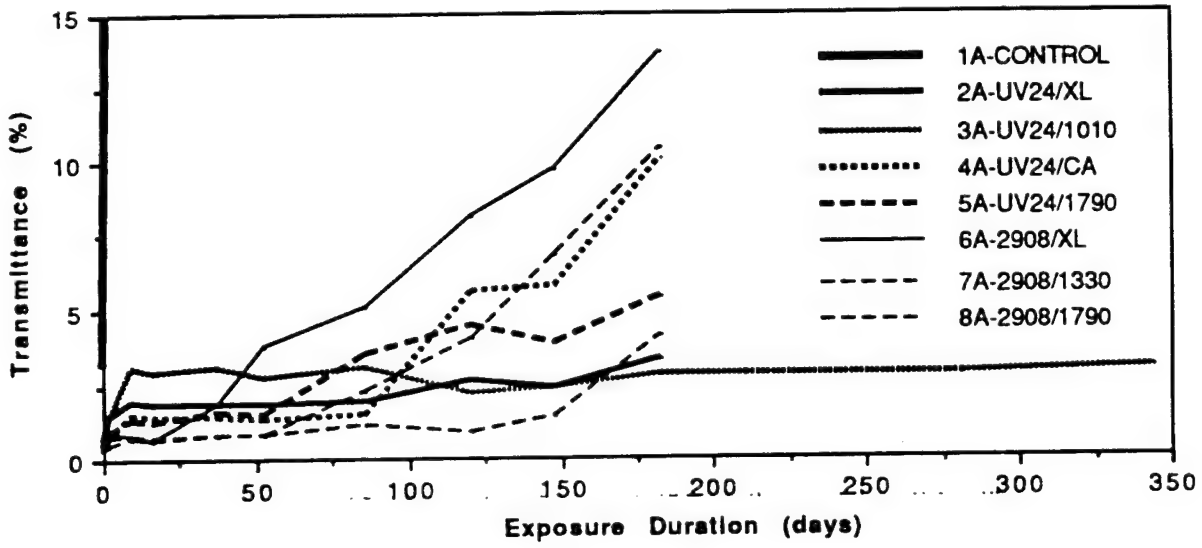

Figure 3-15. Environmental aging response of 20/80 carrier blends.

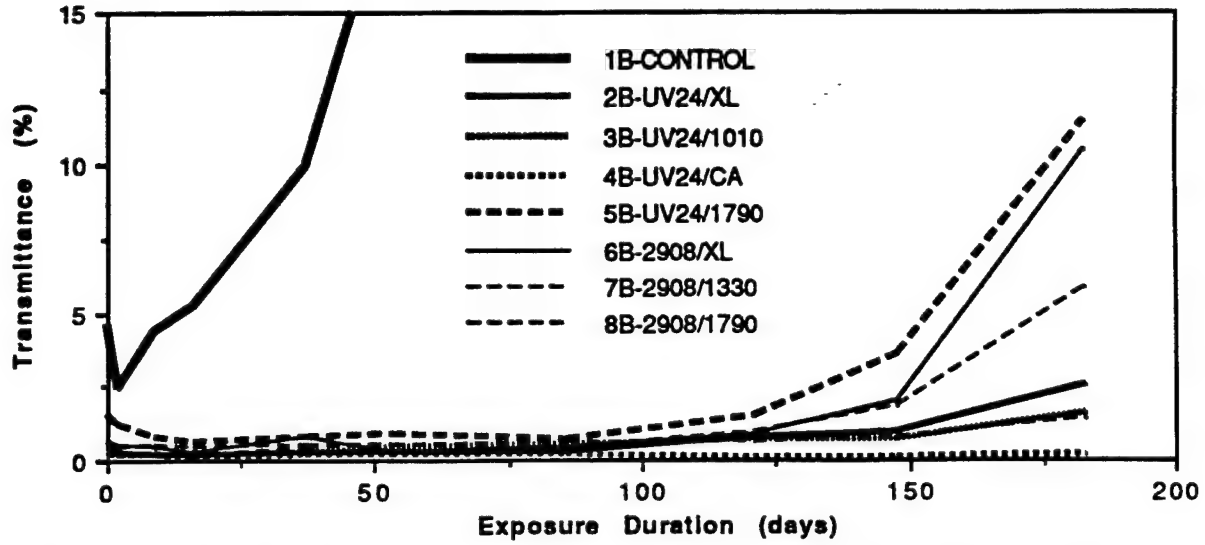

Figure 3-16. Environmental aging response of 50/50 carrier nlends.

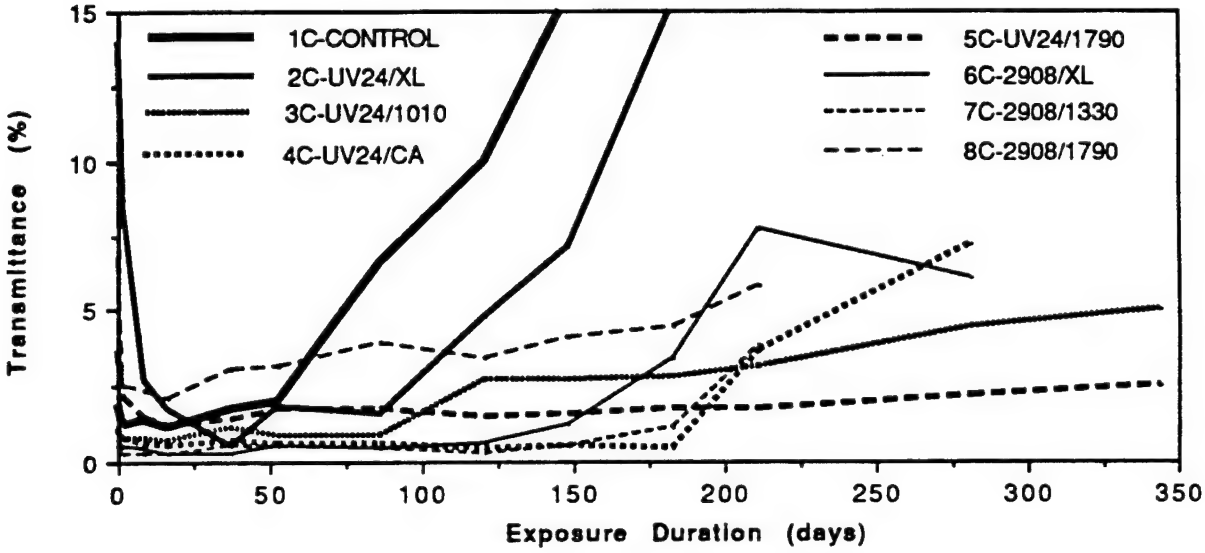

Figure 3-17. Environmental aging response of 80/20 carrier blends.

3.3.1.5 Microencapsulation. Due to the extreme sensitivity of the thermochromic pigment chemistry to the solvent system and polymer components of all candidate paint binders, microencapsulation of the pigment is required for protection of the pigment from these elements of the coating system. The thermochromic pigment functions as an extremely sensitive acid-base reaction between a pH sensitive dye and a weak acid. The change in the dielectric constant of the carrier material as it melts reverses the equilibrium between the dye-activator complex

and the phenolate ion. Likewise, exposure of the color former to an acidic or basic component in the paint binder will also reverse the equilibrium, often permanently. The dye and the activator also tend to be highly soluble in the polar organic solvents most commonly used in paint binders to solubilize the polymer.

The objectives of this task were to identify candidate encapsulation materials with the necessary thermal stability, solvent resistance, and compatibility with candidate binder systems, and to develop a microencapsulation process that is compatible with the TRAC pigment chemistry. These efforts successfully resulted in the development of a dual wall microencapsulation process which retains all of the functional aspects of the unprotected pigment, while providing the required protection for the pigment from the adverse effects of solvents and other potentially incompatible compounds contained in the paint binder.

Identification of the optimum microcapsule wall material was based on diffusion theory in accordance with Fick's Second Law. Accordingly, a capsule material with good barrier properties has some degree of polarity, high chain stiffness, is inert to the permeating species, has close chain packing caused by molecular symmetry, crystallinity, or orientation, some bonding or attraction between chains, and a high glass transition temperature. Critical capsule wall thickness for optimum barrier properties is 10 microns. Below this thickness there are pinholes and microvoids. For multiple layers, the relationship between the wall permeability, P, and the capsule wall thickness, ℓ, is defined mathematically as: $1/P = \ell_1/\ell P_1 + \ell_2/\ell P_2$ where $\ell = \ell_1 + \ell_2$. (Reference 4).

The requirements for solvent resistance of the microencapsulated pigment are dictated by the type of paint binder into which the pigment will be dispersed. The cured topcoat paint film property requirements defined in the TRAC System Specification (Appendix A) are very similar to those of commonly used Mil-Spec aircraft exterior coatings conforming to MIL-C-83286 and MIL-C-85285. Using the information in product literature and Material Safety Data Sheets obtained from vendors of these highly cross-linked polyurethane paint systems, a fairly accurate description of the solvents incorporated into the paint components can be obtained. Typically, these coatings contain aggressive solvents such as methyl ethyl ketone (MEK) and cellosolve acetate in large percentages.

The second consideration in the choice of suitable polymers for microencapsulation of the thermochromic pigment is the set of processing conditions for deposition of the capsule wall material onto the pigment particles (core material). The basic requirement is non-reactivity with the core material. Encapsulation of the thermochromic pigment is a particularly sensitive process due to the inherent incompatibility of the pigment components. The low solubility of the dye and activator in the carrier increases the probability of migration of components into any external medium. Therefore, the microencapsulation medium must have less affinity for the dye and activator than the carrier. Very low pH will solvate the dye, while very high pH will solvate the activator. Polar organic solvents will solvate both the dye and the activator. Non-polar solvents will dissolve the carrier at temperatures in excess of 40°C. It is noteworthy that most polymerization reactions are extremely slow below 40°C unless highly catalyzed, usually at either very high or very low pH, which further illustrates the delicate nature of such a process.

Since the microcapsule wall material is required to protect the pigment, the third criteria is minimal interference with the color of the pigment. Microcapsule walls are typically 2 to 5 microns thick, therefore the passage of light through the wall is likely regardless of polymer choice. Color, however, is highly variable, ranging from white to deep brown.

Careful consideration of these criteria resulted in identification of several encapsulation materials possessing the potential for good solvent resistance and compatibility with the core. These included epoxy, melamine-formaldehyde, phenol-formaldehyde, parylene, and possibly polyurethane. While initially all looked feasible, several were ruled out after cursory examinations. Epoxy microencapsulation is processed as an interfacial polymerization, with the epoxide prepolymer added to the hydrophobic carrier and the amine crosslinker added to the aqueous phase. Several attempts indicated that both the epoxide and the amine interfered with the thermochromic pigment chemistry. For polyurethane it was discovered that the Lewis acid type catalysts used to polymerize the polyurethane over-activated the dye, yielding it non-thermochromic. Phenol-formaldehyde encapsulation resulted in a coating with an opaque red-brown color that completely obscured the thermochromic pigment's color. This left melamine-formaldehyde and parylene as the only remaining viable candidate encapsulants. Parylene appeared to be particularly promising because it is processed by vapor deposition at room temperature from the poly-para-xylylene monomer, a process that would

not interfere with the thermochromic chemistry. However, in practice, coating the thermochromic pigment particles directly resulted in no tangible wall formation, for which the processor had no immediate explanation. Although not verified, one possible explanation is that the poly-para-xylylene monomer was absorbed by the carrier, which possessed similar solubility parameters. Melamine-formaldehyde became, by default, the best candidate material for microencapsulation. This material also has the necessary compatibility with the candidate binder systems and has excellent thermal stability. This choice was reinforced by information from a manufacturer of similar thermochromic pigments stating that this was the capsule wall used by other manufacturers in the industry.

Virtually every known encapsulator in the industry was contacted in our effort to microencapsulate this pigment. While these efforts proved unsuccessful to a large extent, they were valuable in defining critical microencapsulation process parameters. PDA successfully resolved this portion of the processing by developing its own dual wall microencapsulation techniques. The process was then scaled-up to produce sufficient quantities of microencapsulated pigment to support testing requirements, and to verify the feasibility of large-scale production.

The melamine-formaldehyde microencapsulation is processed in an aqueous medium. Partially methylolated melamine-formaldehyde at low molecular weights (average degree of polymerization of 2.5) is soluble in water. The prepolymer, stabilized at pH 8 to prevent premature polymerization, is dissolved in water and catalyzed. The core material is dispersed, completing formulation of the reaction slurry. The melamine-formaldehyde condensation reaction progresses in a step-wise fashion, slowly increasing the molecular weight of the dissolved polymer. The solubility of the polymer in solution decreases until a second phase, oily in nature, begins to form. This hydrophobic phase has great affinity for the non-polar dispersion of thermochromic pigment particles, and micro-droplets begin to wet the suspended pigment particles. The coating of droplets increases until they coalesce to form a continuous coating on the particles. Continued polymerization of the melamine-formaldehyde results in a highly crosslinked polymer wall that is then isolated by filtration. The reaction is defined in Figure 3-18 below as:

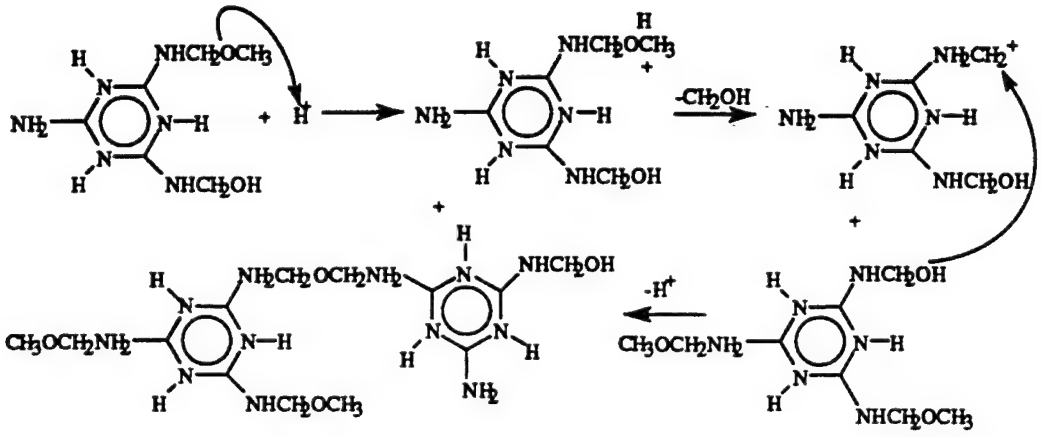

Figure 3-18. Melamine-formaldehyde polymerization reaction.

Success of this process lies in controlling the rate of polymer formation. If the reaction proceeds too quickly, the droplets may harden before coating of the particles can occur. In the industry this is known as nugget formation. Microscopic examination shows pigment particles surrounded by what appears to be snow. Skilled practitioners in the art of microencapsulation endeavor to deposit nuggets on the surface of the particles that are still wet enough to crosslink among themselves. This forms a thick, though more opaque, impervious wall. This is just one aspect of the art of microencapsulation. Many techniques are used to control the rate of reaction and deposition of the polymer onto the pigment particles. Most of the variables examined as potential processing methods are related to this aspect of the microencapsulation. While appearing simple in concept, a large number of variables can be adjusted or added to adapt the process to obtain the desired product. The process variables found to be relevant to microencapsulation of the TRAC pigment are defined in the following paragraphs.

The optimum pH for the TRAC microencapsulation process was dictated by the stability of the pigment chemistry. Experimentation indicated that the ideal pH range was 3.8 to 4.1.

Most melamine-formaldehyde encapsulations are performed in the presence of a suspending agent, used to improve emulsification of a liquid core material. The use of solid pigment particles negated the requirements for emulsification. It was determined that a sodium laural sulfate solution with a concentration of less than 0.5% was effective for promoting dispersion and wetting of the pigment particles.

The cure cycle, in terms of time and temperature, was a critical parameter in obtaining capsule walls with good adhesion and integrity. Patent literature suggested long, high temperature (95°C) cycles for optimum cure and cross-linkage. Experimentation at temperatures within the range of 55°C to 95°C resulted in nugget formation, poor solvent resistance, and low color intensity. In small batches it was found that introducing a holding time of between zero and two hours at room temperature prior to increasing the cure temperature produced acceptable results, but the results from larger batches were inconsistent. It was determined that these cure cycles proceeded too fast to accomplish good wetting of the extremely hydrophobic pigment surface. When the cure temperature was dropped below 55°C, the reaction time to reach 90% cure (45 minutes at 55°C) increased sufficiently to allow for proper wetting and coating of the particles. Thermodynamic theory indicates that reaction times double for every 10°C reduction in the reaction temperature. Three hours was the minimum time required to coat the particles prior to attaining the 90% cure level. The processing ratio of core to total reaction solids determines the ultimate wall thickness of the microcapsules. The optimum range for this parameter was determined to be between 65 and 80%, constrained by low solvent resistance on the high end and darkening of the pigment on the low end.

Evaluation of the solvent resistance properties of the polymerized methylolated melamine-formaldehyde revealed great sensitivity with respect to the catalyst type and concentration. Acetic acid was determined to be highly effective at a pH of 4.0 at the higher cure temperatures. Below 55°C stronger catalysis was required, but without significant alteration of the pH. It was determined that low concentrations (0.5 milliequivalents/10 g. of resin) of the metal salts of ammonia were highly effective in improving the degree of cross-linking in the capsule wall, as evidenced by less than 1% solvent absorption in methyl ethyl ketone, butyl cellosolve acetate, 1-butanol, and mineral spirits after a soak of 6 hours. The combination of these two catalysts accomplished the goals of both stabilizing the pH and promoting complete cure without the necessity of post-curing operations.

Post-activation, an imbibing process which replaces activator lost in the microencapsulation process, involves dispersing the microencapsulated pigment in an aqueous solution of 0.1 to 2% of the activator used in the thermoreactive pigment for one to two hours, preferably at room temperature. This process enhanced the color intensity of the microencapsulated pigment in the benign state, as well as the contrast in the heated state.

U.S. patent #4,957,949 by the Matsui Shikiso Chemical Company, Ltd. outlines the theory behind the use of secondary walls to enhance solvent resistance, which is substantiated by the theory of solvent resistance as presented earlier. The chemical characteristics of the outer wall need to be opposite in polarity to the solvents to be repelled. If the solvents are organic, then a hydrophilic polymer, highly insoluble in organic solvents is appropriate. If the solvents are hydrophilic, then a hydrophobic coating is most resistant. In addition, the coatings should be highly crosslinked and have a high glass transition temperature to reduce chain mobility and, therefore, diffusivity.

The choice of an appropriate secondary wall requires consideration of the method of deposition in addition to the nature of the cured wall. Microencapsulation involves phasing-out the dissolved polymer, inducing precipitation on the particles in the slurry. This can be achieved by altering pH, reacting the polymer with another chemical to promote crosslinking and increasing the molecular weight, through the addition of a non-solvent, or evaporation of the solvent in which the encapsulating polymer is dispersed.

Parylene, the free radical polymerization product of para-xylylene, is a highly solvent resistant coating deposited in the vapor phase at room temperature. The processing method by which it is deposited has excellent compatibility with the thermochromic pigment system in the microencapsulated state. The coating is extremely inert, hydrophobic, and deposition can be controlled to provide a coating with a wall thickness of 4 microns. It has excellent characteristics for a secondary wall on pigments to be used in a water-based binder system, and studies indicate that it has an absorption rate of less than 1% for most organic solvents, making it a promising candidate for use in solvent-based binder systems.

Analysis of the particle size distribution of the dual-wall microencapsulated pigment was performed using a Horiba LA-900 laser diffraction particle size distribution analyzer. The results, shown in Appendix B, indicate that over 78% of the particles fell within a size range of 15 to 50 microns, and that the median size of all particles was 25 microns. This particle size distribution was determined to be sufficient to produce a high quality coating which was suitable for conventional spray application.

The dual-coated pigment is a dark grey color. The pigment, when dispersed in a water-based polyurethane binder, is somewhat darker than the pigment when in powder form by itself. The cured coating exhibits a broadband luminous reflectivity of 6 to 8% in the benign state, which changes to a creamy light grey color with luminous reflectivity of approximately 38% in the heated state. The results of back-side temperature tests of samples of TRAC coated aluminum samples exposed to fluence levels of 36 cal/cm^2 on the PDA Xenon Light Test Bench indicate that the broadband radiant thermal energy reflectance of this pigment dispersed in the binder and coated over a reflective white primer is approximately 67%. The color intensity after transition in the water-based polyurethane binder is approximately 90% of the original value.

As stated earlier, the color intensity of the dual-coated pigment in solvent-based polyurethane binders is excellent under ambient conditions. It transitions at 130°C to a color similar to that seen in the water-based binder. However, the reversion to the original color is less than 25%. Resolution of this problem is unclear at this time. The solvents used to dissolve binder polymers vary in volatility to optimize the flow characteristics of the paint and prevent skinning during the drying cycle. Cellosolve acetate, for instance, has a boiling point of 156°C. The manufacturers state that these high boiling solvents may never completely volatilize, which is considered desirable, as it plasticizes the paint coating, improving flexibility. It is known that the resistance of a polymer matrix to solvent vapors is very much more difficult to achieve than resistance to solvents in the liquid phase and that temperature promotes the diffusion process. The likelihood is high that the solvent vapors plasticize the capsule wall, decreasing its resistance significantly. Studies which include scanning electron microscopy may be a starting point in the analysis of this remaining difficulty.

3.3.2 Binder.

The required properties of the binder material were defined to a large extent by existing specifications for currently used military aircraft coatings. The primary objective of this task was to identify a suitable binder material with these properties and compatibility with the microencapsulated pigment. The cooperation of qualified manufacturers was solicited to facilitate the adaptation of existing binders to the pigment chemistry as well as to assure the potential for scale-up to production levels.

Polyurethane and epoxy binders were the primary candidates for potential binders. The evaluation process included weathering tests, thermal response and backside temperature measurements performed on the PDA Xenon Light Test Bench, and determination of the absorption spectra, before and after thermal exposure to determine bleaching characteristics. From these evaluations, a binder was selected for sub-scale thermal performance evaluations under simulated fireball radiation conditions at the White Sands Solar Facility. The following sections discuss the results of these tests.

Meetings with Mil-Spec paint manufacturers resulted in enthusiastic support of the TRAC program. Commitments had been received from U.S. Paint in St. Louis, Missouri, Crown Metro in Templeton, California, and Deft, Inc. in Irvine, California for technical and materials support. All agreed that the pigment could be added as a third component and mixed just prior to spraying, eliminating the need for excessively long pot lives or 6 month shelf lives in the solvent based components. Deft, Inc. submitted a proposal for complete formulation and evaluation of the final product, and offered the use of test equipment on their premises. Of these, Crown Metro and Deft had the capacity to qualify the final formulation to military specifications.

As refinement of the microencapsulation process neared completion, the sensitivity of the microencapsulated pigment to certain commonly employed solvents became apparent, which dictated the need for custom formulation of the binder material composition At this point, Miles Laboratories Military Coatings Division was contacted for assistance. This division of Miles Laboratories supplies custom tailored polyurethane resins and paint formulations to several major manufacturers of military coatings including Deft, DeSoto, and Crown Metro. In response to our needs, they modified a formulation from their new line of low-volatile organic compound (VOC) polyurethane coatings in order to meet TRAC solvent requirements, with the understanding that compliance with the requirements of MIL-C-85285 was necessary.

3.3.2.1 Compatibility of the Binder with the Microencapsulated Pigment. In the process of evaluating different paint/binder systems in the laboratory, the requirements for compatibility became apparent. The benign state color of the microencapsulated pigment must remain stable upon cure of the paint film. The transition temperature must remain at or above that of the microencapsulated pigment. The heated state color should be at least as light as that of the microencapsulated pigment. The

cured paint/binder system must transition and return to the benign state color upon cooling below the transition temperature.

Many binders, including several non-Mil-Spec qualified materials were screened for compatibility with the microencapsulated pigment. The following binder materials were investigated and disqualified from further consideration for the reasons described. Solvent-based moisture-cured polyurethanes exhibited excellent benign state color upon cure, but the heated state color was dark green. Polyurethane alkyds, which cure by an oxidative process, were extensively investigated because of the known compatibility of their mineral-based solvent system with the thermochromic pigment. The binder, however, turned golden brown upon curing, altering the overall color of the heated state of the paint/binder system. Conventional epoxy systems decolorized the pigment due to the presence of an amine catalyst. Silicone alkyds were evaluated because of their high heat capacity and their mineral spirits based solvent system. However they failed for the same reason as the polyurethane alkyds.

Ultimately, the binder must be Mil-Spec qualifiable, therefore further evaluations focused on the more conventional Mil-Spec aerospace coatings. These included MIL-P-53030 water based clear epoxy primer, and both MIL-C-85285 and MIL-C-83286 solvent based polyurethanes.

Samples were prepared for testing by flow coating 1 by 3-inch glass slides with the candidate paint/binder systems formulated at 50% pigment/total solids ratio. Both melamine-only and melamine/parylene microencapsulated pigments were dispersed in the binders for comparison. Samples were allowed to cure for seven days prior to testing. Coating thicknesses were recorded for tests in which it could affect the results.

The transition temperature remained stable for all polyurethane systems evaluated. The water based MIL-P-53030 epoxy system caused a decrease of 30°C in the transition temperature, sufficient to disqualify it from further consideration. It was however, carried through the bleaching tests described in Section 3.3.2.2.

Tests for pigment/binder compatibility included luminous transmittance ($\%T_{LUM}$) measurements taken in the benign state and reflectance ($\%R_{LUM}$) measurements taken in the heated and benign states. As the transmittance of the coating in the benign state increases, the hiding power of the pigment coating decreases. The percent reflectance in the benign state is a good indicator, without the use of color analyzers, of the darkness of the grey coating. As a point of reference, low gloss grey

coatings with a reflectance of less than 5% generally appear nearly black, those with a reflectance in the range of 5 to 25% appear grey, and coatings with a reflectance above 25% approach white or colorless. The desired characteristics for the coating in the benign state were minimum transmittance (optimum hiding power) with 5 to 10% reflectance (for a dark grey color). The unactivated pigment, which simulates the pigment in its heated state, is approximately 34% reflective and appears to be a very light beige. This is the target value for pigment/binder system in the heated state, when measured without a reflective undercoat.

The values of luminous reflectance and transmittance for the candidate microencapsulated pigment/binder systems of interest, measured at room temperature and in the heated state, are presented in the table below.

Table 3-8. Luminous reflectance and transmittance of candidate microencapsulated pigment/binder systems.

BINDER	PIGMENT COATING	$\%T_{LUM}$ @ r.t.	$\%R_{LUM}$ @r.t.	$\%R_{LUM}$ @ 130°C
MIL-C-85285 Polyurethane	Melamine Formaldehyde/Parylene	4.1	6.6	21.8
MIL-C-85285 Polyurethane	Melamine Formaldehyde	1.9	5.9	19.4
MIL-C-83286 Polyurethane	Melamine Formaldehyde/Parylene	1.0	7.7	20.8
MIL-C-83286 Polyurethane	Melamine Formaldehyde	1.1	5.8	22.4
MIL-P-53030 Epoxy	Melamine Formaldehyde/Parylene	18.1	12.8	36.7
MIL-P-53030 Epoxy	Melamine Formaldehyde	19.5	6.3	30.4
Miles Water-Based Polyurethane	Melamine Formaldehyde/Parylene	0.6	8.6	26.1
Miles Water-Based Polyurethane	Melamine Formaldehyde	3.9	7.1	26.0

The color of the epoxy/pigment binder system improved with increasing dilution of the binder. Epoxies are amine cured and react with the thermochromic pigment, causing some decolorization and a drop in the transition temperature. Epoxies were disqualified as a potential binder system for this reason. All of the polyurethane specimens yielded acceptable results. The water-based polyurethane system had somewhat better heated state color and less bleaching than the solvent-based systems. The bleaching characteristics are discussed in the following section.

3.3.2.2 Bleaching Characteristics. Bleaching of the thermochromic system, resulting in partial permanent loss of color in the benign state which may occur after transition to the uncolored (heated) state, is a result of either thermal or chemical decomposition of the thermochromic pigment. Thermal degradation is caused by decomposition of the dye molecule or activator within the thermochromic pigment. Chemical decomposition, the result of chemical interference with the thermochromic system, may be caused by two different reactions. The first reaction is leaching of dye or activator into the solvent base of the paint binder. The second is reaction of the basic solvent with the acidic activator while in the heated state, often exacerbated by residual high-boiling temperature solvents that remain in the binder long after cure. This form of bleaching varies considerably with the different solvent systems.

Repeated cycling of coating samples performed by heating to 130°C for 30 seconds allowed comparison of the bleaching characteristics related to the different binders. As in the previous tests, both melamine only and melamine/parylene coated capsules were evaluated in the different binders.

The results are shown graphically in Figure 3-19 below. The water-based polyurethane systems interfered the least with the thermochromic system, with the melamine-only (M) coating performing better than the melamine/parylene (M/P) dual coating. The bleaching characteristics of the epoxy/melamine system prepared for this test were excellent, but the reproducibility among samples was poor.

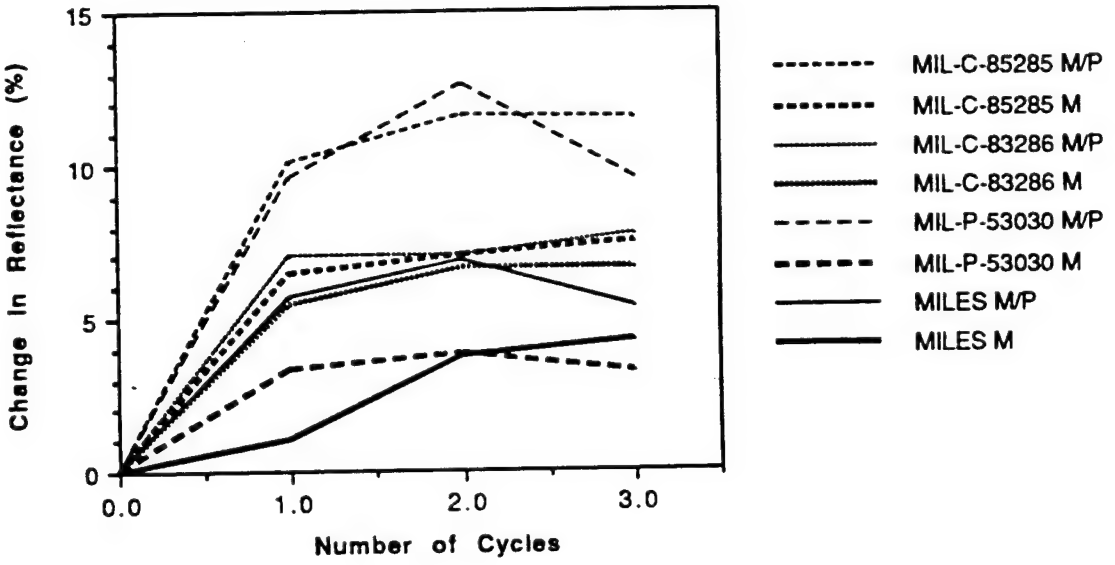

Figure 3-19. Bleaching test binder comparison.

Samples of the completed TRAC cross-section were also tested at the NREL High Flux Solar Furnace for evaluation of bleaching characteristics. The specimens consisted of glass-epoxy clad nomex honeycomb composite material primed with white epoxy primer and topcoated with TRAC pigment dispersed in the Miles water-based polyurethane binder. Specimens were subjected to repeated exposures of a timed, constant-flux thermal pulse of either 5 or 10 cal/cm^2-sec for durations of either 1, 1.5 or 2 seconds.

The data, presented graphically below, indicates that the degree of thermal degradation, as determined by an increase in luminous reflectance, is a function of both the total fluence per cycle to which the sample was exposed, and the number of cycles it endured. When the fluence per cycle was low (less than 7.5 cal/cm^2), the thermal bleaching was minimal beyond the first exposure cycle. As the total fluence approached 10 cal/cm^2, the level of degradation continued to increase with each subsequent exposure. A longer exposure at lower flux levels produced slightly less degradation than a pulse with equivalent fluence at a higher flux level but a shorter duration. It should be noted that the degree of bleaching observed from a 30 second exposure in the laboratory at 130°C was very similar to that seen in samples tested at NREL when subjected to fluences of 10 cal/cm^2.

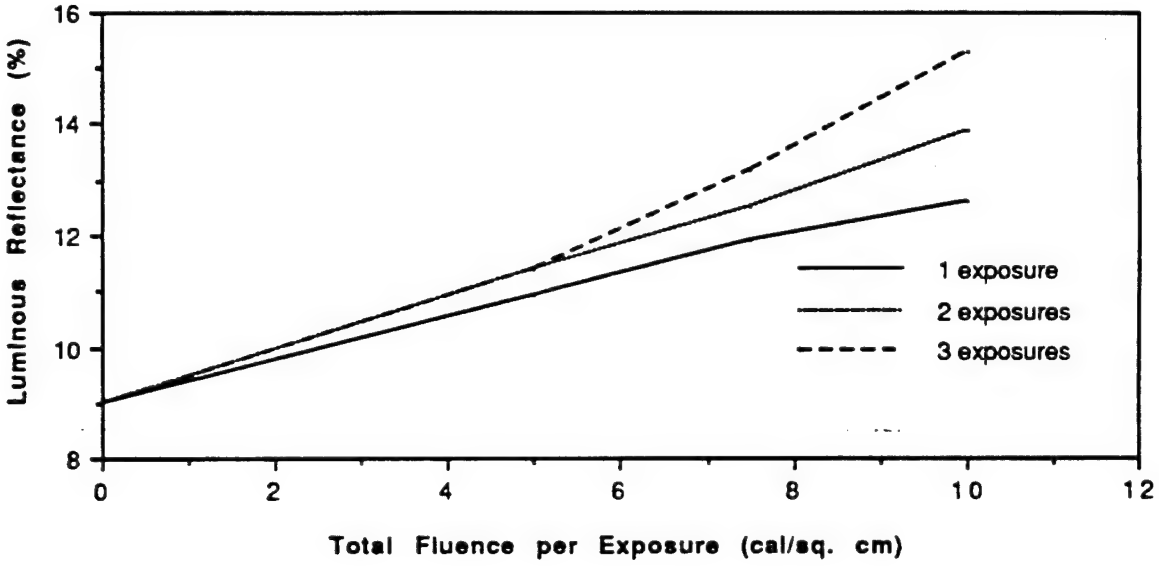

Figure 3-20. Increase in luminous reflectance with fluence per exposure.

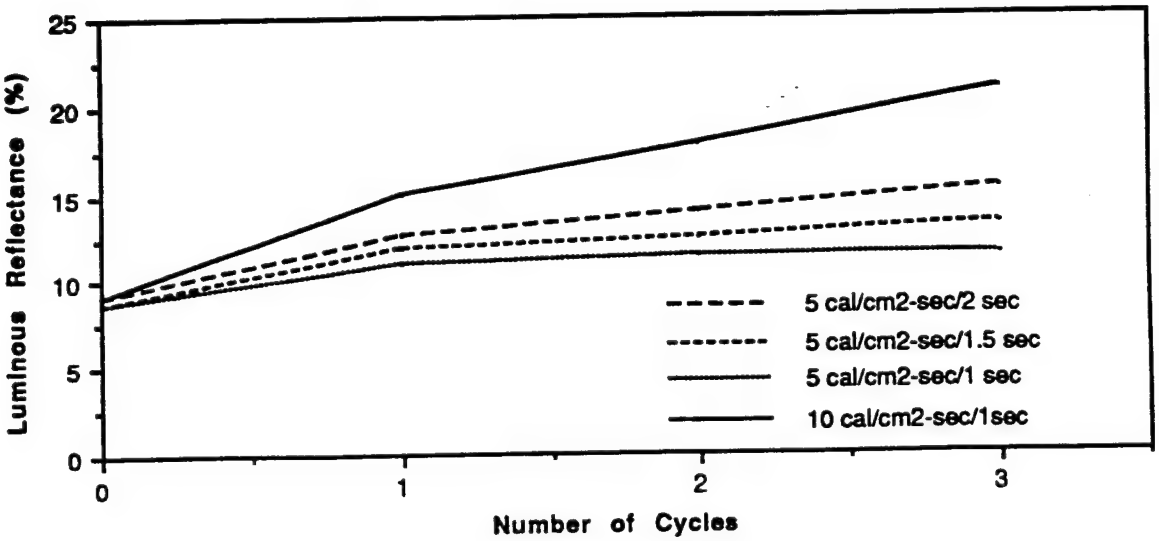

Figure 3-21. Increase in luminous reflectance with number of cycles.

Considerable effort was expended in testing various pigment/binder formulations on the PDA Xenon Light Test Bench (XLTB), which is described later in Section 4.2. This test fixture was configured to subject samples to a flux level of approximately 10 to 12 cal/cm^2-sec focused on a one cm^2 spot, and was used to measure the transmittance of energy through transparent samples.

The XLTB was used to determine the thermal response of various pigment/binder systems coated on clear glass slides to a total thickness of 10 mils. Thermal response was displayed as an increase in the transmittance (ΔT_{XLTB}) of the samples upon transition to the uncolored (heated) state. Measurements made are recorded in Table 3-9 below.

Table 3-9. Transmittance increase of various pigment/binder systems.

BINDER	PIGMENT COATING	ΔT_{XLTB}
MIL-C-85285 Polyurethane	Melamine	30%
MIL-C-83286 Polyurethane	Melamine	23%
MIL-P-53030 Water-Based Epoxy	Melamine	30%
Miles Water-Based Polyurethane	Melamine	19%

The normal cured coating thickness specified in MIL-C-85285 is 1.7 to 2.5 mils, which is only 20% of the coating thickness of the samples tested. Therefore, the transmittance of the final TRAC topcoat, as applied in service is expected to be much higher, although actual transmittance

values were not predicted. This test was performed strictly for comparison of the binders only. It did not take into account other parameters, such as the depressed transition temperature of the pigment in the epoxy binder, which tends to increase its transmittance, or that the water based polyurethane coating was inherently hazier than the solvent based polyurethanes, which also affects its transmittance.

Backside temperature tests give a more straightforward understanding of the thermal response of the complete coating system. Several tests of this type were performed and are discussed in Section 5.3.

3.3.2.3 UV Stabilization of the Binder for Pigment Preservation. Stabilization of the TRAC system was approached conceptually with recognition of the fact that degradation in any one organic component accelerates degradation of all of the other organic components, and that all components are required in their original concentrations for the TRAC pigment to perform properly. Previous sections discussed efforts made to stabilize the pigment. In this section weathering tests of the unstabilized microencapsulated pigment in the binder system are documented, as well as the effects of stabilization of the binder system on the pigment

Qualification of the Miles water-based polyurethane binder system for military use requires meeting the environmental durability requirements of MIL-C-85285. ASTM G53-88 "Standard Practice for Operating Light and Water Exposure Apparatus for Exposure of Nonmetallic Materials" is the most relevant specification related to accelerated weathering of exterior coatings. This specification defines the standard practice for accelerated weathering tests conducted in a fluorescent lamp/condensation exposure apparatus such as the QUV chamber, which is briefly described in Section 3.2 of this report. While this specification calls out the use of UVB 313 lamps as the primary light source, it was determined that the weathering response to both UVB 313 and UVA 340 lamps would provide valuable information. In accordance with MIL-C-85285 which calls for 500 hours of total light exposure time, an exposure cycle of 8 hours UV light exposure at 60°C and 4 hours condensation exposure (without light) at 50°C cycle was used for 31 days. Samples were run in duplicate to accommodate testing of both the benign and heated states, and were removed and inspected weekly in accordance with

ASTM G 53. For comparative purposes, duplicate samples were placed on the roof of the PDA laboratory facility to investigate degradation resulting from natural sunlight exposure.

Samples were prepared by first coating 1 by 3-inch glass slides with MIL-P-53022 white epoxy primer. Sample thermoreactive coatings using unstabilized pigment were then applied over the primer coat. The thermoreactive coatings were formulated in each of two different binder systems, the Miles water-based polyurethane (designated with the prefix "W"), and Deft MIL-C-83286 solvent-based polyurethane (designated with the prefix "S"), both with a 50% pigment to total dry solids ratio. One-third of each set of samples (designated with the suffix "N") was topcoated with the same binder, in unpigmented form, as was used for the thermochromic coating on that sample. Another one-third of the samples (designated with the suffix "T") was topcoated with a 3 mil thick coating of the binder material stabilized with 2.5% UV24, which blocks 100% of the transmission of UV light with wavelengths below 380 nm. The remaining one-third of the samples (without any suffix) was not topcoated. All samples were allowed to cure for 7 days at 23°C prior to testing, in compliance with ASTM G53.

A group of control samples were aged simultaneously, coated over the same white epoxy primer on glass slides, to isolate any anomalies due to the test methods or the base binder systems. These samples included the unpigmented binder material (i.e. the topcoat), both with and without UV24.

Evaluation of the samples, removed in duplicate every 7 days, involved identification of any resulting color change indicative of degradation. Measurements of each sample's luminous reflectance in the benign state were performed Each duplicate sample's reflectance was measured while heated to transition with a heat gun. A second reflectance measurement was made of each transitioned sample upon cooling. All recorded data are presented in Appendix C.

Microscopic analysis of the aged samples at 100 to 200 power magnification showed similar trends for both water and solvent based systems. In general, surface roughness increased with exposure duration, a common characteristic of aged polyurethanes. No cracking was noticed on any of the samples. Voids were apparent at the surface of the samples with no topcoat, however, these same voids were also seen at the pigmented to clear coating interface of the topcoated samples, and may not be an indication of degradation. Degradation of the pigment was severe in those samples which were either not topcoated or were

topcoated without the addition of UV24. It should be noted that the solvent-based polyurethane binder used was a clear polyurethane material which already contained UV stabilizers, so overall it was a more highly protected system than the water-based polyurethane.

The following figures give a visual representation of the aging test results for those samples with stabilized topcoats. Samples coded "SRT", "SAT", and "SBT" represent test specimens with TRAC pigment dispersed in solvent-based polyurethane; samples coded "WRT", "WAT", "WBT" represent water-based polyurethane samples. The second letter in the sample designations, "R", "A", or "B" defines whether sample was aged on the roof, under UVA 340 lamps, or under UVB 313 lamps respectively.

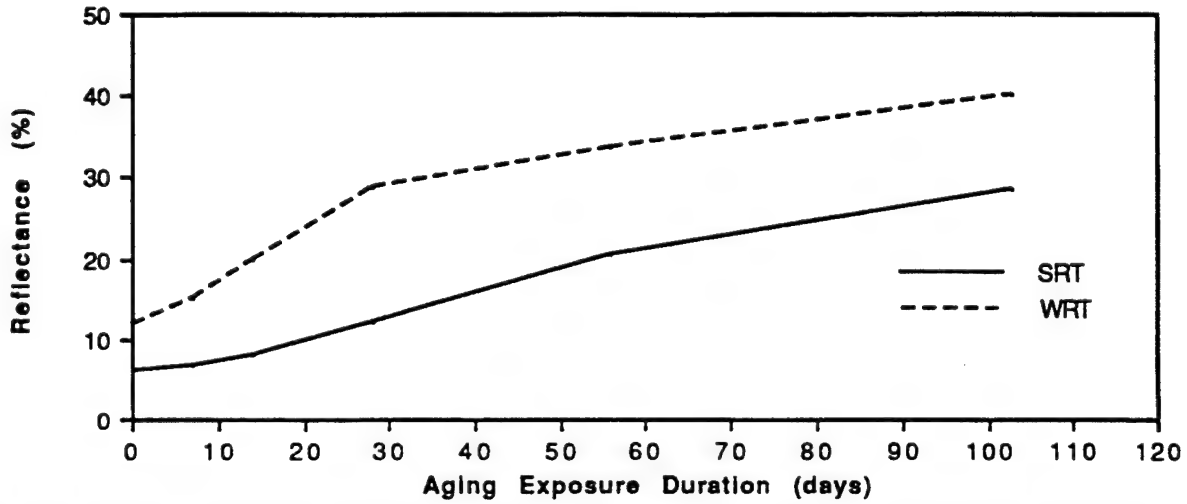

Figure 3-22. Sunlight aging of TRAC system with UV stabilized topcoat.

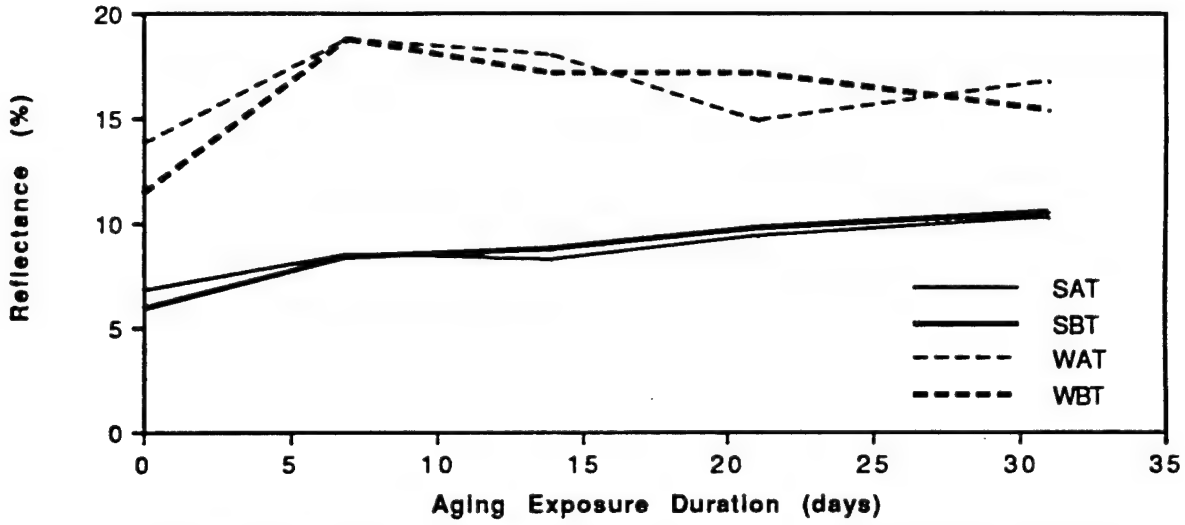

Figure 3-23. QUV aging of TRAC system with UV stabilized topcoat.

All TRAC samples not topcoated with a UV24 stabilized coating turned brown within the first seven days regardless of aging method or binder. Specimens with topcoats containing UV24 faded gradually from black to dark grey to an olive grey color. Their degree of color change from the benign to the heated state decreased to a third of its original value within the first seven days, and then remained constant thereafter. As compared to the solvent-based binder system, the rate and degree of degradation was accelerated slightly in the water-based polyurethane binder system, probably due to the absence of additional stabilizers (Hindered-amine type free radical scavengers) in the binder system. Natural sunlight exposure (rooftop) samples exhibited degradation at a rate greatly accelerated as compared to that of samples aged in the QUV chamber, both with UVA 340 and UVB 313 lamps.

Contrary to the phenomena observed in the raw pigment (described in Section 3.3.1.4.1.1), these weathered samples did not darken additionally after transition. Browning of the pigment is generally attributed to a breakdown in the molecular structure into molecules with decreased conjugation. It is appropriate to assume that these degraded molecules, lacking the molecular structure necessary for thermochromism, would no longer transition to the colorless state. However, because they lacked significant color, degradation did not appreciably decrease their luminous reflectance of the heated state. The delta, or difference in reflectance values between the benign and heated states therefore decreased by an amount equivalent to the loss of color in the benign state. This model seems to hold for the water-based TRAC system and the solvent-based system with no topcoat. In the topcoated solvent-based system, however, the heated state reflectance seemed to increase in proportion to the increase in reflectance in the benign state.

The overall stability of the TRAC pigment in the paint binder is very much lower than that observed in the unstabilized raw pigment. After 103 days on the roof, the raw pigment sandwiched between glass slides had increased in reflectance only 5%. Samples of the TRAC system in the paint binder exposed on the roof increased in luminous reflectance by 20 to 40%. The point of significance in this observation is that while the glass slides do not block out any of the UV light, they do inhibit oxygen migration through the pigment.

In this test, the microencapsulated pigment was dispersed in a binder with 3% of the candidate UVA or HALS based on the total weight of solids in the dry film. The samples were made in quadruplicate, each with variations in the topcoat, with each layer stabilized with the same compound. Samples were either: 1) not topcoated, 2) coated with one coat of unstabilized topcoat, 3) coated with one layer of stabilized topcoat, or 4) coated with two layers of stabilized topcoat. All samples were aged outdoors under natural sunlight (on the roof) for 26 days. The relative effectiveness of the different stabilizers and stabilizing cross-sections was then evaluated.

Chimasorb 944, a hindered amine light stabilizer (HALS), AM 806, an oligomeric HALS, UV 24, a benzophenone type U.V. light absorber (UVA), and AM 205, an organo-nickel compound, were most effective under these conditions. AM 205, possessing an absorption peak from 200-440 nm., had a green tint and was, therefore, less acceptable. As expected, in all cases the samples in which the UV stabilizer was in the binder and both topcoats degraded most slowly.

Considerable work remains to be done in the area of UV stabilization. Thin films of the bulk (unencapsulated) pigment stabilized with Tinuvin 123, UV24, and Cyanox 1790 maintained luminous reflectance values of less than 5% at the conclusion of 344 days of outdoor natural sunlight exposure. To date, this stabilized pigment has not been microencapsulated and dispersed in a binder system for evaluation. This is an obvious next step in the stabilization process. One preliminary experiment was performed to determine an approach to stabilization of the binder and topcoats, but no quantification of the effects has yet been made. Additionally, there remain many more stabilization approaches for application to the topcoat and binder that have not been investigated and new, more effective materials are currently in development. This work should be of primary consideration for future efforts.

3.3.3 Reflective Undercoat.

The thermal reflectivity of the TRAC system is affected to a large extent by the characteristics of the primer coat applied beneath the thermoreactive coating layer. An effective undercoat must be reflective

well into the near infrared, preferably out to 2000 nm wavelength. Its gloss characteristics are unimportant due its position in the coating stack-up, but compatibility with an epoxy or polyurethane binder coat dictated epoxy or polyurethane based coatings as the primary candidate materials.

A wide variety of off-the-shelf candidate undercoat materials were screened in the laboratory for high luminous reflectance. Spectral reflectance measurements were taken on some materials. Samples were then evaluated at the White Sands Solar Facility under thermal flux conditions to determine both broadband reflectance and thermal hardness. From the results of these tests, described in Section 5.2, a white epoxy primer conforming to MIL-P-53022 was selected as the baseline reflective undercoat for subscale testing of the TRAC system on composite materials subjected to simultaneous thermal and mechanical loading, described in Section 5.4.

A more optimized undercoat with broadband reflective properties closer to those of bare polished aluminum would, to some degree, enhance the overall TRAC system effectiveness, but could not be found in a useable form which also had acceptable properties as a bond coat between the TRAC pigmented topcoat and aluminum or composite substrates. The development of such a coating would involve significant additional effort and was determined to be outside of the current scope of this project.

3.4 SUMMARY.

The results of the coating development task were used to select the optimum cross-section for the TRAC coating. Candidate systems, selected for color and spectral characteristics, thermal performance, environmental stability, and component compatibility were prepared for laboratory-scale testing. Samples were subjected to testing on the PDA XLTB and at the WSSF to establish the functionality of the total TRAC system. Specific tests were performed to compare candidate systems with conventional coatings by measuring the back-face temperatures of differently coated substrates. Color, bleaching characteristics, and thermal stability were determined for each test sample.

Upon compilation of all laboratory test data, selection of the optimum binder and the reflective undercoat were made. Quantities of all necessary components were acquired or produced in sufficient quantities to support sub-scale evaluation of coated composite beams subjected to simultaneous thermal and mechanical loading performed at the National Renewable Energy Laboratory (NREL) high flux solar furnace.

SECTION 4
DESCRIPTION OF TEST FACILITIES

4.1 INTRODUCTION.

This section provides general descriptions of the primary facilities and equipment used to support development of the TRAC system. The thermoreactive paint development program consisted principally of laboratory research and development activities, thermal effects testing, environmental durability testing, and limited-quantity TRAC material production.

The PDA laboratory and light manufacturing facility includes a chemistry laboratory, a precision machine shop, the Passive Thermal Protective System (PTPS) production facility, an instrumentation and measurements laboratory, a static testing area, and quality assurance and inspection facilities. Incorporated within these facilities is a large variety of laboratory equipment for chemical processing, as well as facilities for evaluating material response to simulated nuclear thermal flash, spectral analysis of coatings and transparencies, evaluation of accelerated weathering, and measurement of the optical quality of transparencies.

The White Sands Solar Facility (WSSF) at White Sands Missile Range, New Mexico, was used for testing of the thermal response of candidate TRAC pigment formulations, evaluation of the broadband reflectance of candidate undercoats, and spectral analysis of TRAC pigments.

The National Renewable Energy Laboratory (NREL) High Flux Solar Furnace was utilized as an alternate to the WSSF for TRAC system effectiveness evaluations. PDA Engineering, under DNA sponsorship, upgraded this test facility to provide simulated nuclear weapons effects testing capabilities. This was accomplished through the installation of specialized equipment designed and built by PDA.

4.2 PDA LABORATORY AND EQUIPMENT.

PDA maintains a large variety of laboratory equipment and facilities for processing and evaluating optical materials and components, specialized paints and pigments, and aircraft composite materials. Laboratory efforts in support of the TRAC program focused on the chemical formulation and processing of the pigment components, evaluation of the chemical compatibility of the TRAC system components, thermal and spectral response of the thermochromic system,

transmittance and reflectance measurements of coated specimens, and the environmental aging characteristics of the TRAC components.

Spectral transmittance and absorbance data was acquired using PDA's Beckman Acta MIV dual beam spectrophotometer. This instrument measures absorbance and transmittance as a function of wavelength from 200 to 2000 nanometers on samples up to six inches square. This system was used for evaluation of the spectral characteristics of various dyes and pigment formulations. It was also helpful in analyzing the results of pigment aging tests.

Luminous transmittance and reflectance measurements were obtained using a Pacific Scientific XL-211 hazemeter. This device utilizes a Gardner hazemeter design with an integrating sphere and a modified silicon photodetector which closely models the spectral sensitivity of the human eye. This device was utilized primarily for comparative purposes, evaluating the effects of chemical formulation and process variations, thermal exposure, and aging on TRAC pigments, and on the complete coating system.

Spectral reflectance data was acquired using an Oriel InstaSpec III diode array detector system equipped with an integrating sphere. The system was linked to a 386-DX33 computer for system control, data collection, and analysis. Reflectance values were recorded as a function of wavelength from 390 to 1030 nanometers. The system components and their layout are shown diagrammatically in Figure 4-1 below.

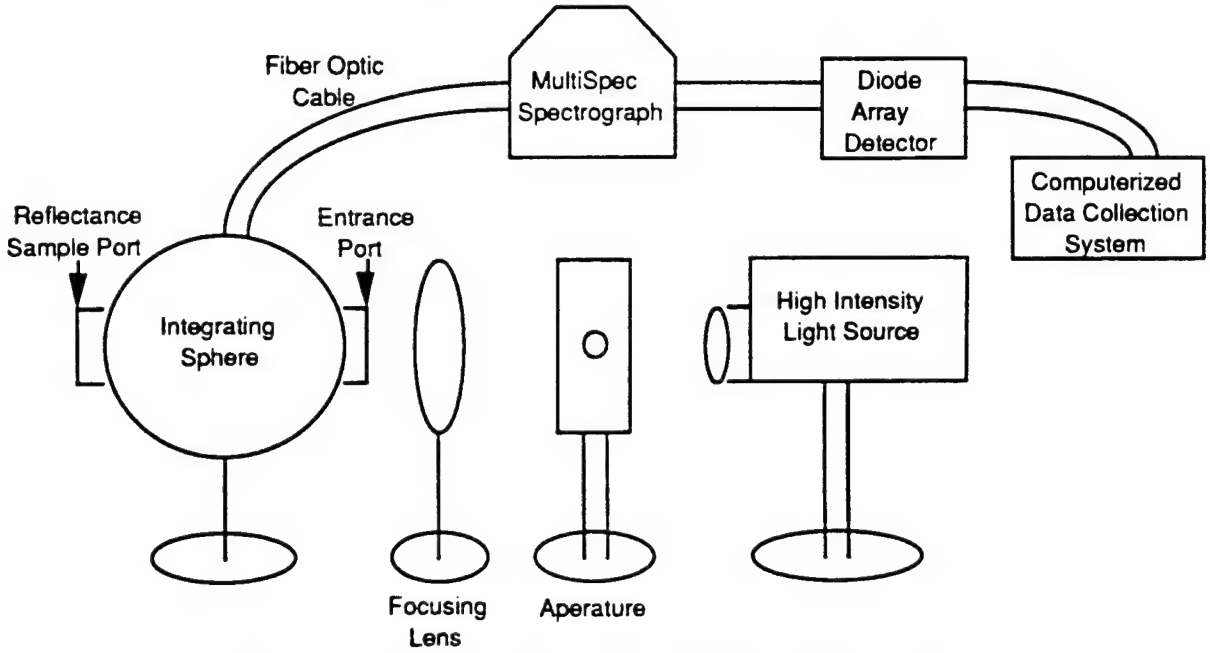

Figure 4-1. Spectral reflectance test setup.

An Olympus BH-2 microscope with a PM-10AK automatic exposure photomicrograph attachment was used for visual evaluation of polymer compatibility, the response of microencapsulated pigments to solvent exposure, the effects of aging on TRAC coating samples, pigment particle size measurements, and general inspection of coating coverage and quality characteristics.

The PDA laboratory also includes a xenon arc lamp test facility, shown in Figure 4-2, known as the Xenon Light Test Bench (XLTB), which is used for screening tests where simulation of the nuclear fireball thermal radiation environment is required. The XLTB focuses the output of a high pressure, air-cooled, 1000 Watt xenon lamp onto a photodetector. The light path includes a convergent lens and mechanical iris shutter between the lamp and the photodetector. The test sample is placed downbeam of the shutter and just forward of the photodetector at the instrument's focal plane. A Nicolet 2090 digital storage oscilloscope is used to record photodiode output as a function of time.

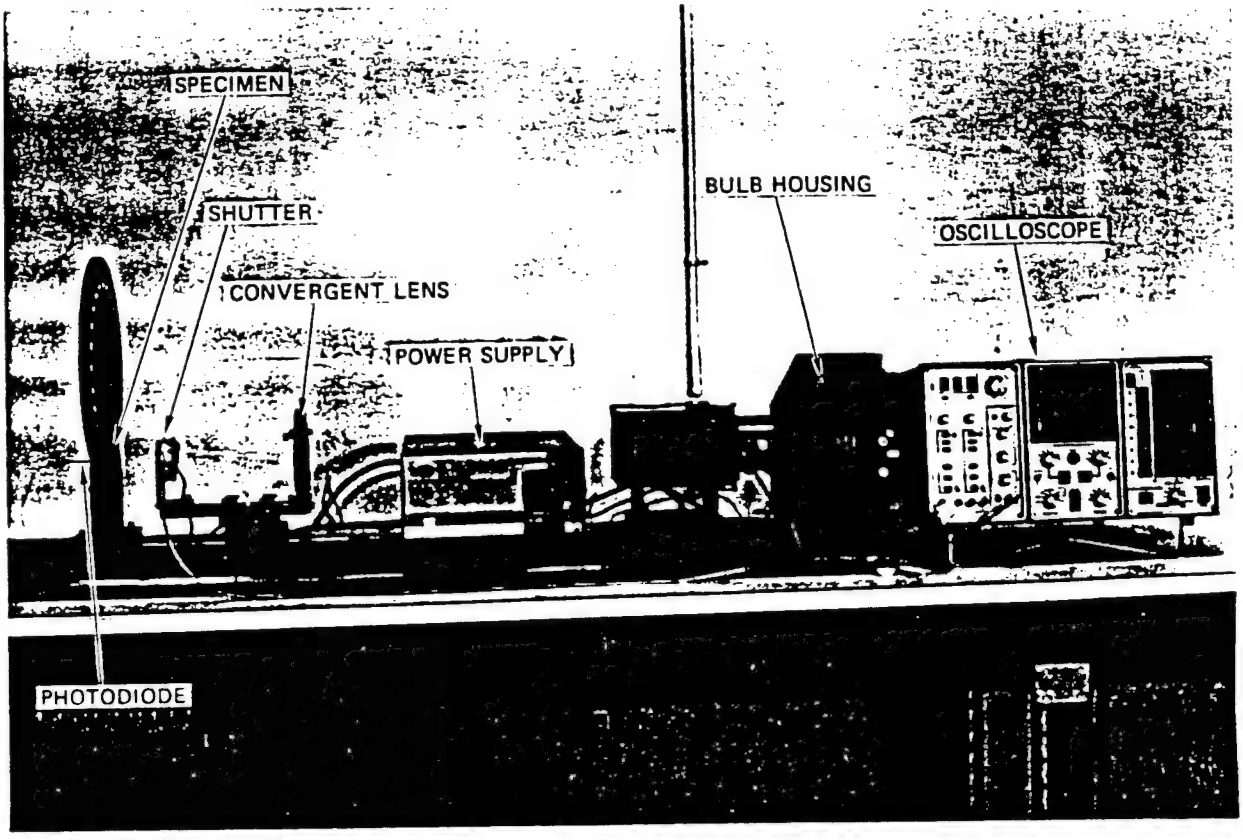

Figure 4-2. Xenon light test bench facility layout.

Output of the photodetector with a test sample in place was compared to reference calibration pulses taken with no sample in the beam. The ratio of transmitted fluence (area under the detector output versus time curve) to the calibration fluence is referred to as $\%T_{xe}$, the transmittance of light from the xenon source through the sample. Figure 4-3 shows an example of the $\%T_{xe}$ response of a thermochromic film as an increase in transmitted light as a function of exposure time.

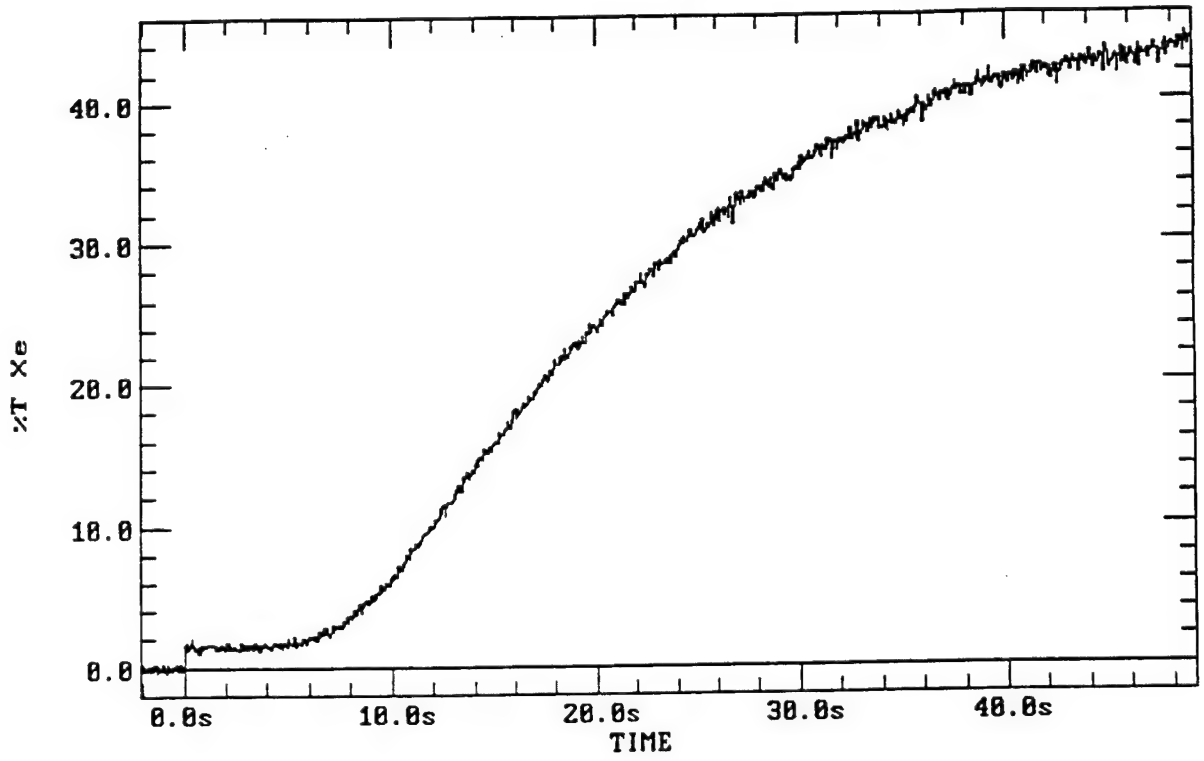

Figure 4-3. Thermochromic film response measured on the xenon light test bench.

Originally designed by PDA for the evaluation of photochromic transparencies for thermal flash protection, this apparatus was adapted for the measurement of the backface temperature of coated aluminum and composite specimens. The specimens, held in a teflon sleeve for insulation from conductive heat loss (shown in Figure 4-4), were exposed to a maximum flux of 15 cal/cm^2-sec on the front, coated side. An Omega model 88102 thermocouple junction surface temperature probe was placed in contact with the back, uncoated side of the specimen to measure the specimen's backside surface temperature response. The probe's output was fed into an Omega OMNI-AMP II B which has a built-in ice point and amplified the signal for the Nicolet digital storage oscilloscope to record. This technique provided important data for evaluation of the effectiveness of various coating systems on aluminum and composite substrates.

Instantaneous backside temperatures were compared for the purpose of evaluating the relative thermal protective value of each coating. Backside temperature response data generated on the XLTB for a representative group of aircraft coatings on an aluminum and a composite substrate are shown in Section 5.3.

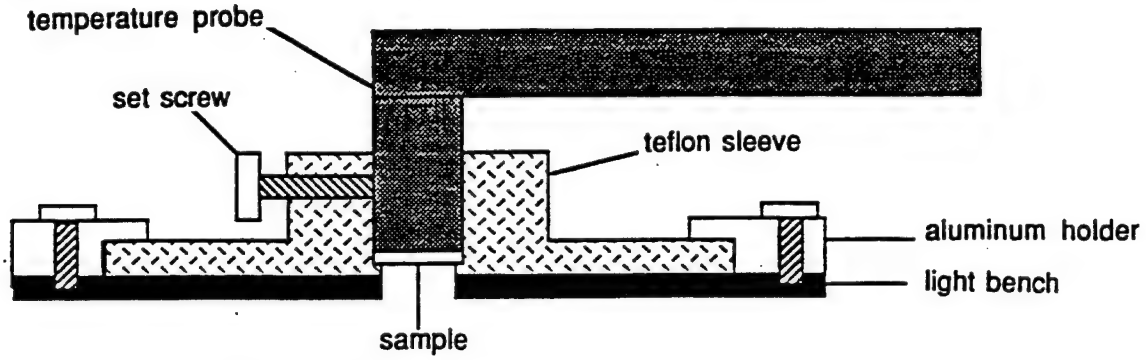

Figure 4-4. Teflon sleeve sample holder.

Accelerated aging tests are an important screening test for all organic and polymeric systems destined for use in an outdoor environment. Two types of accelerated aging equipment have been utilized during the TRAC development program. Initial aging tests were performed in a Sunlighter Model 50 ultraviolet aging chamber, manufactured by Test Lab Apparatus Company of Milford, New Hampshire. This device uses a General Electric RS-4 bulb to age specimens at a rate approximately 50 times faster than natural sunlight exposure. A QUV accelerated weathering chamber, manufactured by Q-Panel Company of Cleveland, Ohio, was later acquired to facilitate accelerated aging with programmable control of hours of exposure to light and dark, temperature, and humidity cycles.

The QUV accelerated weathering chamber employs 48 inch fluorescent lamps as the ultraviolet light source. This feature allows the user to choose from a wide variety of specialty lamps to obtain the spectral energy distribution of light inside the chamber which best duplicates the effects of natural outdoor exposure on the particular type of sample being tested. Most lamps utilized for the purposes of accelerated aging have spectral energy distributions heavily weighted in the short wavelength ultraviolet regions, designated as UVA and UVB. The high energy photons produced in this range typically cause bond scission in organic systems leading to rapid degradation. However, organic pigments with strong absorption curves in the visible range of the spectrum, such as the TRAC pigment, are highly susceptible to excitation by the longer wavelength photons. This results in an excited state that is highly reactive with the most common deteriorating agents: moisture, oxygen, atmospheric pollutants, and other chemical components in the coating

system, causing the types of degradation which are normally observed as the result of long term natural outdoor exposure. PDA identified a prototype lamp manufactured by Sylvania called "Sunblend" which was unique for its high output in the visible and long ultraviolet wavelengths as compared to the more commonly used UVA and UVB lamps. However, due to the extremely limited availability of these lamps, they were used only in the earlier stages of evaluation of the aging characteristics of the TRAC system. UVA-340 lamps, best known for their simulation of the sun's terrestrial spectral energy distribution, and UVB-313 lamps, the most commonly used lamps for testing of exterior coatings, were substituted in the final TRAC aging tests for correlation with the widely recognized ASTM G53-88 weathering test method. A comparison of the spectral energy distributions of the different fluorescent lamps compared to natural sunlight is shown in Figure 4-5 below.

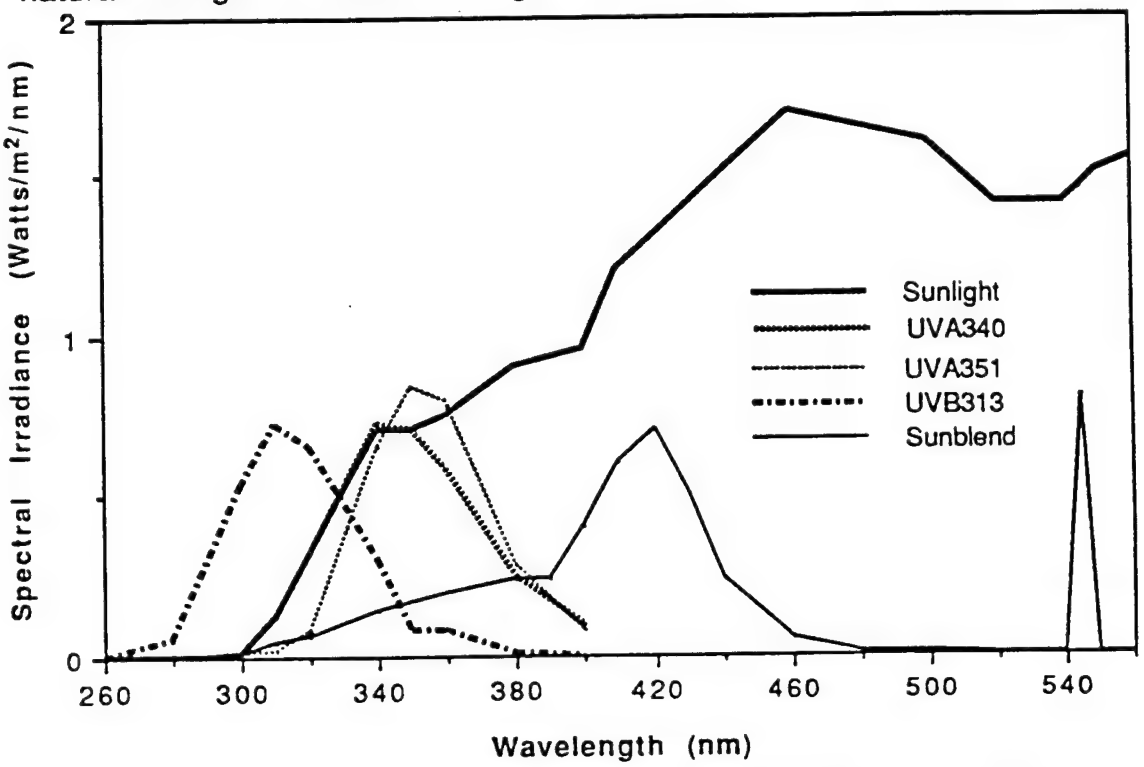

Figure 4-5. Spectral energy distributions of fluorescent lamps compared to sunlight.

The PDA laboratory facility in Santa Ana, California is equipped with a roof mounted fixture for exposing test samples to the natural outdoor aging environment, providing benchmark data for comparison with accelerated aging test results. Samples were positioned facing south at a 34° inclination angle to maximize solar exposure at this latitude, providing a worst case aging environment.

4.3 WHITE SANDS SOLAR FACILITY DESCRIPTION.

The surface of the sun radiates energy at essentially the same blackbody temperature as an atmospheric nuclear fireball (approximately 6000°K), as shown in Figure 4-6. This fact makes a concentrated solar energy facility such as the White Sands Solar Facility ideal for investigation of nuclear thermal effects. Because the TRAC coatings and thermochromic pigments absorb or reflect light as a function of wavelength, it is crucial that testing be conducted with the proper spectral content.

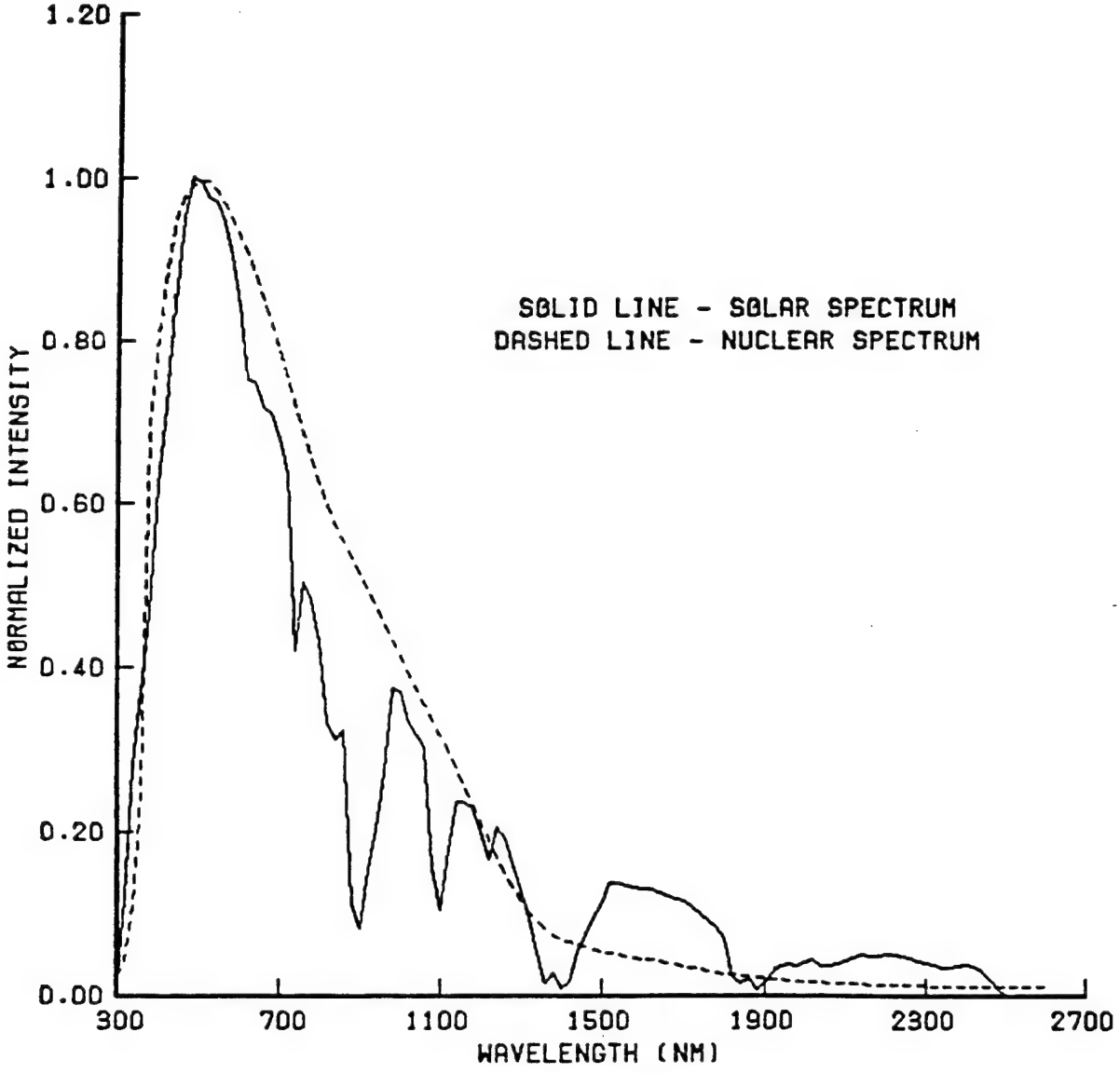

Figure 4-6. Comparison of solar and nuclear spectra.

The WSSF, described in Reference 5, was developed by the U.S. Army specifically for nuclear thermal effects testing. The facility, shown in Figure 4-7, consists of a tracking heliostat, attenuator, focused spherical concentrator, and a test and control chamber. A beam approximately five inches in diameter is produced at the focal plane. High speed shutters and pulse-shaping apparatus provide the capability of producing a rectangular (constant flux) pulse or a time varying (nuclear) shaped pulse. Flux levels up to 80 cal/cm^2-sec are obtainable, depending on atmospheric conditions.

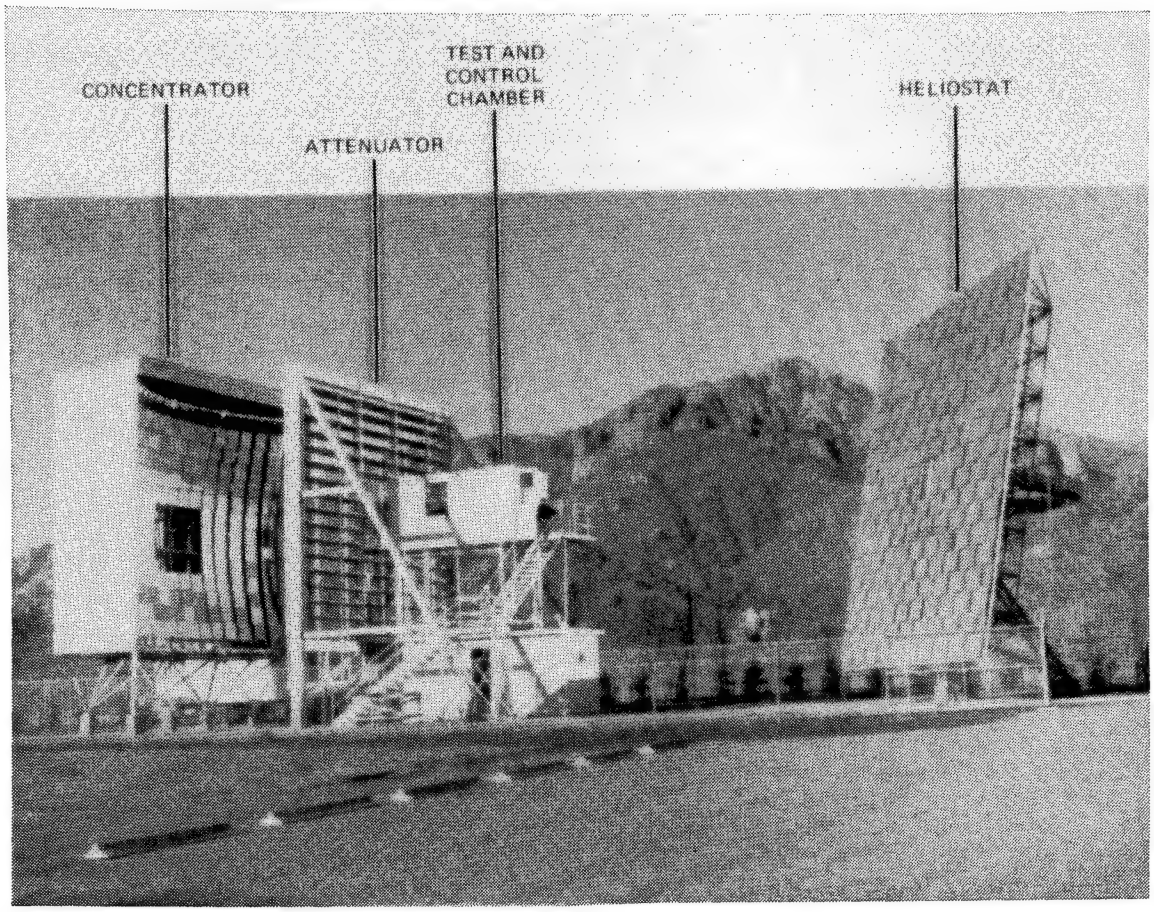

Figure 4-7. White sands solar facility.

The heliostat consists of 356 flat, front-surface coated mirrors positioned in a 36 x 40-foot array. The heliostat automatically tracks the sun, maintaining the axis of the concentrated solar energy beam in a fixed position during the course of experimentation. The position of the focal plane is fixed in the test chamber by the concentrator design and spherical curvature of the individual concentrator mirrors.

The attenuator, which is located between the heliostat and the concentrator, is used to adjust the flux level at the focal plane by partially blocking the passage of light from the heliostat to the concentrator. This is accomplished by mechanically moveable metal louvers mounted horizontally in a vertical plane. The attenuator is operator controlled and is adjusted to attain the desired incident flux level at the test position.

The test and control chamber is 8 x 8 feet in cross-section and 16 feet in length. The chamber contains the shutters and pulse-shaping apparatus, an XYZ table for positioning test hardware at the focal plane, calibration heat flux gages, data collection systems, facility control systems, and related safety equipment. An interior view of the chamber looking upbeam toward the focal plane is shown in Figure 4-8. The figure shows the shutter, oscilloscopes used for data collection, facility control panels, and an aircraft windshield in the sample test position.

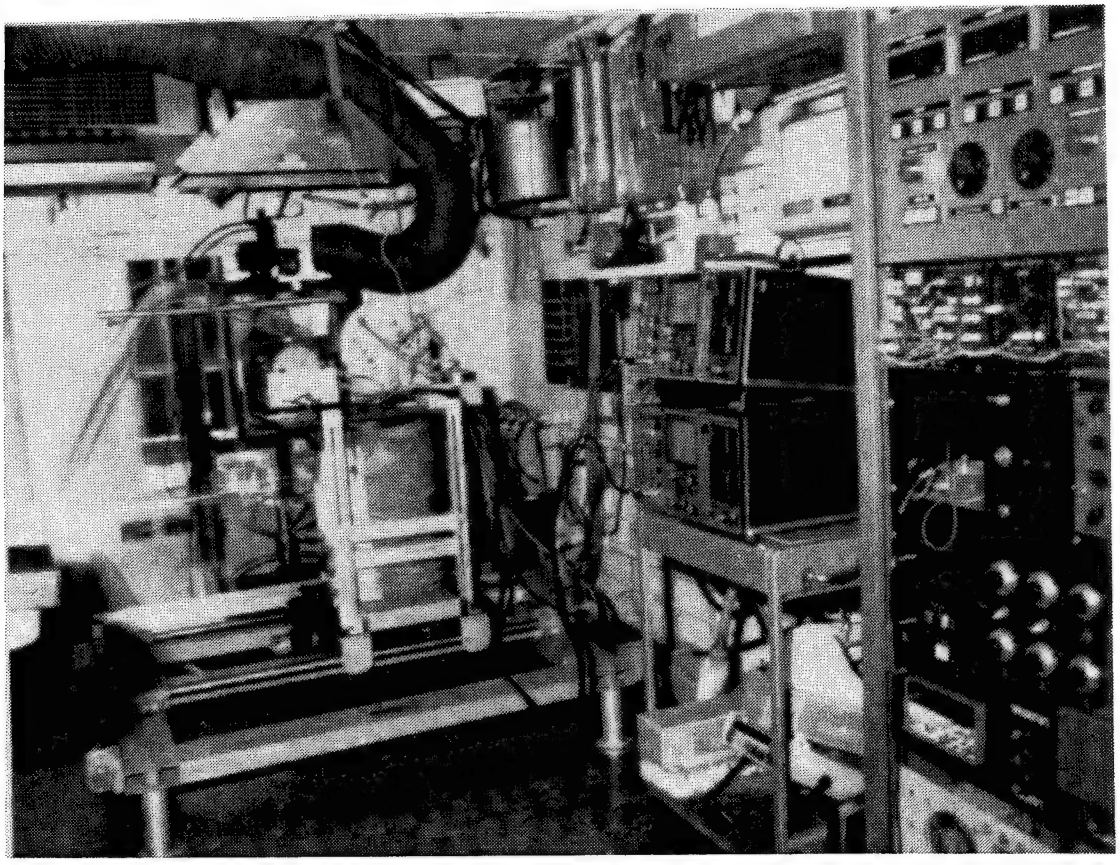

Figure 4-8. White Sands solar furnace test chamber interior.

The test procedure employed at the WSSF for evaluation of the thermal performance of TRAC pigment formulations involved adjustment of the incident flux to the desired level and verification of shutter timing with a blackbody heat flux gage (thin foil type calorimeter). Four second duration rectangular (constant flux) pulses were used for most tests. A "calibration exposure" was then performed and recorded without a sample in the test position. The solar constant (indicating the intensity of sunlight reaching the earth's surface) and wind velocity at that time were noted. Samples were then inserted into the test position and exposed to an identical pulse immediately after calibration. Solar constant and wind velocity were again noted to verify that no significant changes occurred since the calibration data were taken. Wind velocity is important in that it may affect heliostat positioning, resulting in displacement of the beam relative to the facility axis. Energy transmitted through each sample was measured continuously during the pulse and recorded on the facility's computer or on a Nicolet 2090 digital storage oscilloscope. Thermal energy transmittance was calculated by dividing the total transmitted fluence by the total calibration fluence.

4.4 NREL HIGH FLUX SOLAR FURNACE.

The High Flux Solar Furnace at the National Renewable Energy Laboratory (NREL), described in Reference 6, is located in Golden Colorado and began operation in December 1989. This facility offers testing capabilities similar to those of the WSSF, but this system is not an aligned axis system like that of the White Sands Solar Facility. The NREL solar furnace heliostat redirects solar radiation onto a stationary primary concentrator with a long focal length-to-diameter ratio, which focuses the beam off-axis through an attenuator and shutter and into the test chamber which is located at ground level.

Diagrams of this facility and its general layout are shown in Figures 4-9 and 4-10. The 31.8 m^2 flat heliostat, computer driven and controlled, tracks the sun and directs its rays onto the 11.5 m^2 fixed primary concentrator, consisting of 23 hexagonal facets or mirrors. The facets, each 762 mm in diameter, are ground and polished to a spherical curvature with a radius of 14.6 meters and are front-surface coated with a UV-enhanced aluminum coating. Each facet provides a concentration of more than 100 suns at the focal point. Flux levels may be controlled by covering a portion of the facets thus attenuating the beam.

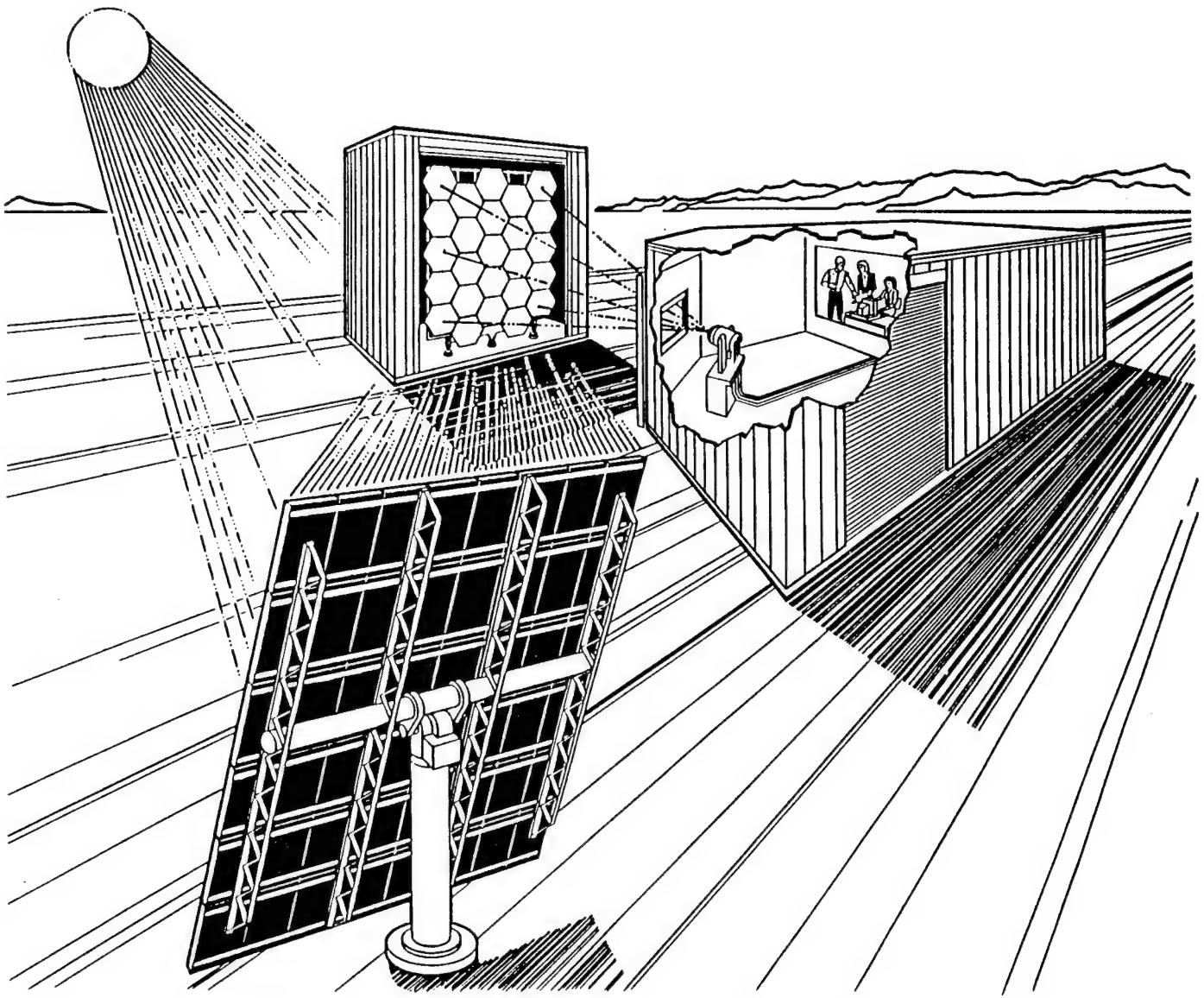

Figure 4-9. NREL high flux solar furnace.

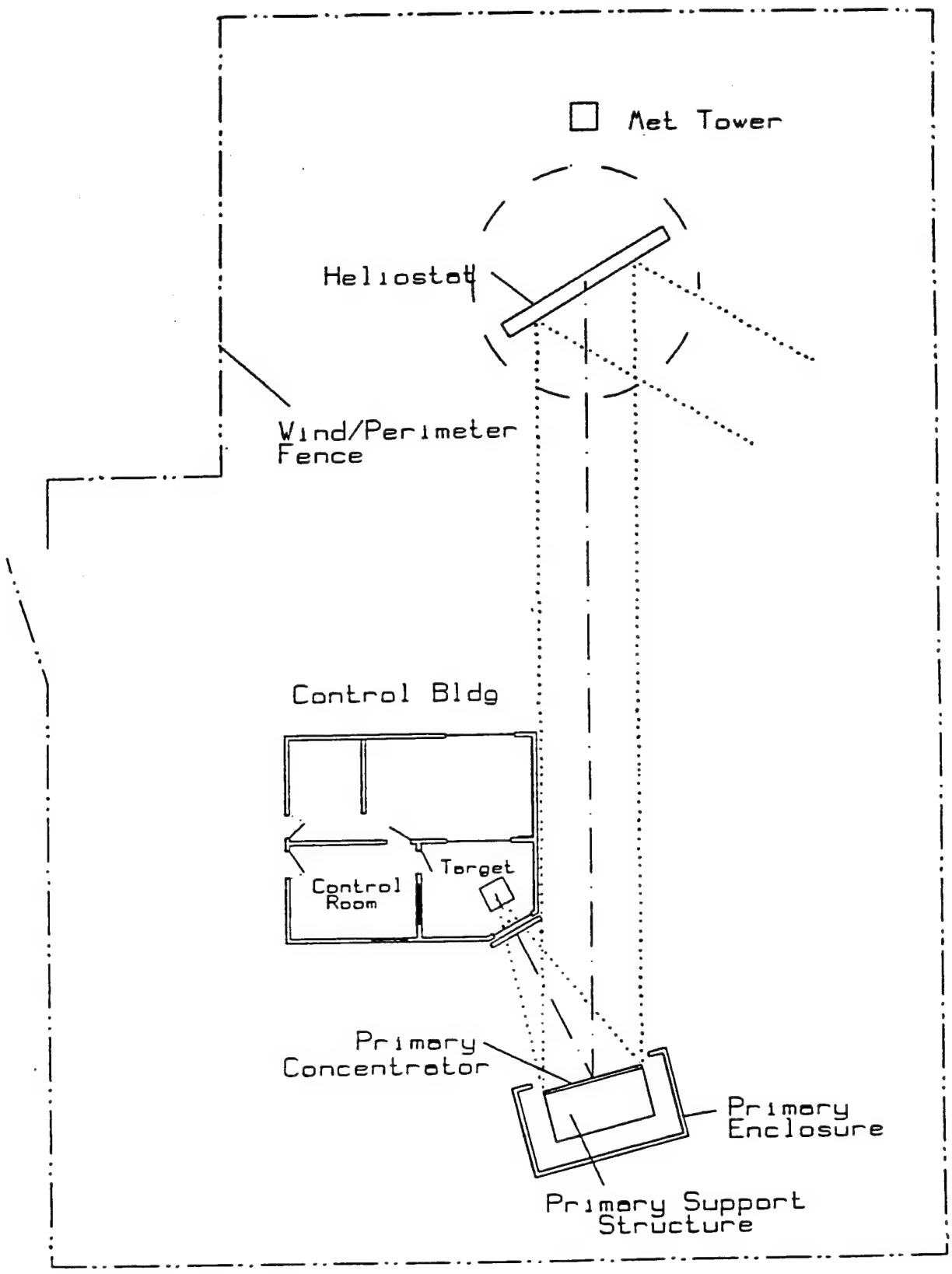

Figure 4-10. NREL solar furnace facility layout.

The primary concentrator redirects the flux 30 degrees off-axis through the attenuator. The off-axis design allows the test chamber to be located outside the beam at ground level between the heliostat and the primary concentrator. In this room, an air-activated, actively cooled shutter is located in front of the focal point. Samples are placed atop a three axis XYZ positioner, with the focal point defined by use of two one mW helium neon lasers. Facility operations are carried out from the adjacent control room, shown in Figure 4-11, where data acquisition systems, video monitoring, flux mapping, and temperature control systems are available to the experimenter.

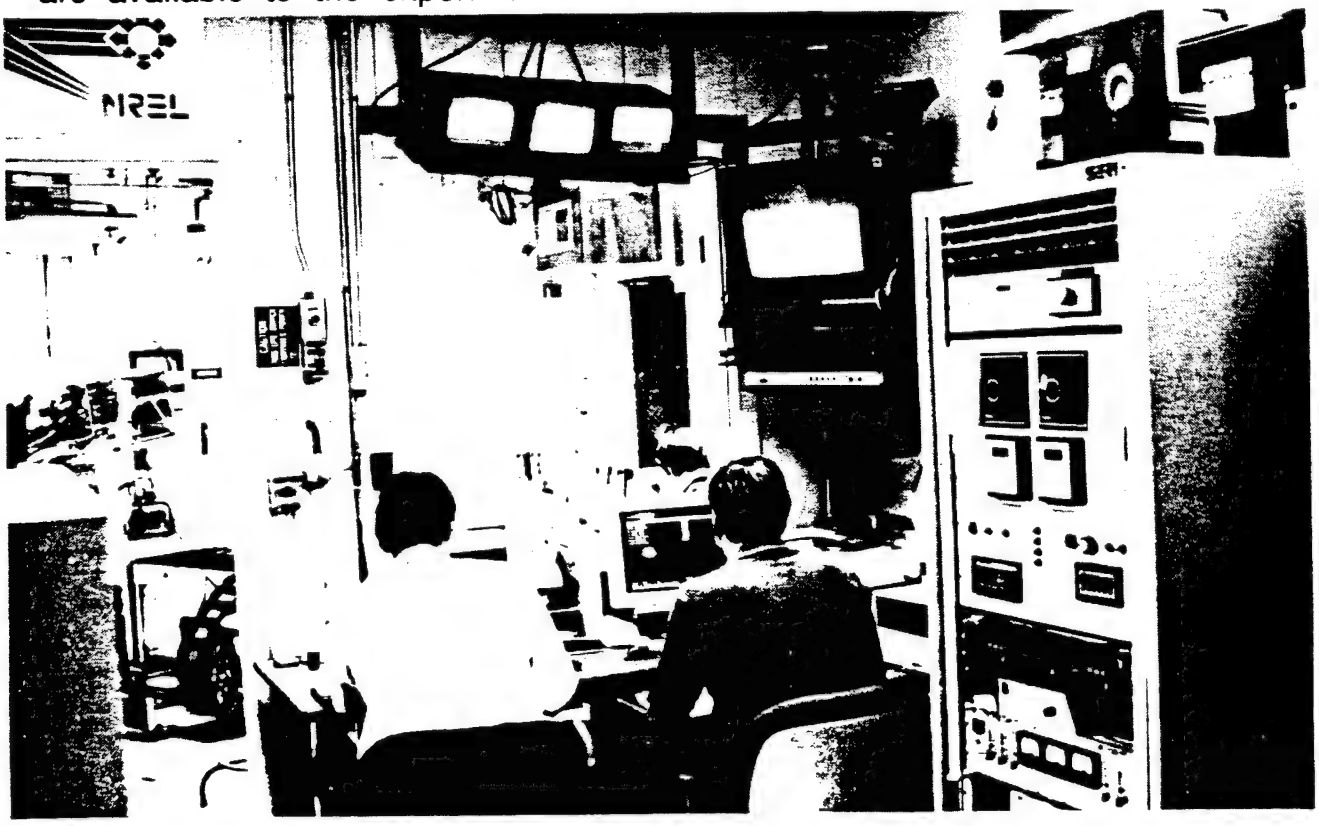

Figure 4-11. NREL solar furnace control room.

The attenuator provides fine tuning of the level of flux focused on the sample. Designed to operate in either automatic or manual modes, it consists of two 1.0 m^2 vertically opposing plates located 1.8 meters in front of the target and 5.2 meters from the center facet of the primary concentrator. The size of the attenuator opening has no effect on the circular shape of the image or the nearly Gaussian flux profile at the test position.

Under DNA sponsorship, PDA was directed to evaluate the suitability of NREL's solar furnace as an alternative to the WSSF for the

purpose of nuclear thermal effects testing. After an initial visit in April 1992, it was determined that the physical and optical characteristics of the facility, although somewhat different from those at the WSSF, appeared suitable, however additional equipment would be required for thermal pulse exposure duration and pulse shaping control. Following DNA approval, a fast shutter, pulse shaper wheel and control system was designed, built and installed at NREL by PDA. A more complete description of these tasks, and the measured performance of this hardware is given in Reference 7.

The PDA fast shutter, shown in Figure 4-12, is a pneumatically driven pair of 6 x 10-inch stainless steel plates which act in a guillotine fashion to precisely control the timed duration of flux exposure to a sample. It was installed downbeam of (behind) the existing facility water-cooled shutter, and just ahead of the test sample position. Operational control of the shutter including flux exposure duration timing is accomplished using a microprocessor-based control system designed and built under PDA IR&D. The flux versus time history of a rectangular pulse obtained at NREL (shown in Figure 4-13) using the newly installed fast shutter is compared to a similar pulse generated at WSSF in Figure 4-14, indicating comparable results.

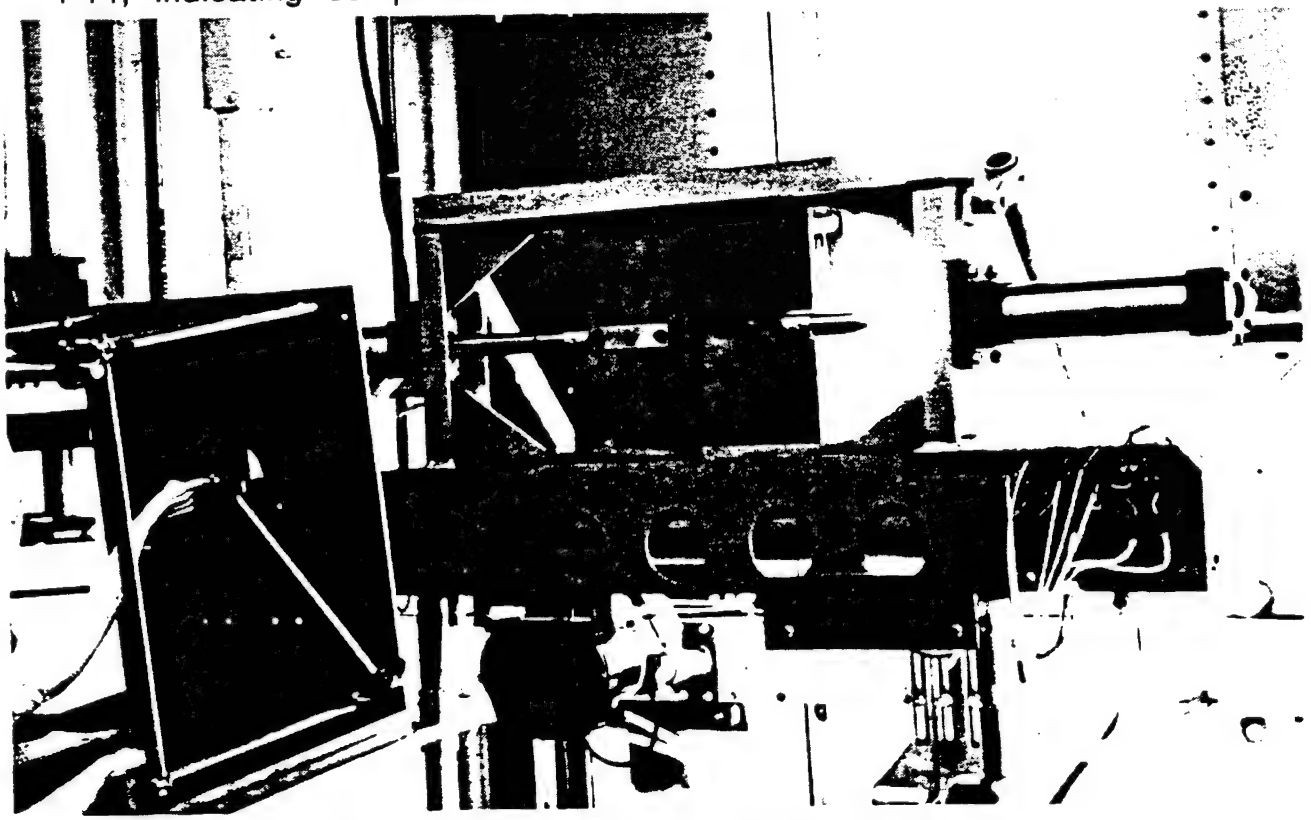

Figure 4-12. PDA fast shutter assembly.

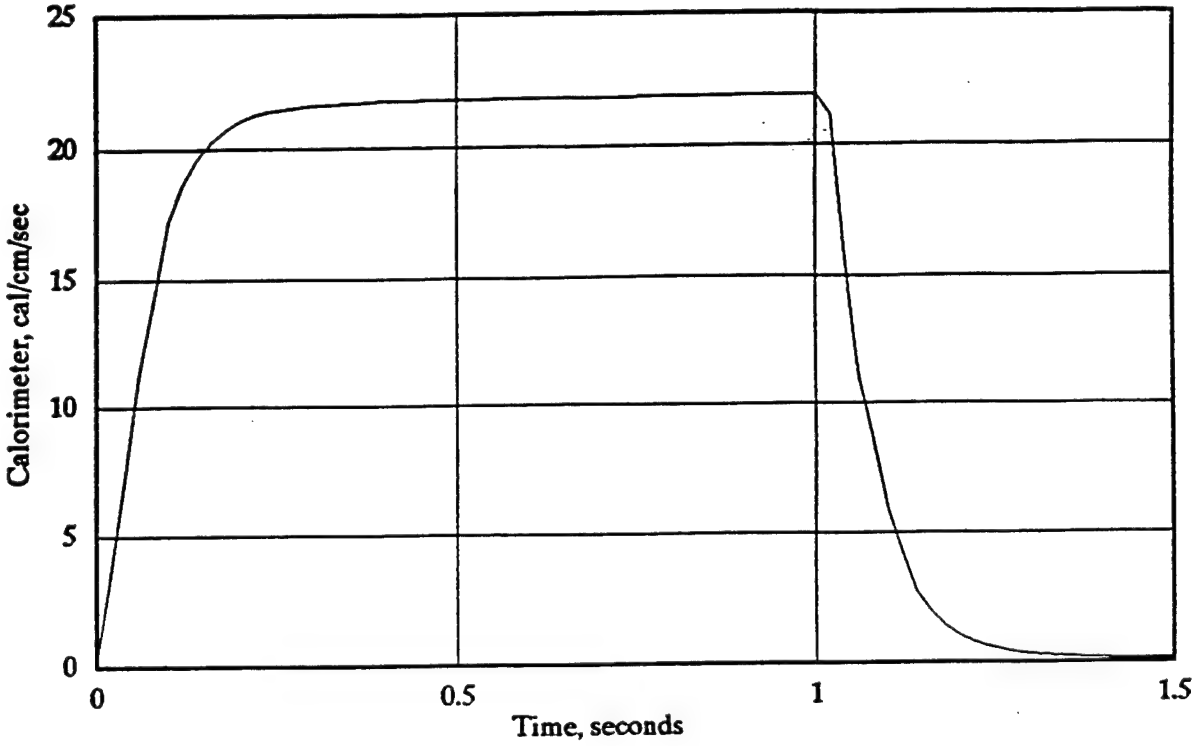

Figure 4-13. NREL solar furnace rectangular thermal pulse.

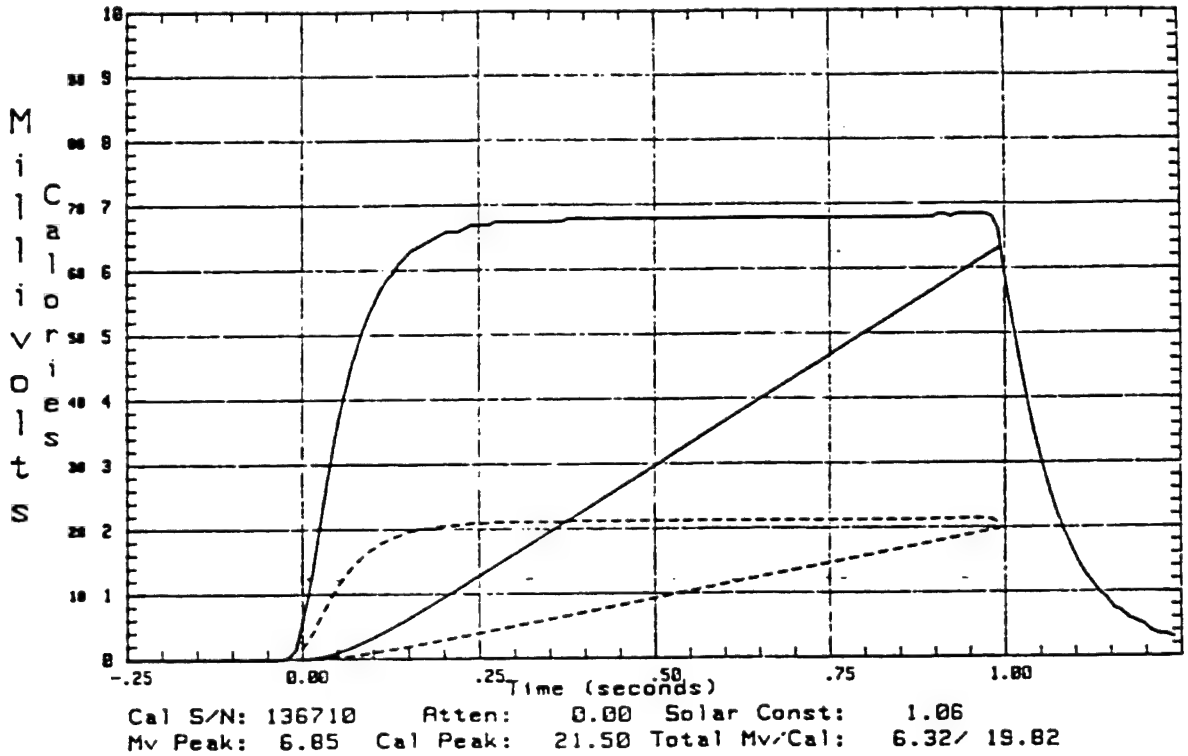

Figure 4-14. White Sands solar furnace rectangular thermal pulse.

In order to simulate the rapid rise, peak and gradual tail-off in flux as a function of time that is associated with an atmospheric nuclear weapon detonation, a pulse shaper wheel must be placed downbeam of the fast shutter to act as a "filter" whose optical density changes as a function of time. The 40-inch diameter PDA pulse shaper wheel, shown in Figures 4-15, is divided into 40 wedge shaped sectors, each constructed from thin aluminum plates drilled with many small holes.

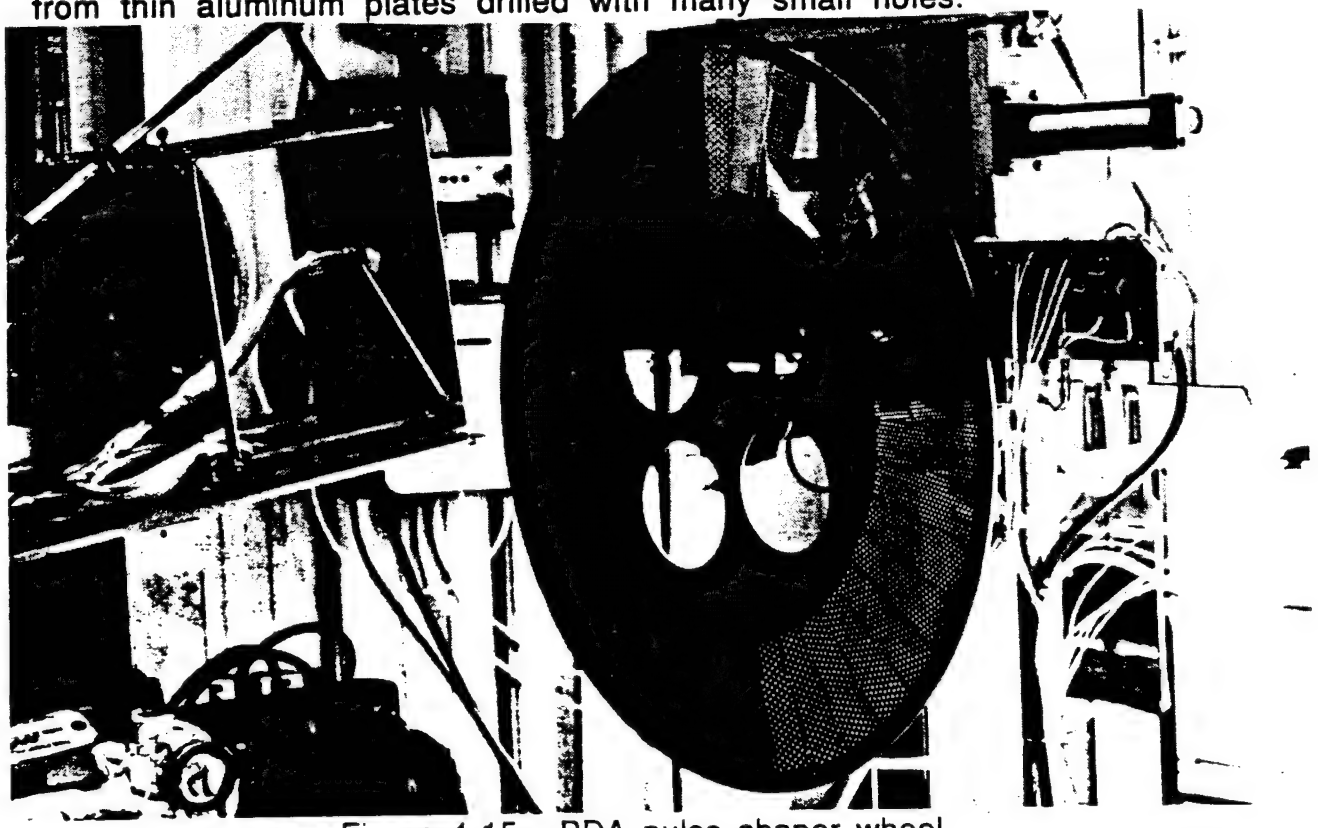

Figure 4-15. PDA pulse shaper wheel.

By varying the number and size of the holes in each sector, the open-to-blocked area ratio can be controlled in a semi-continuous manner as a function of the rotational angle of the wheel. As the wheel is rotated, each sector passes through the radiant energy beam, reducing its intensity by an amount proportional to the open-to-blocked area ratio. Therefore, through proper tailoring of this ratio as a function of wheel rotation angle, the desired flux level versus time behavior can be achieved. Control of the pulse shaper wheel speed and synchronization of the wheel's rotational position with the opening and closing of the fast shutter is accomplished using the same controller that drives the fast shutter. The flux versus time history of a shaped pulse obtained at NREL (shown in Figure 4-16) using the newly installed pulse shaped wheel is compared to a similar pulse generated at WSSF shown in Figure 4-17, indicating comparable results.

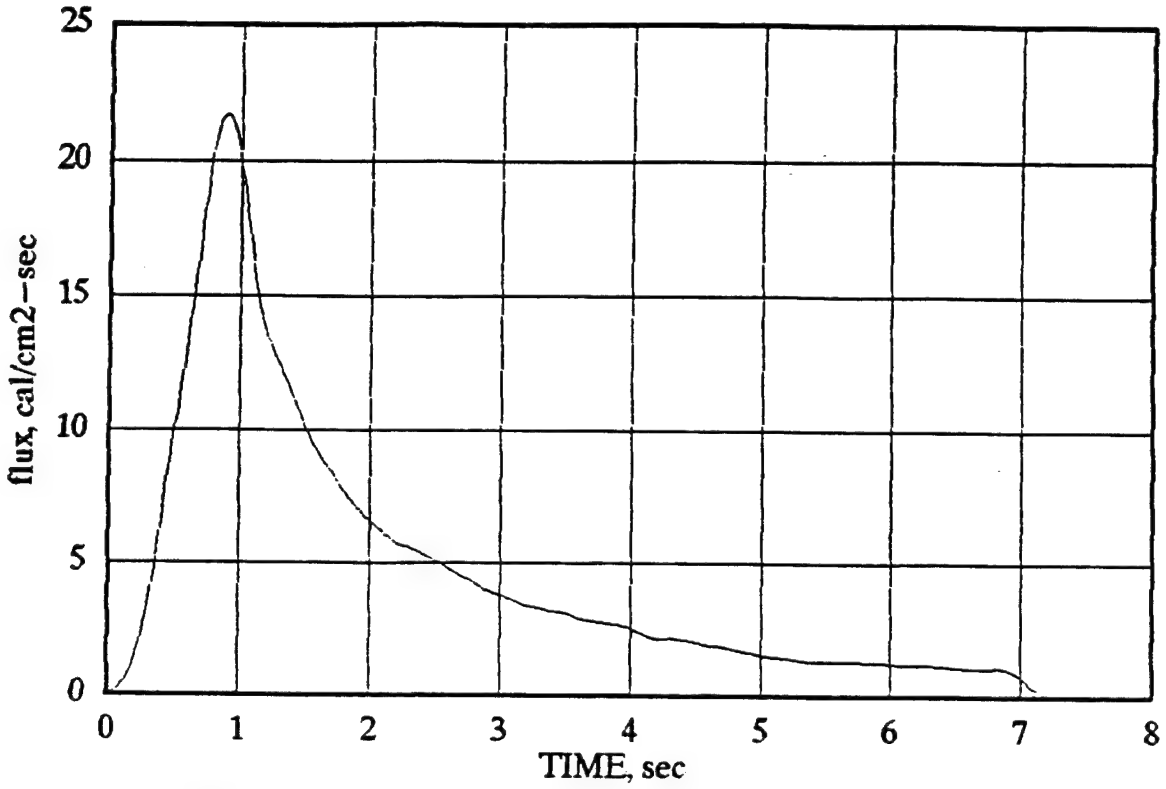

Figure 4-16. NREL solar furnace shaped thermal pulse.

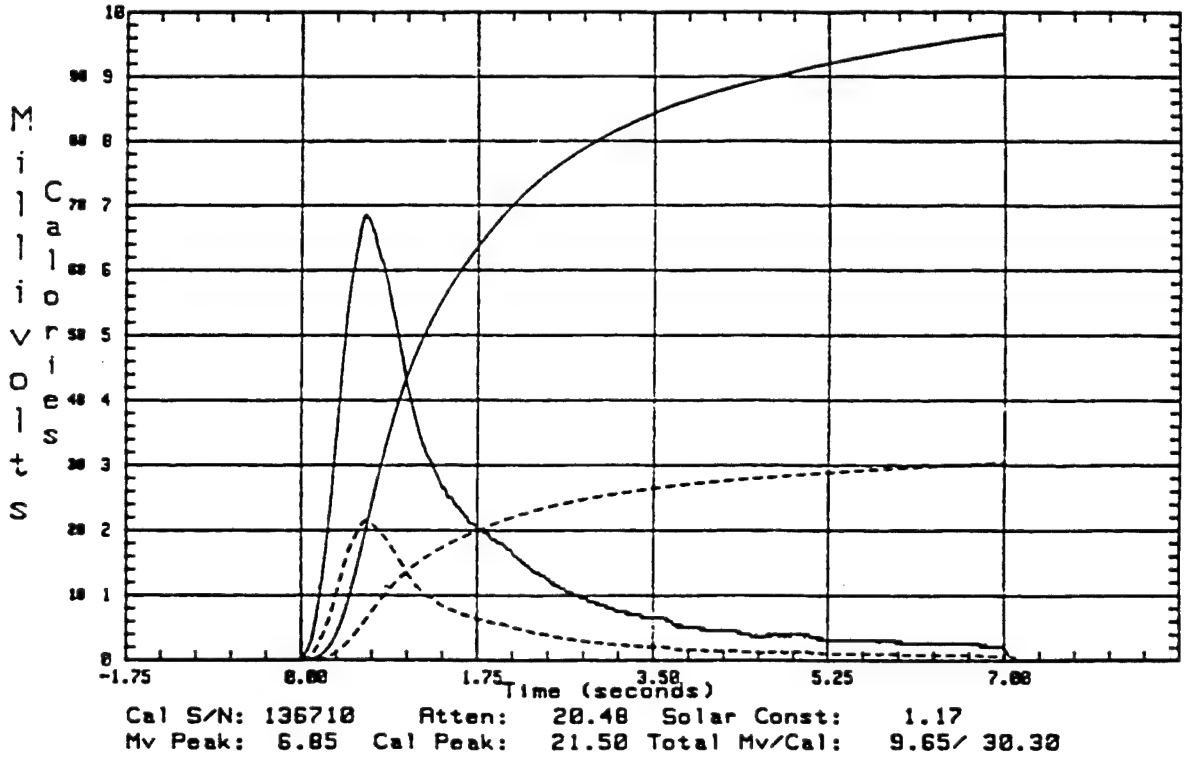

Figure 4-17. White Sands solar furnace shaped thermal pulse.

Following installation of the above described hardware, thorough testing, described in Reference 7, was conducted at NREL in September of 1992 to evaluate the ability of the facility to adequately simulate the thermal environment required for nuclear effects testing. The benchmark testing was performed using a large database of samples representative of B-1, B-2, and other classified weapons systems programs previously tested at WSSF. Comparison of the results from NREL to those from WSSF using identical test methods allowed an accurate analysis of the equivalency of the two facilities. It was concluded that with the exception of tests conducted at flux levels in excess of 60 cal/cm^2-sec, the capabilities of the NREL solar furnace appear to be equal to, and in some cases superior to the WSSF. In addition, the facility is well maintained, operated efficiently, and available at a much lower cost per day of testing than the current charges at WSSF.

SECTION 5
TEST RESULTS

5.1 INTRODUCTION.

Test methods that are practical, repeatable and reliable which isolate, control and measure the experimental parameters of interest have been developed and validated. The test methods used in support of this development effort closely replicate the principal aspects of the nuclear thermal threat environment while minimizing the effects of unwanted or uncontrolled variables. From the results of tests performed under this program, parametric data which demonstrate the effects of different coating types, colors, and preparation processes on the surface temperature, structural failure modes, and damage thresholds of aircraft exterior surface materials exposed to the nuclear thermal threat environment have been quantified. This in turn provides for a better understanding of the interactive response mechanisms involved, which can be used to make improvements to the TRAC system and its performance. Ultimately, it is our intention to demonstrate the advantage gained in thermal hardness when Thermal Reactive Aircraft Coatings are applied to materials representative of modern aircraft structural materials.

5.2 REFLECTANCE TESTS.

One of the key issues related to the development of the TRAC system was the selection of the undercoat or primer to be used as the bottom layer of the coating system. For this application, the primer must satisfy two uniquely different functional requirements. First, the primer must function as a bond coat, providing the necessary adhesion between the substrate (which could be either aluminum or a fiber reinforced composite) and the subsequent topcoats. This is the traditional role of a primer, and narrows the choice of materials to mostly epoxies and urethanes which have been specifically formulated for this purpose. The second functional requirement is the radiant energy reflectance of the primer, and its ability to withstand elevated temperatures.

As has been previously described in this report, an "ideal" primer would reflect 100% of the thermal energy which passes through the thermochromic topcoat in its heated state. In practice, however, any "real" primer will reflect somewhat less than 100% of the incident radiant energy, depending on its color (spectral reflectance of visible light), infra-red (IR) reflectance, and surface texture. The reflectance of visible light from the surface of coated aircraft exterior surfaces is easily measured using a variety of commonly available measuring devices,

such as those described in Section 4.2. A Gardner type hazemeter was used to measure the total reflectance, in the visible waveband, of various coated and uncoated materials. A spectrophotometer was used to measure the spectral reflectivity of surfaces in the visible and near-IR wavebands. However, in order to measure the broadband reflectance of surfaces exposed to the entire nuclear thermal radiant energy spectrum, a special apparatus and test method were required.

5.2.1 Broadband Reflectance Test Method.

A simple test was devised which placed 3 x 3.5-inch painted aluminum samples (one at a time) at a 45° angle to the incident radiant energy beam. A blackbody calorimeter was positioned at 90° to the beam on a ray which intersected the incident beam at the sample position, thus measuring the reflected energy from the sample. Each sample was exposed to a one second rectangular pulse of between 15 and 16.5 cal/cm^2 total fluence, and tested twice in order to assess the repeatability of the measurement method. Although this method measures neither pure specular reflectance (because the beam is not collimated) nor total reflectance (because an integrating sphere is not used), but rather something in between, it does provide a relative level for ranking the various coatings from highest to lowest reflectance. The use of the WSSF allows for good simulation of the nuclear weapon generated radiant energy spectrum, providing the proper "weighting" of each coating's spectral reflectance to its measured overall broadband reflectance value. Prior to testing at the WSSF, the luminous reflectance of each sample was measured using our Pacific Scientific hazemeter. It was of interest to see how well the relative ranking among measured values of luminous reflectance correlates to the WSSF broadband reflectance values.

5.2.2 Broadband Reflectance Test Results.

Reflectance testing of coating samples was accomplished during two separate test entries at the WSSF, conducted during the weeks of April 29 through May 3 and August 12 - 16, 1991. It should be noted that due to the relatively large cone angle of the WSSF incident energy beam (approximately 45° included angle) combined with the setback distance of the calorimeter from the test sample, a large amount of the reflected energy does not strike the face of the calorimeter. This causes the WSSF broadband reflectance values to be abnormally low, as compared to true total reflectance values, but is still valid for relative comparisons of broadband reflectance among the samples. The tables below give the WSSF measured broadband reflectance values, as a percent of incident for each sample tested, along with the measured luminous reflectance values.

Table 5-1. Reflectance test data from April 29 - May 3, 1991 WSSF entry.

SAMPLE COATING	BROADBAND REFLECTANCE (%)	LUMINOUS REFLECTANCE (%)
Bare Aluminum	32.7, 32.2	65.3
Lomit (1)	27.3, 28.2	83.3
Zynolyte 0917 Gloss Clear Lacquer	25.3, 25.7	60.7
Zynolyte 0537 Clear Epoxy	23.3, 23.3	61.3
Deft MIL-P-53022 White Epoxy Primer	12.2, 12.1	90.4
Krylon 1501 Glossy White	11.5, 11.8	85.2
Krylon 9189 Flat White	9.5, 9.7	79.7
Deft MIL-P-53030 White Epoxy Primer (2)	7.9, 7.7	59.1
Deft MIL-P-53030 White Epoxy Primer (3)	7.4, 7.3	56.2
Deft MIL-C-83286 Camouflage Grey Urethane	3.8, 3.7	24.9
Experimental Thermochromic Paint over Krylon 9189 Flat White	7.3, 8.1	10.0, 39.1 (4)

Footnotes:
(1) A product of Solar Energy Corporation, Princeton, New Jersey
(2) Sample prepared by Deft
(3) Sample prepared by PDA using Deft material
(4) Before/After WSSF testing

Table 5-2. Reflectance test data from August 12-16, 1991 WSSF entry.

SAMPLE COATING	BROADBAND REFLECTANCE (%)	LUMINOUS REFLECTANCE (%)
Bare Aluminum	37.3, 37.5	61.1
Lomit	31.9, 32.1	82.7
DeSoto 821 x 641 White Polyurethane	16.4, 16.3	96.2
DeSoto 821 x 400 White Polyurethane	15.8, 15.8	99.8
DeSoto 821 x 557 White Polyurethane	14.8, 14.7	86.2
Deft MIL-P-53022 White Epoxy Primer	14.7	90.4
Deft MIL-C-83286 Camouflage Grey Urethane	3.8, 3.7	24.9

It should be noted that among the four samples tested in both WSSF entries, the values of broadband reflectance measured from the second entry are slightly higher. This is a natural consequence of the test method, due to small differences in positioning of the test fixture relative to the WSSF focal plane. This discrepancy is not of great concern, as the bare aluminum sample can be used as a standard for comparison in both test entries.

In reviewing the data, there are some interesting points to take note of. The silver colored samples (bare and clear coated aluminum as well as Lomit) had higher broadband reflectances than the white samples, which had the highest luminous reflectances. This must be attributed to differences in IR reflectance, suggesting that the pigments used in the white paints do absorb significant amounts of IR energy. Lesser amounts of IR energy are absorbed in the clear binders (lacquer and epoxy), and even less by the Lomit. Unfortunately, Lomit is a silicone based material, and is unsuitable for use as a primer. It was of interest in this study because it was specifically developed for high broadband reflectance, which was proven to be second only to bare aluminum.

As expected, glossy samples tended to be slightly more reflective than their "flat" counterparts of the same color. The Deft primers, both MIL-P-53022 and 53030 had flat finishes, as well as the camouflage grey MIL-C-83286 urethane paint which was included in the matrix for reference. When used as an undercoat, the flatness of the primer is unimportant as this effect is more or less eliminated once a topcoat is applied over it. It should be noted that the MIL-P-53030 primer was an off-white or light grey color, as compared to the MIL-P-53022 primer which was pure white. This color difference, as opposed to any differences in the primers' chemical formulations, accounts for the observed differences in their measured reflectance values. Also note that the DeSoto 821 x 400 paint, which is composed of pure titanium dioxide untinted white pigment dispersed in a polyurethane binder, demonstrated nearly 100% luminous reflectance, yet had only 42% of the broadband reflectance of bare aluminum.

An experimental thermochromic paint sample was also tested, which used Krylon 9189 Flat White paint as a base coat. Although this sample was significantly bleached (permanently) after testing, it did exhibit a broadband reflectance nearly as high as its base coat during exposure, and had a relatively low luminous reflectance before and after testing.

In summary, none of the potential candidate primers exhibited broadband reflectance values anywhere near as high as that for bare aluminum. Bare aluminum, however, cannot be coated directly with a thermochromic topcoat, as the adhesion of non-primer type coatings to aluminum is typically very poor. Additionally, application of the TRAC system to composite materials will also require a base primer coat for proper environmental durability. Since the broadband reflectance values of the white primers tested were not greatly different, it appears that the overall TRAC system performance is unlikely to be highly sensitive to the

particular choice of primer, but that performance can be optimized by using the purest white colored primer that functions acceptably as a bond coat between the substrate and the thermochromic topcoat. Based on these conclusions, the MIL-P-53022 primer was selected as the "baseline" undercoat material.

5.2.3 Spectral Reflectance Tests.

Spectral reflectance measurements were taken on a variety of coatings as well as on bare aluminum, using the spectral reflectance test setup which was shown in Figure 4-1 of Section 4.2. For our purposes, spectral reflectance tests were used primarily as a diagnostic tool. Data obtained from spectral scans is most useful in illustrating where, in the radiant energy spectrum, certain coatings have their highest reflectivity, and how variable this reflectance is as a function of wavelength. As is shown in Figure 5-1, all of the coatings tested, with the exception of Lomit, exhibit a marked decrease in reflectance at the shorter wavelengths. This phenomenon is most likely due, at least in part, to certain organic components, possibly UV absorbers purposely added for environmental protection, which are incorporated into the binders of these polyurethane and epoxy coatings. In contrast, by design Lomit has a very broad, constant, wavelength-independent reflectivity, superior even to bare aluminum.

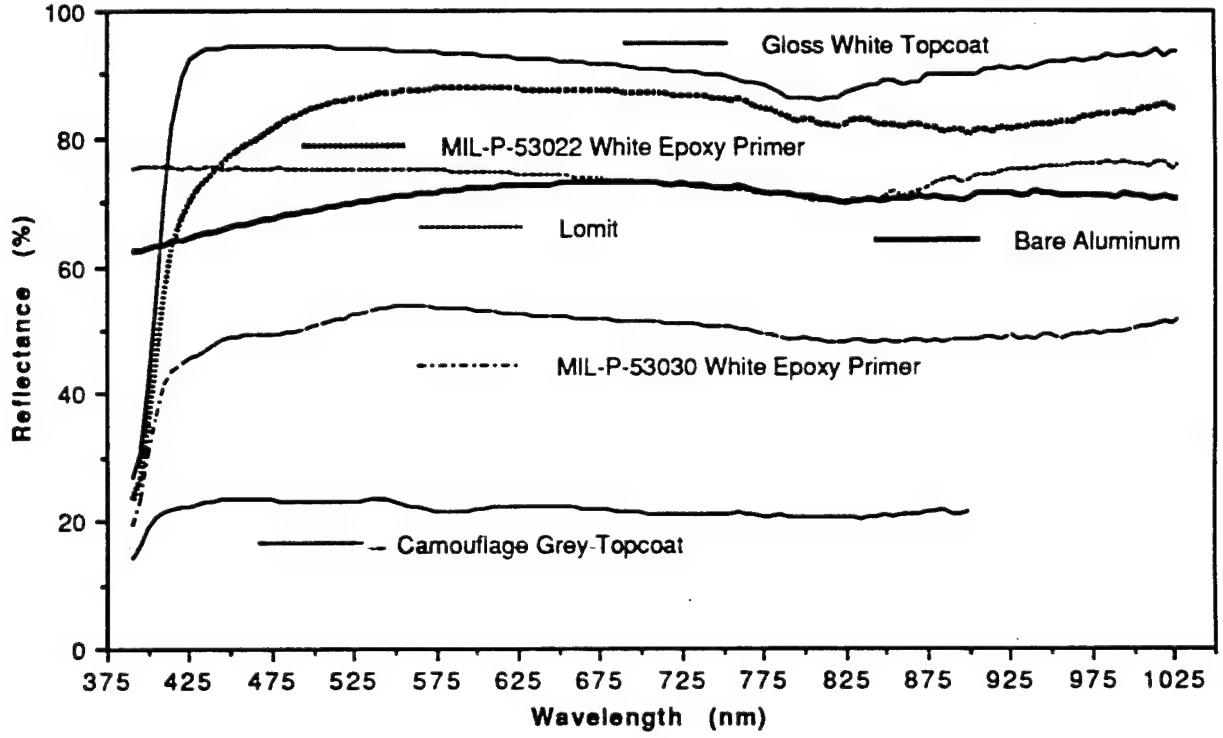

Figure 5-1. Spectral reflectance of bare and coated aluminum.

Reflectance values at 550 nm are in generally good agreement with the broadband luminous reflectance values reported in Tables 5-1 and 5-2. This is consistent with the fact that luminous reflectance is the integral of spectral reflectance weighted to the human eye sensitivity curve, which peaks at 550 nm.

5.3 LABORATORY THERMAL RESPONSE TESTS.

Preliminary tests of coating thermal response to simulated nuclear fireball radiation were performed in the PDA laboratory using the Xenon Light Test Bench (XLTB), which was described in Section 4.2. This test technique provided important data for evaluation of the effectiveness of various coating systems in a nuclear thermal environment when applied over both aluminum and composite substrates. Coated substrate backside temperatures were measured during and immediately following thermal exposure, and the peak temperatures and rise rates were compared in order to evaluate the relative thermal protective value of each coating tested.

5.3.1 Laboratory Thermal Response Tests on Aluminum Substrate.

Aluminum discs, 0.5-inch in diameter were punched from 0.017-inch thick sheet stock to simulate aluminum aircraft skin. These small discs were then processed and coated with materials representative of those used on military service aircraft. The preparation processes and coatings used on the individual samples are shown in the table below.

Table 5-3. Description of aluminum disc samples.

SPECIMEN DESIGNATION	SURFACE PREPARATION	PRIMER COAT	TOPCOAT
A	None (1)	None	None
C	Chemfilm (2)	None	None
P	Chemfilm (2)	White Epoxy (3)	None
W	Chemfilm (2)	White Epoxy (3)	Gloss White
G	Chemfilm (2)	White Epoxy (3)	Lusterless Grey
B	Chemfilm (2)	White Epoxy (3)	Lusterless Black
T	Chemfilm (2)	White Epoxy (3)	TRAC

Footnotes:
(1) Bare aluminum with mill finish
(2) Chemical conversion coating per MIL-C-5541
(3) White epoxy primer per MIL-P-53022B Type II
(4) White polyurethane per MIL-C-83286, color no. 17925
(5) Grey polyurethane per MIL-C-83286, color no. 36440
(6) Black polyurethane per MIL-C-83286, color no. 37038

The aluminum disc samples were subjected to three second duration timed radiant thermal energy exposures of 12 cal/cm^2-sec on the PDA Xenon Light Test Bench. Each sample was placed in a holding fixture, which was shown in Figure 4-4 of Section 4.2, and the instantaneous backface temperature during and immediately following exposure was measured using a spring loaded contact thermocouple probe. The output of the thermocouple was amplified and recorded as a function of time using a Nicolet digital storage oscilloscope. The stored oscilloscope traces were then reviewed and plotted as graphs of backface temperature rise as a function of time.

Figure 5-2 illustrates how the heat reflecting/absorbing properties of aluminum are modified by various surface treatments and coatings which are commonly applied to an aircraft's external aluminum skin surfaces.

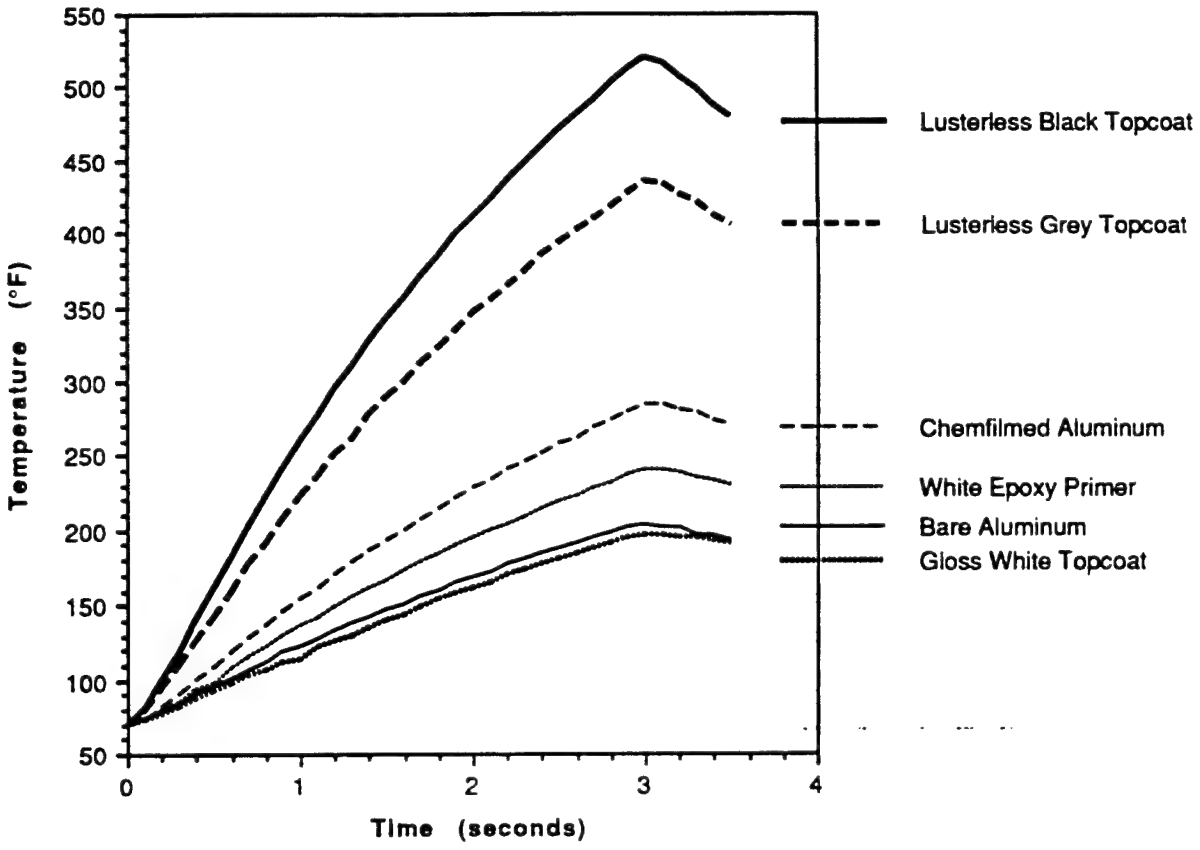

Figure 5-2 Backface temperature response of aluminum disc samples.

It is not surprising that the lusterless black topcoated sample experienced the greatest and most rapid temperature rise, due to the coating's low luminous and broadband reflectance. Conversely, bare aluminum and white topcoated aluminum exhibited the lowest temperature rises, indicating that much of the incident radiant energy was reflected away rather than absorbed into the aluminum substrate. Application of a chemical conversion coat, or "chemfilm" process, which is necessary for proper adhesion of a primer to aluminum, significantly dulls the finish (as compared to "bare" aluminum) and imparts a slightly golden color. This results in reduced reflectance, causing increased absorption of the incident radiant energy.

The backface temperature response of black, grey and white topcoated aluminum disc samples are compared with the response of two candidate TRAC system coated samples in Figure 5-3 below.

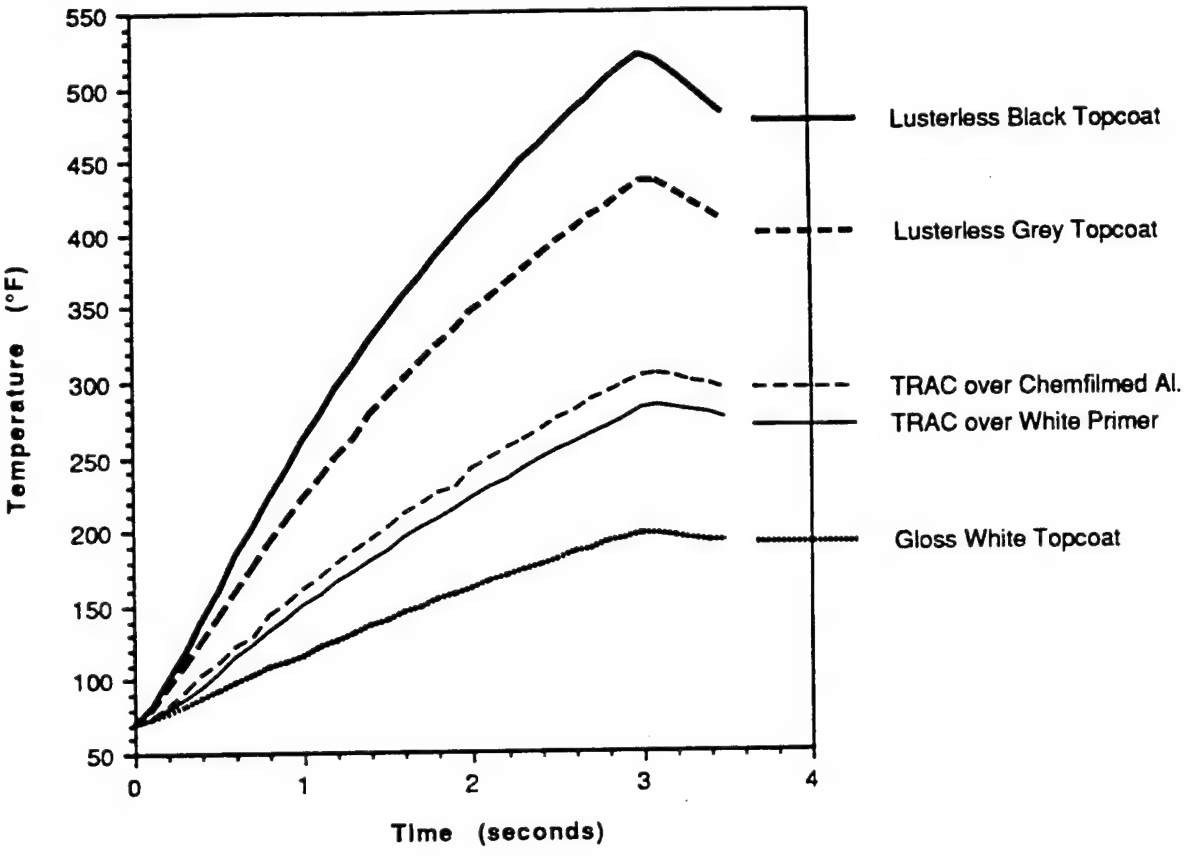

Figure 5-3. Comparison of black, grey, white and TRAC coated aluminum disc sample thermal response.

The relatively low temperature rise rate of both TRAC coated samples compares very favorably with the temperature rise rate of the grey topcoated sample, especially when one considers that in the benign state the TRAC coating is visibly much darker (luminous reflectance = 7%) than the grey topcoat (luminous reflectance = 25%). When the TRAC pigmented topcoat is applied directly over chemfilmed aluminum (without any primer) the system's thermal performance is slightly reduced as compared to the TRAC topcoat applied over white primer (the "baseline" system). This is not surprising, as it was shown in Figure 5-2 that the white primer by itself is more reflective (smaller temperature rise) than the chemfilmed aluminum. Carrying this argument further, one might expect that the TRAC topcoat applied over bare aluminum would exhibit even better performance since the bare aluminum exhibits even better heat reflectance than the white primer. However, the adhesion of polymeric coatings to bare untreated aluminum is typically poor, and such a system would not be recommended and is therefore unrealistic. The fact that in Figure 5-2 the gloss white topcoat was shown to be more reflective than the white primer suggests that the addition of more titanium dioxide (TiO_2) pigment to the primer might enhance its thermal reflective properties.

5.3.2 Laboratory Thermal Response Tests on a Composite Substrate.

Simulated nuclear thermal pulse testing of 0.5-inch diameter discs cut from glass-epoxy skin/nomex honeycomb core composite material was also performed on the PDA Xenon Light Test Bench at an incident flux level of 12 cal/cm^2-sec. The particular composite material from which samples were cut was chosen to be representative of a modern aircraft's skin material and is described below:

Face Sheets: 7781 E-glass, harness satin, MIL-C-9084/TYVIIIB
F161 epoxy resin, 350°F cure, MIL-R-9300 B
(Hexcel designation for impregnated fabric: 7781-38"-F161)
Thickness: 0.02-inch (two ply)

Core: Nomex paper honeycomb, HRH 10-1/8-6.0
Thickness: 0.188-inch

As was the case for the aluminum disc samples, the composite samples were prepared with various different surface coatings in order to measure and compare thermal response as a function of coating color and

type. All samples were primed with white epoxy primer conforming to MIL-P-53022B, and then topcoated with either a white, grey, or black polyurethane coating per MIL-C-83286, or the baseline TRAC topcoat material. Each sample was fitted with a thermocouple bonded to the center of the backside of the outer (exposed side) face sheet. The thermocouple output was amplified and recorded as a function of time during exposure using a Nicolet digital storage oscilloscope. From this data the backface temperature response plots shown in Figure 5-4 were generated.

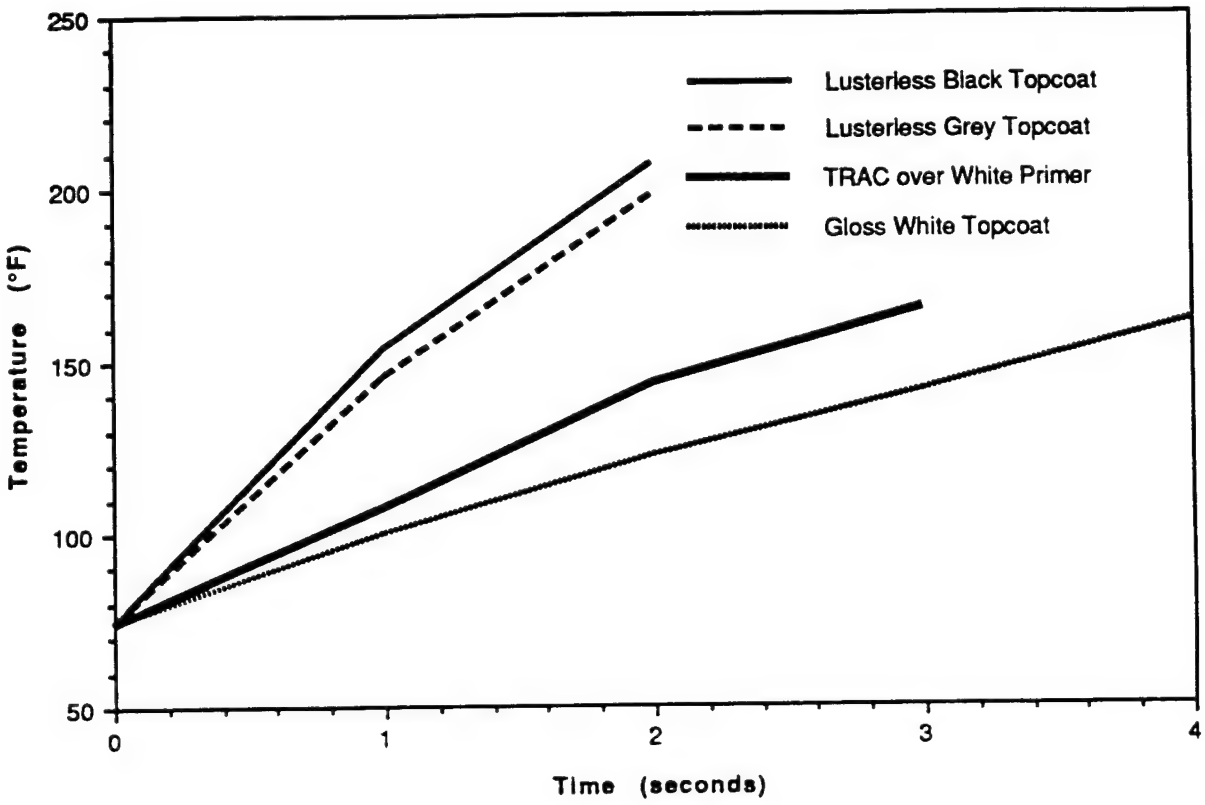

Figure 5-4 Backface temperature response of composite disc samples.

Compared to the data shown in Figure 5-3, measured temperature rises on the backface of the composite samples were much smaller than those measured from aluminum samples with the same coatings. This is due to the relatively low conductivity (as compared to aluminum) of heat through the glass-epoxy skin. On the exterior (exposed) surface however, we know that the temperatures on the composite material samples were much higher than those on the aluminum samples. On the aluminum samples a significant portion of the absorbed radiant energy (heat) was

conducted away from the surface to the substrate below, whereas the highly insulative composite face sheet material significantly inhibits the diffusion of heat into the substrate, trapping most of it in the coating itself.

This effect was evidenced by the fact that significant coating degradation, in the form of blistering and charring, was observed after only 2 seconds of exposure (24 cal/cm^2 total fluence) on the black and grey composite samples, at which point the test exposures were terminated. In contrast, previously tested black and grey coated aluminum disc samples exhibited no visible degradation after 3 seconds (36 cal/cm^2 total fluence) of exposure. TRAC coated composite disc samples exhibited the first signs of degradation after three seconds exposure, and white composite samples required approximately 4 seconds (48 cal/cm^2) of exposure to cause blisters.

Once again, the TRAC coated samples compared very favorably, from both a temperature rise and degradation standpoint, to the visibly lighter, lusterless grey samples. In fact, the thermal performance of the TRAC coating closely rivaled the performance of the gloss white topcoat when tested on this composite material under the same conditions

5.4 COMBINED THERMAL-MECHANICAL TESTING OF COMPOSITE BEAMS.

Direct measurement of TRAC effectiveness has been accomplished through measurement of substrate temperature response to incident thermal fluence, as described in the previous sections. However, a more direct simulation of aircraft structural response to thermal loading is required to assess the operational advantage associated with the application of the TRAC system to aircraft operating in a nuclear threat environment. While simple substrate temperature response is of interest, it does not provide a direct assessment of TRAC system operational effectiveness. Complex analyses are required to predict the effect of substrate temperature response on failure of structural materials subjected to simultaneously or subsequently applied mechanical loading.

Analytical methods currently used for evaluation of composite aircraft structures exposed to thermal loading (Reference 8) assess the potential for failure under thermal loading on the basis of critical substrate temperatures for delamination and debond. These assessments assume that the structure is unloaded during thermal exposure. The retained strength of the composite after exposure is estimated from the

maximum temperature rise and is used as a basis for prediction of failure during application of subsequent mechanical loads.

Preliminary testing was conducted under PDA IR&D in which composite-honeycomb materials with stressed skins were subjected to simultaneous thermal loading. It was shown that the presence of skin compressive stress during thermal loading greatly affects the skin buckling response of the materials. Failure was observed at relatively low temperatures in composite samples loaded to 50% of their ultimate room temperature buckling stress.

These data suggest that the currently used analysis methodology is nonconservative. A composite material with stressed skins resulting from normal flight loads may fail by skin buckling if subjected to thermal exposure. The current methodology would assign only a degraded strength to this composite structure unless the skin temperature rise exceeded the criteria for delamination or debond.

Therefore, a new test methodology, including associated specimen and fixture design concepts, was developed under PDA sponsored IR&D (Reference 9) for evaluation of the behavior of aircraft composite skin materials subjected to combined simultaneous mechanical loading and thermal flash conditions. A unique test sample configuration was designed to provide a constant flexure stress distribution over the surface exposed to thermal fluence while supported in a fixture which applies a constant, regulated mechanical load, and is instrumented to monitor the applied load, sample end deflection, incident flux level and face sheet backside temperature response during and after thermal exposure. The fixture was designed for convenient location in the test section of either the WSSF or the NREL solar furnace. The test sample configuration, test fixture, test method, and results are described separately below.

5.4.1 Composite Beam Test Sample Design.

A test sample material was selected that is representative of a modern aircraft's skin material, is well characterized, and is readily available at a reasonable cost. This glass-epoxy skin/nomex paper honeycomb composite is the same material that was described in Section 5.3.2. In addition to the reasons already listed, this particular material's combination of face sheet strength, thickness and core thickness provided acceptable predicted deformations within the planned loading envelope (Reference 10).

Since composite materials have lower compressive strengths than tensile, aircraft wings, for example, are likely to be more vulnerable to nuclear thermal flash exposure on surfaces under compressive stress. Therefore it was planned that the test sample, in the form of a uniformly stressed beam, be loaded so that the surface exposed to the thermal flash is under a constant compressive stress state.

The constant stress test sample is a cantilever sandwich beam of variable width with a concentrated applied end load. The unique planform shape, shown in Figure 5-5, provides a large area of near uniform flexure stress in the central portion (the area exposed to thermal fluence) when loaded at the lower end by a concentrated applied load. The flexure stress in a simple cantilever beam with a triangular planform (load applied at the apex) is theoretically non-varying over the length. The actual beam planform shape is larger at the load point and at the gripped end for practical purposes.

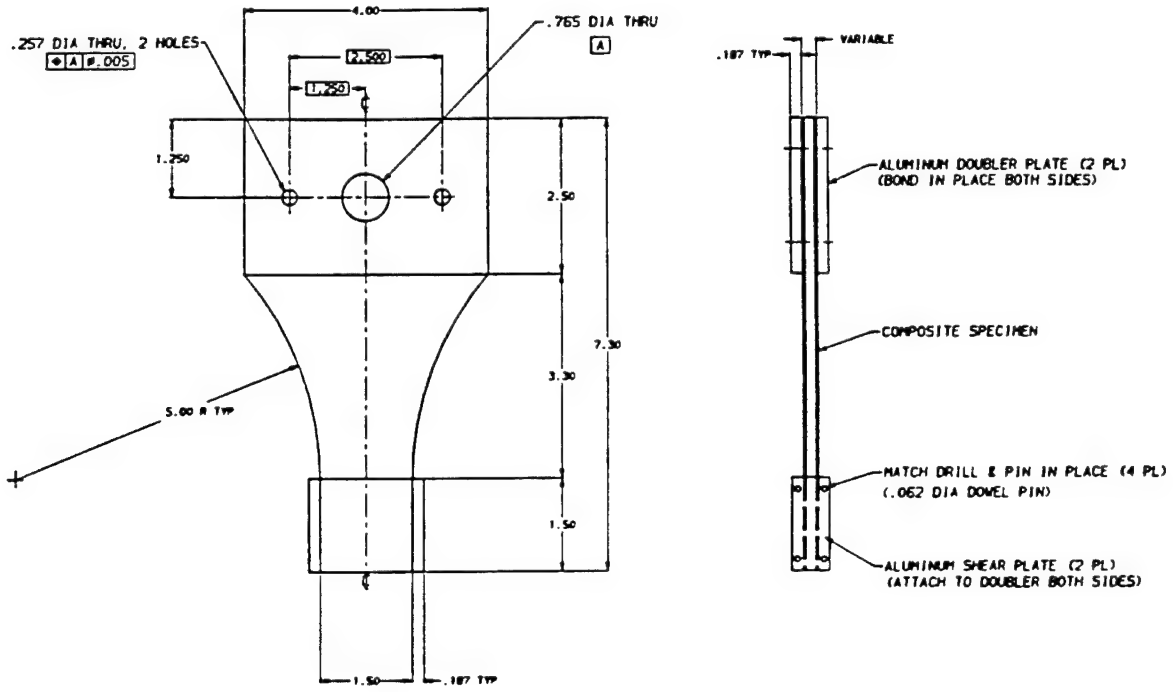

Figure 5-5. Constant stress composite beam test sample configuration.

Preliminary test sample design was conducted with closed-form beam theory. The analysis was used to trade off sample deflection, load and skin stress. A single, selected design configuration was verified by finite element analyses (Reference 11), which confirmed the magnitudes and uniformity of stress in the test section.

All samples fabricated and tested during this program were cut from a single large sheet of the composite sandwich material, thus eliminating any possible sheet to sheet variations which could affect the test results. Sample preparation involved cutting the planform shape from the sheet material, attachment of the aluminum doubler plates by bonding and pinning, and installation of thermocouples, as shown in Figure 5-6, on selected samples for measurement of backface temperatures during thermal exposure.

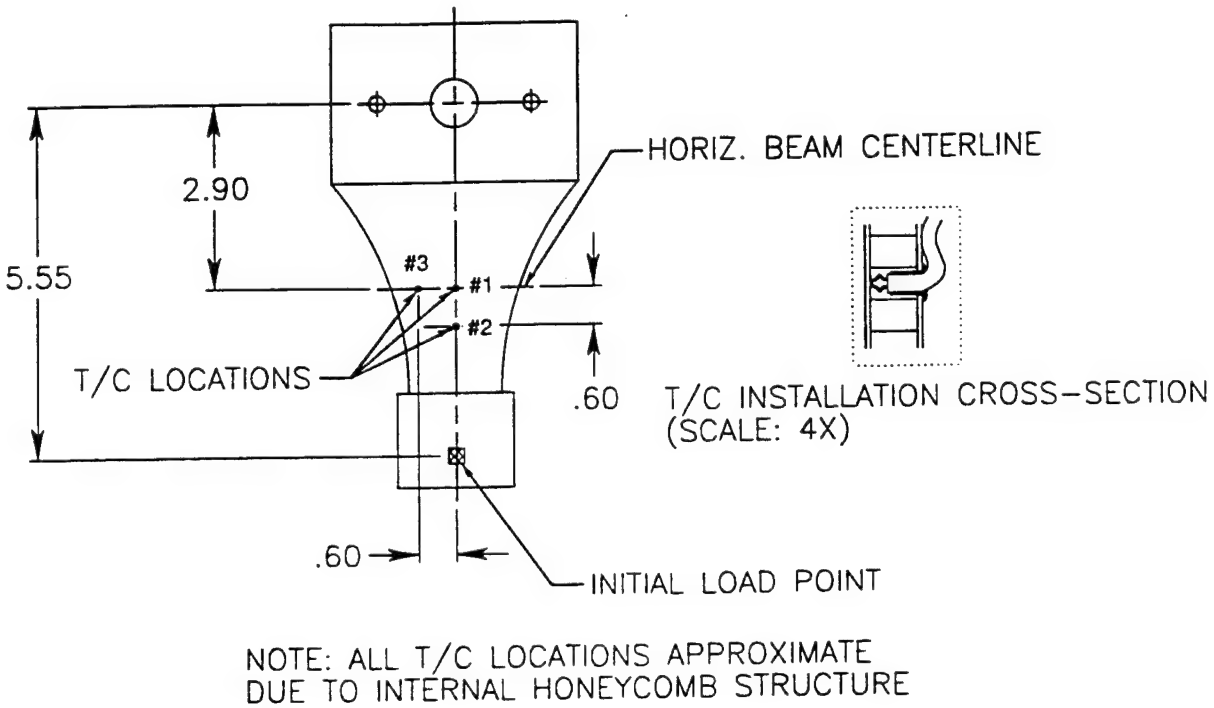

Figure 5-6. Test sample thermocouple installation details.

Prior to testing, each sample was primed and topcoated with either a gloss white (color no. 17925 per FED-STD-595A), lusterless grey (color no. 36440), or lusterless black (color no. 37038) aliphatic isocyanate (polyurethane) coating per MIL-C-83286, or with the baseline TRAC topcoat material. White, grey and black samples utilized a green epoxy-polyamide primer per MIL-P-23377 Type II, and TRAC samples employed a white epoxy primer per MIL-P-53022B Type II. All coatings were deposited by spray application using techniques which simulated actual aircraft preparation as closely as possible. All coatings were allowed to cure at room temperature for a minimum of 7 days prior to testing.

5.4.2 Test Fixture for Combined Thermal-Mechanical Loading.

A specialized, purpose-built test fixture was designed, developed and fabricated under PDA IR&D sponsorship (Reference 12) to support testing of composite beams for the TRAC program. The test fixture, shown in Figures 5-7 through 5-12, is a portable, self-contained structural assembly used for the application of a controlled mechanical load to the cantilevered beam test sample while positioned in a solar furnace for simultaneous application of thermal loading. The concentrated end load is applied with a pneumatic actuator on a controlled pressure supply system. Applied load is monitored with a load cell, while sample end deflection is measured with a linear differential transformer (LVDT). Calorimeters are positioned on the test sample centerline, for thermal flux calibration purposes, and to either side of the sample to measure incident thermal flux during testing. Three thermocouple interfaces are also provided to facilitate the measurement of sample face sheet backface temperatures during testing. The output signals from the load cell, LVDT, calorimeters and thermocouples are routed to a Macintosh-based data acquisition system where they are monitored and recorded immediately before, during, and after thermal exposure.

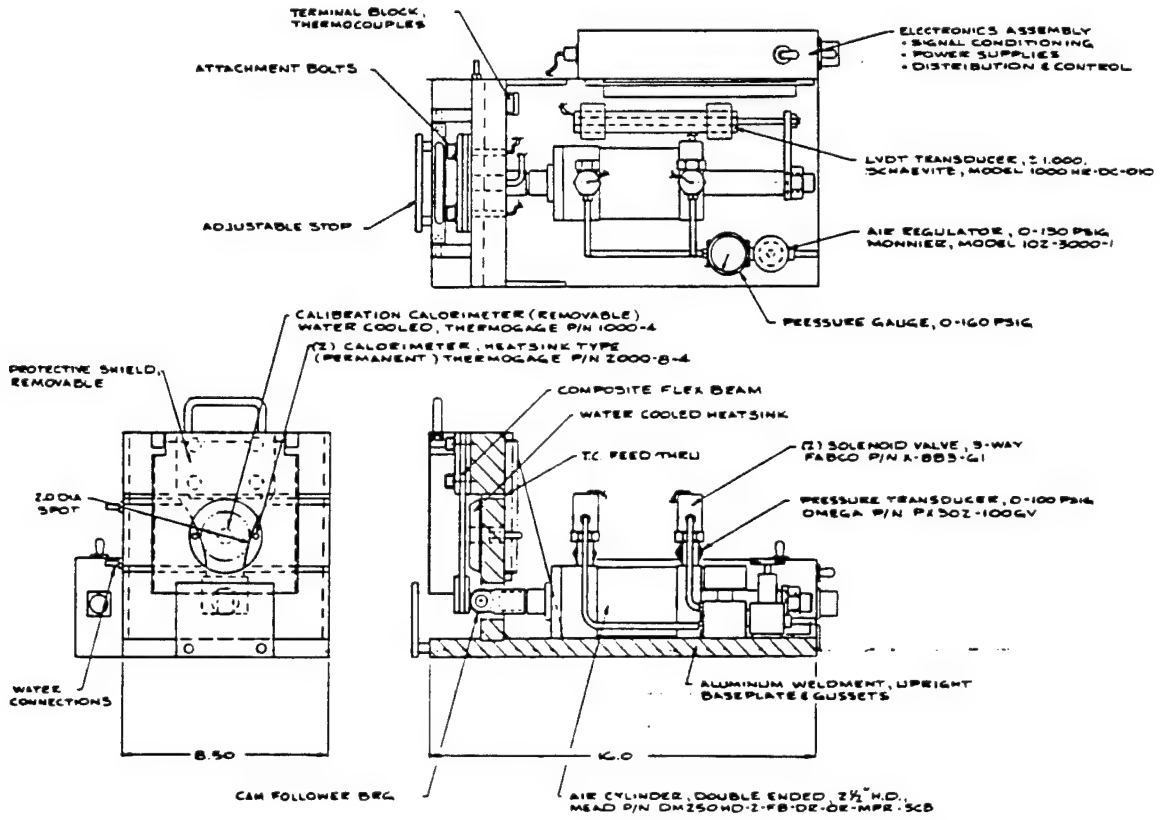

Figure 5-7. Combined thermal-mechanical test fixture assembly drawing.

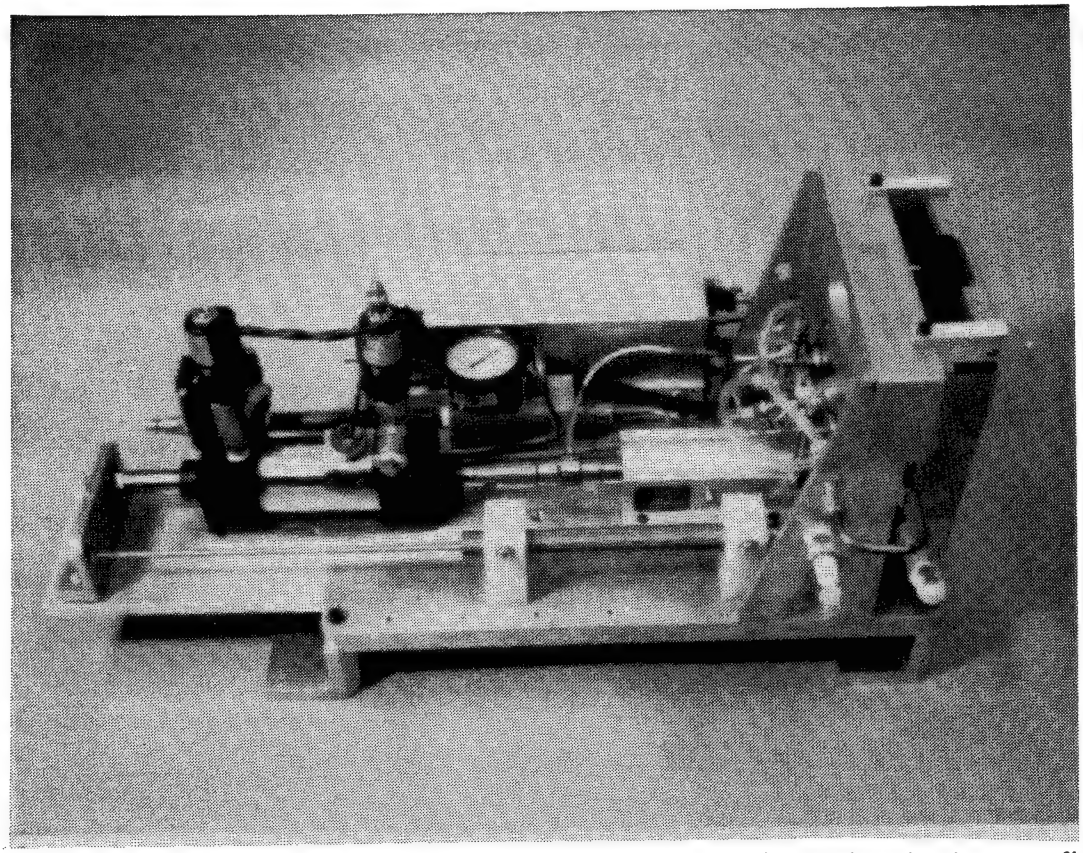

Figure 5-8. Left side view of combined thermal-mechanical test fixture.

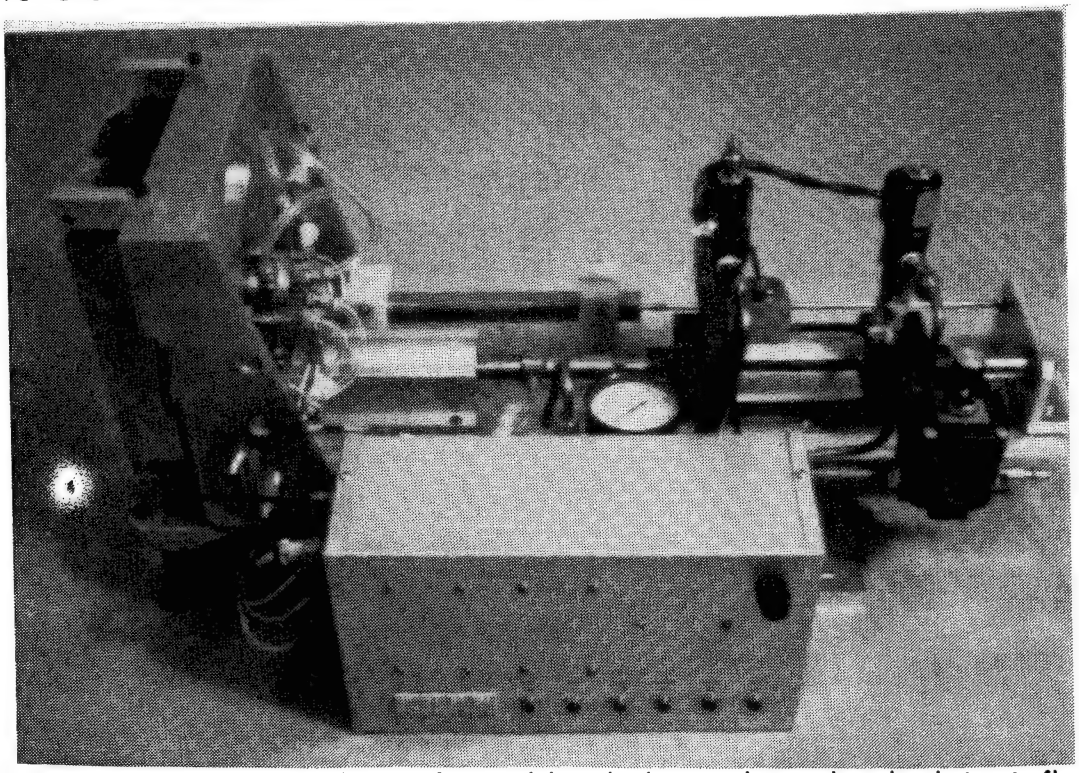

Figure 5-9. Right side view of combined thermal-mechanical test fixture.

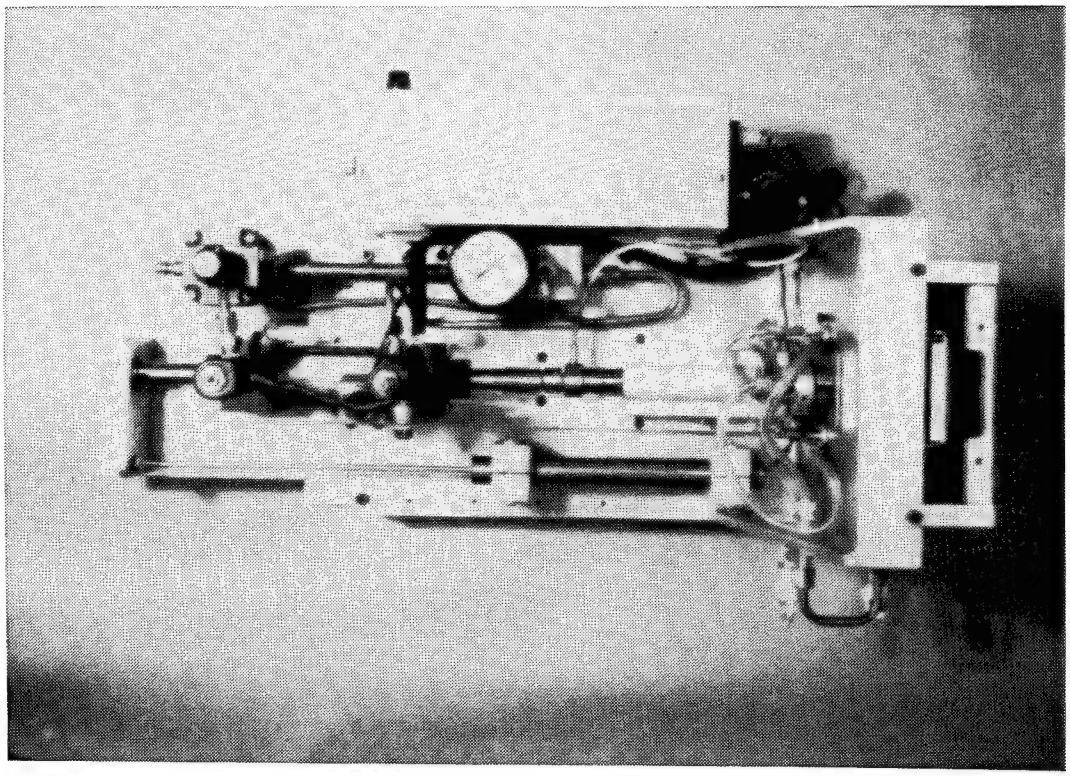

Figure 5-10. Top view of combined thermal-mechanical test fixture.

Figure 5-11. Test fixture with macintosh-based data acquisition system.

Figure 5-12 shows a side view of the front face of the test fixture with a machined aluminum sample, used for calibration purposes, mounted in the test position. Note the deflection of the end of the beam as it is subjected to mechanical loading applied to its lower end.

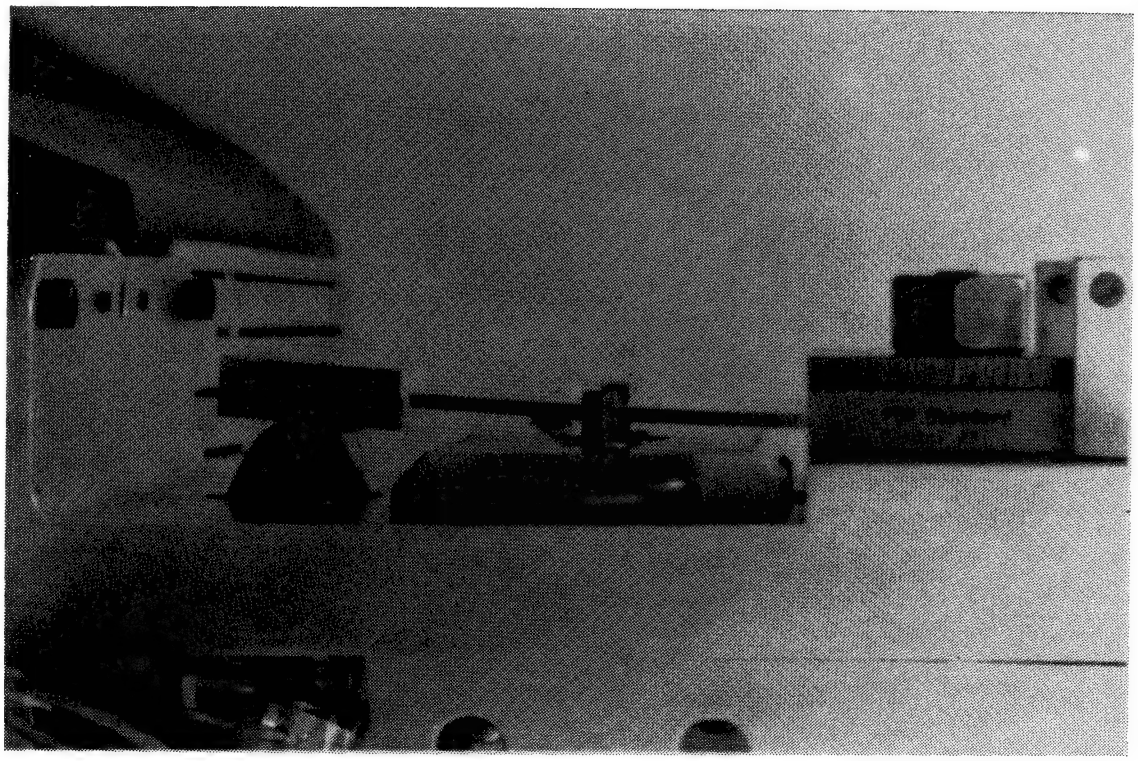

Figure 5-12. Side view of face of fixture with aluminum calibration beam installed.

5.4.3 Combined Thermal-Mechanical Loading Test Method.

5.4.3.1 Test Objectives. A test method was developed which, through the use of simultaneously or sequentially applied mechanical load combined with radiant thermal energy exposure, provides a direct simulation of stressed aircraft skin exposed to a nuclear thermal pulse. The primary objective of tests conducted using this method was to determine the failure threshold of selected composite materials as a function of steady-state mechanical load, total thermal fluence and topcoat color. From this data a "failure envelope" can be generated which illustrates the critical thermal environment as a function of mechanical stress for each material/topcoat combination tested. Additional objectives were to investigate, determine and describe the composite material's failure mechanisms, and demonstrate the advantages of a white coating for increasing thermal hardness. As a result of the tests and data collected using the test method described below, it was possible to clearly demonstrate that the TRAC system provides the thermal hardness benefits of a white coating while retaining a dark camouflage color under benign conditions.

5.4.3.2 Test Fixture and Sample Verification Procedure. As described in Reference 13, prior to testing any of the composite beam samples, the test fixture (described in Section 5.4.2) was first checked in the laboratory for proper operation. A machined aluminum "calibration beam" (which was shown in Figure 5-12) with attached strain gauges was mounted in the fixture and subjected to a gradually increasing mechanical load while continuously recording the load cell, LVDT (sample end deflection), strain gauge outputs, and the air cylinder input pressure. This was continued until a steady load of 40 pounds was reached, which was then held for one minute, at which time the beam was gradually unloaded. The measured stress and strain were then plotted as a function of applied load and compared to analytical predictions (Reference 14) to verify that the system performed properly.

Several test samples conforming to the description presented in Section 5.4.1, some with attached strain gauges, were then mounted in the test fixture and subjected to a gradually increasing mechanical load (at room temperature without radiant thermal flux exposure) until failure occurred. The load to failure values were averaged together to establish the average test samples' ultimate load capacity. Measured strains were again compared to analytical predictions to verify that the sample material behaved as predicted. From these tests it was determined that

for the configuration described in Section 5.4.1, the test samples' average ultimate load capacity is 75 pounds.

5.4.3.3 Combined Thermal-Mechanical Test Procedure. All combined thermal-mechanical testing was accomplished at the NREL solar furnace using the PDA fast shutter, pulse shaper wheel (used for some tests) and control system which was described in Section 4.4. The test fixture was mounted atop the facility XYZ table and positioned so that the facility's radiant energy beam was centered on the test sample's central area. Test fixture verification, as described above, was then performed to ensure that the entire system performed properly and was not damaged from shipping. The NREL facility video camera was positioned and focused to provide a view of the test sample during exposure.

A detailed test plan, which had been written prior to each test entry indicated the test conditions (mechanical preload and incident flux level) for each sample to be tested. Immediately prior to each test, the incident thermal flux level was adjusted to the desired level using the facility attenuator. A calibration exposure was performed without a sample mounted in the fixture by opening the fast shutter and measuring the incident flux level with all three calorimeters, the one on the test sample centerline and the ones on either side. Outputs from the side calorimeters were compared to each other to verify proper alignment of the radiant energy beam, and compared to the output from the center calorimeter to establish a ratio which was used to determine the flux level during subsequent test exposures. Because the center calorimeter is blocked when a test sample is mounted in the fixture, flux measurements taken from the side calorimeters are multiplied by the previously determined ratio in order to calculate the incident flux on the beam centerline during tests.

Following completion of an acceptable calibration exposure, a test sample was mounted in the fixture and mechanically preloaded in accordance with the test plan. The facility video recorder was started and the stressed area of the sample was then exposed to the radiant energy beam until structural failure occurred, as indicated by a large, rapid increase in sample end deflection. The PDA fast shutter was then immediately closed, video recording stopped, and the sample was removed. Each sample was closely inspected to determine the failure mode, and to take note of any visible degradation of the surface coating in the exposed area. Video recordings were reviewed afterwards to observe smoke generation (if any) from each sample's outer surface during exposure.

5.4.4 Results of Combined Thermal-Mechanical Loading of Composite Beams.

Testing of composite material samples subjected to combined mechanical and thermal loading was performed by PDA Engineering during three separate test entries conducted during the weeks of March 15 - 19, May 17 - 21, and September 27 - October 1, 1993 at the National Renewable Energy Laboratory (NREL) High Flux Solar Furnace located in Golden, Colorado. Test results from each entry are described in detail in References 15, 16 and 17 respectively. Because the test conditions used in the last entry were of a somewhat different nature from those employed in the previous two entries, the test conditions, results, and discussion pertaining to the third entry are presented in separate sections (5.4.4.3 and 5.4.4.4).

5.4.4.1 Results from the March 15 - 19 and May 17 - 21 Test Entries. A total of 28 samples were tested during these two test entries at the NREL solar furnace. These consisted of three white, three black, eight grey and fourteen TRAC painted samples. All samples conformed to the description given in Section 5.4.1, and all but eight of the TRAC samples had thermocouples installed which were used to measure the backface temperature response of the samples' outer (exposed) face sheets.

Testing was performed in accordance with the test method described in Section 5.4.3. As stated earlier, in laboratory tests performed with mechanical loads only, (no radiant thermal energy exposure) it was determined that this sample configuration has an ultimate strength (the load at which structural failure occurs) of approximately 75 pounds. For all tests performed with radiant thermal energy exposure during these two test entries, the applied mechanical load was set to either 25, 50 or 75 percent of ultimate, which corresponds to 19, 38 or 56 pounds respectively. With the solar furnace radiant thermal energy beam adjusted to a flux level within a range of 4.3 to 18.5 cal/cm^2-sec, each mechanically preloaded sample was exposed to the radiant energy beam until structural failure was observed.

Videotape recordings of each test were made, and upon review, most tests showed some degree of smoke generation from the painted surfaces of the samples prior to failure. Plots of sample end deflection and total fluence (the time integral of flux) as a function of time for 20 of the 28 tests are shown in Figures D-1 through D-20 (Appendix D). In each case, the time at which a sharp increase in deflection is observed is designated as the time to failure (t_f), and the corresponding fluence at

that time is designated as the fluence to failure (ϕ_f). Unfortunately, during the other 8 tests a data acquisition problem was encountered which interfered with the proper recording of data. For these tests the time to failure was determined by reviewing the videotape, and the incident flux level was determined from pre- and post-test calibration exposures performed with the NREL facility calorimeter array.

Photographs of the failed test samples are shown in Figures D-21 through D-30 (Appendix D). From a cursory review of the photos, it is obvious that most of the samples are clearly broken, whereas some others (e.g. White Sample #3) appear unbroken. Upon closer examination of the actual samples, it becomes clearly evident that there are two distinctly different failure modes responsible for these different failed sample appearances. In those samples which appear "fractured" it was found, upon close examination of the damaged area with magnification, that the failure mechanism was breaking of the fiber bundles in the face sheet in the exposed area. It is hypothesized that heating of the resin surrounding these fibers causes sufficient softening to allow the compressively stressed fibers to lose their rigidity, buckle, and break. For the other samples which do not appear "fractured", the outer skin (face sheet) was found to have delaminated from the Nomex honeycomb core, leaving the sample with little or no rigidity in the loaded direction. In these cases it appears that the adhesive used to bond the face sheet to the core has simply softened to the point where the unbroken face sheet comes apart from the core, and therefore no longer contributes to the composite material's stiffness.

The test conditions, times and fluences to failure, failure modes and observations from tests of each sample are shown in Table 5-4. The failure modes of the samples have been designated as either "Face Sheet Fiber Buckling" (FSFB) for those samples with "fractured" face sheets, or "DELAM" for samples with debonded yet unbroken face sheets. Temperature readings at the time of failure, obtained from thermocouples attached to the back of the outer face sheet of selected samples are also given in the table. The location of each thermocouple (T/C 1, 2 and 3) in relation to the exposed area of each sample was shown in Figure 5-6 (Section 5.4.1). Plots of the measured temperatures as a function of time are presented in Figures D-31 through D-43 (Appendix D). The uniquely shaped response curves shown in Figures D-40 and D-42 are particularly noteworthy, as they show the sharp reduction in output (shown as temperature) which occurred when the face sheet delaminated and lost contact with the thermocouple junction (sensing area).

Table 5-4. Results from the March 15-19 and May 17-21 combined thermal-mechanical load tests.

SAMPLE IDENTIFICATION	INCIDENT FLUX LEVEL (cal/sq cm-sec)	PRELOAD (lbs)	TIME TO FAILURE (sec)	FLUENCE TO FAILURE (cal/sq cm)	FAILURE MODE	SMOKE DURING TEST?	POST-TEST PAINTED SURFACE APPEARANCE	BACKFACE TEMP. AT FAILURE (°F) T/C 1	T/C 2	T/C 3
WHITE #1	9.3	38	3.55	33.0	FSFB	NO	Lightly Wrinkled	131	114	128
WHITE #2	9.4	19	4.54	42.7	FSFB	NO	Lightly Wrinkled	No Data	No Data	No Data
WHITE #3	4.5	38	7.08	31.9	DELAM	NO	Lightly Blistered	No Data	No Data	No Data
GREY #1	9.4	19	1.25	11.7	FSFB	YES	Lt. Char, Mod. Blistered	109	105	98
GREY #2	8.5	38	0.95	8.1	FSFB	YES	Mod. Bleached, No Blist.	92	93	92
GREY #3	8.4	56	0.50	4.2	FSFB	NO	Lightly Blistered	73	71	73
GREY #4	4.7	19	2.34	11.0	FSFB	YES	Moderately Blistered	No Data	No Data	No Data
GREY #5	4.6	38	1.70	7.8	FSFB	NO	Lightly Blistered	113	93	99
GREY #6	4.6	56	1.24	5.7	FSFB	NO	No Blisters	No Data	No Data	No Data
GREY #7	4.7	19	2.60	12.3	FSFB	YES	Moderately Blistered	144	105	126
GREY #8	4.3	56	0.70	3.0	FSFB	NO	No Blisters	80	74	75
BLACK #1	4.5	19	1.71	7.7	FSFB	YES	Moderately Blistered	No Data	No Data	No Data
BLACK #2	4.3	38	1.45	6.2	FSFB	NO	Very Lightly Blistered	85	100	92
BLACK #3	8.4	38	0.80	6.7	FSFB	YES	Heavily Blistered	97	91	86
TRAC #1	9.3	19	4.50	41.9	DELAM	YES	Heavily Charred	No Data	No Data	No Data
TRAC #2	9.1	38	2.70	24.6	DELAM	YES	Lt. Char, Hvy. Blistered	139	99	128
TRAC #3	9.3	56	2.14	19.9	FSFB	YES	Moderately Bleached	No Data	No Data	No Data
TRAC #4	9.3	19	4.45	41.5	FSFB	YES	Hvy. Char & Blistered	181	150	148
TRAC #5	4.6	19	7.40	34.0	DELAM	YES	Lt. Char, Hvy. Blistered	160	129	177
TRAC #6	4.7	19	7.30	34.6	DELAM	YES	Lt. Char, Hvy. Blistered	189	145	147
TRAC #7	9.2	56	1.88	17.3	DELAM	YES	Mod. Bleached & Blistered	No T/C's Installed on this Sample		
TRAC #8	7.1	56	1.10	7.8	DELAM	YES	Mod. Bleached & Blistered	No T/C's Installed on this Sample		
TRAC #9	4.6	38	3.20	14.6	FSFB	YES	Mod. Bleached & Blistered	No T/C's Installed on this Sample		
TRAC #10	4.8	56	2.15	10.4	FSFB	NO	Slighlly Bleached	No T/C's Installed on this Sample		
TRAC #11	12.7	38	1.05	13.3	FSFB	YES	Mod. Charred & Blistered	No T/C's Installed on this Sample		
TRAC #12	18.5	38	1.15	21.3	FSFB	YES	Hvy. Char & Blistered	No T/C's Installed on this Sample		
TRAC #13	9.2	38	1.70	15.7	DELAM	YES	Lightly Charred	No T/C's Installed on this Sample		
TRAC #14	4.6	38	4.95	23.0	FSFB	YES	Mod. Bleached & Blistered	No T/C's Installed on this Sample		

5.4.4.2 Conclusions from the March 15 - 19 and May 17 - 21 Test Results. A more straightforward interpretation of these test results can be obtained by reviewing the data as presented in Table 5-5 below.

Table 5-5. Comparison of fluence to failure vs. test sample color.

TEST CONDITION		TEST SAMPLE COLOR				FLUENCE TO FAILURE COMPARISON		
LOAD	FLUX LEVEL	WHITE	GREY	BLACK	TRAC			
(% of Ultimate)	(cal/sq cm-sec)	Refl.=90%	Refl.=22%	Refl.=3%	Refl.=8%	TRAC/WHITE	TRAC/GREY	TRAC/BLACK
25%	4.5 - 4.7	-	11.0 , 12.3	7.7	34.0 , 34.6	-	294%	445%
25%	9.3 - 9.4	42.1	11.7	-	41.9 , 41.5	98%	356%	-
50%	4.3 - 4.6	31.9	7.8	6.2	14.6 , 23.0	59%	241%	303%
50%	8.4 - 9.3	33.0	8.1	6.7	24.6 , 15.7	61%	249%	301%
50%	12.7	-	-	-	13.3	-	-	-
50%	18.5	-	-	-	21.3	-	-	-
75%	4.3 - 7.1	-	5.7 , 3.0	-	7.8 , 10.4	-	418%	-
75%	8.4 - 9.3	-	4.2	-	19.9 , 17.3	-	443%	-

Here the fluence to failure values ($ø_f$), given in cal/cm^2, are shown in a matrix arranged vertically by test condition and horizontally by test sample color. By reading down any column (white, grey, black or TRAC) one can examine the relationships between $ø_f$ versus increasing incident flux level and/or increasing mechanical preload for samples of the same color. By reading across any row, one can examine the effect of sample color on $ø_f$ for any particular test condition. In the last three columns to the right, the $ø_f$ values for TRAC samples are ratioed to the $ø_f$ values for white, grey and black samples tested under the same conditions. In cases where two data points exist for a particular sample color/test condition, those values are averaged together before the ratio is determined. Some very significant conclusions can be drawn from this data as presented:

1. The magnitude of the mechanically induced preload has a large effect on the fluence to failure. The higher the preload, the lower the fluence to failure. This relationship has been observed to be basically linear.

2. Fluence to failure values do not appear to be particularly sensitive to incident flux level. For a given sample color and preload condition, increasing the incident flux level tends to reduce the time to failure proportionally, resulting in the same or nearly the same fluence to failure.

3. The color of the sample has a large effect on the fluence to failure. For any particular test condition, black samples always have the lowest ϕ_f values, grey samples have slightly higher values, TRAC samples have considerably higher values, and white samples have the highest ϕ_f values. TRAC samples compare quite favorably to white samples, and are much better than grey samples even though TRAC has a much lower reflectance under benign conditions. The comparisons presented in the right hand portion of Table 14 demonstrate the effectiveness of TRAC in numerical terms. TRAC improved the thermal hardness of the samples by a factor of 2.4 to 4.4 (depending on test conditions) over grey or black samples, and demonstrated hardness values between 59 and 98% of white painted samples under equivalent conditions.

5.4.4.3 Results from the September 27 - October 1 Test Entry. A total of 25 samples were tested during this test entry at the NREL solar furnace. These consisted of two white, two black, nine grey and twelve TRAC painted samples. All samples conformed to the description given in Section 5.4.1, and twelve of the samples had thermocouples installed which were used to measure the backface temperature response of the samples' outer face sheets within the heated area.

Testing was performed in general accordance with the test procedure described in Section 5.4.3.3, however some changes and additional procedures were added, which in their modified form, comprised three distinctly different test methods. For the purpose of clarity, each "modified" test method and its results are described separately below.

In this first series of tests, for which the results are presented in Table 5-6, the mechanical load applied during radiant thermal energy exposure was considerably lower than what had been used during any of the previous tests. As described previously, in laboratory tests performed with mechanical loads only, (no radiant thermal energy exposure) it was determined that this sample configuration has, on average, an ultimate strength (the load at which structural failure occurs) of approximately 75 pounds. For all previous tests performed with radiant thermal energy exposure, the applied mechanical load was set to either 25, 50 or 75 percent of ultimate, which corresponds to 19, 38 or 56 pounds

respectively. For this new series of tests however, it was of interest to investigate sample behavior at 10 percent of ultimate load, which corresponds to approximately 8 pounds applied load.

Table 5-6. Results from low preload/constant flux tests.

SAMPLE IDENTIFICATION	INCIDENT FLUX LEVEL (cal/sq cm-sec)	TIME TO FAILURE (sec)	FLUENCE TO FAILURE (cal/sq cm)	FAILURE MODE	SMOKE DURING TEST?	POST-TEST PAINTED SURFACE APPEARANCE	BACKFACE TEMP. AT FAILURE (°F) T/C 1	T/C 2	T/C 3
WHITE #4	10.4	6.85	71.0	DELAM	YES	Mod. Char, Hvy. Blistered	201	240	201
WHITE #5	9.7	4.00	38.9	DELAM	YES	Lt. Char, Hvy. Blistered	No T/C's Installed on this Sample		
GREY #9	9.5	3.00	28.6	DELAM	YES	Hvy. Char & Blistered	188	164	156
GREY #10	8.8	2.05	18.1	DELAM	YES	Hvy. Char & Blistered	No T/C's Installed on this Sample		
BLACK #4	9.2	3.50	32.3	DELAM	YES	Hvy. Char & Blistered	178	175	178
BLACK #5	8.9	2.15	19.1	DELAM	YES	Hvy. Char & Blistered	No T/C's Installed on this Sample		
TRAC #17	10.0	5.25	52.6	DELAM	YES	Hvy. Char & Blistered	176	193	181
TRAC #18	8.9	2.45	21.8	DELAM	YES	Hvy. Char & Blistered	No T/C's Installed on this Sample		
TRAC #19	9.8	3.30	32.4	DELAM	YES	Hvy. Char & Blistered	No T/C's Installed on this Sample		

With the solar furnace radiant thermal energy beam adjusted to a flux level within a range of 8.8 to 10.4 cal/cm^2-sec, each mechanically preloaded sample was exposed to the radiant energy beam until structural failure was observed. Videotape recordings of each test were made, and upon review showed that all tests resulted in a considerable amount of smoke generation from the painted surface of each sample prior to failure. Plots of sample end deflection and total fluence (the time integral of flux) as a function of time for all nine tests of this type are shown in Figures E-1 through E-9 (Appendix E). In each case, the time at which a sharp increase in deflection is observed is designated as the time to failure (t_f), and the corresponding fluence at that time is designated as the fluence to failure (ϕ_f).

As described in the previous test results section (5.4.4.1), there are two distinctly different modes by which failure of the samples occurs. In the Face Sheet Fiber Buckling (FSFB) mode the outer (exposed) face sheet of the failed sample appears to be "fractured", which is the result of breaking of the fiber bundles in the face sheet in the exposed area. It is hypothesized that heating of the resin surrounding these fibers causes sufficient softening to allow the compressively stressed fibers to lose their rigidity, buckle, and break. In the other mode, the failed sample does not appear "fractured", but its outer skin (face sheet) is delaminated from the Nomex honeycomb core, leaving the sample with little or no rigidity in the loaded direction. In these cases it appears that the adhesive used to bond the face sheet to the core has simply softened to the point where the unbroken face sheet comes apart from the core, and therefore no longer contributes to the composite material's stiffness.

As can be seen from Table 5-6, all samples in this series of tests failed by delamination (DELAM), which is not surprising considering the high fluence to failure values (as compared to those from the previous test results) and low applied mechanical load. Photographs of the failed test samples presented in Figures E-10 through E-13 (Appendix E) show the severe charring and blistering of the painted surfaces and underlying face sheets of the test samples caused by the high total fluence exposures to which they were subjected. This undoubtedly caused large amounts of heat to be absorbed into and conducted through the face sheets and into the adhesive behind them, causing softening and ultimately delamination. This explanation is further supported by the high backface temperatures at failure reported in the table (as compared to those reported in Table 5-4 of the previous test results section) which were obtained from the thermocouple response vs. time plots shown in Figures E-14 through E-17 (Appendix E).

The shapes of the temperature response curves give us some insight into what was happening to the face sheet just before failure. For example, in Figure E-14 we see the temperatures measured from thermocouples #1 and 2 peak and then drop just before failure, while thermocouple #3 peaks just at the moment of failure. We surmise that the sudden drop in measured temperature is the result of loss of contact between the outer face sheet and the thermocouple itself due to delamination of the face sheet from the core. If we assume this to be true, then the curves in this figure seem to indicate that localized delaminations occurred at TC1 and TC2 about 1.5 seconds prior to failure which ultimately took place when the face sheet completely delaminated from the core, and lost contact with TC3 at that time.

For this series of tests, no mechanical preload was applied to the samples during exposure to radiant thermal energy. Instead, following thermal exposure each sample was allowed to completely cool back down to room temperature, and then was subjected to a gradually increasing mechanical load (using the same test fixture, but without radiant thermal energy exposure) until structural failure of the sample was achieved. The post-pulse failure load was recorded and compared to a typical untested sample's ultimate strength (determined to be 75 pounds, as noted previously) in order to ascertain the post-exposed sample's percentage of "retained strength". The concept of retained strength provides a measure of structural load carrying capability for materials which have been "degraded" as a result of radiant thermal energy exposure.

Each of the nine samples tested in this series was exposed to a "shaped" radiant thermal energy pulse with a total fluence of between 10.1 and 32.8 cal/cm^2 and a duration of seven seconds, simulating the thermal pulse from a one megaton weapon yield. Figures F-1 through F-9 (Appendix F) show the flux time histories and time integrals (fluence) for each test sample in this series.

The results from tests in this series are given in Table 5-7. Note that the TRAC sample numbers are not in numerical order, but instead are presented in the order of increasing fluence to make comparisons among them more convenient. Photographs of the failed test samples, presented in Figures F-10, F-11 and F-12 (Appendix F), are also arranged in this same order. It is important to note that in contrast to the data presented in Table 5-6, none of the samples in Table 5-7 failed in the "DELAM" mode. It is postulated that the loss in bond strength between the face sheet and core due to softening of the adhesive during thermal exposure is, to a great extent reversible, so that after cooling the bond strength "recovers" back to near its original condition. During this series of tests there was no mechanical load applied while the adhesive was in its "soft" state, therefore no delamination was initiated. In laboratory tests conducted at room temperature, a delamination type failure has never been observed. The fibers of the face sheets themselves are the weakest link, and normally the side in compression fails by buckling. However, on rare occasions a failure on the tension (back) side occurs, usually initiated at one of the thermocouple installation locations. This is what happened to TRAC sample #20, hence the notation "Backface" for the failure mode of this sample.

Table 5-7. Results from no preload/shaped pulse tests.

SAMPLE	PEAK INCIDENT FLUX	TOTAL FLUENCE	POST-PULSE	FAILURE	SMOKE	POST-TEST PAINTED	TEMP. AT END OF PULSE (°F)		
IDENTIFICATION	LEVEL (cal/sq cm-sec)	(cal/sq cm)	FAILURE LOAD	MODE	DURING TEST?	SURFACE APPEARANCE	T/C 1	T/C 2	T/C 3
GREY #11	4.4	10.1	76 lbs	FSPB	NO	No Visible Degradation	155	134	160
GREY #12	6.9	16.7	50 lbs	FSPB	YES	Lt. Char, Hvy. Blistered	169	166	136
GREY #13	7.8	17.8	56 lbs	FSPB	YES	Mod. Char, Hvy. Blistered	164	154	111
TRAC #20	4.6	10.7	85 lbs	Backface	NO	Moderately Bleached	131	111	131
TRAC #22	5.8	12.8	82 lbs	FSPB	NO	Moderately Bleached	137	112	130
TRAC #21	6.9	15.9	86 lbs	FSPB	NO	Moderately Bleached	132	142	162
TRAC #15	10.8	20.5	90 lbs	FSPB	NO	Moderately Bleached	No T/C's Installed on this Sample		
TRAC #23	12.5	29.0	71 lbs	FSPB	YES	Mod. Bleached & Blistered	182	161	155
TRAC #24	14.0	32.8	62 lbs	FSPB	YES	Lt. Char, Hvy. Blistered	191	194	180

It is also important to note that the post-pulse failure loads for the first four TRAC samples listed in Table 5-7 are significantly above the "nominal" virgin sample strength of 75 pounds, and that only those samples (including the grey samples) that produced smoke and blisters as a result of thermal exposure exhibited significant post-exposure retained

strength degradation. The association between the production of smoke and blisters and reduced retained strength is certainly a logical one, but a lack of smoke and blisters should not necessarily imply that no degradation has occurred. The apparent "increase" in strength observed for TRAC sample #'s 20, 22, 21 and 15 remains unexplained at this time.

Plots of thermocouple response as a function of time for each sample (except for TRAC sample #15) during and after test are given in Figures F-13 through F-20 (Appendix F). The plots indicate that in most cases, the temperatures measured at the end of the pulse (reported in Table 5-7) were equal to or only slightly below the peak measured temperatures.

In this final series of tests, a mechanical preload of either 19 or 38 pounds (which corresponds to 25 and 50% of the sample's ultimate strength) was applied to each of the seven samples during exposure to a seven second duration shaped pulse with a total fluence between 7.9 and 23.5 cal/cm^2. Total fluence values of the incident thermal pulses were chosen in order to "bracket" the fluence to failure of grey and TRAC coated samples subjected to the aforementioned mechanical preloads. Samples that did not fail during radiant thermal energy exposure were allowed to cool back down to room temperature and were then subjected to a gradually increasing mechanical load (as in the previously described series of tests conducted with no mechanical preload) until structural failure of the sample was achieved. The post-pulse failure load was recorded and compared to a typical untested sample's ultimate strength (determined to be 75 pounds, as noted previously) in order to ascertain the post-exposed sample's percentage of "retained strength".

The results from tests in this series are given in Table 5-8. Note once again that the samples are not shown in numerical order but rather are grouped by coating type (grey or TRAC) and mechanical preload (19 or 38 pounds). In each group we have at least one sample that did not fail during thermal exposure, and one that did, thus "bracketing" the fluence to failure for each group. In Figures G-1 through G-7 (Appendix G) the flux and fluence time histories are shown for the samples that did not fail during thermal exposure (grey sample #'s 14 and 17 and TRAC sample #'s 25 and 26), and the sample end deflection and total fluence as a function of time plots are shown for the samples that did fail during thermal exposure (grey sample #'s 15 and 16 and TRAC sample #16). Photographs of all seven samples, grouped together as in Table 5-8, are shown in Figures G-8, G-9 and G-10 (Appendix G).

Table 5-8. Results from combined mechanical preload/shaped pulse tests.

SAMPLE IDENTIFICATION	PEAK INCIDENT FLUX LEVEL (cal/sq cm-sec)	PRELOAD (lbs)	TIME TO FAILURE (sec)	FLUENCE TO FAILURE (cal/sq cm)	TOTAL FLUENCE (cal/sq cm)	POST-PULSE FAILURE LOAD	FAILURE MODE	SMOKE DURING TEST?	POST-TEST PAINTED SURFACE APPEARANCE
GREY #14	5.8	19	Did Not Fail During Pulse		11.1	90 lbs	FSFB	NO	Lightly Blistered
GREY #15	5.7	19	5.90	10.6	10.7	Failed During Pulse	DELAM	YES	Moderately Blistered
GREY #17	3.7	38	Did Not Fail During Pulse		7.9	93 lbs	FSFB	NO	No Visible Degradation
GREY #16	4.9	38	3.35	8.8	12.5	Failed During Pulse	DELAM	NO	Lightly Blistered
TRAC #25	8.7	19	Did Not Fail During Pulse		16.0	85 lbs	FSFB	NO	Moderately Bleached
TRAC #26	12.1	19	Did Not Fail During Pulse		21.9	63 lbs	FSFB	YES	Heavily Bleached
TRAC #16	12.3	19	5.90	23.2	23.5	Failed During Pulse	DELAM	YES	Lt. Char, Hvy. Blistered

Comparing the data for tests of grey sample #'s 14 and 15, we see that #14 actually "survived" a higher fluence (11.1 cal/cm^2) than #15 which failed at 10.6 cal/cm^2. It is also interesting to note that grey sample #14 produced no smoke and had slightly less visible post-test surface degradation than grey sample #15. This apparent anomaly is probably due to small sample to sample variations which can easily contribute to test data scatter. In any case, it seems reasonable to conclude that the "failure threshold" for this sample type/test condition combination is approximately 11 cal/cm^2. This result is in close agreement with test data reported in Table 5-4 of Section 5.4.4.1, where grey samples with the same applied preload failed at 11.0, 12.3 and 11.7 cal/cm^2 when subjected to constant flux level thermal pulses.

For grey sample #'s 16 and 17 the results are clearer. These two tests employed a 38 pound (50% of ultimate) mechanical preload instead of the 19 pound load which was applied to grey sample #'s 14 and 15. The result was that the failure threshold was reduced from approximately 11 cal/cm^2 down to somewhere between 7.9 and 8.8 cal/cm^2. This result is also in very good agreement with previously reported test data, where grey samples loaded to 38 pounds failed at 7.8 and 8.1 cal/cm^2 when subjected to constant flux level thermal pulses. One additional point of interest are the thermocouple response curves shown in Figures G-11 and G-12 (Appendix G). Grey sample #16's response clearly shows the drop in response that is associated with delamination of the face sheet, whereas the response for grey sample #17 (which did not fail during the pulse) exhibits a continuous, smooth temperature rise throughout the pulse duration. Close inspection also reveals that both samples responded identically (same temperature rise as a function of time) during the first three seconds of thermal exposure.

A comparison of the data from tests of TRAC sample #'s 25, 26 and 16 indicates a failure threshold of between 21.9 and 23.2 cal/cm^2. This is considerably below the fluence to failure values of 34.0, 34.6, 41.9 and 41.5 cal/cm^2 reported in Table 5-4 of Section 5.4.4.1 for TRAC samples loaded to 19 pounds while exposed to constant flux level pulses.

Also from Table 5-8 we can see that TRAC sample #26 suffered some degradation in retained strength, (63 pounds = 84% of the assumed 75# pre-test strength) and produced smoke during exposure, as compared to TRAC sample #25 which produced no smoke and failed at 85 pounds.

It is important to note that all of the samples (grey and TRAC) in this series of tests that failed during radiant thermal energy exposure failed in the DELAM mode, whereas all of the others, which were mechanically loaded to failure after cooling, failed by face sheet fiber buckling (FSFB). This is particularly significant in that it implies that the observed failure mode is highly influenced by the test method or "sequence of events". And again, as was noted from the data presented previously in Table 5-7, several samples which did not fail during thermal exposure which were mechanically loaded after cooling required loads well in excess of the 75 pound "nominal" virgin sample strength to cause failure. The apparent "increase" in strength observed for grey sample #'s 14 and 17 and TRAC sample #25 remains unexplained at this time.

5.4.4.4 Conclusions from the September 27 - October 1 Test Results. The intent of this series of tests was to investigate sample behavior at low preloads while exposed to radiant thermal flux levels of approximately 10 cal/cm^2-sec. This was done in an attempt to "extend the envelope" of known sample response to simultaneous mechanical and thermal loading. Previous tests, described in Section 5.4.4.1, investigated sample behavior at preloads corresponding to 25, 50 and 75% of the sample's ultimate strength. It was observed, as one would expect, that the time to failure and resulting fluence to failure of any particular specimen type (white, grey, black or TRAC) increases as the mechanical preload is decreased. Taking this concept to the extreme, when no preload is applied, the time to failure becomes infinite. When low preloads (on the order of 10% of ultimate) are applied, times to failure are quite long, and the results are quite variable. As we have seen from the test data, these test conditions result in delamination type failures which are highly sensitive to face sheet to core bond integrity. If this integrity varies from sample to sample, which is the case in all composite laminate materials to some extent, the test results will inherently be variable. Therefore it is not surprising that the data from these tests does not exhibit the high degree of consistency that was attained in previous tests conducted with higher preloads. If, however, we average the fluence to failure values together for each specimen type (color), we can conclude that for these test conditions the fluence to failure for TRAC coated samples is, on average, 45% higher than the fluence to failure for grey or black samples. This increase in thermal hardness provided by the TRAC coating under these

low preload test conditions is considerably smaller than has been demonstrated under higher preload test conditions (as shown in Table 5-5 of Section 5.4.4.2). When comparing to white samples, we find that the fluence to failure values for TRAC samples are approximately 65% of those for white samples. This comparison is generally consistent with what has been observed from previous tests.

The objective of this series of tests was to investigate and evaluate the effect of radiant thermal energy exposure on samples without mechanical preloads applied during exposure. It was postulated that any degradation in mechanical properties that had resulted from radiant thermal energy exposure would be evidenced in the form of reduced post-exposure breaking strength, which we refer to as "retained strength. However, as was shown in the test results (Section 5.4.4.3), several of the TRAC samples actually demonstrated an apparent increase in strength following thermal exposure, for which no logical explanation has been proposed.

If we overlook this anomaly for the moment and consider these particular samples to have simply experienced no loss in retained strength, we can draw some important conclusions from the test data. Compared to the previously determined unexposed sample strength of 75 pounds, it appears that for grey samples, no loss in strength results from a 10 cal/cm^2 exposure, and that a loss in strength of between 25 and 33% results from a 16 to 18 cal/cm^2 exposure. For TRAC samples an exposure to 20 cal/cm^2 or less results in no loss of strength, approximately 5% degradation results from a 29 cal/cm^2 exposure, and approximately 17% degradation results from a 33 cal/cm^2 exposure. A comparison between grey and TRAC samples suggests that the TRAC samples have at least twice the thermal hardness of the grey samples when tested under these conditions. It must be kept in mind that these particular conclusions apply specifically to seven second duration shaped pulses only, and would most likely be significantly different for constant flux level pulses or shaped pulses of other durations.

This series of tests was successful in determining the critical total fluence threshold values of a seven second shaped pulse which will cause failure of a grey sample loaded to 25 or 50% of its ultimate load capacity, and of a TRAC sample loaded to 25% of its ultimate load capacity. The failure threshold fluence values for grey samples subjected to seven second shaped pulses were found to be consistent with those measured for constant flux level pulses performed in earlier tests. For TRAC samples however, the measured shaped pulse threshold fluence was

approximately 40% lower than the constant flux pulse threshold fluence measured previously for the same mechanical load condition. Upon comparing threshold values determined from these tests for grey and TRAC samples, we see that the TRAC samples have roughly twice the thermal hardness of grey samples when subjected to the same mechanical load condition (19 pound preload). This two to one improvement factor is consistent with the results from the no preload/shaped pulse tests.

One somewhat surprising result of the tests conducted in this series is that samples which were subjected to thermal pulses near their failure threshold yet remained intact exhibited either only slightly less (in the case of TRAC sample #26) or "increased" retained strength upon cooling after exposure. This phenomenon was also observed during the no preload/shaped pulse tests.

SECTION 6
SUMMARY AND RECOMMENDATIONS

6.1 INTRODUCTION.

PDA Engineering has developed a Thermoreactive Aircraft Coating (TRAC) which appears dark in the visible light range under benign conditions, yet becomes highly reflective to radiant energy under conditions of thermal flux exposure. When the TRAC system is used in place of conventional paint it can provide aircraft or other weapon systems with the thermal hardness benefits of a white coating while retaining a dark camouflage color under benign conditions, thus providing reduced vulnerability for weapons systems and crew operating in a nuclear threat environment.

The TRAC system, which can be applied by conventional spray techniques, consists of a white, heat reflective primer topcoated with a passively reactive, thermally activated coating which reversibly changes from dark grey to white when the coating's temperature exceeds a designed transition temperature. By setting the designed transition temperature for the coating to a level just above the standard operating temperature for an aircraft's external surfaces, the TRAC coated surfaces are effectively protected from large additional temperature increases and resultant degradation from incident fireball radiation by significantly reducing the fraction of thermal energy absorbed by those surfaces. The increased thermal hardness benefits afforded by the TRAC system are particularly well suited for application to composite materials where rapid temperature rises in thin, dark colored (camouflage) skins bonded to insulative cores can result in structural failure at fairly low fluence levels.

6.2 COATING DEVELOPMENT.

As noted above, the TRAC system consists of a two layer coating. The undercoat is a highly reflective, white epoxy primer which was selected from a wide range of candidate materials on the basis of highest broadband reflectivity (as measured at the White Sands Solar Facility) and compatibility with the thermoreactive topcoat as well as the primary candidate substrate materials (aluminum and composites). The thermoreactive topcoat consists of microencapsulated thermoreactive pigment particles dispersed in a clear, water-reducible polyurethane

binder material. The selected binder material is a product of Miles Laboratories which was formulated to meet the requirements of this program. These requirements included compatibility with the microencapsulated pigment material as well as conformance to the dry film properties specified in MIL-C-85285. Both topcoat and primer are formulated for application with conventional paint spraying equipment.

The majority of the development effort conducted under this program focused on the thermoreactive pigment formulation and the microencapsulation process. Because the pigment is the key and only "active" ingredient in the system, its properties have the greatest influence on the entire system's performance. Principal properties of the pigment include its benign state color, heated state color and transition temperature. For this program, a dark grey (5 to 10% visible light reflectance) benign state color was chosen to be representative of a "dark camouflage" color. A clear to translucent white heated state color is necessary for maximum radiant energy rejection (to expose the white, heat reflective undercoat), and a transition temperature in the range of 85 to 105°C was selected for the "baseline" coating which was evaluated during thermal testing. It is important to note that these three principal properties can all be varied, fairly independently from one another, in order to tailor the thermoreactive coating to satisfy various end-users' different application requirements. For example, nearly any desired benign state color can be created from the five basic dyes which were formulated; black, blue, green, orange and red, and transition temperatures can be varied from below room temperature up to approximately 150°C.

The processing sequence for production of a pigment for incorporation into a thermoreactive coating is to reduce the bulk thermoreactive pigment material down into discrete particles with a size in the range of 5 to 25 microns, microencapsulate the particles in a solvent-resistant polymeric coating, and then disperse the microencapsulated material into the selected solvent-based paint binder. To optimize the solvent resistance of the microcapsules, spherical shaped particles are required, and to facilitate the microencapsulation process, a dry powder or aqueous suspension is desired. These objectives were ultimately achieved, but only after numerous difficulties were overcome through considerable effort and ingenuity.

The task of reducing the bulk pigment into particles was first approached through traditional methods such as emulsification, solvent dispersion and cryogenic grinding. For a variety of reasons, all of these

methods produced only limited success and were generally unsatisfactory. Modification of a conventional spray drying process ultimately proved to be the preferred method of particle formation. In cooperation with Yamato Scientific, a process and supporting apparatus was developed to successfully atomize the heated, liquified pigment material into droplets which when cooled, comprised a powder with the desired attributes. The apparatus was purchased from Yamato, and after further modifications and process optimization, produced sufficient size batches of material to satisfy all subsequent requirements in support of this program.

Due to the extreme sensitivity of the thermochromic pigment chemistry to the solvent system and polymer components of all of the candidate paint binders, microencapsulation of the pigment is required for protection of the pigment from these elements of the coating system. The aggressive solvent characteristics of binder materials which possessed the required dry film properties (polyurethanes) dictated the need for an extremely low permeability microcapsule wall material. As was the case for the particle formation task, much experimental work was required to select, develop and optimize the encapsulation material and process. A determination was made that no single capsule wall material successfully met all of the requirements. The solution to this problem was a dual wall coating consisting of a melamine-formaldehyde inner wall overcoated with a vapor deposited wall of parylene.

Concurrent with and as part of the pigment formulation and binder development tasks was the UV stabilization of both the pigment and the binder. The environmental durability or weatherability of organic pigments and polymeric coatings is critically dependant on their ability to resist the degradational effects of long term exposure to sunlight (ultraviolet light in particular). Much experimental work was conducted in the laboratory with a wide range of commercially available UV stabilizers including UV absorbers, benztriazoles, hindered amine light stabilizers and hindered phenolic antioxidants. A large number of samples employing various combinations of these stabilizers was subjected to screening tests in an accelerated aging chamber. The most successful combinations were identified and further optimized. Although the addition of the selected UV stabilizers greatly improved the weatherability of the unstabilized pigment and binder, further effort in this area is recommended for extending the TRAC system useful lifespan.

6.3 TEST RESULTS.

Specialized test methods and apparatus developed in support of this program were used to evaluate TRAC component and system performance. The majority of testing in support of coating formulation development was performed in the PDA laboratory. These tests included spectral analysis of thermochromic dyes and carrier materials, measurements of transition temperature, spectral and luminous reflectance and transmittance of reflective undercoats and thermoreactive topcoats, and evaluation of candidate coating systems under accelerated aging (weathering) conditions. Broadband reflectance measurements of candidate reflective undercoats was performed at the White Sands Solar Facility, and a small amount of other testing, such as particle size analysis was performed at outside laboratories.

Preliminary screening tests of candidate coating thermal performance were conducted on the PDA Xenon Light Test Bench (XLTB). Using a 1000 Watt focused high pressure xenon arc lamp as the radiant energy source, the XLTB provides a laboratory-based simulation of the nuclear fireball thermal radiation environment. The backface temperature response (rise rate) of coated aluminum and composite samples was measured in this simulated nuclear thermal threat environment in order to evaluate coating effectiveness in protecting the substrate from thermally induced degradation.

The overall effectiveness of the baseline TRAC system was demonstrated through tests of white, grey, black and TRAC coated test samples constructed from composite/honeycomb sandwich material, simulating aircraft skin, which were subjected to combined radiant thermal energy exposure and simultaneous mechanical loading. This testing was conducted at the National Renewable Energy Laboratory (NREL) High Flux Solar Furnace using a unique test apparatus specifically built for this purpose. These tests were the first of their kind in that they provided a direct simulation of stressed aircraft skin exposed to a radiant thermal energy pulse. Test conditions employed various levels of mechanical preload and incident flux, using both rectangular (constant flux vs. time) and nuclear "shaped" thermal pulses.

The test results provide clear evidence of the effects of surface coating color and mechanical load on composite hardness in a thermal pulse environment. Both the mechanical preload level (stress) and coating reflectivity were shown to have a large effect on survivability under thermal loading. Two distinctly different failure modes for the composite

test samples were observed, and the critical thermal environment as a function of coating color and mechanical load was established for the tested sample configuration.

Test results indicate that, compared to comparably painted grey samples, the TRAC system provides up to a 443% improvement in thermal hardness, and is up to 98% as effective as gloss white paint in protecting the composite substrate from damage induced by radiant thermal energy exposure.

6.4 RECOMMENDATIONS.

6.4.1 Formulation Modifications.

As the test results clearly indicate, the use of the TRAC system on aircraft or other weapon systems with nuclear missions provides for dramatic opportunities in increasing the hardness and survivability of such systems. However, in its current state, some reformulation of the coating will be required for the TRAC system to meet all of the requirements of a Mil-Spec qualified exterior coating for aerospace vehicles. It is recommended that additional effort be spent on UV stabilization of the pigment and binder in order to increase the coating's resistance to environmental degradation, thus extending its useful lifespan. Bleaching of the thermochromic system, resulting in partial permanent loss of color in the benign state, which has been observed to some degree after transition to the heated state, may be significantly reduced or eliminated through changes in the binder's solvent components and/or improvements in the integrity and solvent resistance of the pigment particles' microcapsule walls. Optimization of the reflective undercoat to increase its broadband reflectivity may also have the potential of further enhancing the overall TRAC system effectiveness. And of course, a wide range of benign state colors will be required to satisfy the requirements of various potential end-users, which can be made available through the incorporation of existing alternate colored thermochromic dyes.

6.4.2 Additional Combined Thermal-Mechanical Testing.

The data presented in this report illustrates the usefulness of the combined thermal-mechanical test technique for the determination of material response to nuclear thermal threat environments. The effects of changing design variables such as skin material, thickness, lay-up pattern, core material, core density, core thickness, core-skin adhesive, paints and

coatings can be easily evaluated. Test results can be used to produce plots of the effects of material and design variables on thermal hardness, which can then be used to refine aircraft designs for optimum strength/weight/thermal hardness tradeoffs. Validation of widely used nuclear response codes such as TASL and TRAP can also be accomplished once a comprehensive database has been generated from combined thermal-mechanical tests on a wide variety of aircraft structural materials.

The portability of the test apparatus lends itself to utilization in other test facilities and environments. For instance, simultaneous or sequential mechanical loading combined with high energy laser exposure is also possible and may be of considerable interest. Another possibility would be to conduct standard "benchmark" tests at different nuclear weapons effects simulation facilities in order to get a comparison among the various test facilities and simulated threat environments.

In summary, a very versatile yet straightforward new test technique has been demonstrated for evaluating the behavior of a wide array of structural materials upon exposure to a nuclear threat environment. It is recommended that this potential be fully exploited in order to establish a comprehensive materials response database which would serve as a valuable resource to the aerospace design and analysis communities.

SECTION 7
REFERENCES

1. Oeding, R. G., J. C. Schutzler and K. E. Jechel, "Evaluation of Thermal Radiation Effects on Cockpit Materials," (Unclassified) PDA TR-1087-30-03; DNA TR-85-395; 31 December 85. (Unclassified).

2. Jechel, K. E. and J. C. Schutzler, "Flight Evaluation of a Passive Thermal Protection System for Cockpit Transparencies," (Unclassified) Final Report PDA TR-1618-00-05; DNA-TR-84-44, December 1983. (Secret).

3. Schutzler, J. C. and K. E. Jechel, "A Passive Thermal Protection System (PTPS) for the B-1B Forward Cockpit," (Unclassified) Report DNA-TR-87-217, 30 July 1987. (Unclassified).

4. J. Comyn, "Polymer Permeability," (Unclassified) Elsevier Applied Science Publishers, London, 1986, pp. 315-321. (Unclassified).

5. "White Sands Solar Furnace Experimenter's Guide," (Unclassified) Nuclear Weapon Branch, White Sands Missile Range, 1977. (Unclassified).

6. Bingham, C., and A. Lewandowski, 1991, "Capabilities of SERI's High Flux Solar Furnace," (Unclassified) *Proceedings of the 1991 ASME/JSME/JSES International Solar Energy Conference*, pp. 541-545. (Unclassified).

7. "Interim Report, Nuclear Thermal Effects Testing Capabilities of the National Renewable Energy Laboratory Solar Furnace," (Unclassified) prepared under DNA contract DNA001-89-C-0066 by PDA Engineering, 5 February 1993. (Unclassified).

8. "Nuclear Blast/Thermal Vulnerability Assessment of the VH-60 Helicopter," (Unclassified) DNA TR 89-88, (ADC 045763), January 1990. (Secret).

9. Schutzler, J. C., "Preliminary Design of Constant-Stress Test Specimen for Thermal Effects Evaluation of Aircraft Composite Materials," (Unclassified) PDA IRAD TM 90-4469-00-306, 30 June 1990. (Unclassified).

10. Schutzler, J. C., "Recommended Baseline Composite Material for TRAC Evaluations," (Unclassified) PDA TM 91-1161-06, 7 October 1992. (Unclassified).

11. Gilliam, R. Pat, "Constant Stress Sandwich Beam Flexural Test Specimen Evaluation," (Unclassified) Informal Report, June 1990. (Unclassified).

12. Schutzler, J. C., "Design and Fabrication of a Fixture for Composite Materials Testing," (Unclassified) PDA IRAD TM 92-4646-00-329A, 30 June 1992. (Unclassified).

13. "Test Plan: Validation of Flex Beam Test Method for Thermoreactive Aircraft Coatings Program," (Unclassified) prepared under DNA contract DNA001-89-C-0066 by PDA Engineering, 23 October 1992. (Unclassified).

14. Schutzler, J. C., "Analytical Method for Prediction of the Stress, Strain and Deformation Responses of a Composite Flexure Beam," (Unclassified) PDA IRAD TM 92-4646-00-329B, 30 June 1992. (Unclassified).

15. "Interim Report, Preliminary Test Results from a New Method for Thermal Effects Evaluation of Aircraft Composite Materials," (Unclassified) prepared under DNA contract DNA001-89-C-0066 by PDA Engineering, 31 March 1993. (Unclassified).

16. "Interim Report, Test Results from a New Method for Thermal Effects Evaluation of Aircraft Composite Materials," (Unclassified) prepared under DNA contract DNA001-89-C-0066 by PDA Engineering, 31 August 1993. (Unclassified).

17. "Interim Report, Additional Test Results from a New Method for Thermal Effects Evaluation of Aircraft Composite Materials," (Unclassified) prepared under DNA contract DNA001-89-C-0066 by PDA Engineering, 13 December 1993. (Unclassified).

APPENDIX A

SYSTEM SPECIFICATION FOR THERMOREACTIVE AIRCRAFT COATINGS

This system specification serves as a Product Function Specification for the thermoreactive aircraft coating system. This draft specification, which addresses the requirements of a wide variety of candidate military end-users, was used as a guideline for development and evaluation of the thermoreactive coating system developed under this program. Copies of this draft specification were sent to the candidate end-user representatives listed in Section 3.2 of this report.

A.1 DEFINTION.

The purpose of a Thermoreactive Aircraft Coating is to provide thermal protection for painted aircraft surfaces in the event of a nuclear fireball encounter while retaining a camouflage color scheme. Typical dark camouflage colors absorb most of the incident thermal energy and are damaged by the resulting temperatures. A thermoreactive coating will change to a reflective state at a predetermined transition temperature, thereby limiting further temperature increases. As the intensity of the incident radiant energy decreases, the temperature will drop below the transition level, and the coating will return to its camouflage color scheme.

The term "colored-state" refers to the camouflage color of the coating under benign conditions. "Reflective-state" describes the coating above the transition temperature. The "transition temperature" is the temperature at which the coating makes the change from camouflage to reflective or reflective to camouflage.

Activation of the thermoreactive coating shall be completely passive and self-contained, and will occur only as function of the coating temperature. The return to the colored-state shall be similarly passive and temperature dependent.

A.2 APPLICABLE DOCUMENTS.

The following documents may be used to define the characteristics of the thermoreactive coating system, its components and test procedures.

SPECIFICATIONS

Federal

TT-N-95	Naptha, Aliphatic
TT-P-143	Paint, Varnish, Lacquer and Related Materials; Packaging, Packing, and Marking
TT-S-735	Standard Test Fluids; Hydrocarbon
TT-T-291	Thinner: Paint, Volatile Mineral Spirits

Military

MIL-C-18263	Color, Exterior, Naval Aircraft: Requirements for
MIL-C-22750	Coating, Epoxy, VOC Compliant
MIL-C-46168	Coating, Aliphatic Polyurethane, Chemical Agent Resistant
MIL-C-83286	Coating, Urethane, Aliphatic Isocyanate, for Aerospace Applications
MIL-C-85285	Coating, Polyurethane, Aliphatic, Weather Resistant, Low Infrared Reflective
MIL-F-7179	Finishes and Coatings: Protection of Aerospace Weapons Systems, Structures and Parts; General Specification for
MIL-F-18264	Finishes, Organic, Weapons Systems, Application and Control of
MIL-P-23377	Primer Coating; Epoxy, Chemical and Solvent Resistant
MIL-P-52192	Primer Coating, Epoxy

MIL-P-53022	Primer, Epoxy Coating, Corrosion Inhibiting, Lead and Chromate Free
MIL-P-53030	Primer Coating, Epoxy, Water Reducible, Lead and Chromate Free
MIL-P-85582	Primer Coatings, Epoxy, VOC Compliant, Chemical and Solvent Resistant
MIL-R-7705	Radomes, General Specifications for
MIL-T-81772	Thinner, Aircraft Coating

STANDARDS

Federal

FED-STD-595	Colors
FED-STD-141	Paint, Varnish, Lacquer, and Related Materials; Method of Inspection, Sampling, and Testing

Military

MIL-STD-105	Sampling Procedures and Tables for Inspection by Attributes
MIL-STD-109	Quality Assurance Terms and Definitions
MIL-STD-129	Marking for Shipment and Storage

American Society of Testing Materials (ASTM)

B-117	Salt Spray (Fog) Testing
D-185	Coarse Particles in Pigments and Paints
D-523	Specular Gloss, Standard Test Method
D-562	Standard Test Method for Consistency of Paints
D-1210	Fineness of Dispersion of Pigment-Vehicle Systems
D-1296	Odor of Volatile Solvents and Diluents, Standard Test for
D-1308	Test Method for Effects of Pigments
D-1475	Density of Paint, Varnish, Lacquer, and Related Products, Test Method for
D-1544	Color of Transparent Liquids (Gardner Color Scale)
D-1640	Drying, Curing or Film Formation of Organic Coatings at Room Temperature
D-1729	Practice for Visual Evaluation of Color Differences of Opaque Materials
D-1738	Hiding Power of Nonchromatic Paints
D-1849	Package Stability of Paints, Standard Test Method for
D-2197	Adhesion of Organic Coatings
D-2244	Color Differences of Opaque Materials
D-2267	Method of Test for Aromatics in Light Napthas, Reformates, and Gasolines by Gas Chromatograpy
D-2369	Volatile Content of Paints, Standard Test Method for
D-2805	Hiding Power of Paints, Standard Test Method for
D-3951	Standard Practices for Commercial Packaging
D-3960	Volatile Organic Content of Paints and Related Coatings
E-97	Directional Reflectance Factor, 45°, 0°, of Opaque Specimens by Broad Band Filter Reflectometry
E-308	Spectrophotometry and Description of Color in CIE 1931 System, Standard Recommended Practice for

A.3 CHARACTERISTICS OF THE THERMOREACTIVE COATING SYSTEM.

Military Specifications for primer materials include MIL-P-23377, MII-P-52192, MIL-P-53022, MIL-P-53030, and MIL-P-85582. Specifications for topcoats include MIL-C-22750, MIL-C-46186, MIL-C-83286, MIL-C-85582, MIL-F-7179 and MIL-F-18264. These specifications will be used as guidelines for the development of the thermoreactive coating systems. Specifically, design will be focused on the characteristics required in MIL-P-23377 and MIL-P-85582 (high and low VOC epoxy primers) and MIL-C-83286 and MIL-C-85285 (high and low VOC topcoats), as these are the materials currently specified for most military aircraft applications.

A.3.1 Application Characteristics.

The goal of this program is to develop a thermoreactive coating which will meet the application requirements of a conventional primer/topcoat system. Requirements for drying time, pot life, viscosity, weight per gallon and volatile organic content will be established from MIL-C-83286, MIL-C-85285, MIL-P-23377 and MIL-P-85582. The nature of the thermoreactive pigments may necessitate changes in other characteristics as follows:

Thermoreactive materials may not be compatible with the process of pigmenting the polyester resin, and therefore may be added to the system during mixing in either component, in a separate solvent (component C), or as a pigment powder. This may affect the mixing procedure, dilution ratio, condition in the container and/or storage stability of the thermoreactive coating system. In the event of any change, the revised procedure shall be feasible for large scale production and application, and shall be fully tested and documented to ensure that the materials will function as intended.

A.3.2 Film Properties - Physical.

Once the coatings are applied to the substrate, they shall function according to the physical requirements of MIL-C-83286, MIL-C-85285, MIL-P-23377 and MIL-P-85582 for all conditions below the transition temperature as defined in Section 4.1. This includes characteristics such as adhesion, lifting, flexibility, and resistance to weathering, fluids, humidity and corrosion.

A.3.3 Film Properties - Optical.

All optical properties shall apply to the coating system when tested below the transition temperature as defined in Section 4.1.

A.3.3.1 Color. Initial development of the thermoreactive coatings shall be limited to two colors as specified by FED-STD-595 number 14087 (high gloss olive drab) and 36231 (lusterless dark gray). This is necessary to reduce the initial development time. As the processing becomes established, other colors may be added as necessary to target the requirements of specific applications. In the development stage these standard colors shall be used as guidelines. Actual color is dependent on the availability of thermoreactive materials with the proper spectral absorption characteristics and on the ability to mix thermoreactive systems to achieve a desired color match.

A.3.3.2 Gloss. Both the gloss and lusterless colors shall be examined as discussed in Section 3.3.1. The specular gloss shall be measured in accordance with the methods of MIL-C-83286 or MIL-C-85285.

A.4 PERFORMANCE.

A.4.1 Transition Temperature.

The coating systems described herein shall change from the colored-state to the reflective-state at a temperature between 90°C and 120°C. Below the transition temperature, the color shall not vary significantly as a function of temperature. Above the transition temperature, the coating ceases to function as a camouflage coating.

A.4.2 Activation and Recovery Time.

Transition of the coating between colored-state and reflective-state shall be completely passive, requiring only a change in the temperature of the coating to above or below the transition temperature.

The coating temperature will depend upon the thermal capacity of the substrate, airflow cooling and the ambient temperature in addition to the thermal pulse characteristics and the thermal properties of the coating itself. Recovery to temperature below the transition temperature will be dependent principally upon the airflow cooling and the thermal capacity of the substrate.

Time requirements for transition to the reflective-state can only be established on the basis of thermal performance tests for specific substrates and threat conditions. Consequently, no reaction time for transition from the colored-state to the reflective-state is specified.

The coating is required to transition from the reflective-state to the colored-state within 5 seconds after the temperature of the coating decays to below the transition temperature.

A.4.3 Thermal Performance.

Response of the thermoreactive coating to the thermal flash environment is dependent on the characteristics of the substrate, coating system and the environmental conditions. Therefore, specifications for evaluation of thermal performance under test conditions shall be based upon side-by-side comparisons with conventional coatings applied to identical substrates. The following sections specify requirements for test and evaluation under simulated thermal flash conditions.

A.4.3.1 Test Conditions. All side-by-side tests shall compare conventional coatings to thermoreactive coatings when applied to identical substrates under identical environmental conditions. Substrates of interest include thin gauge aluminum and graphite-epoxy, glass-epoxy, and graphite-polyimide composite materials used in aircraft structures and radomes. Comparisons between the performance of thermoreactive coatings and conventional coatings shall be made on the basis of one or more of the following criteria:

1. Reponse of thermocouples imbedded in the substrate materials.

2. Post-test evaluation of retained properties and/or visual and micrographic examination of thermal-induced damage to the substrate materials.

3. Face sheet failure as indicated by deflection of composite materials tested with applied compressive loading.

Developmental testing shall be done using either a focused xenon lamp source such as the PDA Xenon Light Test Bench or a focused solar arrangement such as White Sands Solar Facility, White Sands Missile Range, New Mexico. Large scale testing shall be done using the Central Receiver Test Facility at Sandia National Laboratories in Albuquerque, New Mexico. Prior to thermal testing, all samples shall be equilibrated to a temperature below the transition point. Incident flux shall not exceed 50 cal/cm^2 sec. and shall not be applied for more than 10 seconds. Total integrated fluence shall not exceed 100 cal/cm^2.

A.4.3.2 Substrate Temperature. The output from imbedded thermocouples shall be monitored on an oscilloscope. The temperature profiles of thermoreactive and conventional coatings shall be compared to determine which systems provide effective substrate temperature control under a given set of conditions.

A.4.3.3 Maximum Deflection Under Load. Coated composite specimens shall be tested under thermal radiation conditions with applied static flexure loading. The thermal flux shall be imposed on the compressive face of the specimen and the deflection monitored during test. The total integrated flux (fluence) applied prior to failure of the specimen, as indicated by rapidly increasing deflection from the original (unheated) position, shall be considered the critical fluence corresponding to a specified applied compressive stress.

Comparison of thermoreactive coating systems to conventional coatings shall be made on the basis of plots of the critical fluence versus applied compressive face sheet stress for identical composite materials.

A.4.3.4 Retained Properties. A visual inspection shall be made of all specimens after thermal testing to check for materials degradation including blistering, charring, peeling, discoloration, melting and other signs of degradation.

In addition, the flexure and compressive properties of some coated substrates may be tested as function of coating system, incident thermal fluence level and environmental conditions. This will be used to establish failure criteria and relative benefits provided by thermoreactive coatings.

A.5 ENVIRONMENTAL.

The thermoreactive coatings systems shall be subjected to the standard environmental tests as specified by MIL-C-83286 or MIL-C-85285.

A.6 QUALITY ASSURANCE PROVISIONS.

All materials shall be subject to Quality Assurance procedures outlined in MIL-C-83286, MIL-C-85285, MIL-P-23377, or MIL-P-85582. Exception shall be taken to any requirements which interfere with the function of the thermoreactive coating system as described in Sections 3.0 and 4.0. At such time as the test methods are better understood, these exceptions shall be documented as formal Quality Assurance Provisions.

APPENDIX B

PARTICLE SIZE DISTRIBUTION DATA

The graphs and tabular data presented in this appendix describe the particle size distribution of the unencapsulated pigment powder produced from the hot atomization process, described in Section 3.3.1.2.4, and the particle size distribution of the dual-wall microencapsulated pigment powder described in Section 3.3.1.5.3. Measurements of the unencapsulated material were made using a Horiba LA-700 laser diffraction particle size analyzer, and measurements of the encapsulated material were performed with a Horiba LA-900 laser diffraction particle size analyzer.

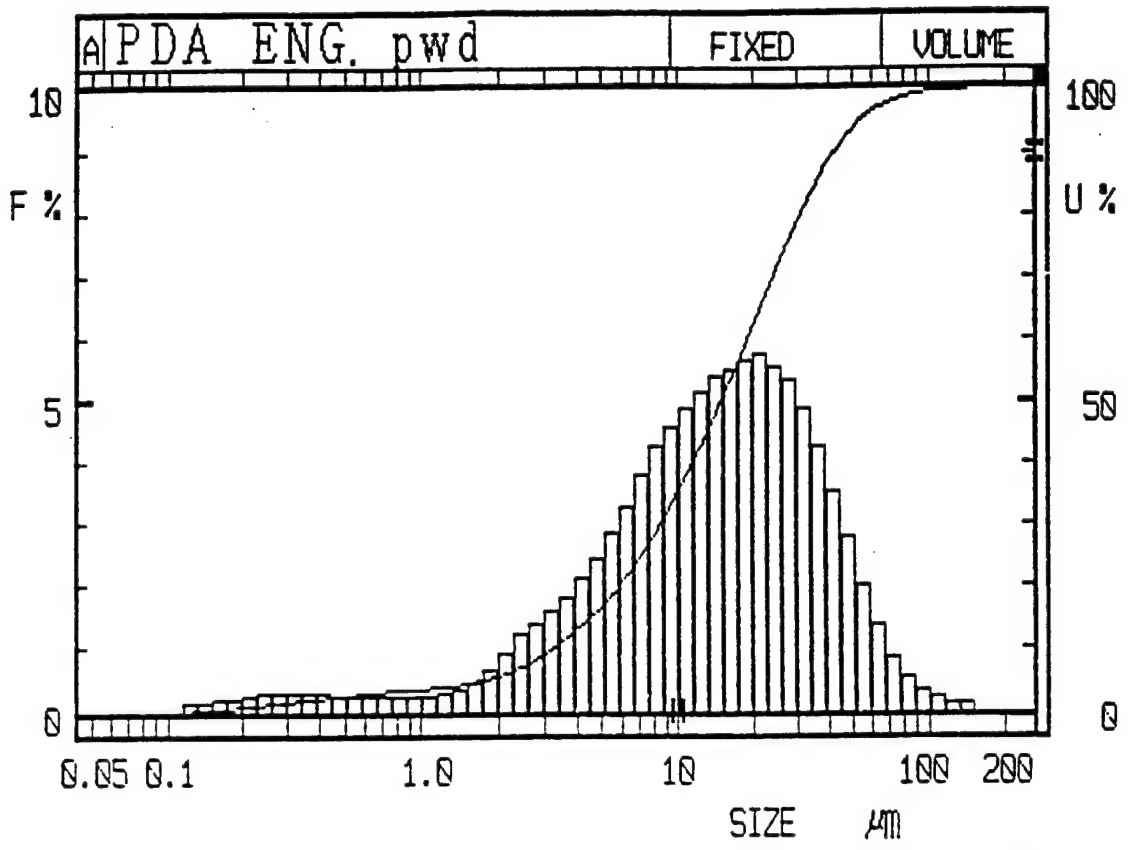

Figure B-1. Particle size distribution graph for the unencapsulated pigment powder.

Table B-1. Particle size distribution for the unencapsulated pigment powder.

DISTRIBUTION TABLE

SEG #	SIZE (μm)	INTVL %	UNDER SIZE%
(01)	262.4	0.0	100.0
(02)	229.1	0.0	100.0
(03)	200.0	0.0	100.0
(04)	174.6	0.0	100.0
(05)	152.4	0.1	100.0
(06)	133.1	0.2	99.9
(07)	116.2	0.2	99.7
(08)	101.4	0.4	99.5
(09)	88.58	0.6	99.2
(10)	77.34	0.9	98.6
(11)	67.52	1.4	97.7
(12)	58.95	2.0	96.4
(13)	51.47	2.8	94.4
(14)	44.94	3.5	91.6
(15)	39.23	4.2	88.1
(16)	34.25	4.9	83.8
(17)	29.91	5.3	79.0
(18)	26.11	5.6	73.6
(19)	22.80	5.8	68.1
(20)	19.90	5.7	62.3
(21)	17.38	5.5	56.6
(22)	15.17	5.4	51.1
(23)	13.25	5.1	45.7
(24)	11.56	4.9	40.6
(25)	10.10	4.6	35.7
(26)	8.82	4.3	31.2
(27)	7.70	3.8	26.9
(28)	6.72	3.2	23.1
(29)	5.87	2.8	19.9
(30)	5.12	2.4	17.1
(31)	4.47	2.1	14.6
(32)	3.90	1.8	12.5
(33)	3.41	1.6	10.7
(34)	2.98	1.4	9.1
(35)	2.60	1.2	7.7
(36)	2.27	0.9	6.5
(37)	1.98	0.7	5.6
(38)	1.73	0.5	4.9
(39)	1.51	0.3	4.5
(40)	1.32	0.3	4.1
(41)	1.15	0.3	3.9
(42)	1.00	0.2	3.6
(43)	0.88	0.2	3.4
(44)	0.77	0.2	3.1
(45)	0.67	0.2	2.9
(46)	0.58	0.2	2.7
(47)	0.51	0.2	2.4
(48)	0.45	0.3	2.2
(49)	0.39	0.3	1.9
(50)	0.34	0.3	1.7
(51)	0.30	0.3	1.4
(52)	0.26	0.3	1.1
(53)	0.23	0.2	0.8
(54)	0.20	0.2	0.6
(55)	0.17	0.2	0.4
(56)	0.15	0.1	0.3
(57)	0.13	0.1	0.1
(58)	0.11	0.0	0.0
(59)	0.10	0.0	0.0
(60)	0.09	0.0	0.0
(61)	0.08	0.0	0.0
(62)	0.07	0.0	0.0
(63)	0.06	0.0	0.0
(64)	0.05	0.0	0.0

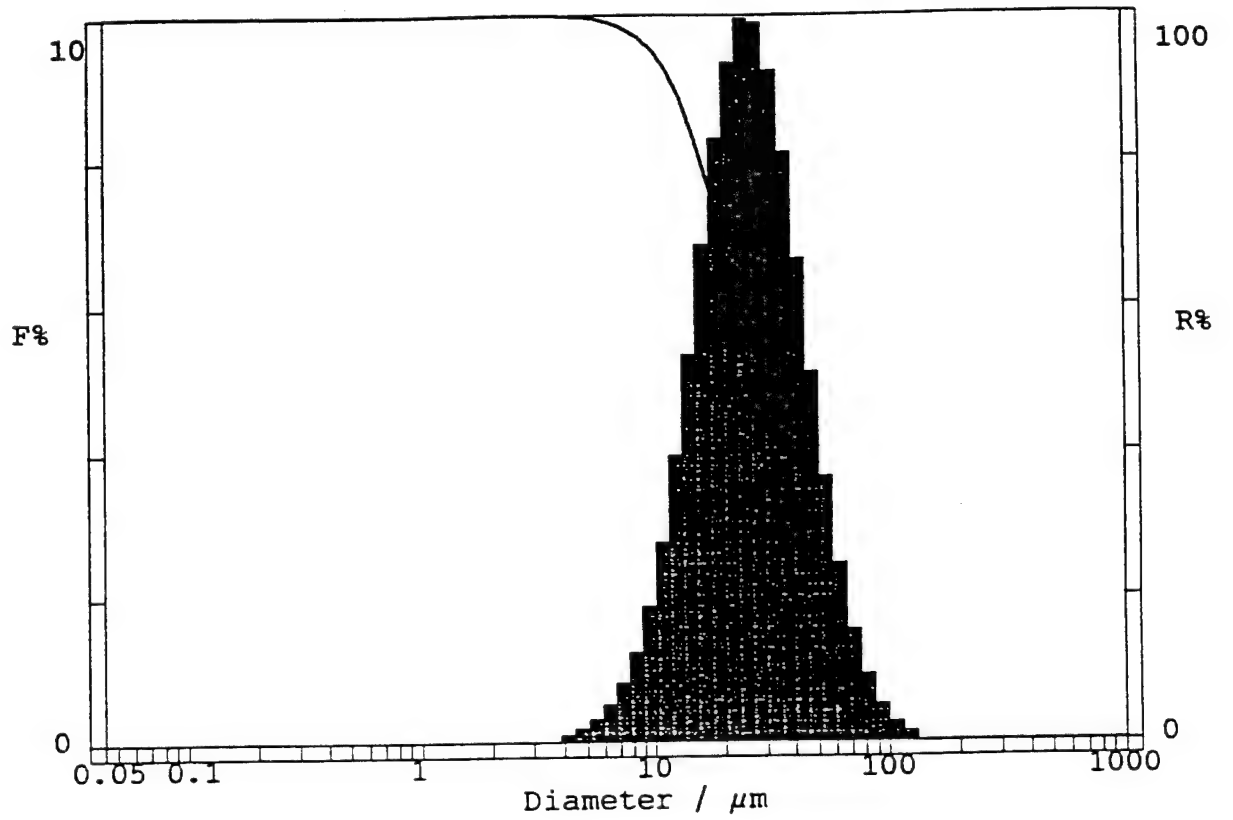

Data:

Median Diameter= 25.573(μm) Specific surface area = 2763cm2/cm3
Standard deviation = 16.706(μm)
Diameter on % [1] 10.0% = 50.790μm
[2] 20.0% = 40.241μm
[3] 30.0% = 33.925μm
[4] 40.0% = 29.329μm
[5] 50.0% = 25.573μm

% on Diameter 70.00μm = 2.9%

Figure B-2. Particle size distribution graph for the dual-wall microencapsulated pigment powder.

Table B-2. Particle size distribution for the dual-wall microencapsulated pigment powder.

#	Size μm	Frequency %	OVER SIZE%	#	Size μm	Frequency %	OVER SIZE%
(1)	1019.5	0.0	0.0	(38)	6.719	0.5	98.8
(2)	890.1	0.0	0.0	(39)	5.866	0.3	99.3
(3)	777.1	0.0	0.0	(40)	5.122	0.1	99.7
(4)	678.5	0.0	0.0	(41)	4.472	0.1	99.8
(5)	592.3	0.0	0.0	(42)	3.904	0.0	100.0
(6)	517.2	0.0	0.0	(43)	3.408	0.0	100.0
(7)	451.5	0.0	0.0	(44)	2.976	0.0	100.0
(8)	394.2	0.0	0.0	(45)	2.598	0.0	100.0
(9)	344.2	0.0	0.0	(46)	2.268	0.0	100.0
(10)	300.5	0.0	0.0	(47)	1.980	0.0	100.0
(11)	262.3	0.0	0.0	(48)	1.729	0.0	100.0
(12)	229.0	0.0	0.0	(49)	1.509	0.0	100.0
(13)	200.0	0.0	0.0	(50)	1.318	0.0	100.0
(14)	174.6	0.0	0.0	(51)	1.150	0.0	100.0
(15)	152.4	0.0	0.0	(52)	1.004	0.0	100.0
(16)	133.1	0.1	0.0	(53)	0.877	0.0	100.0
(17)	116.2	0.3	0.1	(54)	0.765	0.0	100.0
(18)	101.4	0.5	0.4	(55)	0.668	0.0	100.0
(19)	88.58	0.9	0.9	(56)	0.583	0.0	100.0
(20)	77.33	1.5	1.8	(57)	0.509	0.0	100.0
(21)	67.52	2.5	3.4	(58)	0.445	0.0	100.0
(22)	58.95	3.6	5.8	(59)	0.388	0.0	100.0
(23)	51.47	5.1	9.5	(60)	0.339	0.0	100.0
(24)	44.93	6.6	14.5	(61)	0.296	0.0	100.0
(25)	39.23	8.1	21.2	(62)	0.258	0.0	100.0
(26)	34.25	9.2	29.3	(63)	0.225	0.0	100.0
(27)	29.90	9.9	38.5	(64)	0.197	0.0	100.0
(28)	26.11	10.0	48.4	(65)	0.172	0.0	100.0
(29)	22.79	9.3	58.4	(66)	0.150	0.0	100.0
(30)	19.90	8.3	67.7	(67)	0.131	0.0	100.0
(31)	17.37	6.8	76.0	(68)	0.114	0.0	100.0
(32)	15.17	5.3	82.9	(69)	0.100	0.0	100.0
(33)	13.24	3.9	88.2	(70)	0.087	0.0	100.0
(34)	11.56	2.7	92.2	(71)	0.076	0.0	100.0
(35)	10.09	1.9	94.9	(72)	0.066	0.0	100.0
(36)	8.815	1.2	96.8	(73)	0.058	0.0	100.0
(37)	7.696	0.8	98.0	(74)	0.050	0.0	100.0

APPENDIX C

WEATHERING DATA

The following data was generated from weathering tests of coating samples, as described in Section 3.3.2.3.1, "Baseline Weathering Tests". Samples were prepared on 1 by 3-inch glass slides and exposed to either natural sunlight for 103 days, or in a QUV accelerated weathering chamber for 31 days using either UVA 340 or UVB 313 lamps. The luminous reflectance values reported in this appendix were measured from all samples in the benign, heated and recovered (after cooling) states at regular time intervals during testing.

Two, three and four letter designations indicate the sample type and test condition. The first letter indicates if the sample was prepared using a solvent-based (S) or water-based (W) binder material. The second letter indicates if the sample was exposed to natural sunlight outdoors on a rooftop (R), or in a QUV chamber using UVA 340 (A) or UVB 313 (B) lamps. If a letter "U" appears in the third position, this indicates that this is an unpigmented (clear) control sample. A suffix "T" indicates that the sample had a topcoat of UV stabilized clear binder material applied over it, and a suffix "N" indicates that no topcoat was applied. Samples whose designation contains neither a "T" nor an "N" were topcoated with unstabilized clear binder material.

SAMPLE ID	DAYS AGED	BENIGN STATE		HEATED TO 130°C		RECOVERED STATE	
		R_B (%)	COLOR	R_H (%)	R_H-R_B (%)	R_{REC} (%)	R_B-R_{REC} (%)
SAT	0	6.7	BLACK	27.8	21.1	20	13.3
	7	8.5	DARK GRAY	14.7	6.2	13.9	5.4
	14	8.2	DARK GRAY	14.2	6	13.4	5.2
	21	9.4	DARK GRAY	14.3	4.9	13.3	3.9
	31	10.3	ALMOST OLIVE	16.8	6.5	14.3	4
SA	0	7.3	BLACK	27	19.7	21.3	14
	7	6.3	BROWN	15.4	9.1	11.3	5
	14	7	BROWN	11.4	4.4	10.5	3.5
	21	6.5	BROWN	10.4	3.9	9.3	2.8
	31	7.7	MOTTLED BROWN	10.8	3.1	9	1.3
SAN	0	9.7	BLACK	17.9	8.2	12.8	3.1
	7	12.1	BROWN	14.3	2.2	14.3	2.2
	14	18.2	MEDIUM BROWN	18.5	0.3	18.1	-0.1
	21	18.5	MEDIUM BROWN	19.7	1.2	17.9	-0.6
	31	21.6	LIGHT BROWN	22.2	0.6	19.2	-2.4
SAU	0	90.2	UNPIGMENTED SAMPLE - VALUES NOT APPLICABLE				
	7	79.8					
	14	77.4					
	21	79					
	31	78.3					
SAUT	0	86.5	UNPIGMENTED SAMPLE - VALUES NOT APPLICABLE				
	7	75.6					
	14	73					
	21	74.6					
	31	74.5					
SBT	0	5.9	BLACK	10.2	4.3	10.5	4.6
	7	8.4	DARK GRAY	13.5	5.1	13.9	5.5
	14	8.8	DARK GRAY	14.1	5.3	13.6	4.8
	21	9.8	ALMOST OLIVE	15.8	6	14.6	4.8
	31	10.5	OLIVE	16.2	5.7	15.1	4.6
SB	0	7.8	BLACK	14.1	6.3	13.8	6
	7	6.9	DARK BROWN	10.6	3.7	10.7	3.8
	14	6.8	DARK BROWN	10.6	3.8	10	3.2
	21	7.2	DARK BROWN	10.4	3.2	10.2	3
	31	7.2	DARK BROWN	11.1	3.9	10.7	3.5
SBN	0	9.3	BLACK	18.2	8.9	12.8	3.5
	7	12	BROWN	13.6	1.6	12.8	0.8
	14	15	BROWN	14.4	-0.6	13.7	-1.3
	21	17	MEDIUM BROWN	16.5	-0.5	13.8	-3.2
	31	16.3	MEDIUM BROWN	17.4	1.1	15.4	-0.9

SAMPLE TYPE	DAYS AGED	BENIGN STATE		HEATED TO 130°C		RECOVERED STATE	
		R_B (%)	COLOR	R_H (%)	R_H-R_B (%)	R_{REC} (%)	R_B-R_{REC} (%)
SBU	0	90.2	UNPIGMENTED SAMPLE - VALUES NOT APPLICABLE				
	7	79.2					
	14	77.2					
	21	77.7					
	31	75.5					
SBUT	0	85.9	UNPIGMENTED SAMPLE - VALUES NOT APPLICABLE				
	7	74.9					
	14						
	21	74.6					
	31	72.2					
SRT	0	6.2	BLACK	11.9	5.7	12.1	5.9
	7	6.8	DARK GRAY	12.5	5.7	11.1	4.3
	14	8	DARK GRAY	14.5	6.5	12.2	4.2
	28	12.1	MOTTLED OLIVE	17.5	5.4	12.6	0.5
	56	20.5	MOTTLED OLIVE	24.1	3.6	19.7	-0.8
	103	28.6	MOTTLED OLIVE	34.1	5.5	29	0.4
SR	0	7	BLACK	11.6	4.6	11.6	4.6
	7	6.8	DARK BROWN	11.3	4.5	10.4	3.6
	14	7.5	DARK BROWN	12.7	5.2	11.4	3.9
	28	10.5	MOTTLED BROWN	18.8	8.3	17.7	7.2
	56	23.5	MOTTLED BROWN	27.6	4.1	26.9	3.4
	103	27	MOTTLED BROWN	30.5	3.5	32	5
SRN	0	9.9	BLACK	19.9	10	13.6	3.7
	7	14.7	BROWN	18.9	4.2	16.5	1.8
	14	20.4	BROWN	23.3	2.9	21.7	1.3
	28	27.8	LIGHT BROWN	29.6	1.8	27.9	0.1
	56	36.3	LIGHT BEIGE	36.7	0.4	33.5	-2.8
	103	45.1	LIGHT BEIGE	43	-2.1	39.4	-5.7
SRU	0	89.5	UNPIGMENTED SAMPLE - VALUES NOT APPLICABLE				
	7	84.7					
	14	84.8					
	28	84.7					
	56	84.2					
	103	85					
SRUT	0	84.5	UNPIGMENTED SAMPLE - VALUES NOT APPLICABLE				
	7	81.5					
	14	80					
	28	83.7					
	56	79.4					
	103	81.6					

SAMPLE TYPE	DAYS AGED	BENIGN STATE		HEATED TO 130°C		RECOVERED STATE	
		R_B (%)	COLOR	R_H (%)	R_H-R_B (%)	R_{REC} (%)	R_B-R_{REC} (%)
WAT	0	13.7	BLACK	29.7	16	16	2.3
	7	18.7	LIGHT GRAY	27.7	9	18.8	0.1
	14	18	LT. GRAY/BROWN	26.9	8.9	18.6	0.6
	21	14.9	BROWN	22.6	7.7	15.1	0.2
	31	16.8	BROWN	25.3	8.5	17.2	0.4
WA	0	10	BLACK	24.9	14.9	12	2
	7	11	BROWN	15.6	4.6	12.2	1.2
	14	18.6	LIGHT BROWN	23.4	4.8	20	1.4
	21	17.2	LIGHT BROWN	21.6	4.4	19.5	2.3
	31	18.3	LIGHT BROWN	22.9	4.6	20.2	1.9
WAN	0	10.8	BLACK	24.7	13.9	13.4	2.6
	7	15	BROWN	19.8	4.8	16.4	1.4
	14	21.5	LIGHT BROWN	25	3.5	21.6	0.1
	21	24.5	LIGHT BROWN	27.9	3.4	23	-1.5
	31	26.1	BEIGE	30	3.9	26	-0.1
WAU	0	88.3	UNPIGMENTED SAMPLE - VALUES NOT APPLICABLE				
	7	82.5					
	14	80.4					
	21	80.1					
	31	80.5					
WAUT	0	89.9	UNPIGMENTED SAMPLE - VALUES NOT APPLICABLE				
	7	84.8					
	14	83.5					
	21	82					
	31	81.6					
WBT	0	11.4	BLACK	25.8	14.4	13.3	1.9
	7	18.7	DARK GRAY	26.8	8.1	17.8	-0.9
	14	17.1	DARK GRAY	25.7	8.6	18.6	1.5
	21	17.1	DK. BROWN/GRAY	25.5	8.4	17.5	0.4
	31	15.4	BROWN	24.3	8.9	16.3	0.9
WB	0	10.5	BLACK	27.1	16.6	12.6	2.1
	7	10.6	BROWN	14.8	4.2	11.6	1
	14	15.2	MEDIUM BROWN	18.9	3.7	15.5	0.3
	21	17	MEDIUM BROWN	21.2	4.2	17.6	0.6
	31	12.8	BROWN	17	4.2	14.3	1.5
WBN	0	10.7	BLACK	26	15.3	14	3.3
	7	14.4	BROWN	19.4	5	14.3	-0.1
	14	19.6	LIGHT BROWN	24	4.4	19.4	-0.2
	21	23.4	BEIGE	26.1	2.7	21.2	-2.2
	31	26.8	BEIGE	29.2	2.4	24.3	-2.5

SAMPLE TYPE	DAYS AGED	BENIGN STATE		HEATED TO 130°C		RECOVERED STATE	
		R_B (%)	COLOR	R_H (%)	R_H-R_B (%)	R_{REC} (%)	R_B-R_{REC} (%)
WBU	0	88.8	UNPIGMENTED SAMPLE - VALUES NOT APPLICABLE				
	7	79.6					
	14	75.2					
	21	76.5					
	31	74.3					
WBUT	0	91.1	UNPIGMENTED SAMPLE - VALUES NOT APPLICABLE				
	7	83.2					
	14	82.5					
	21	81.6					
	31	78.8					
WRT	0	11.7	BLACK	28.3	16.6	13.5	1.8
	7	15.1	DK. BROWN	24.4	9.3	17.2	2.1
	14	19.8	LT. BROWN	24.5	4.7	19.4	-0.4
	28	29	BEIGE	33.2	4.2	30.1	1.1
	56	33.8	BEIGE	34.5	0.7	33.4	-0.4
	103	40	BEIGE	39.9	-0.1	37.8	-2.2
WR	0	10.8	BLACK	25.8	15	12.5	1.7
	7	10.7	BROWN	17.3	6.6	11.4	0.7
	14	13.9	MED. BROWN	19.4	5.5	16.1	2.2
	28	19.7	LT. BROWN	22.8	3.1	20.4	0.7
	56	27.1	BEIGE	30	2.9	29.6	2.5
	103	33.5	BEIGE	35.4	1.9	34.2	0.7
WRN	0	10.6	BLACK	25.7	15.1	13.9	3.3
	7	16.4	BROWN	22.5	6.1	17.1	0.7
	14	25.6	BEIGE	28.7	3.1	24.7	-0.9
	28	34.8	BEIGE	36.3	1.5	34.9	0.1
	56	42.3	BEIGE	43.6	1.3	42.6	0.3
	103	53	LT. BEIGE	52.3	-0.7	50.6	-2.4
WRU	0	86.9	UNPIGMENTED SAMPLE - VALUES NOT APPLICABLE				
	7	86.8					
	14	84.8					
	28	83.3					
	56	84.3					
	103	81.9					
WRUT	0	90.5	UNPIGMENTED SAMPLE - VALUES NOT APPLICABLE				
	7	84.8					
	14	81.4					
	28	81.5					
	56	76.6					
	103	77.4					

APPENDIX D

TEST SAMPLE RESPONSE PLOTS AND PHOTOGRAPHS FROM TESTS WITH SIMULTANEOUS THERMAL FLUX AND 25, 50 OR 75% MECHANICAL PRELOAD

The following data was generated from combined thermal-mechanical testing of composite beams conducted at the National Renewable Energy Laboratory High Flux Solar Furnace during two separate test entries conducted during the weeks of March 15 - 19, and May 17 - 21, 1993. Results from these tests are described in Section 5.4.4.1.

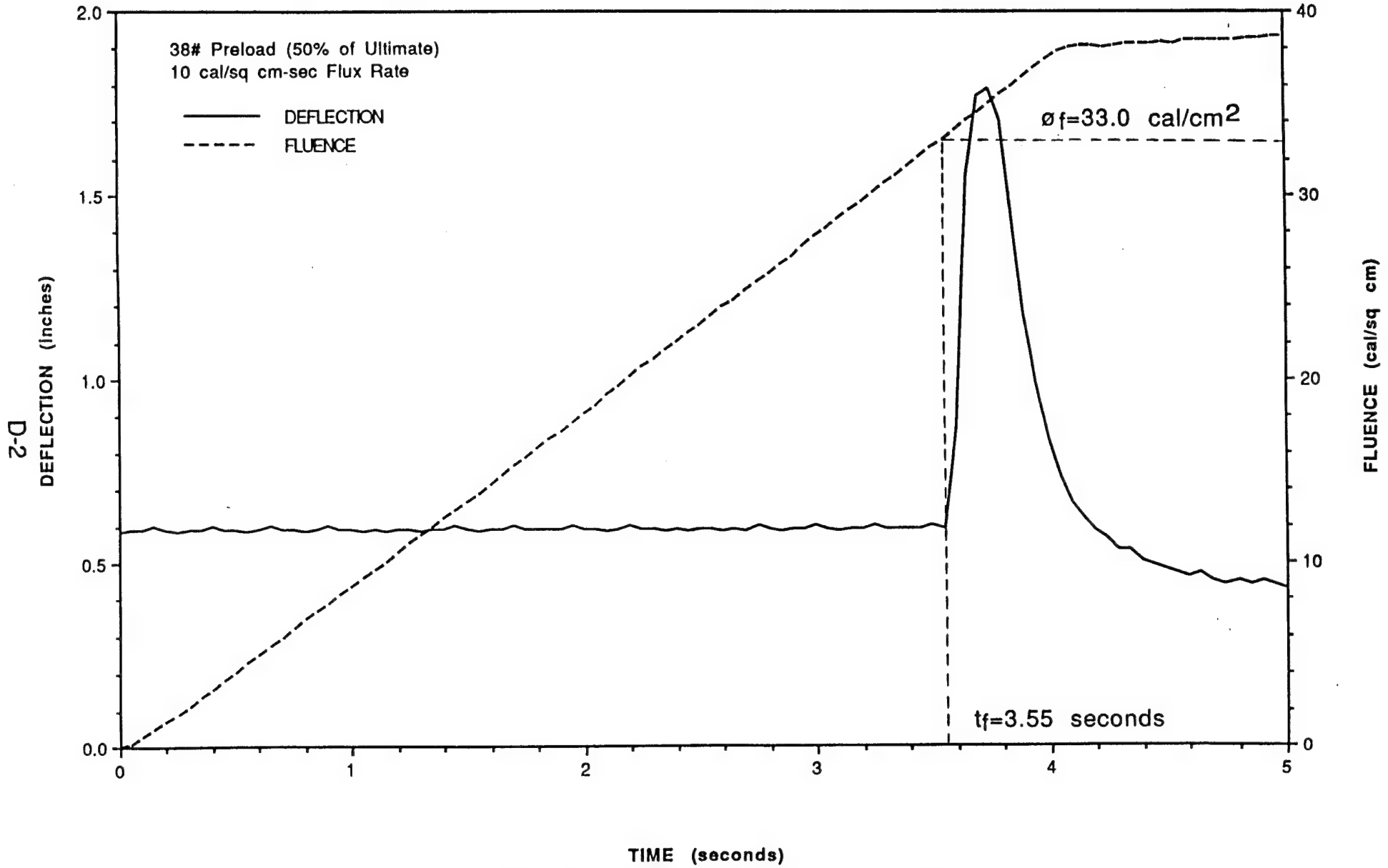

Figure D-1. Deflection and fluence vs. time for white sample #1.

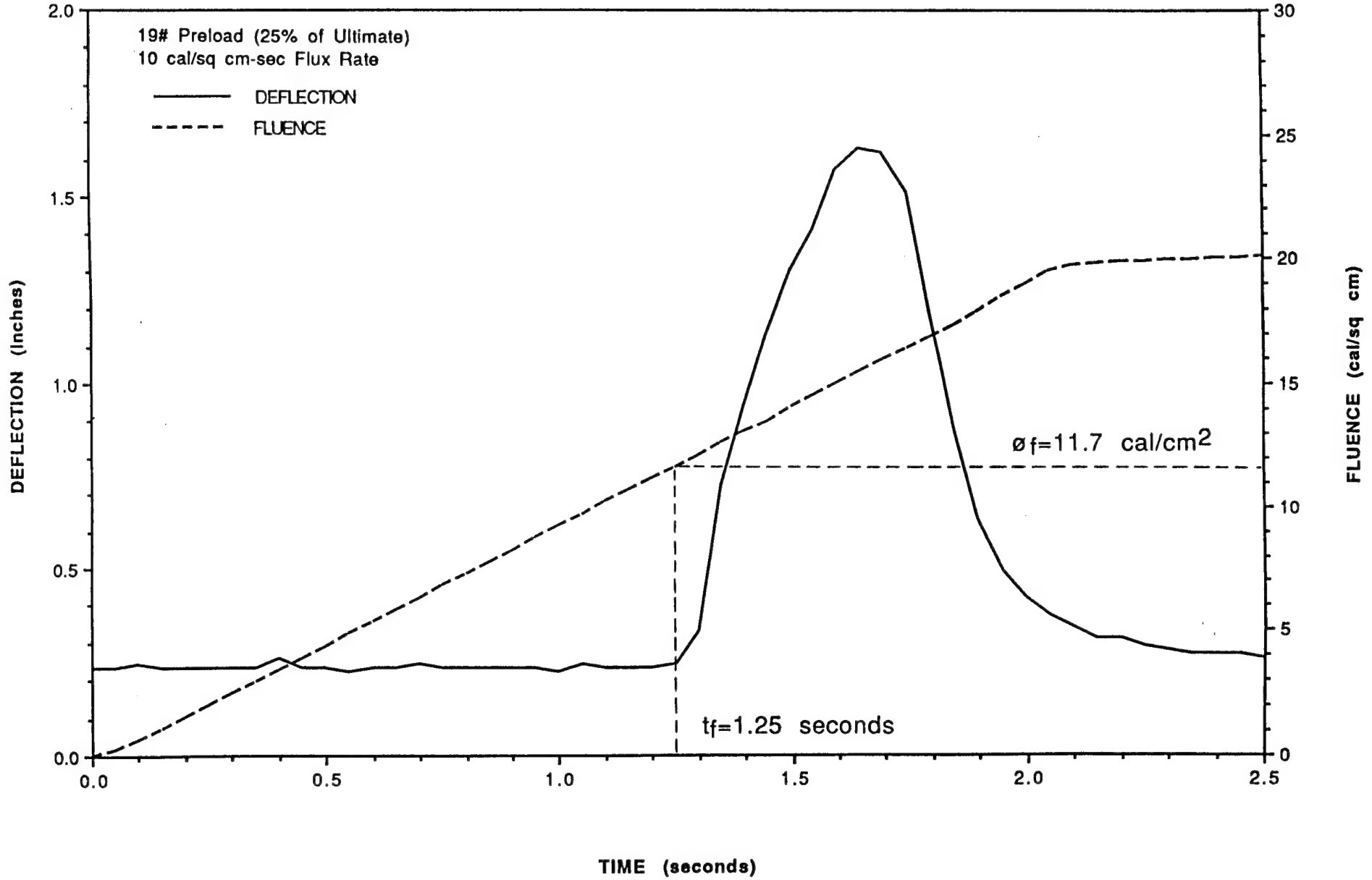

Figure D-2. Deflection and fluence vs. time for grey sample #1.

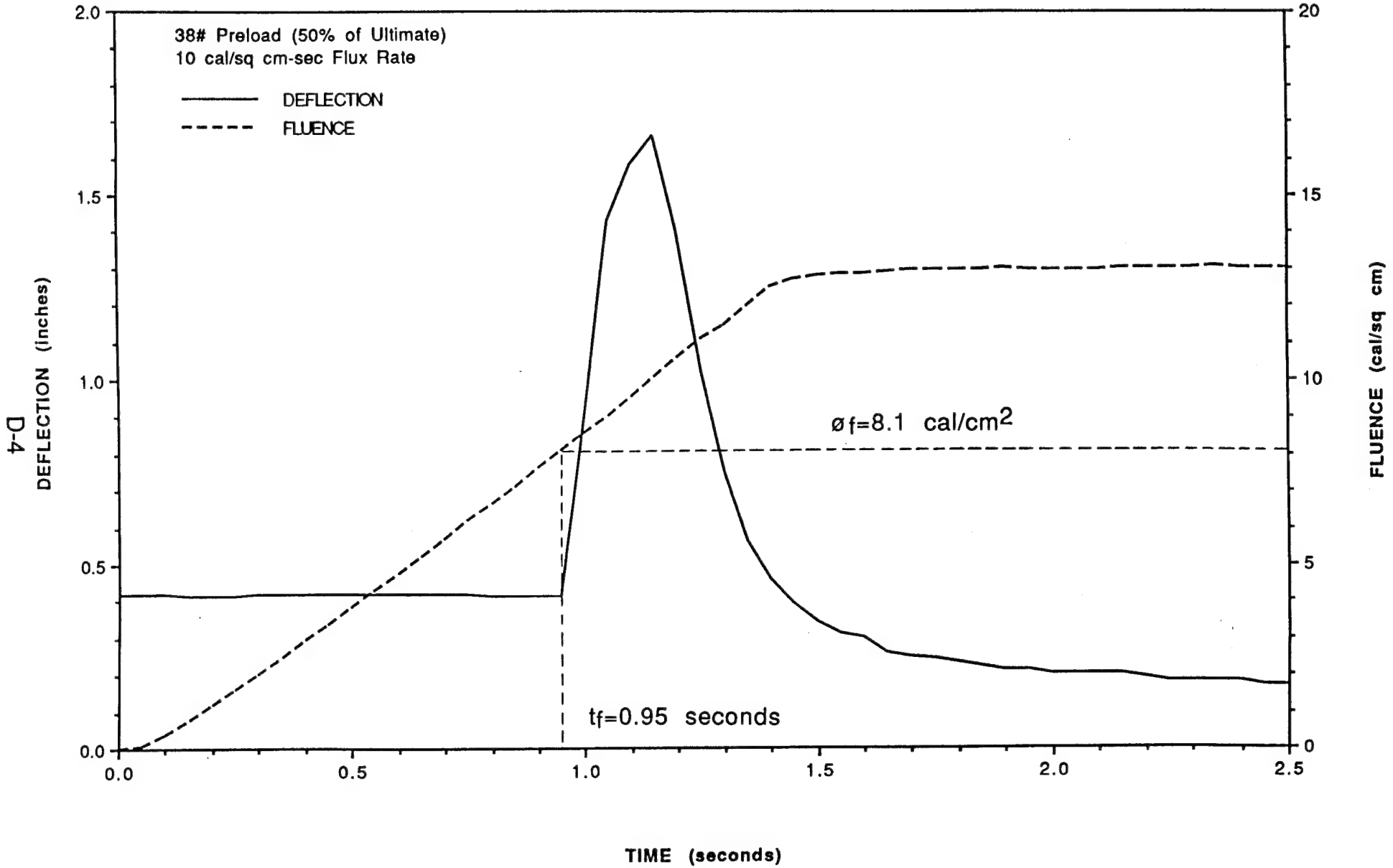

Figure D-3. Deflection and fluence vs. time for grey sample #2.

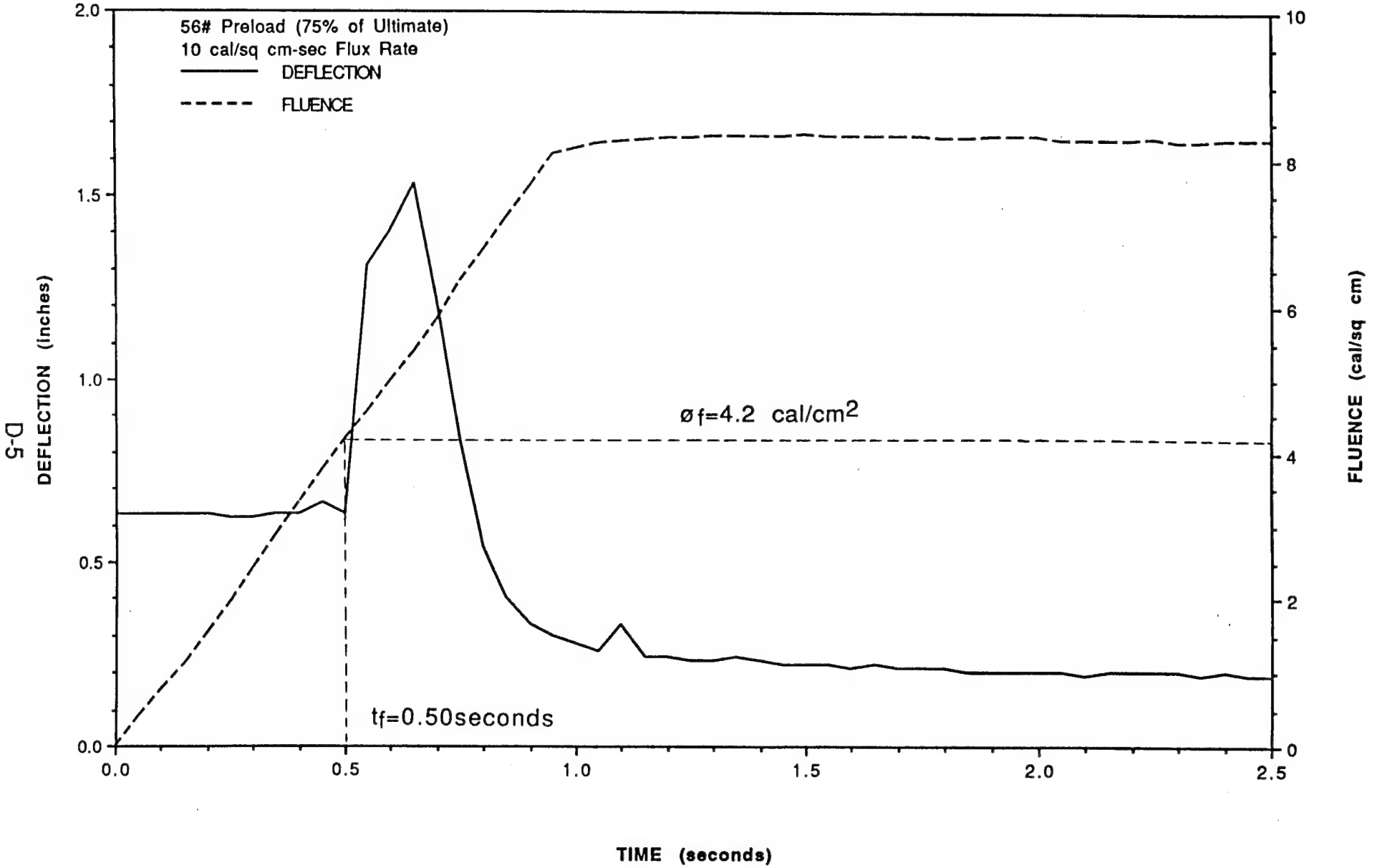

Figure D-4. Deflection and fluence vs. time for grey sample #3.

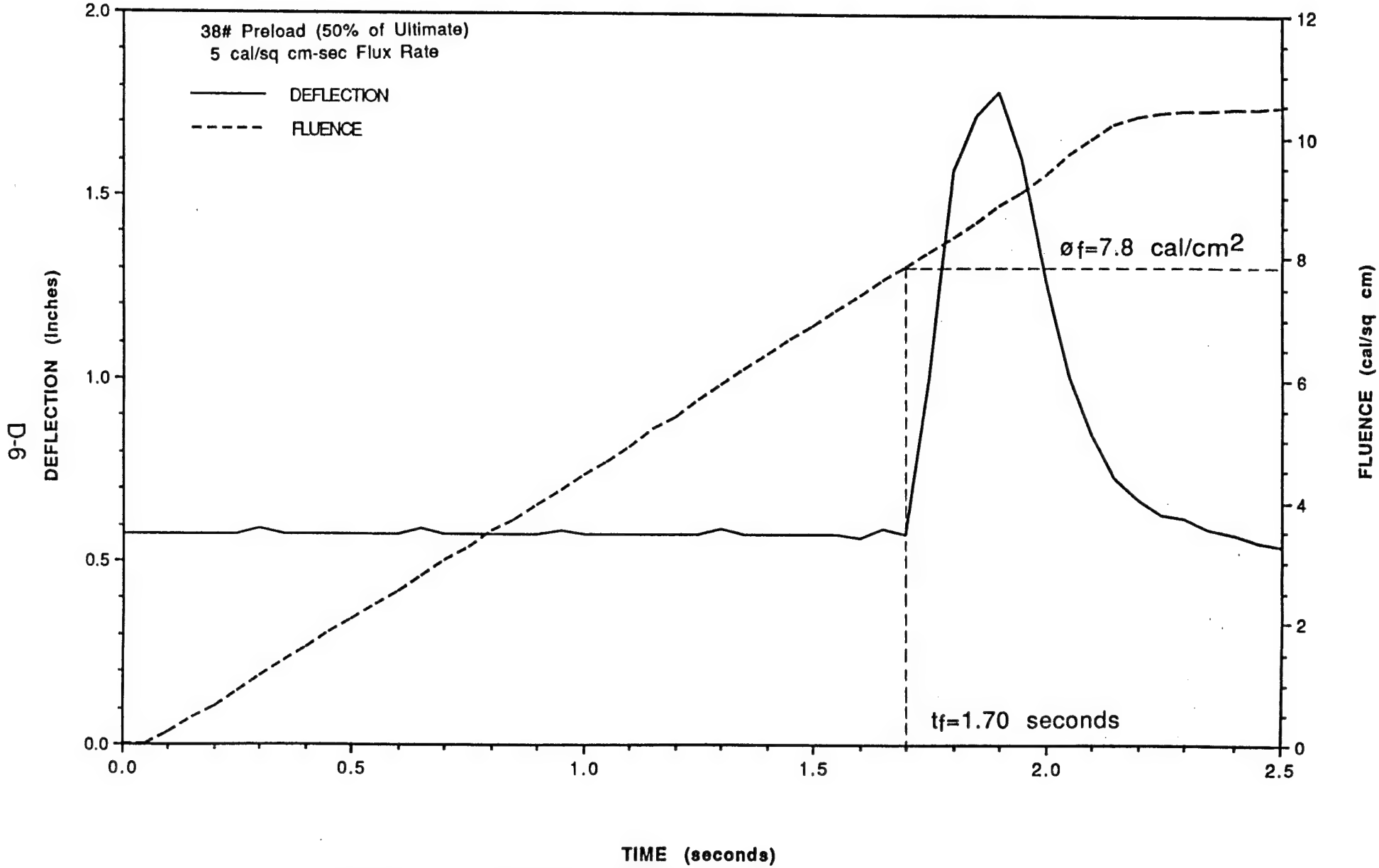

Figure D-5. Deflection and fluence vs. time for grey sample #5.

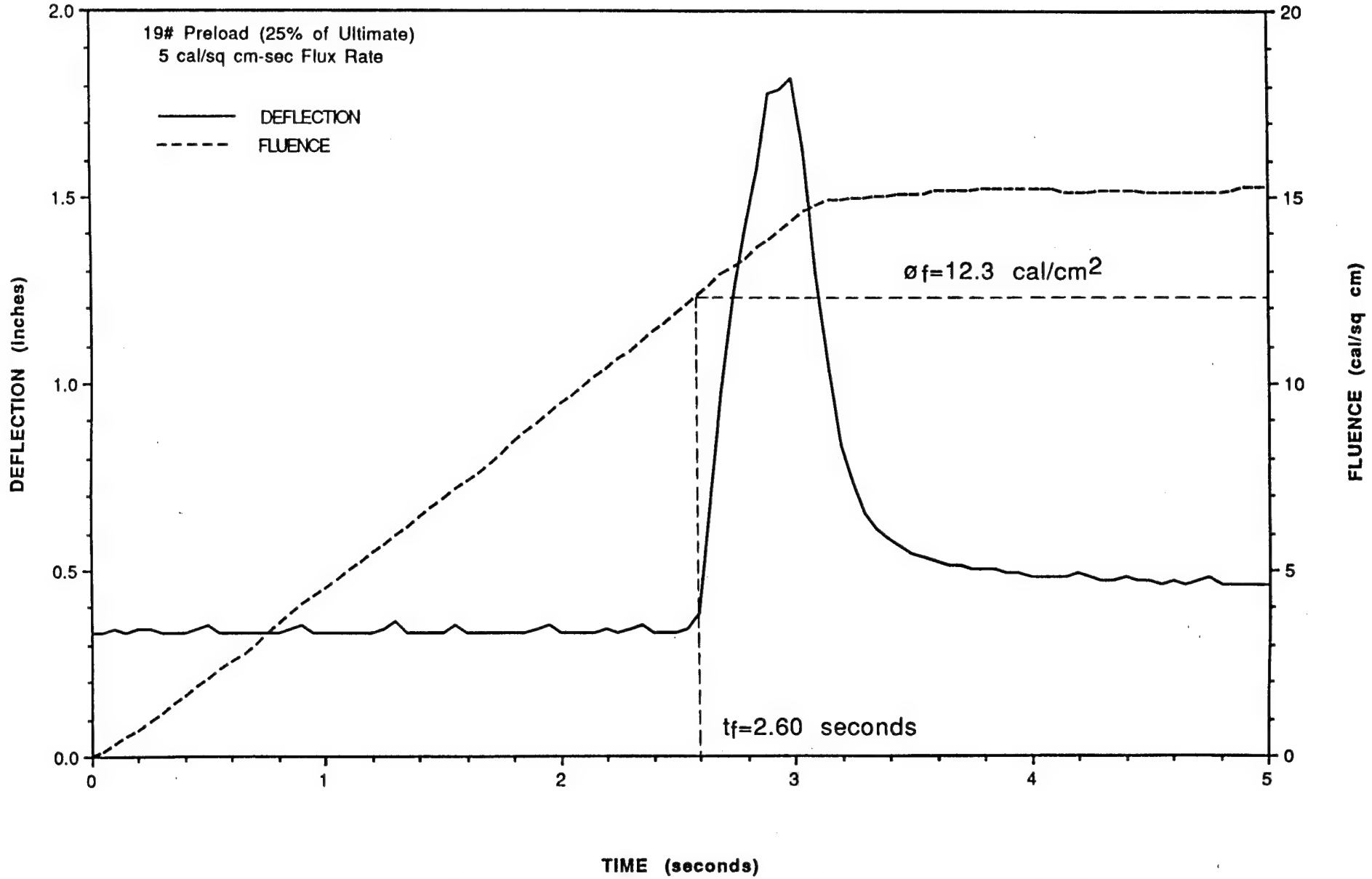

Figure D-6. Deflection and fluence vs. time for grey sample #7.

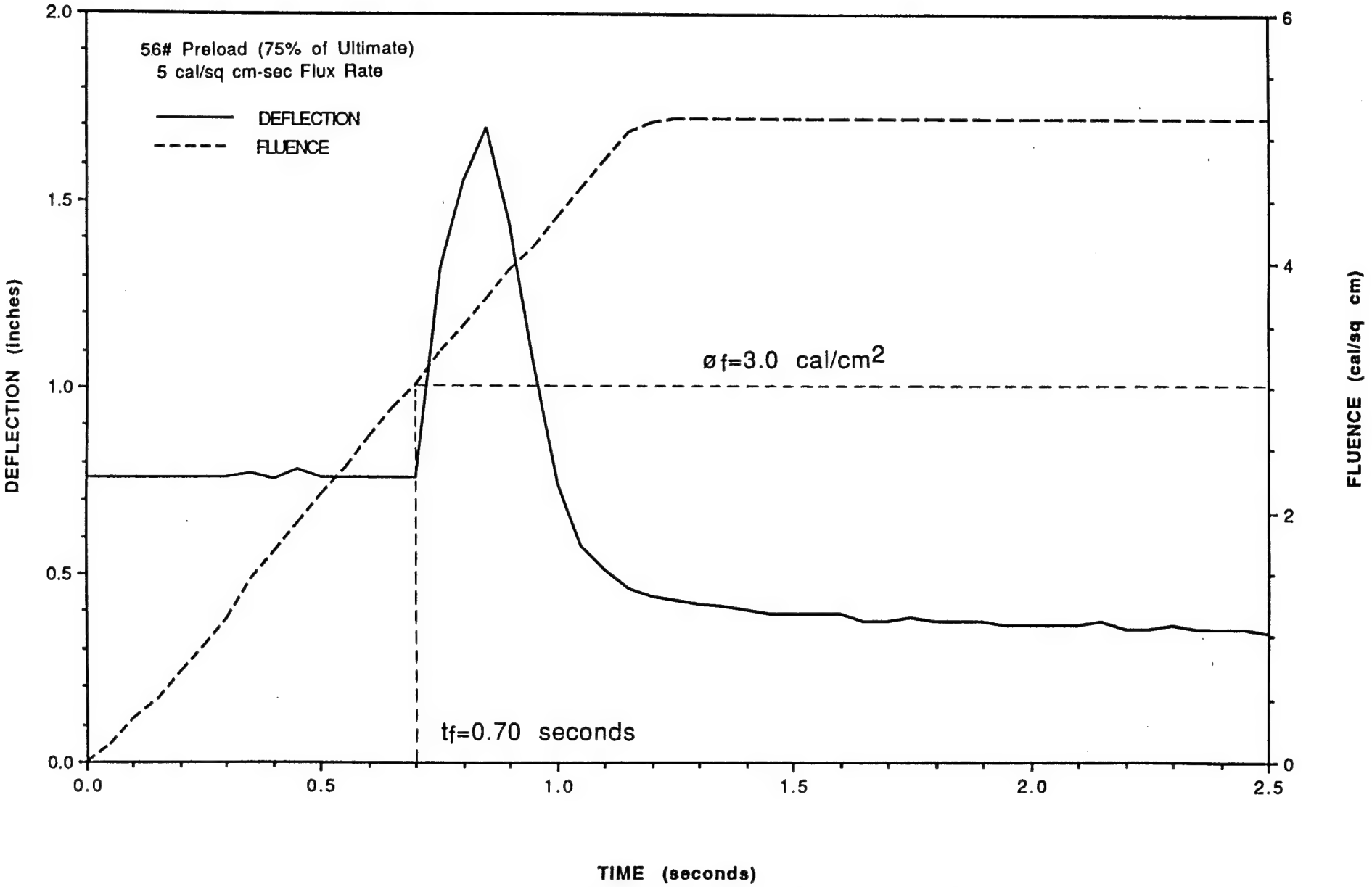

Figure D-7. Deflection and fluence vs. time for grey sample #8.

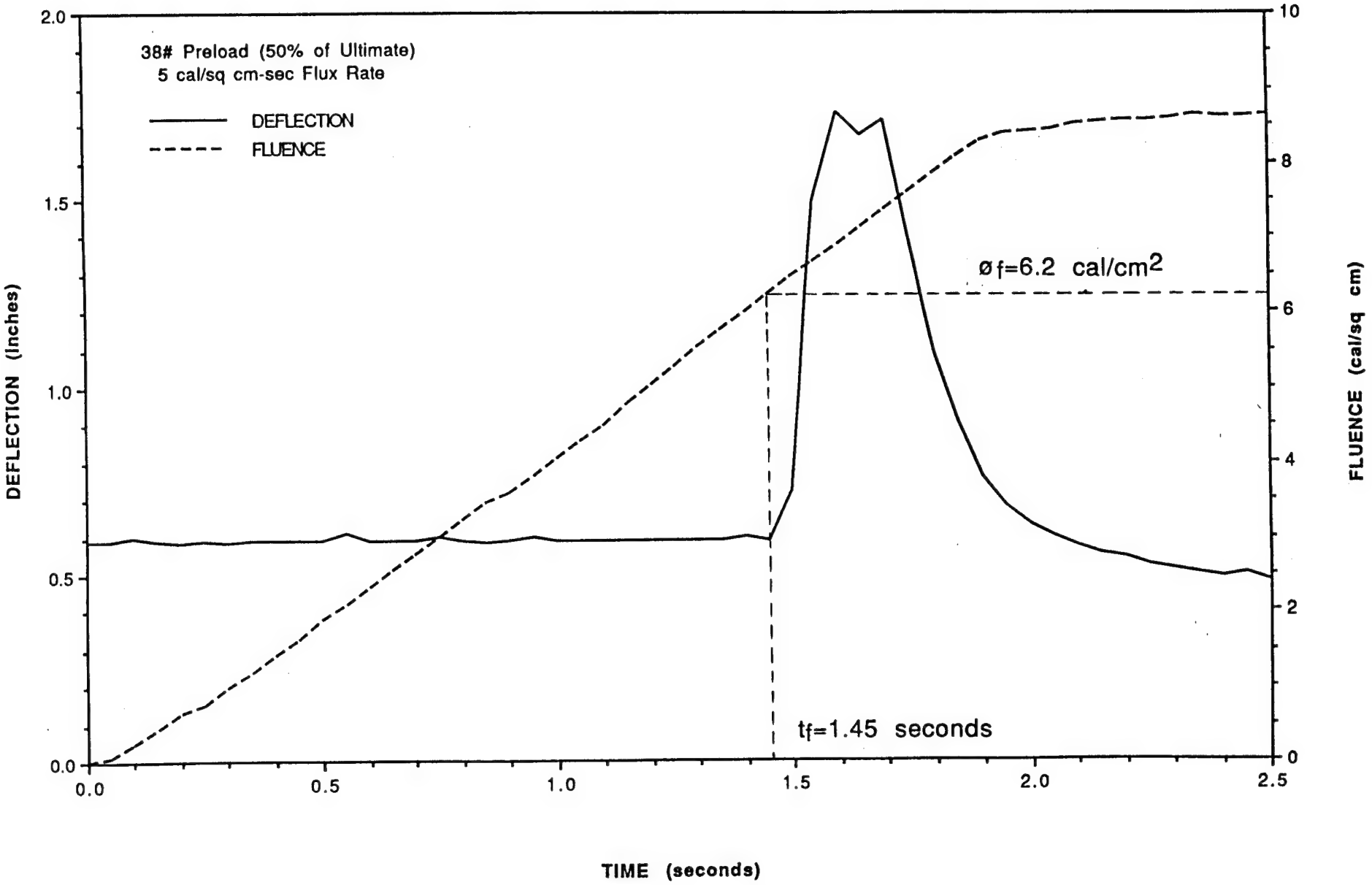

Figure D-8. Deflection and fluence vs. time for black sample #2.

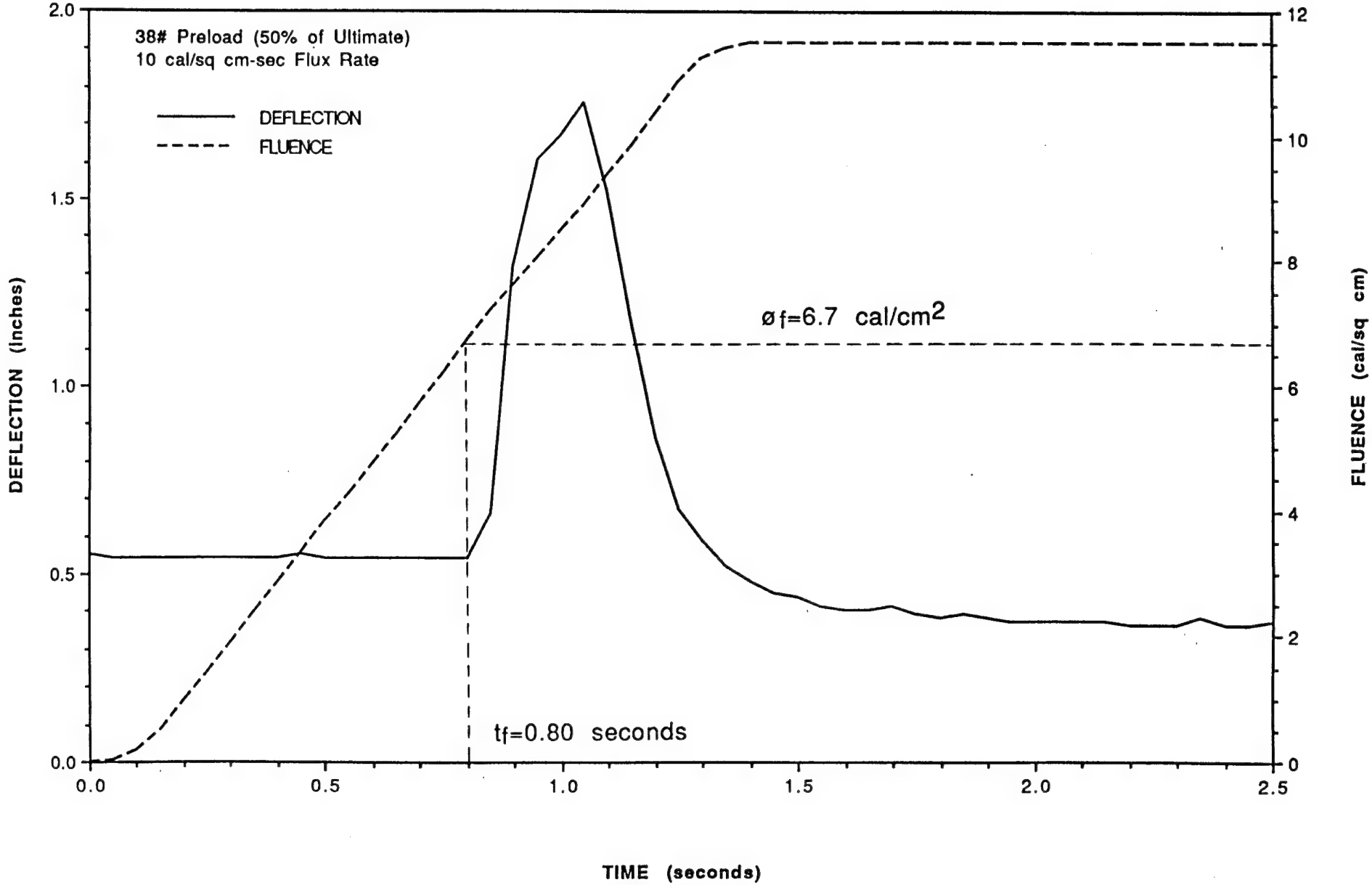

Figure D-9. Deflection and fluence vs. time for black sample #3.

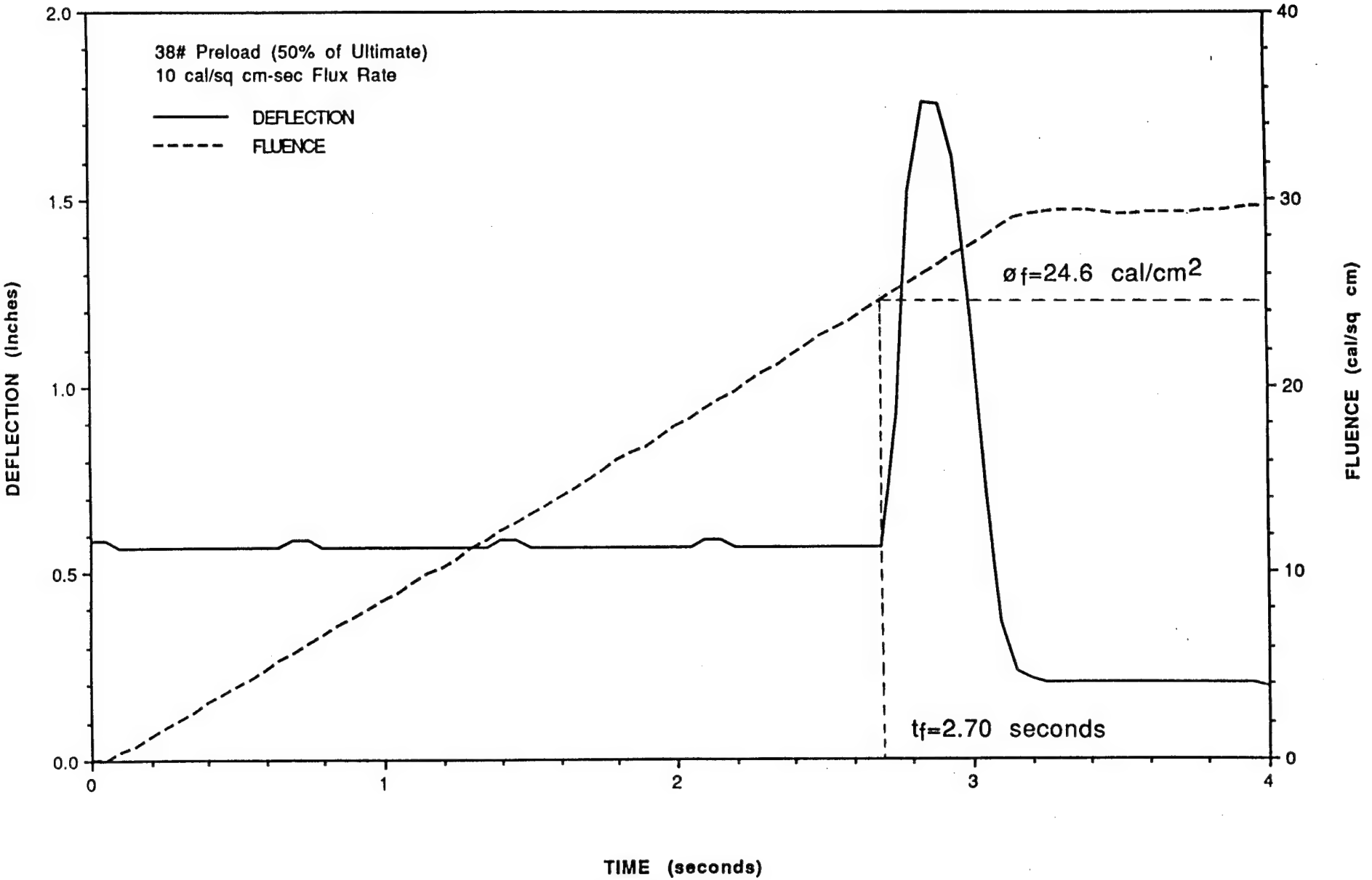

Figure D-10. Deflection and fluence vs. time for TRAC sample #2.

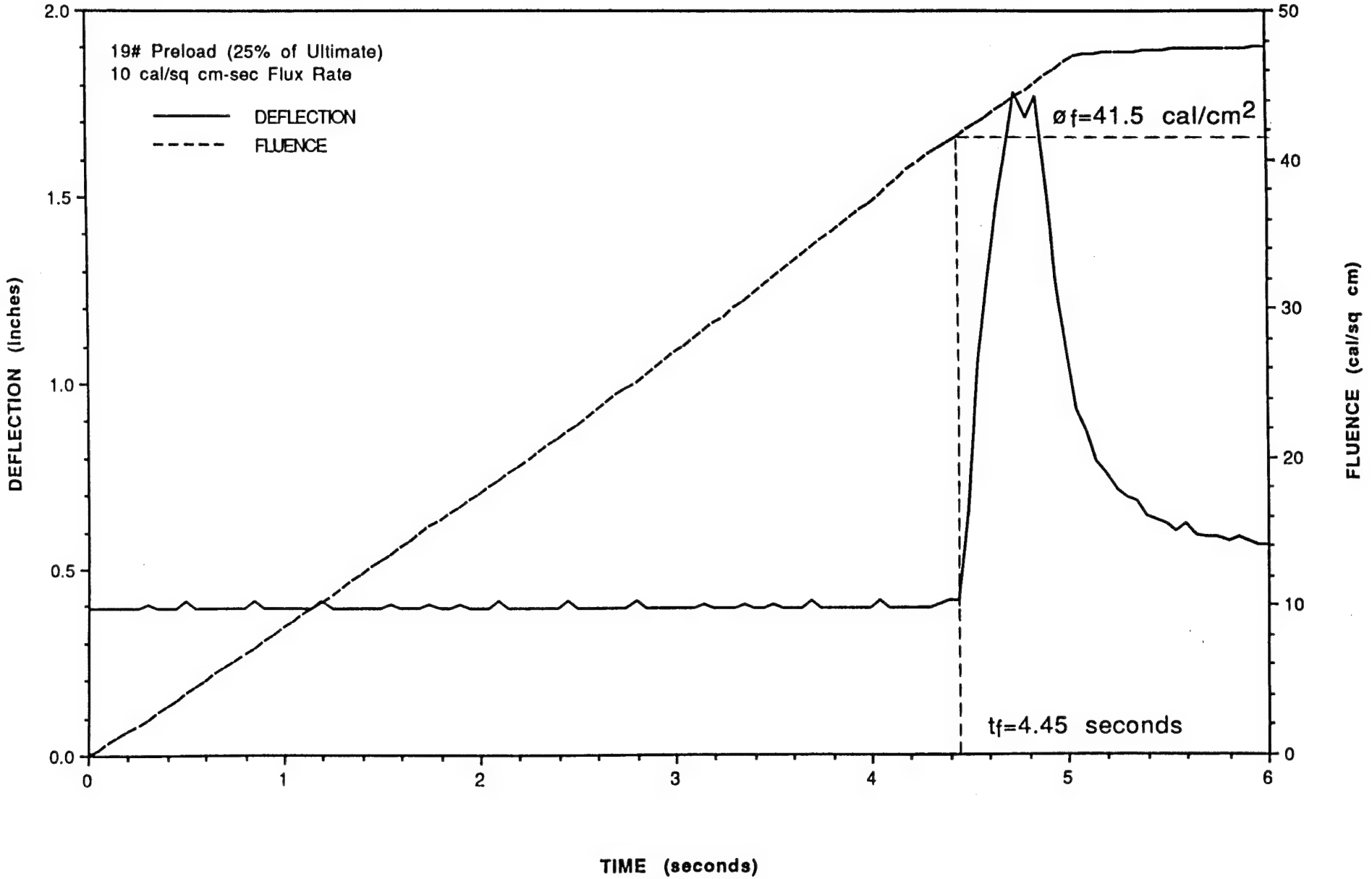

Figure D-11. Deflection and fluence vs. time for TRAC sample #4.

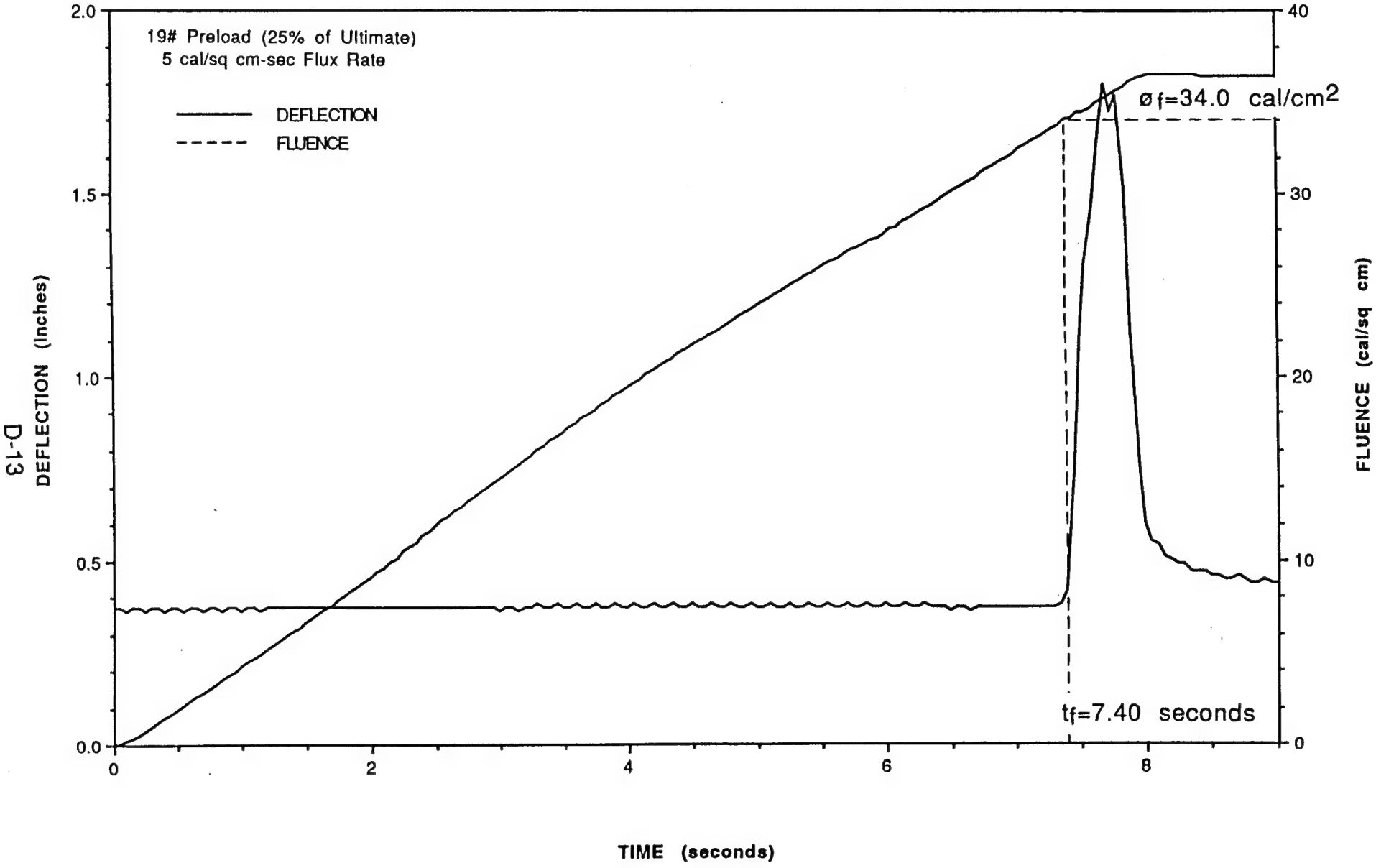

Figure D-12. Deflection and fluence vs. time for TRAC sample #5.

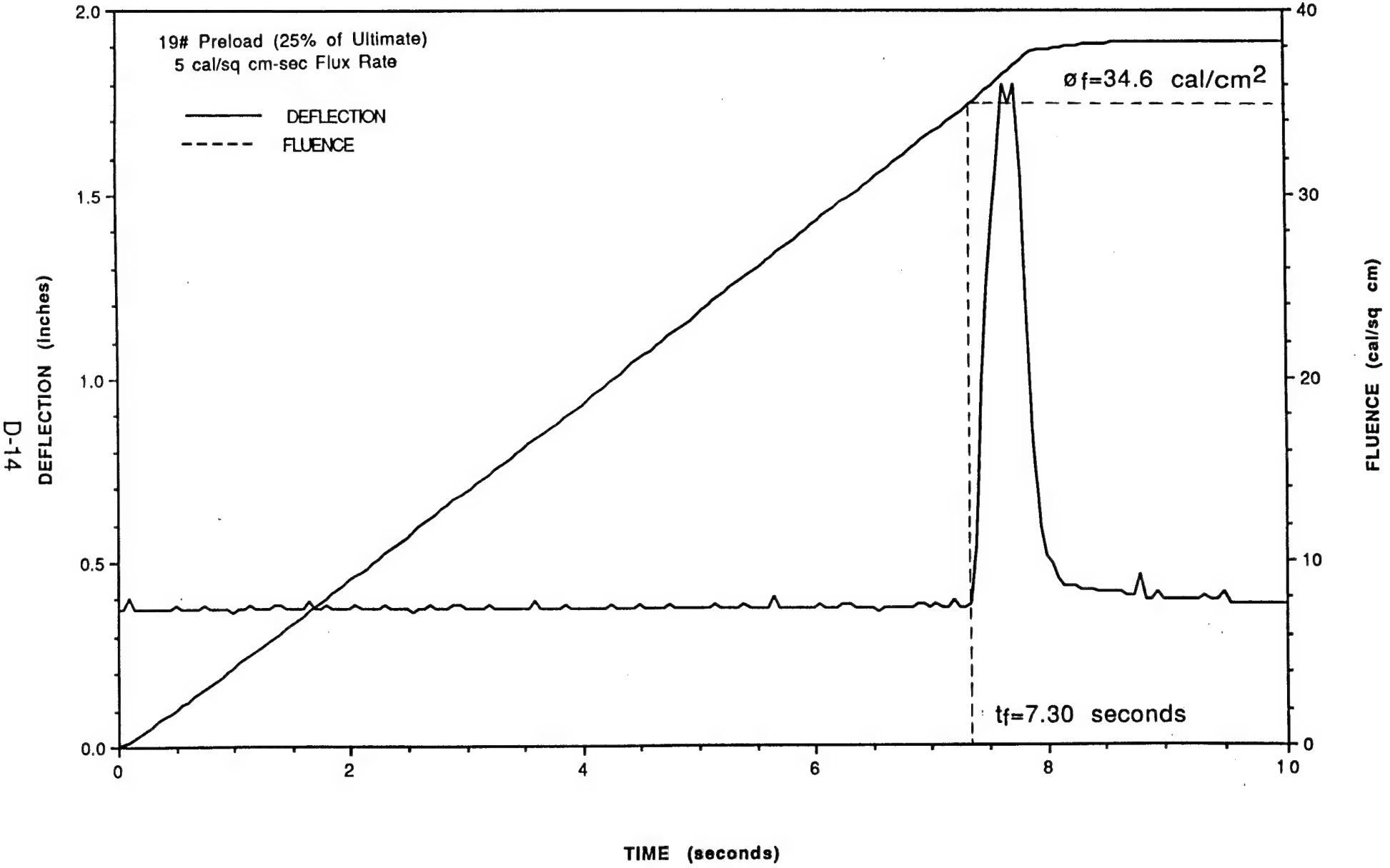

Figure D-13. Deflection and fluence vs. time for TRAC sample #6.

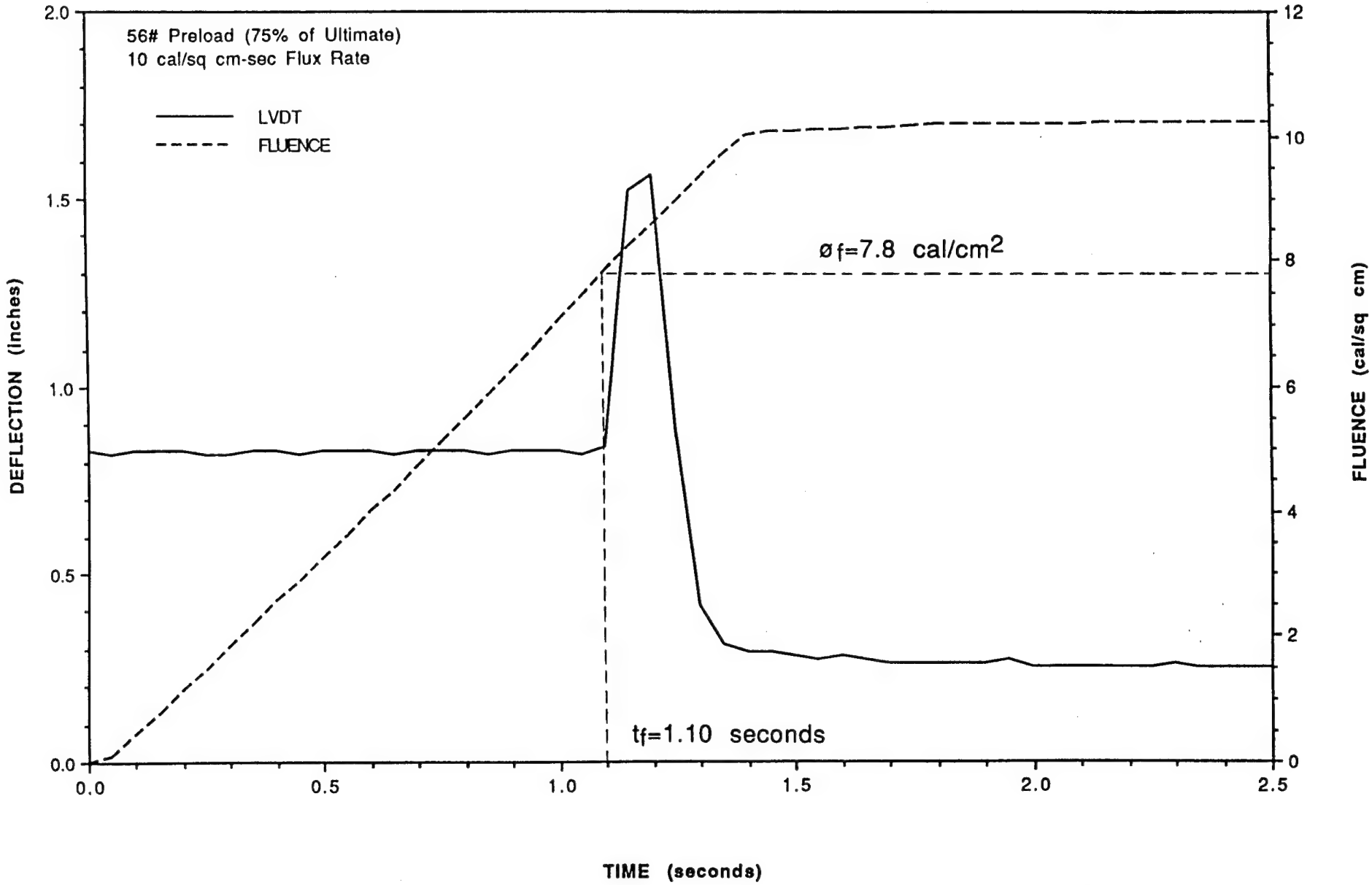

Figure D-14. Deflection and fluence vs. time for TRAC sample #8.

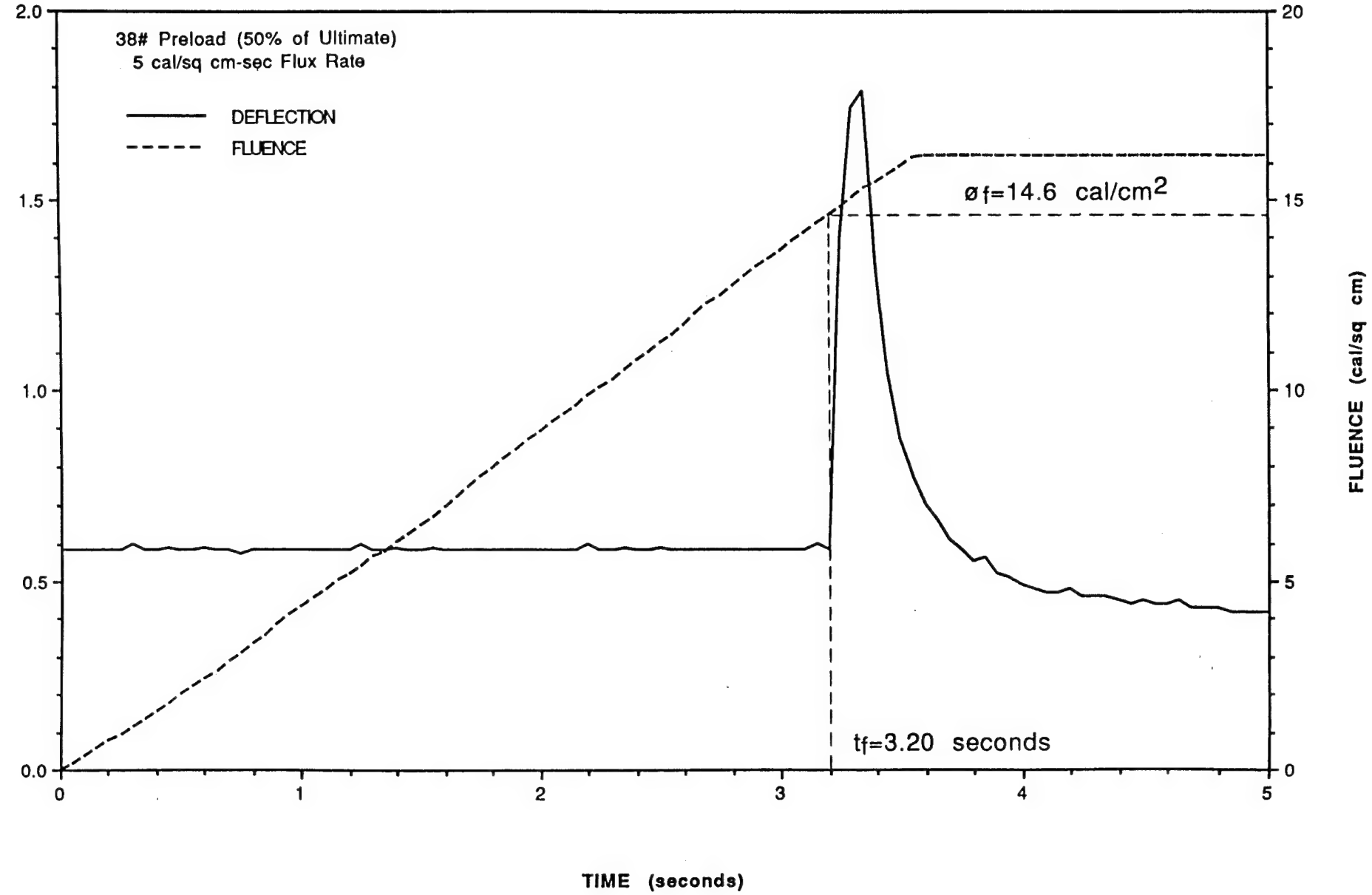

Figure D-15 Deflection and fluence vs. time for TRAC sample #9.

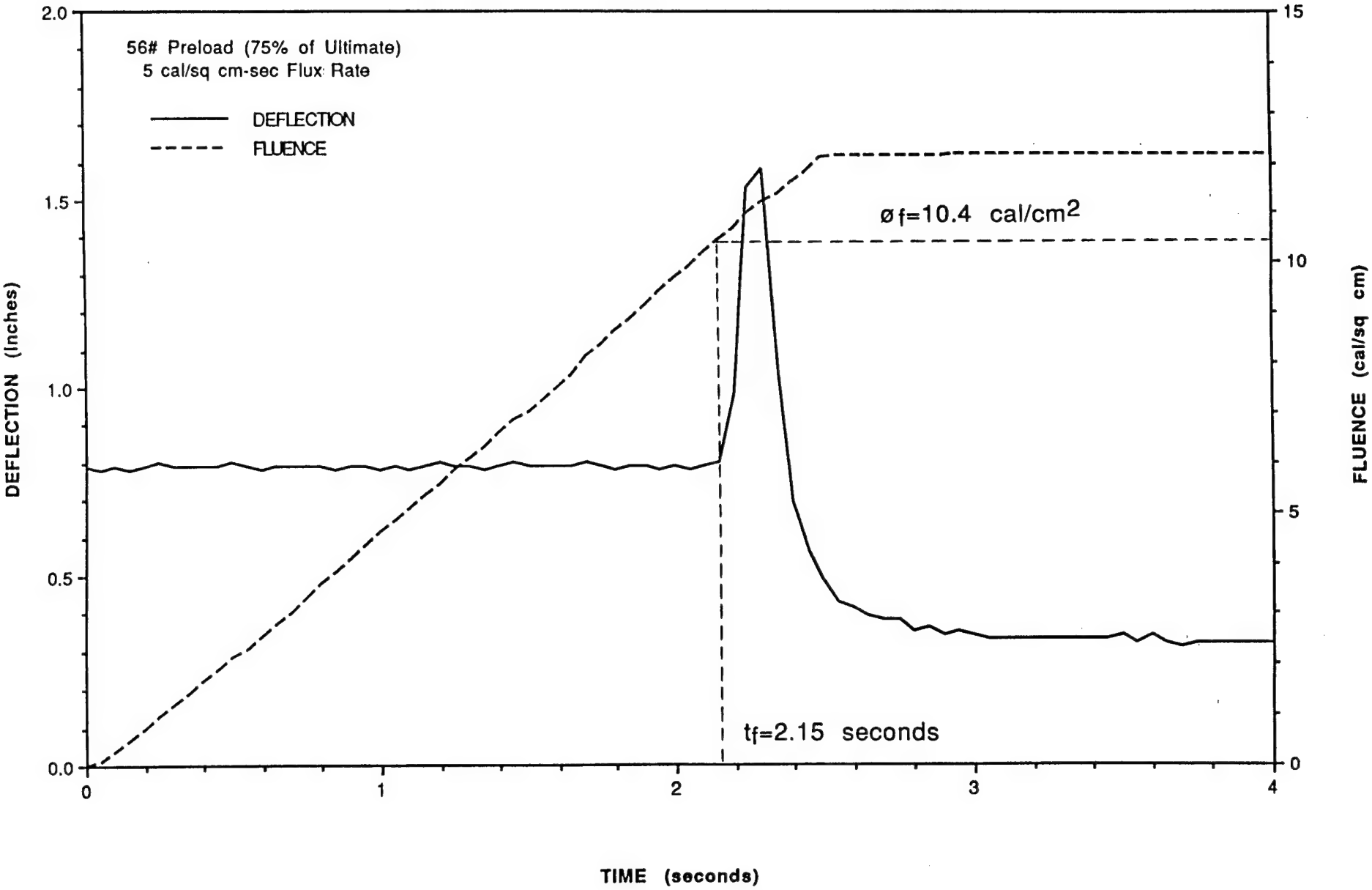

Figure D-16. Deflection and fluence vs. time for TRAC sample #10.

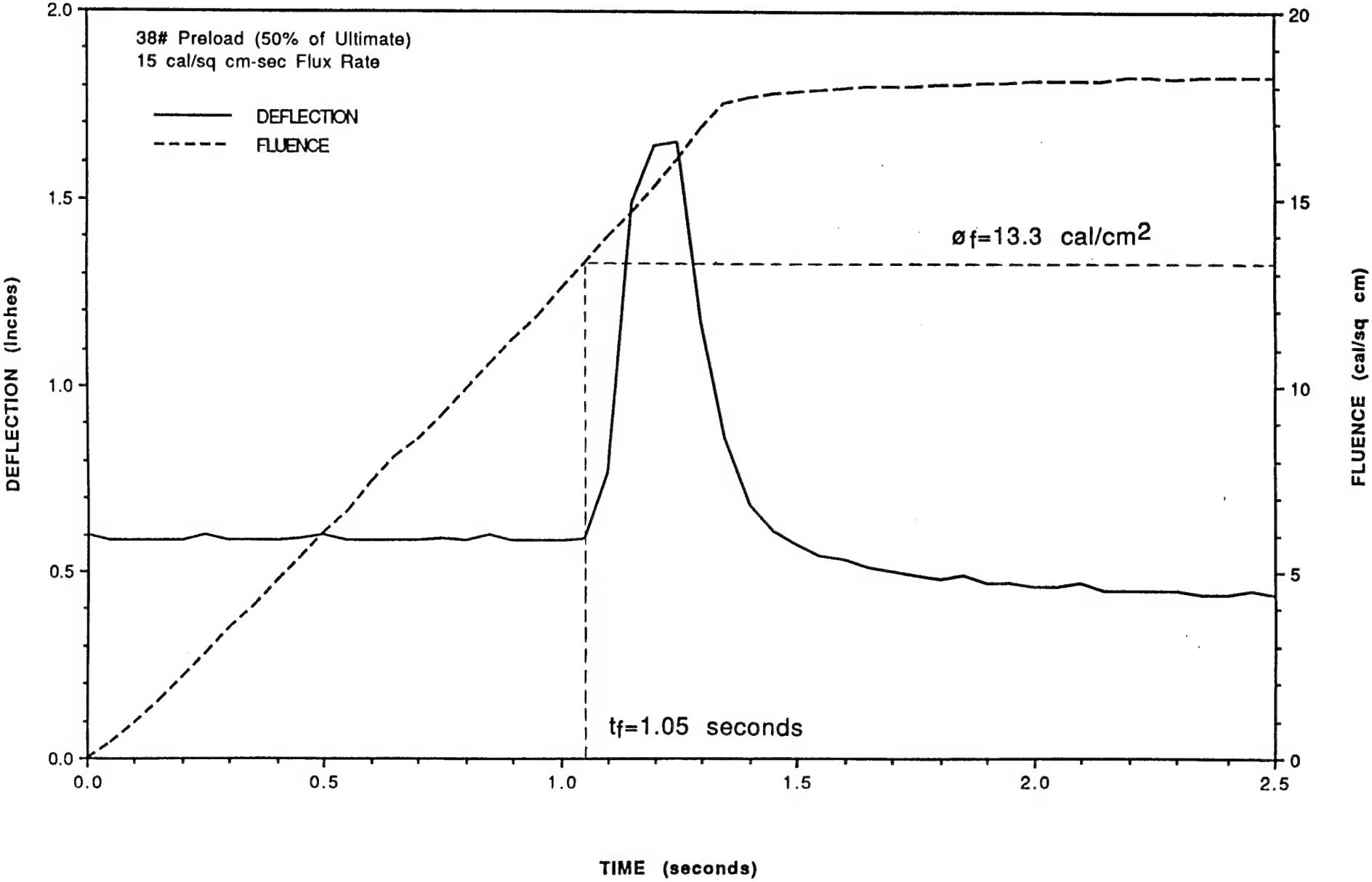

Figure D-17. Deflection and fluence vs. time for TRAC sample #11.

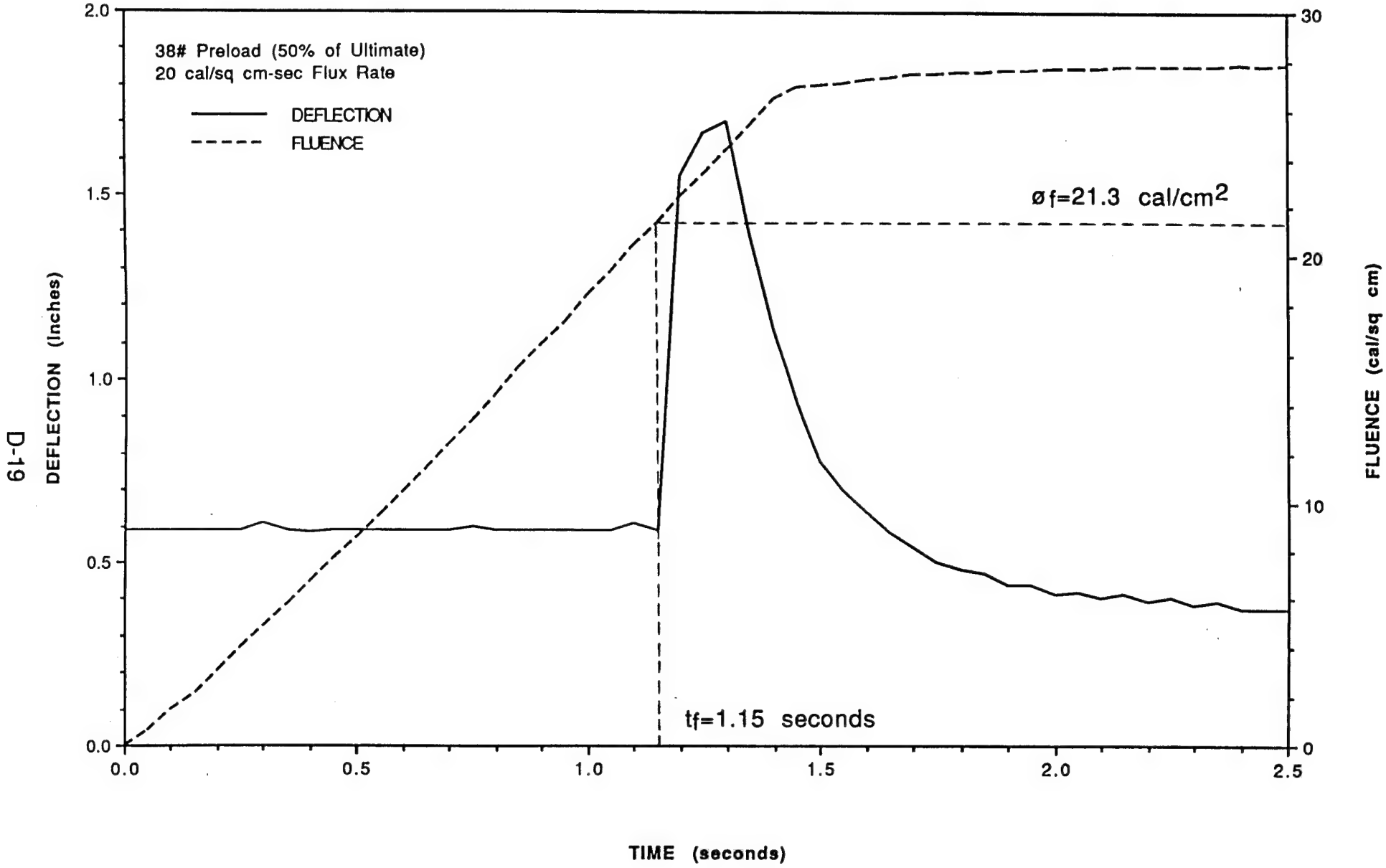

Figure D-18. Deflection and fluence vs. time for TRAC sample #12.

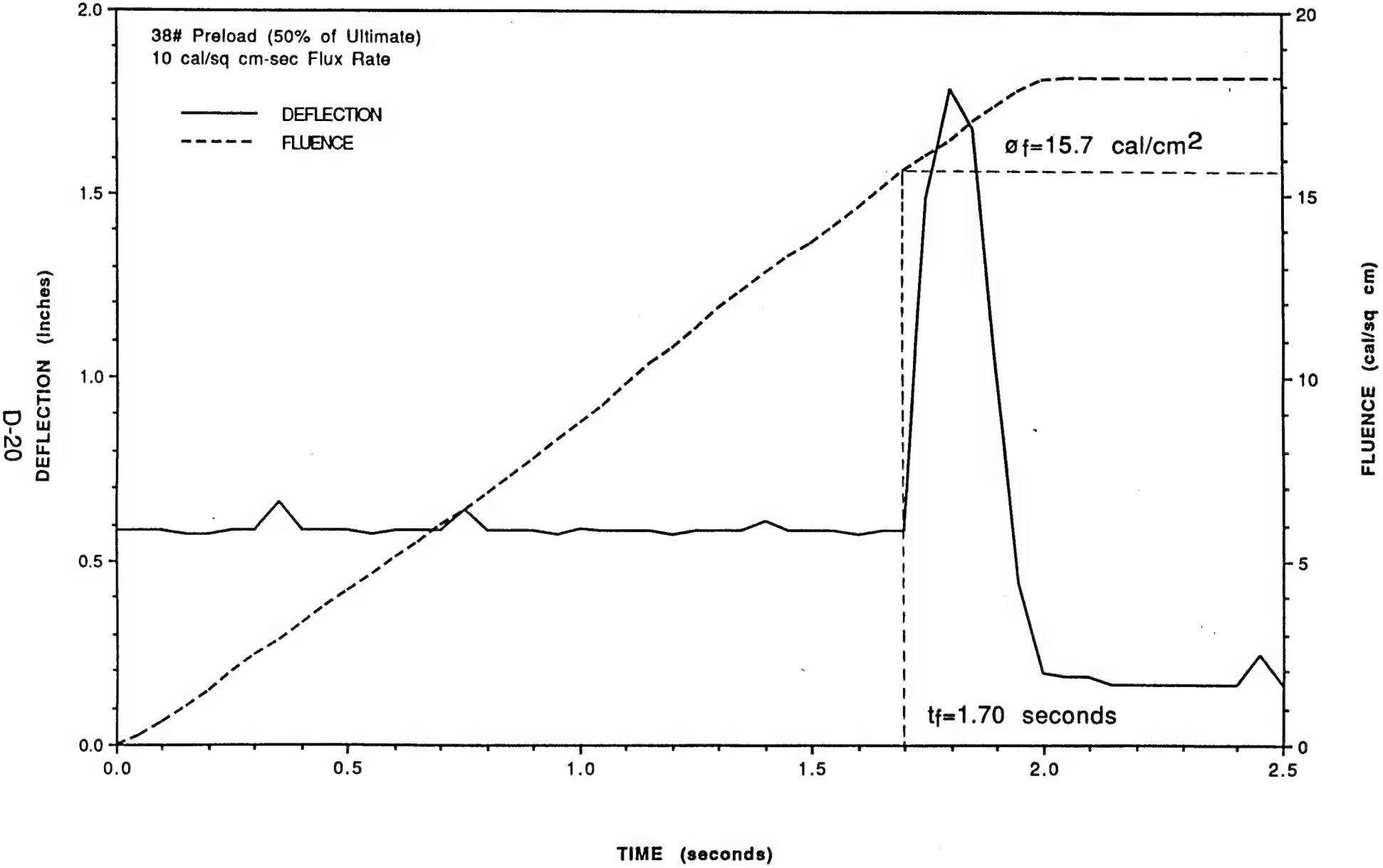

Figure D-19. Deflection and fluence vs. time for TRAC sample #13.

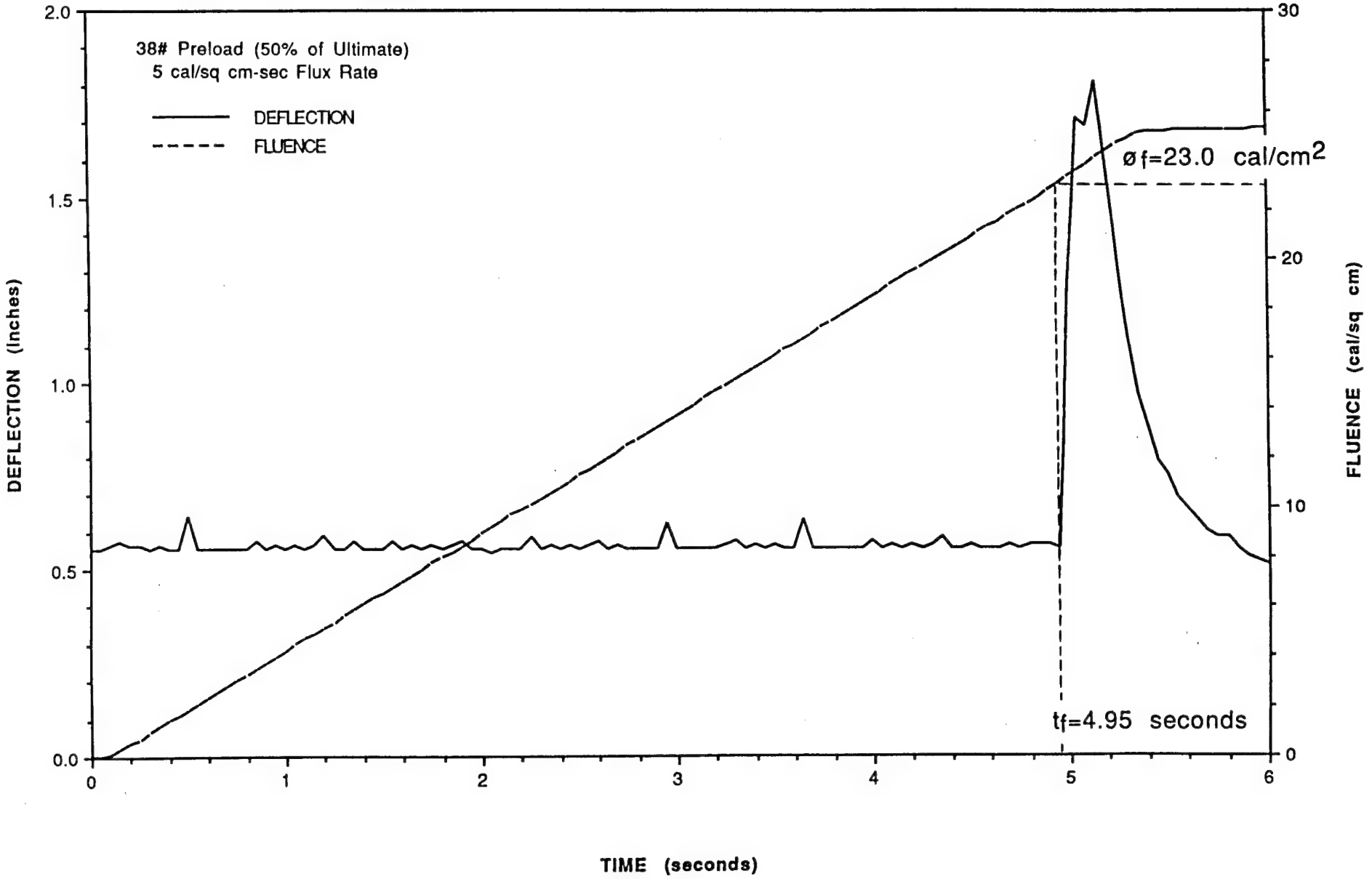

Figure D-20. Deflection and fluence vs. time for TRAC sample #14.

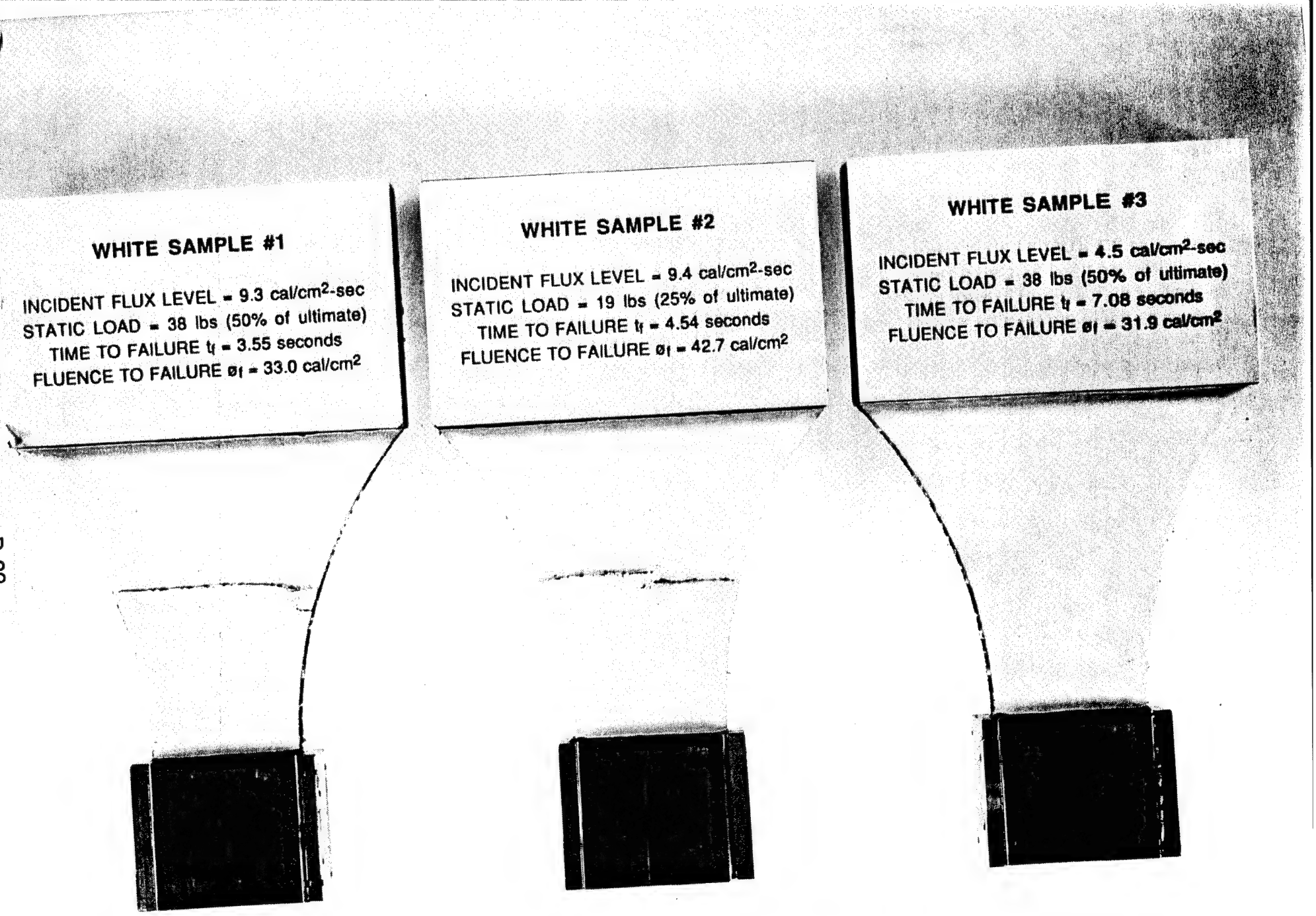

Figure D-21. Post test photograph of white samples #1, #2 and #3.

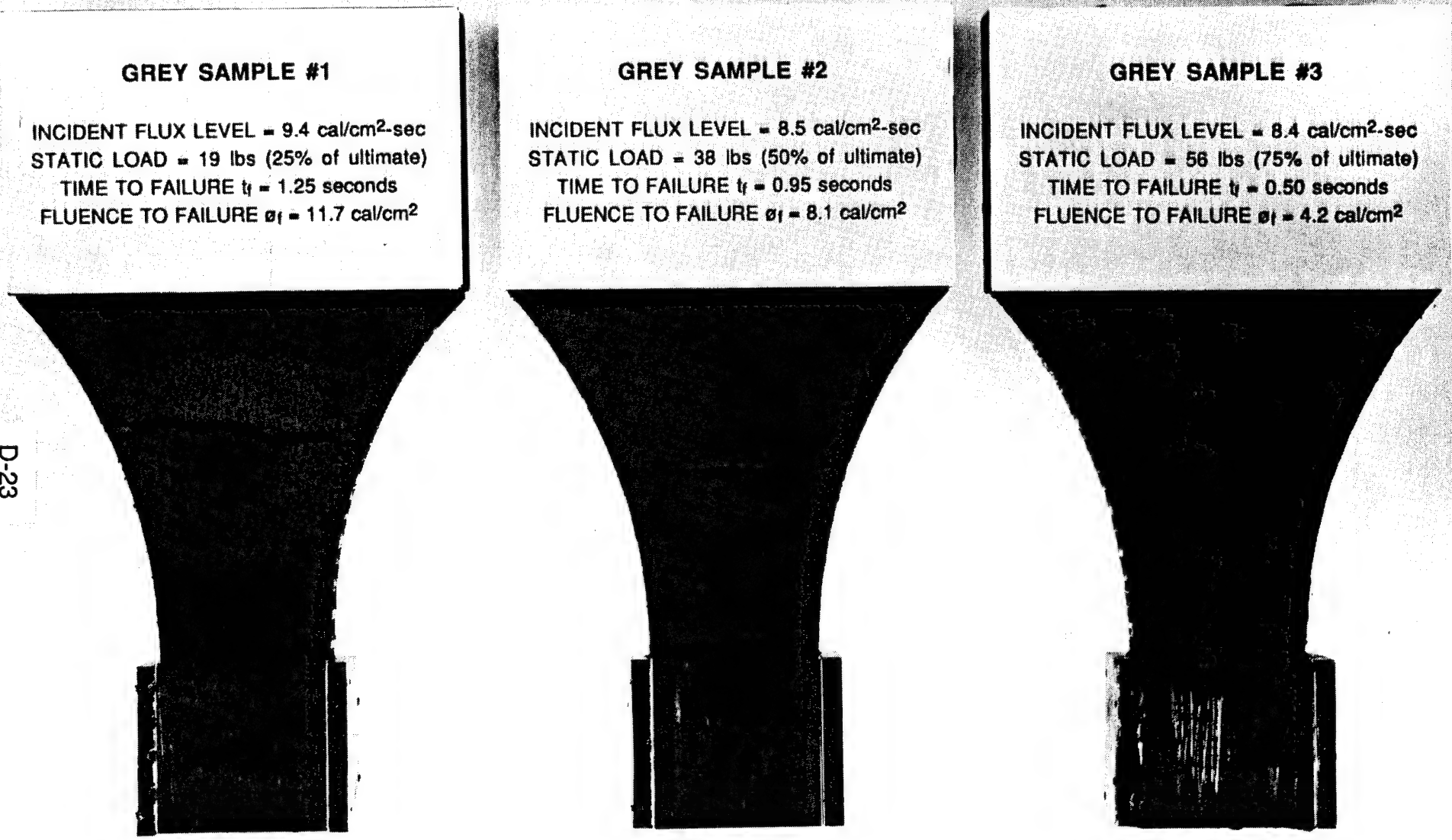

Figure D-22. Post test photograph of grey samples #1, #2 and #3.

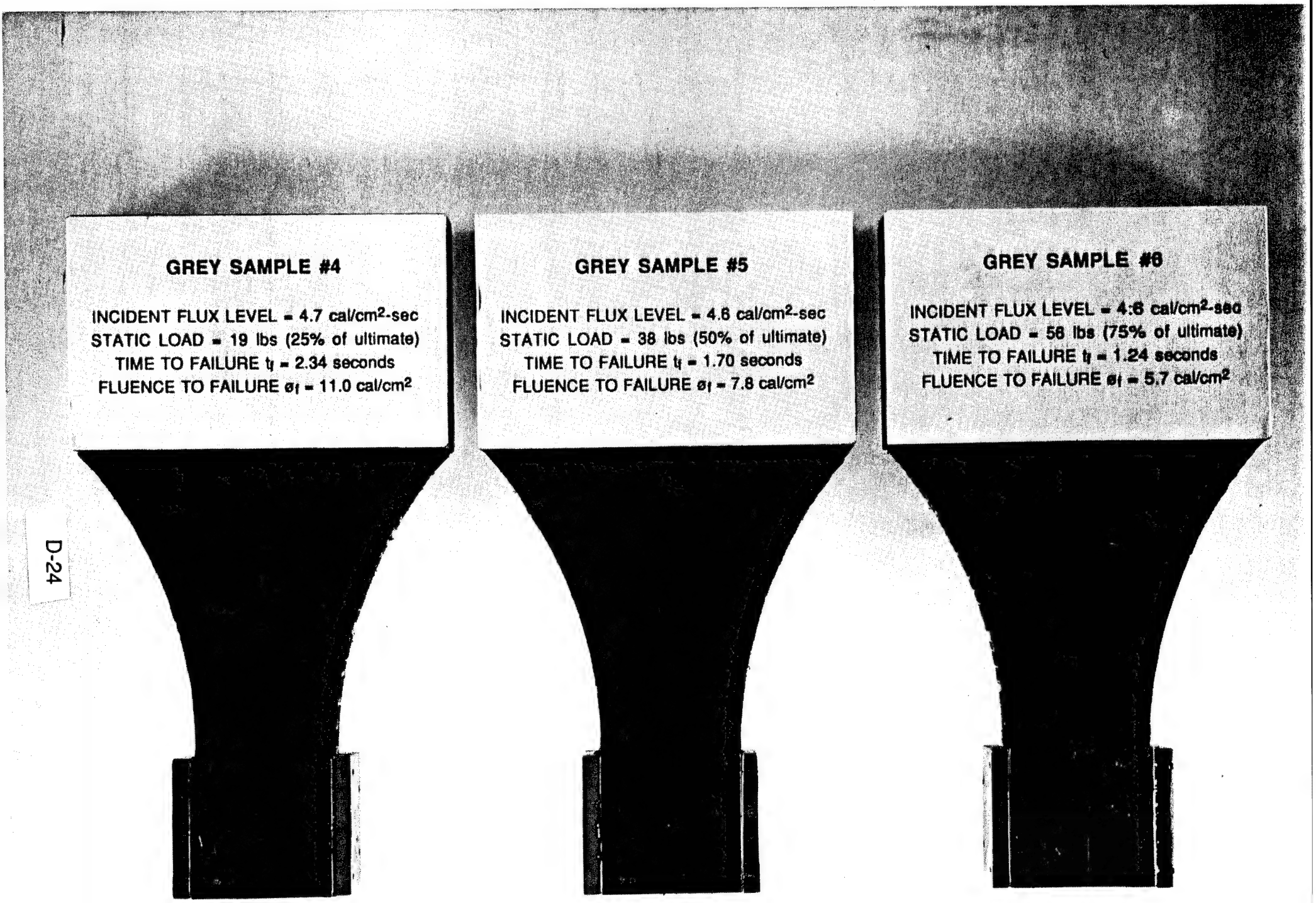

Figure D-23. Post test photograph of grey samples #4, #5 and #6.

GREY SAMPLE #7

INCIDENT FLUX LEVEL = 4.7 cal/cm^2-sec
STATIC LOAD = 19 lbs (25% of ultimate)
TIME TO FAILURE t_f = 2.60 seconds
FLUENCE TO FAILURE ϕ_f = 12.3 cal/cm^2

GREY SAMPLE #8

INCIDENT FLUX LEVEL = 4.3 cal/cm^2-sec
STATIC LOAD = 56 lbs (75% of ultimate)
TIME TO FAILURE t_f = 0.70 seconds
FLUENCE TO FAILURE ϕ_f = 3.0 cal/cm^2

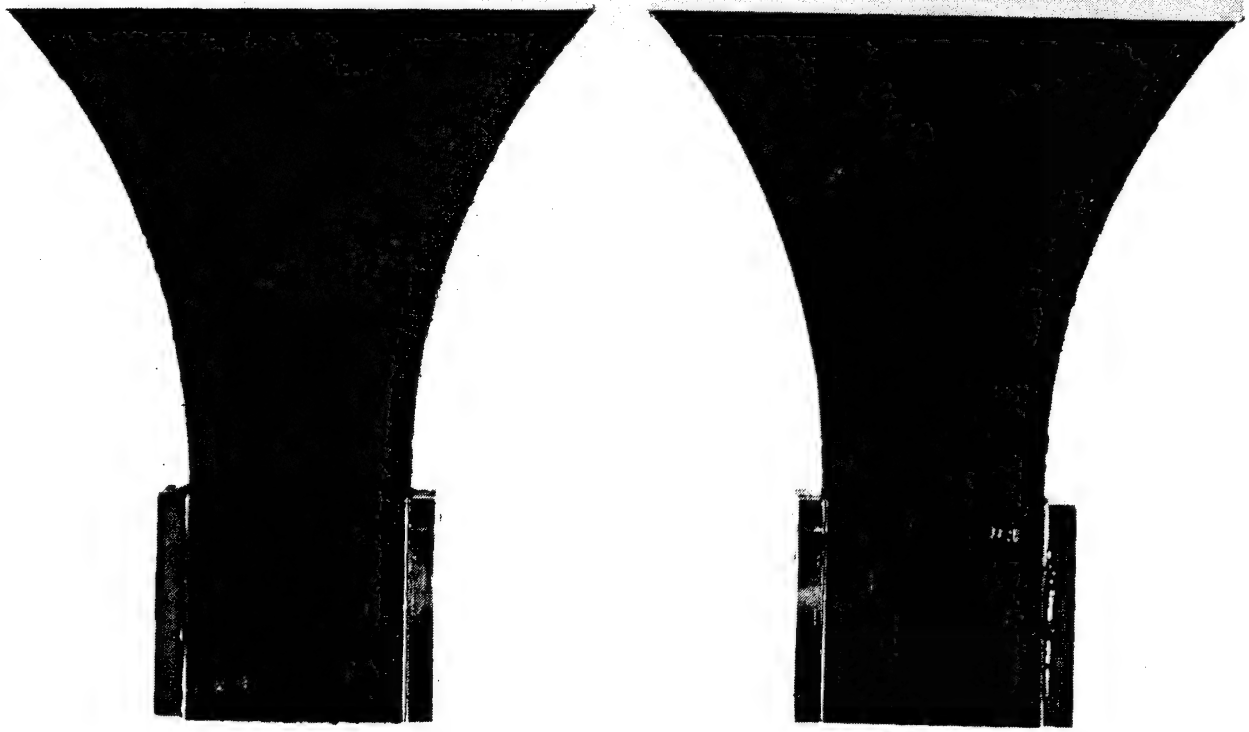

Figure D-24. Post test photograph of grey samples #7 and #8.

BLACK SAMPLE #1

INCIDENT FLUX LEVEL = 4.5 cal/cm^2-sec
STATIC LOAD = 19 lbs (25% of ultimate)
TIME TO FAILURE t_f = 1.71 seconds
FLUENCE TO FAILURE ϕ_f = 7.7 cal/cm^2

BLACK SAMPLE #2

INCIDENT FLUX LEVEL = 4.3 cal/cm^2-sec
STATIC LOAD = 38 lbs (50% of ultimate)
TIME TO FAILURE t_f = 1.45 seconds
FLUENCE TO FAILURE ϕ_f = 6.2 cal/cm^2

BLACK SAMPLE #3

INCIDENT FLUX LEVEL = 8.4 cal/cm^2-sec
STATIC LOAD = 38 lbs (50% of ultimate)
TIME TO FAILURE t_f = 0.80 seconds
FLUENCE TO FAILURE ϕ_f = 6.7 cal/cm^2

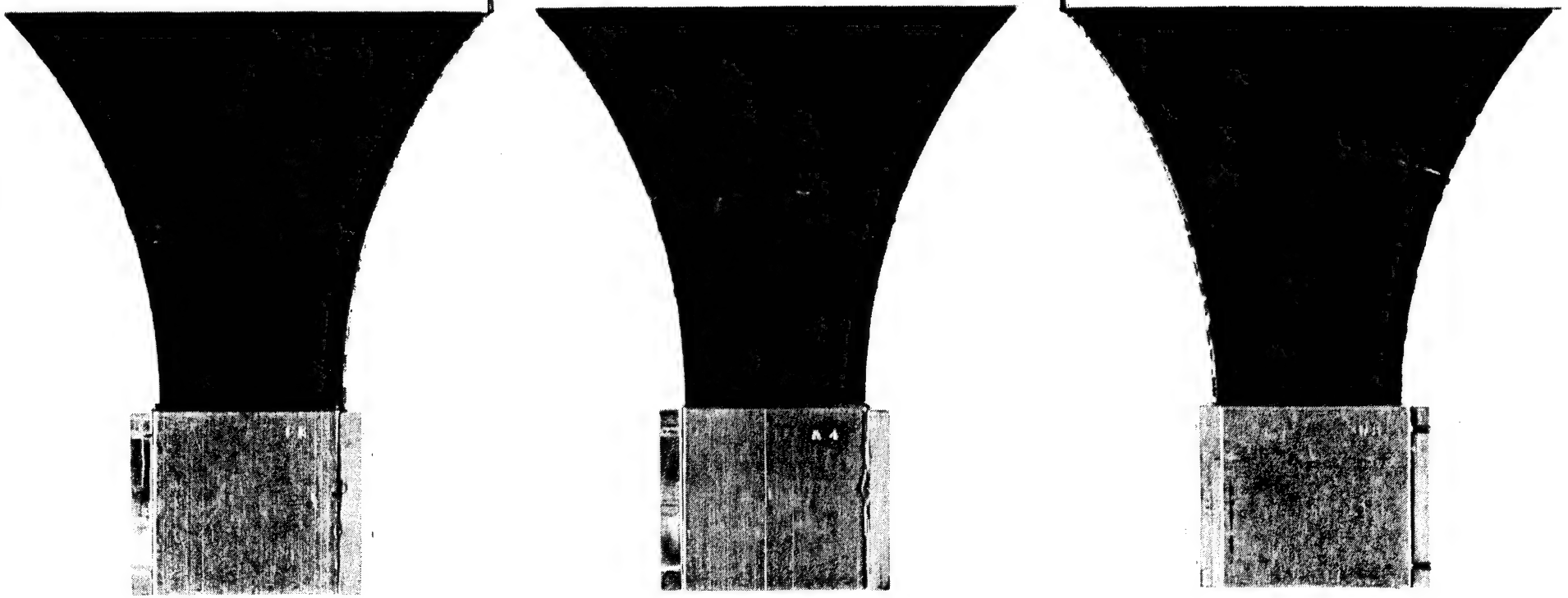

Figure D-25. Post test photograph of black samples #1, #2 and #3.

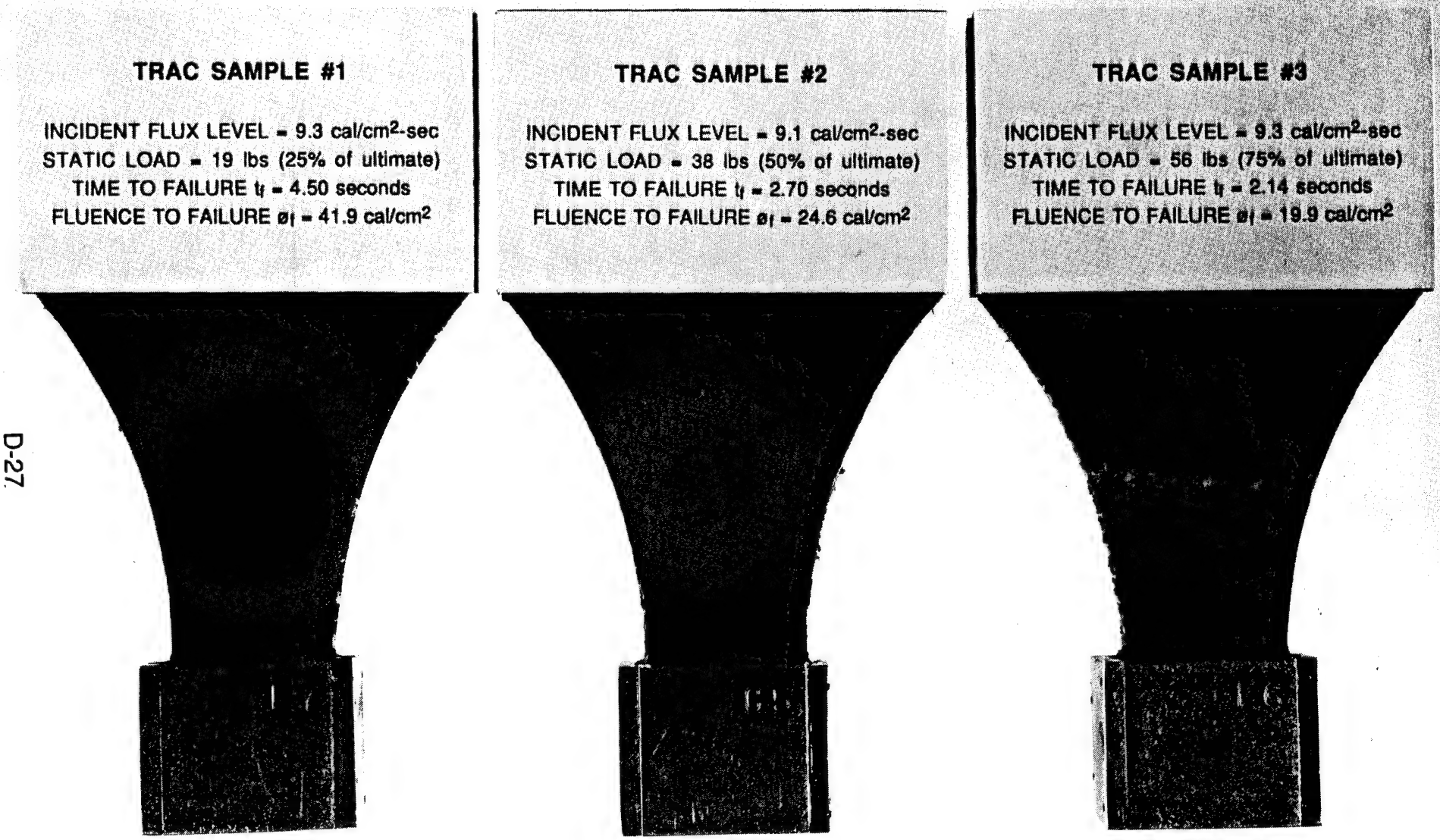

Figure D-26. Post test photograph of TRAC samples #1, #2 and #3.

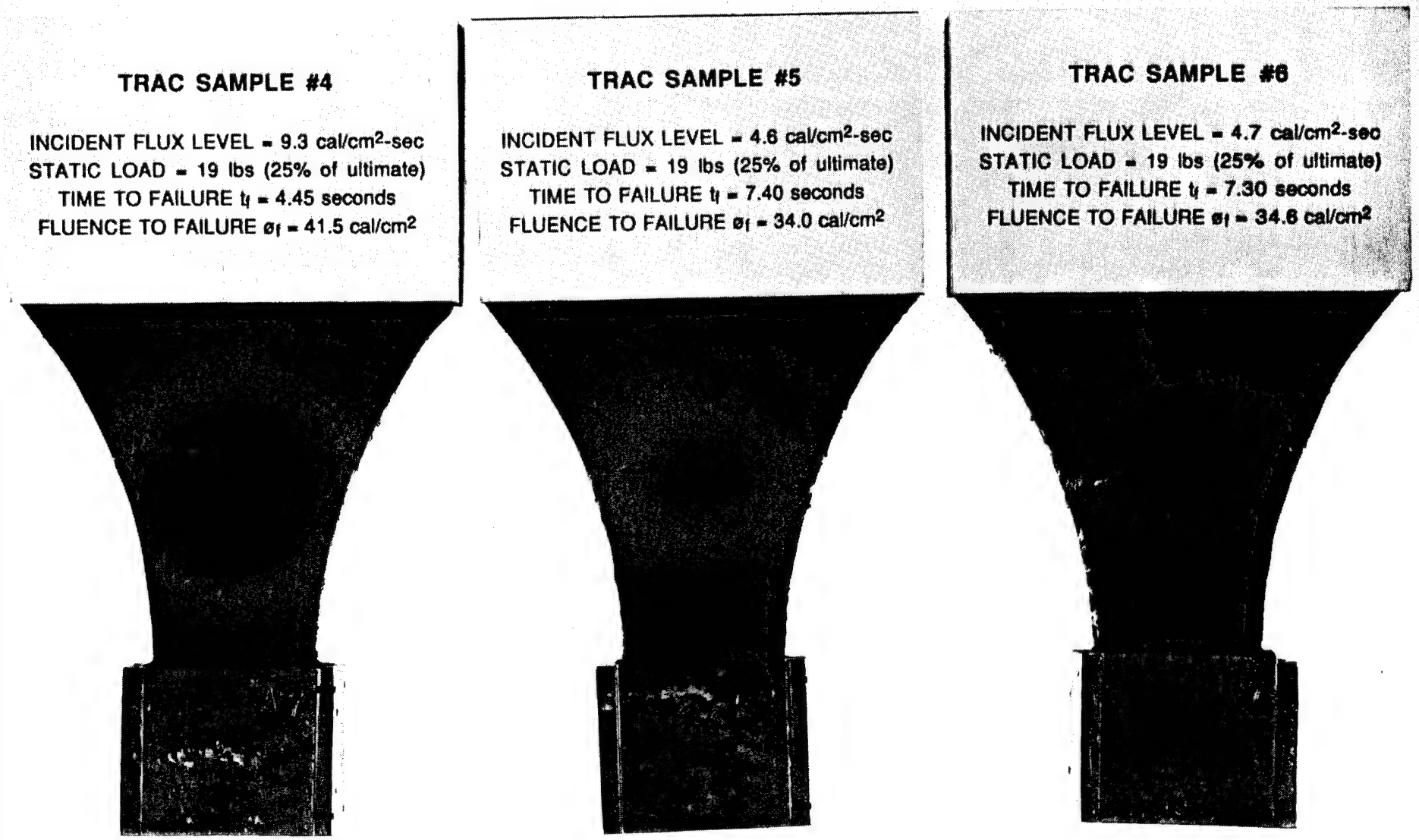

Figure D-27. Post test photograph of TRAC samples #4, #5 and #6.

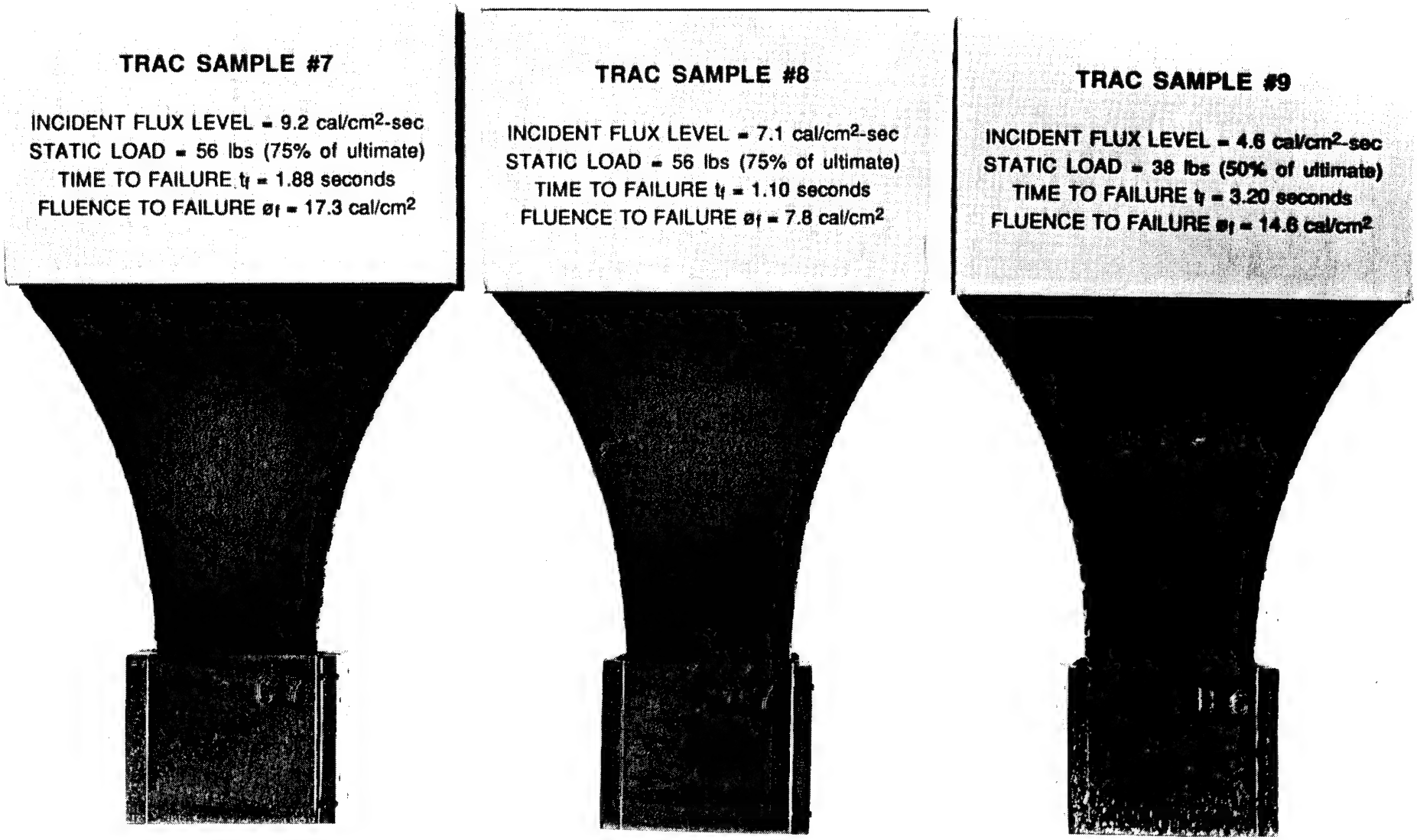

Figure D-28. Post test photograph of TRAC samples #7, #8 and #9.

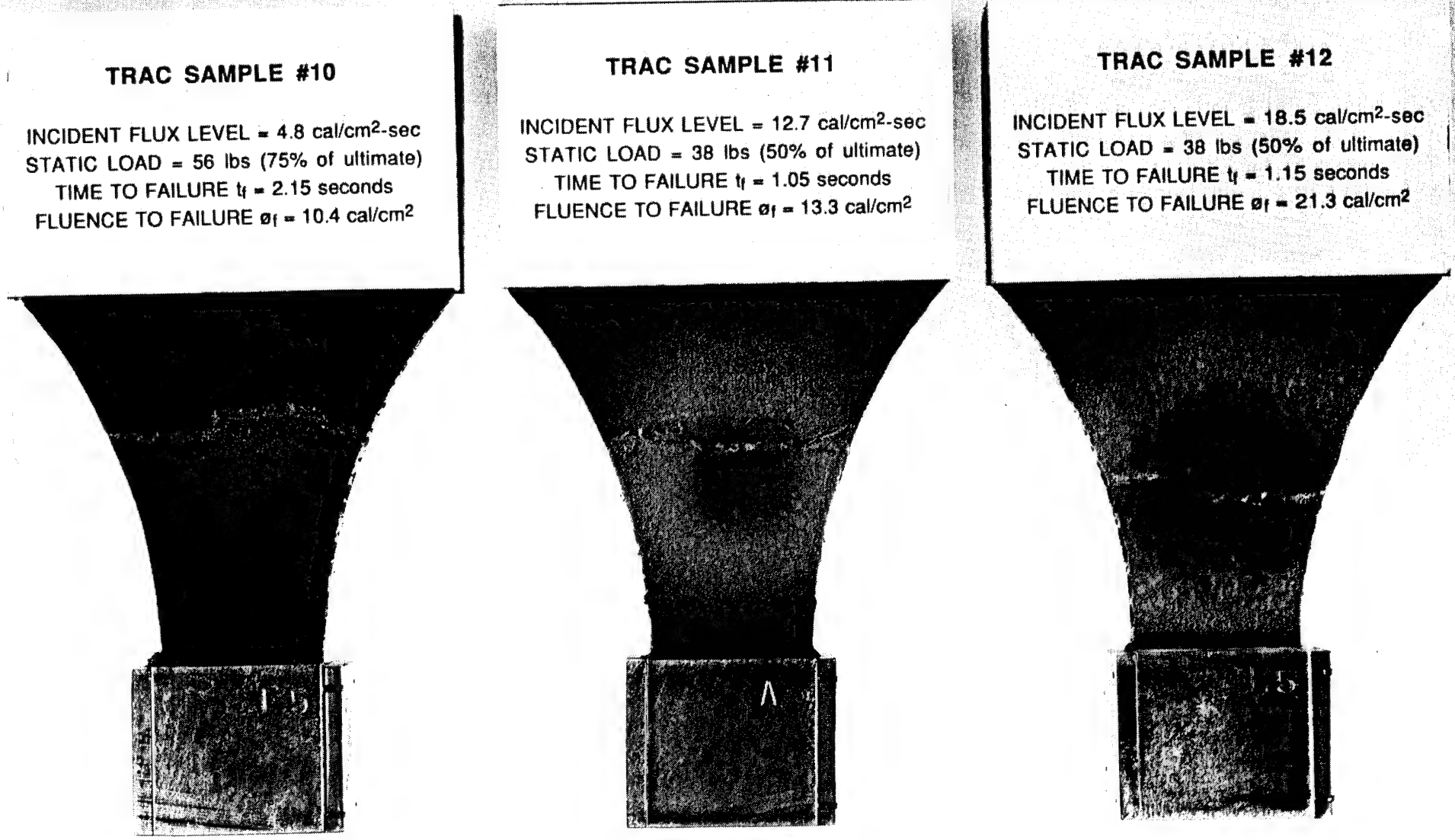

Figure D-29. Post test photograph of TRAC samples #10, #11 and #12.

Figure D-30. Post test photograph of TRAC samples #13 and #14.

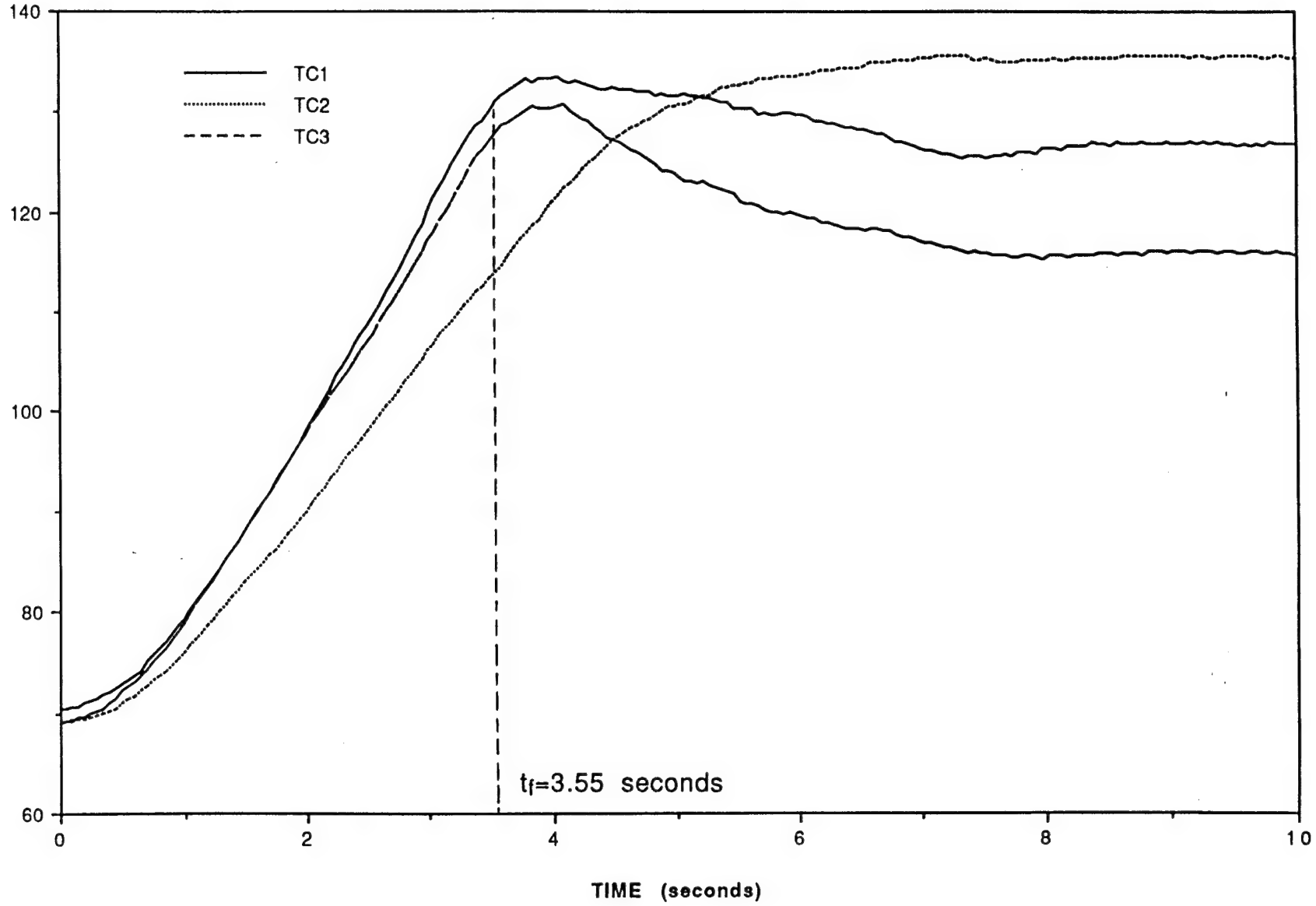

Figure D-31. Thermocouple response vs. time for white sample #1.

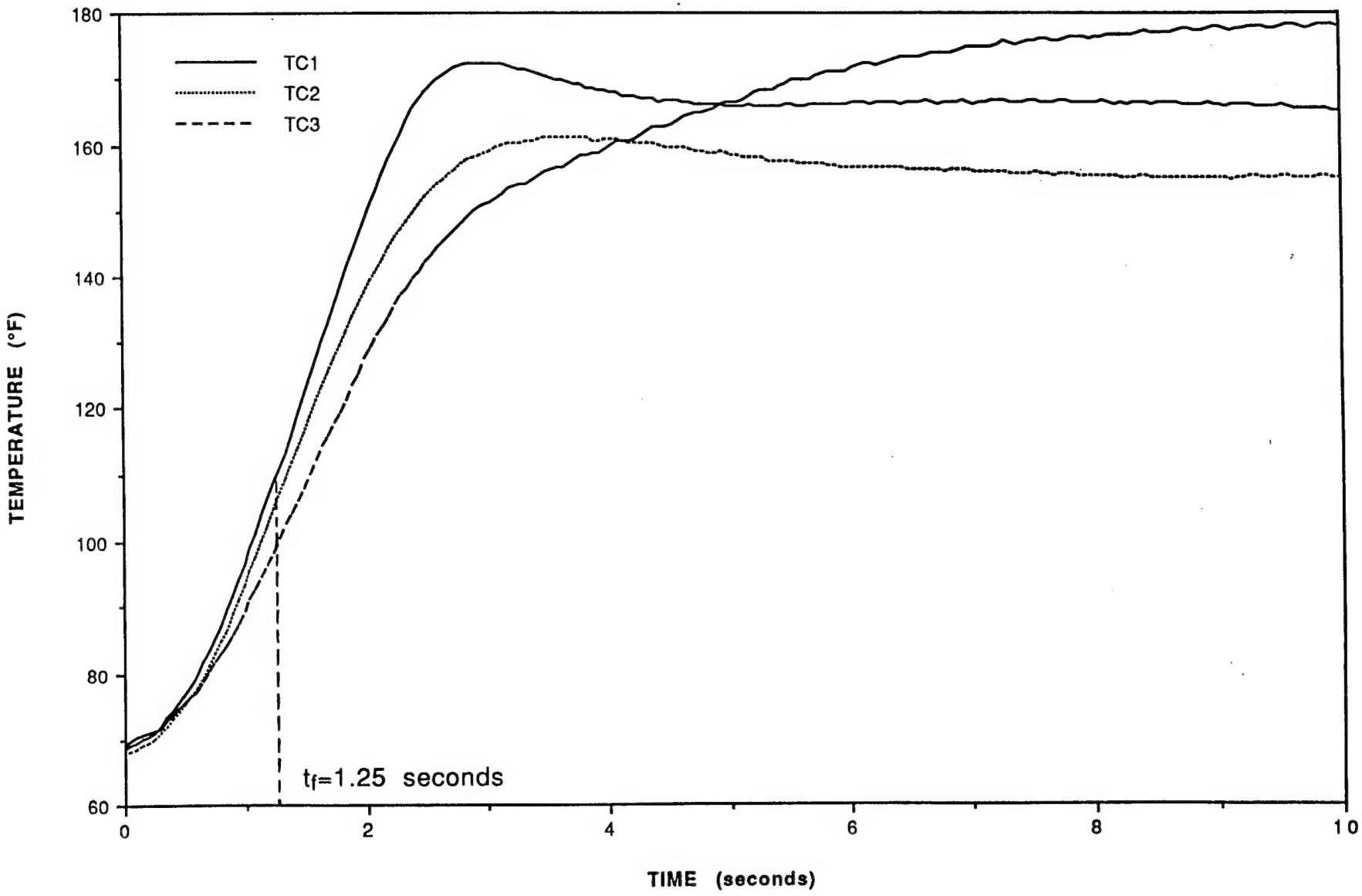

Figure D-32. Thermocouple response vs. time for grey sample #1.

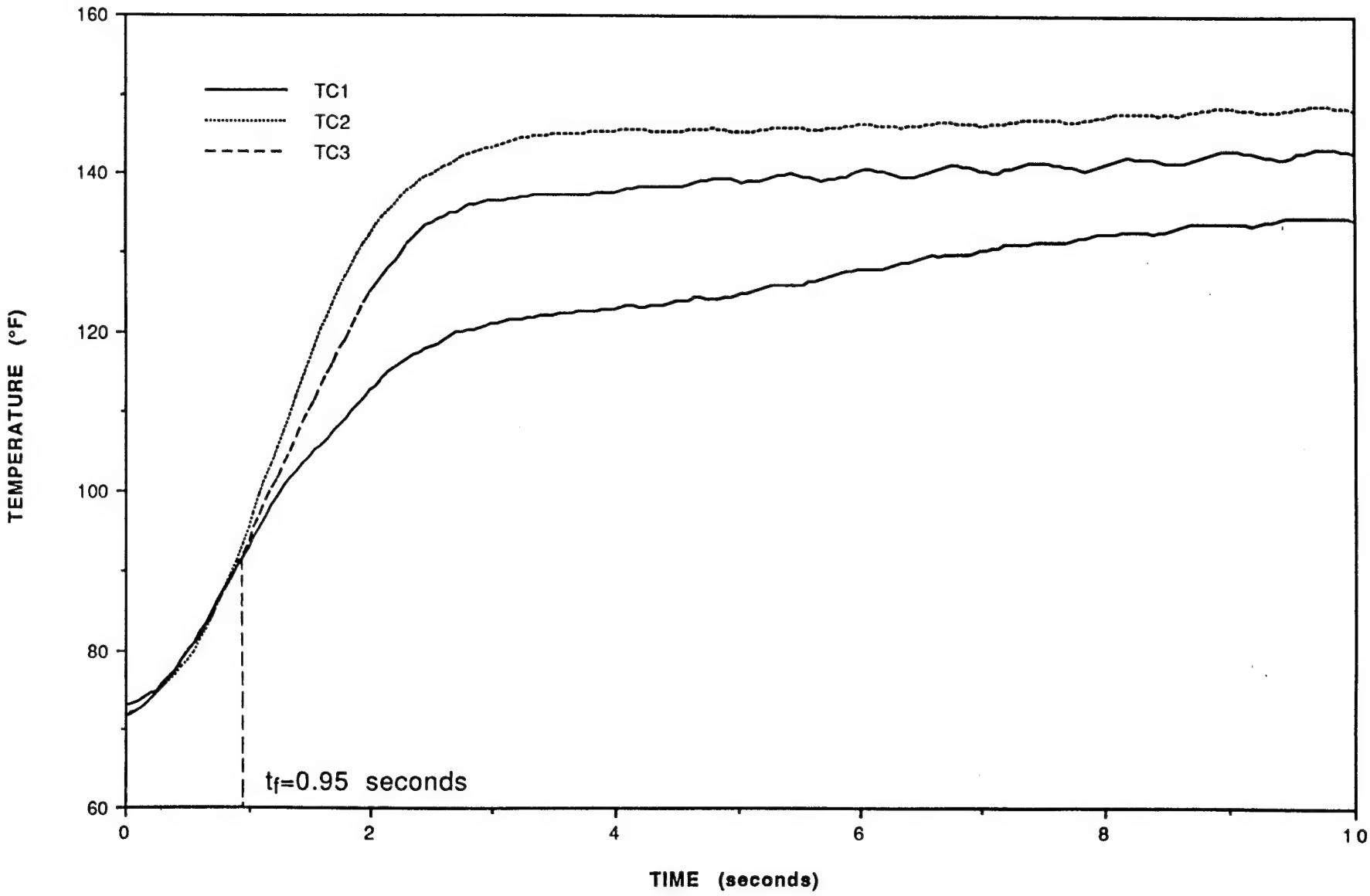

Figure D-33. Thermocouple response vs. time for grey sample #2.

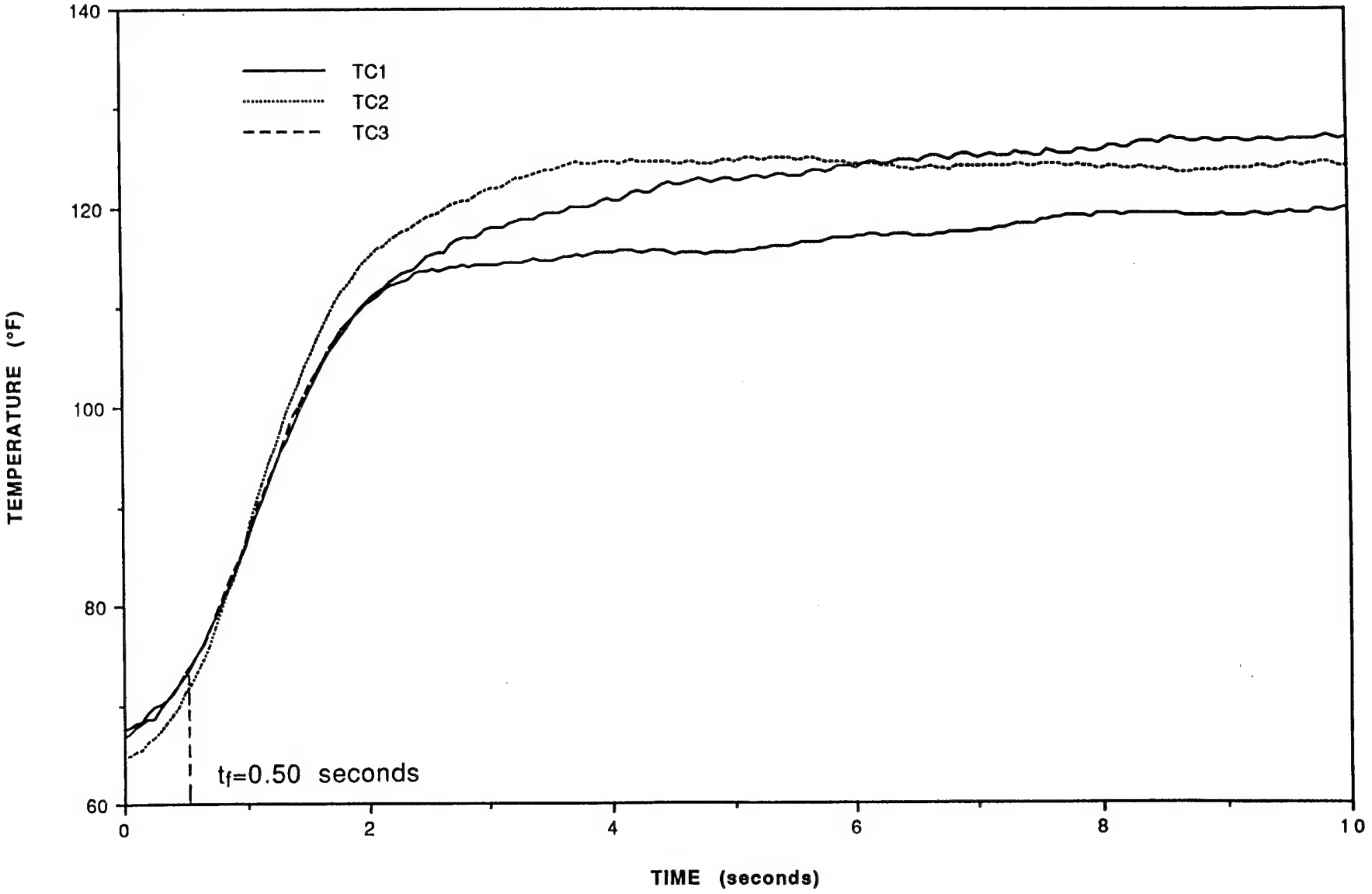

Figure D-34. Thermocouple response vs. time for grey sample #3.

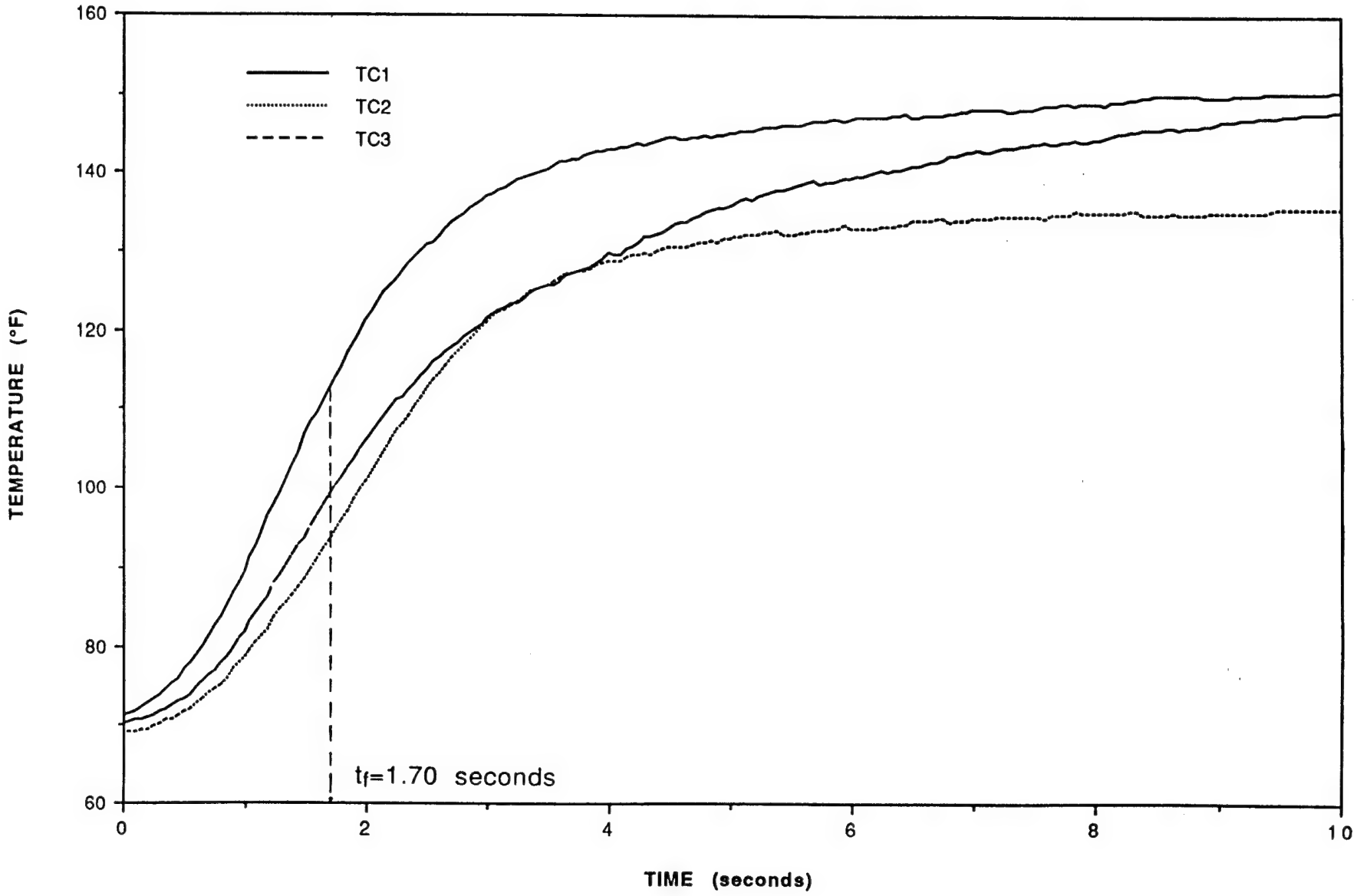

Figure D-35. Thermocouple response vs. time for grey sample #5.

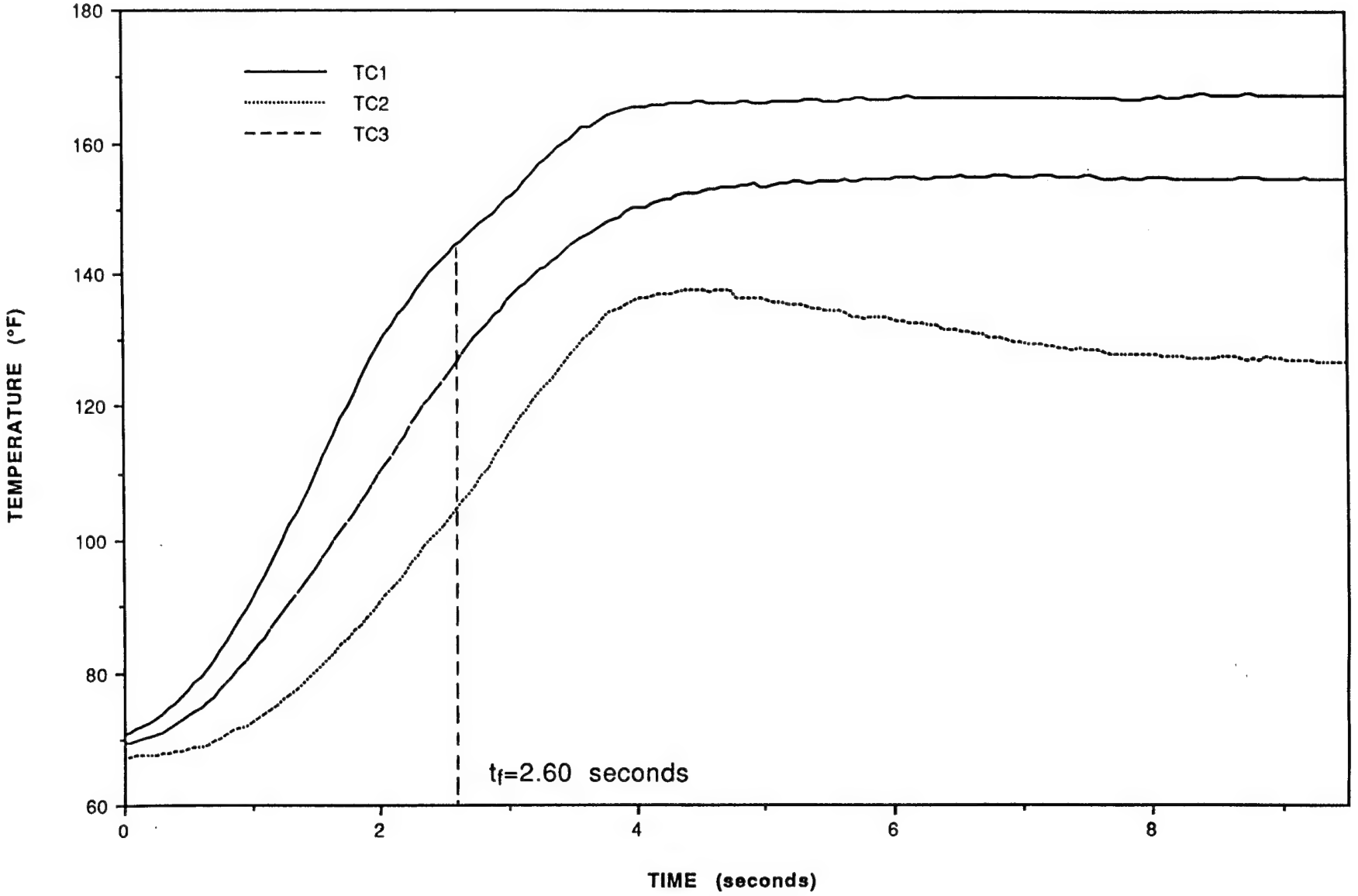

Figure D-36. Thermocouple response vs. time for grey sample #7.

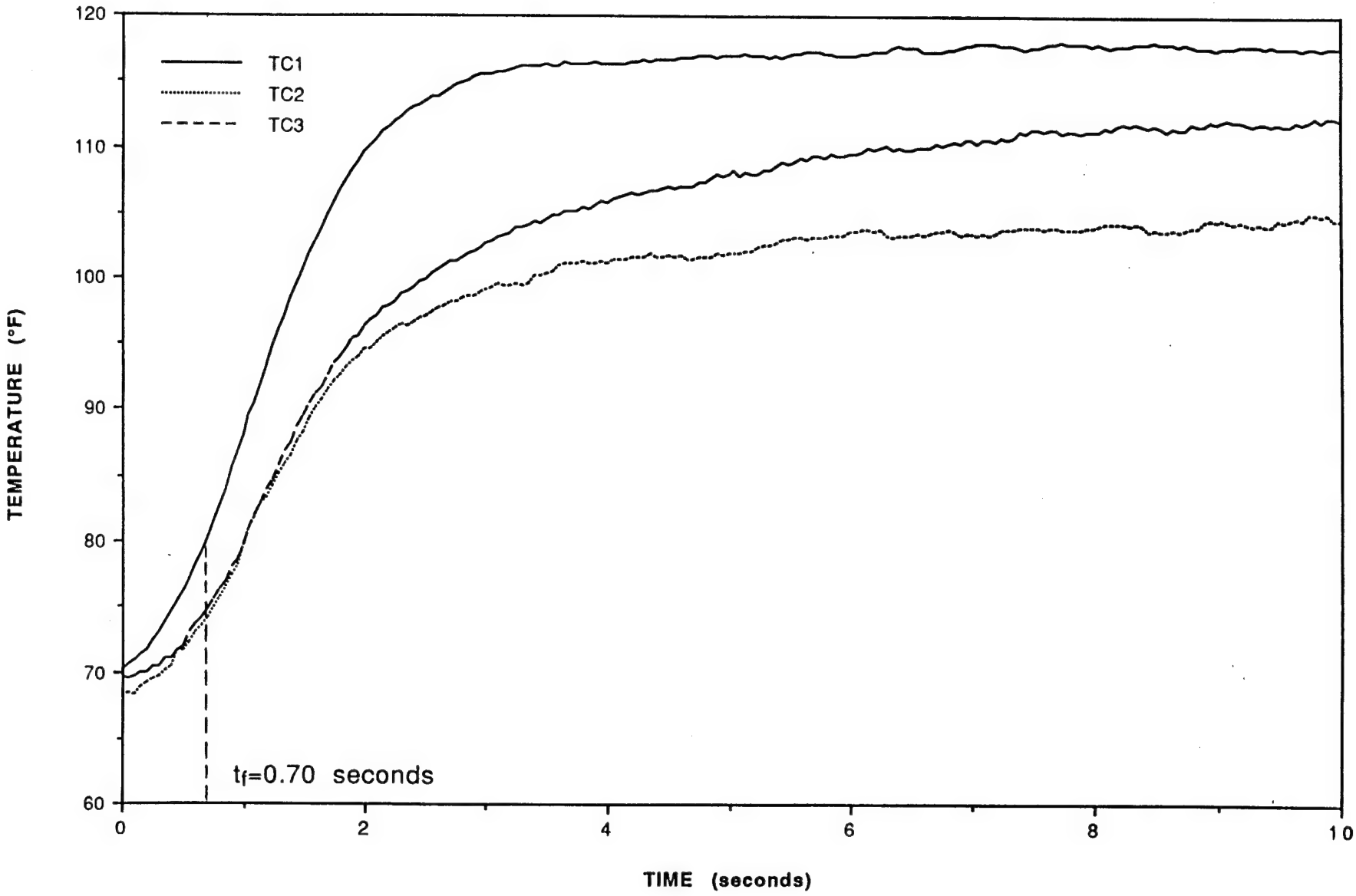

Figure D-37. Thermocouple response vs. time for grey sample #8.

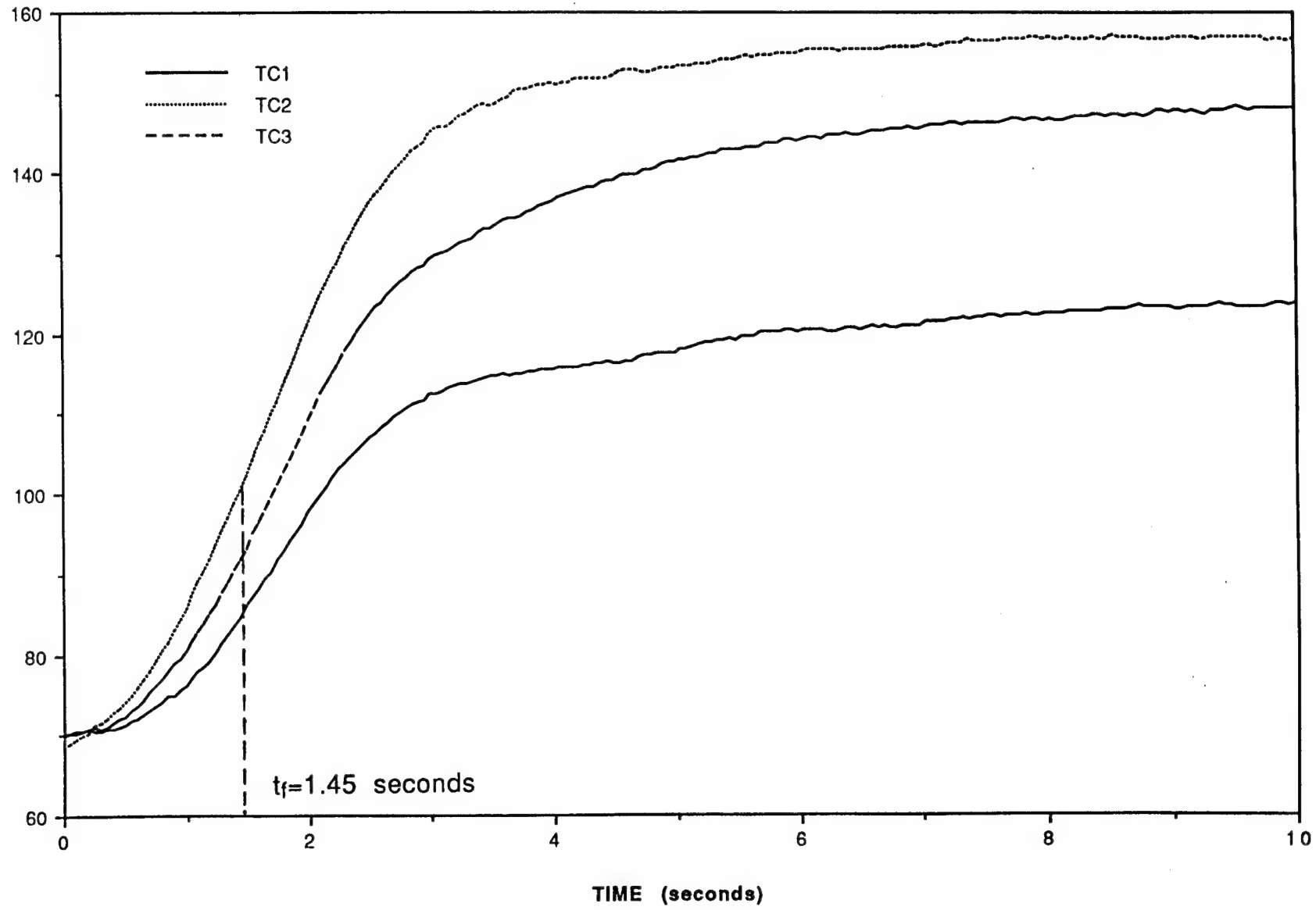

Figure D-38. Thermocouple response vs. time for black sample #2.

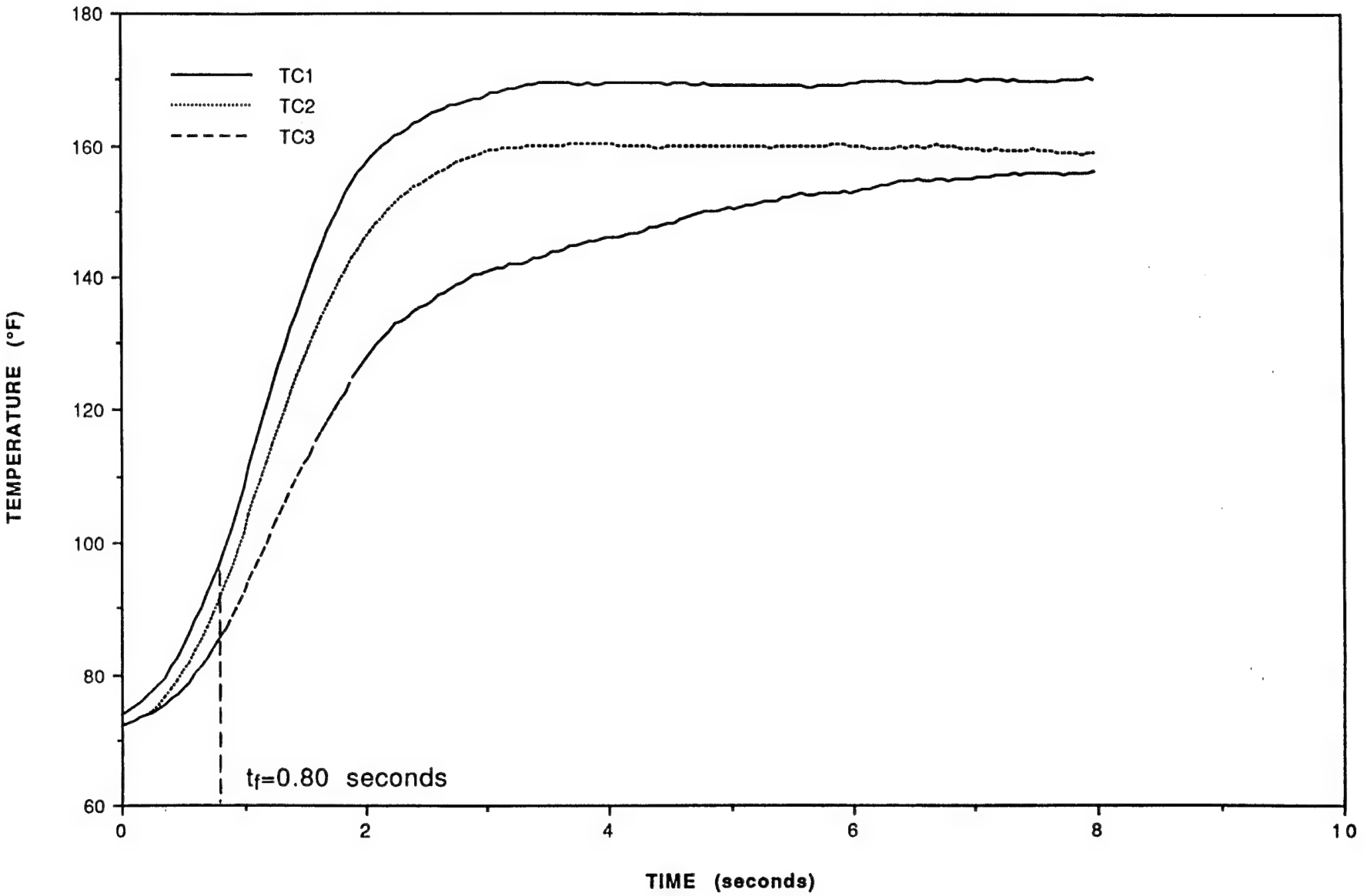

Figure D-39. Thermocouple response vs. time for black sample #3.

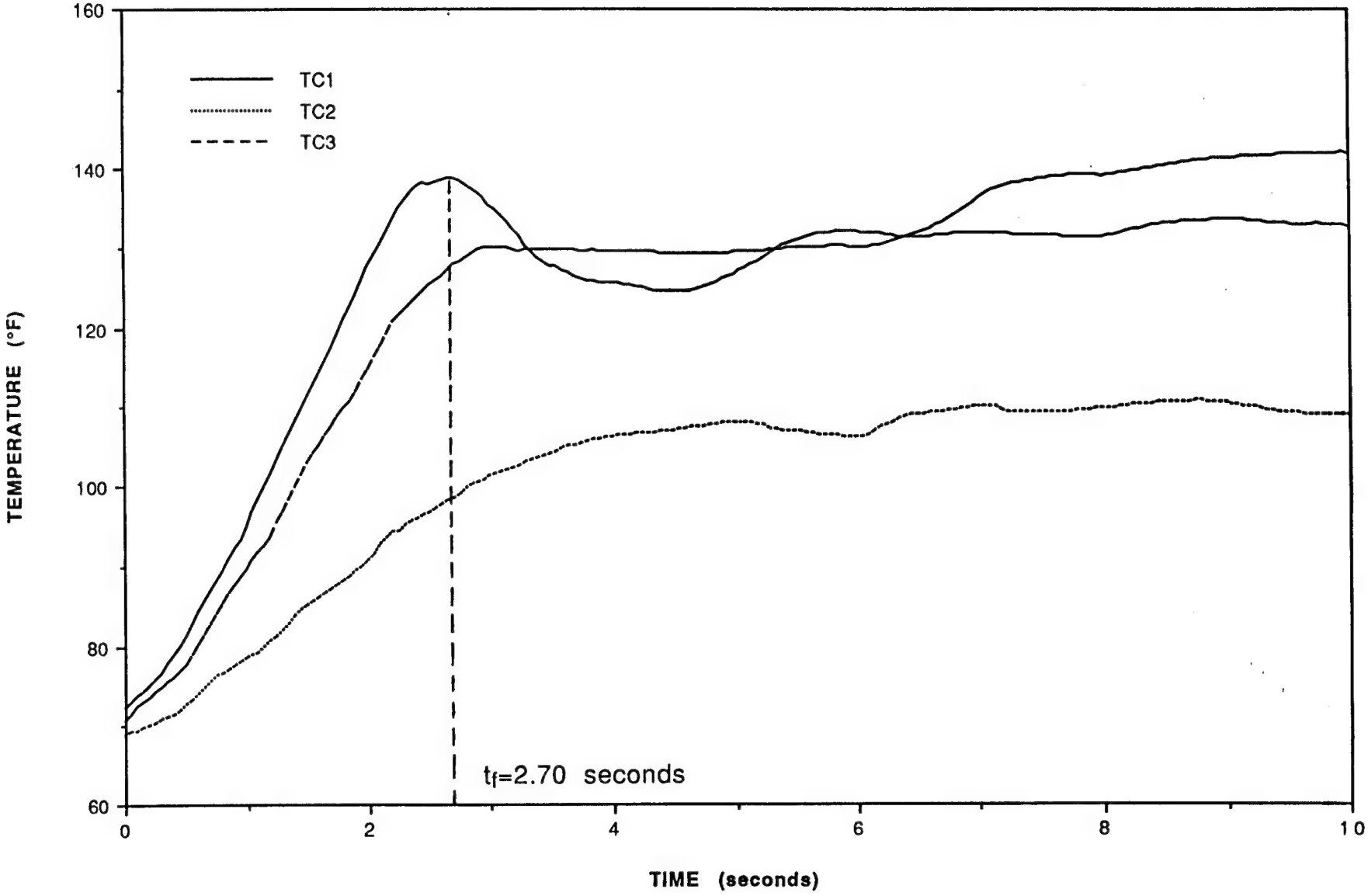

Figure D-40. Thermocouple response vs. time for TRAC sample #2.

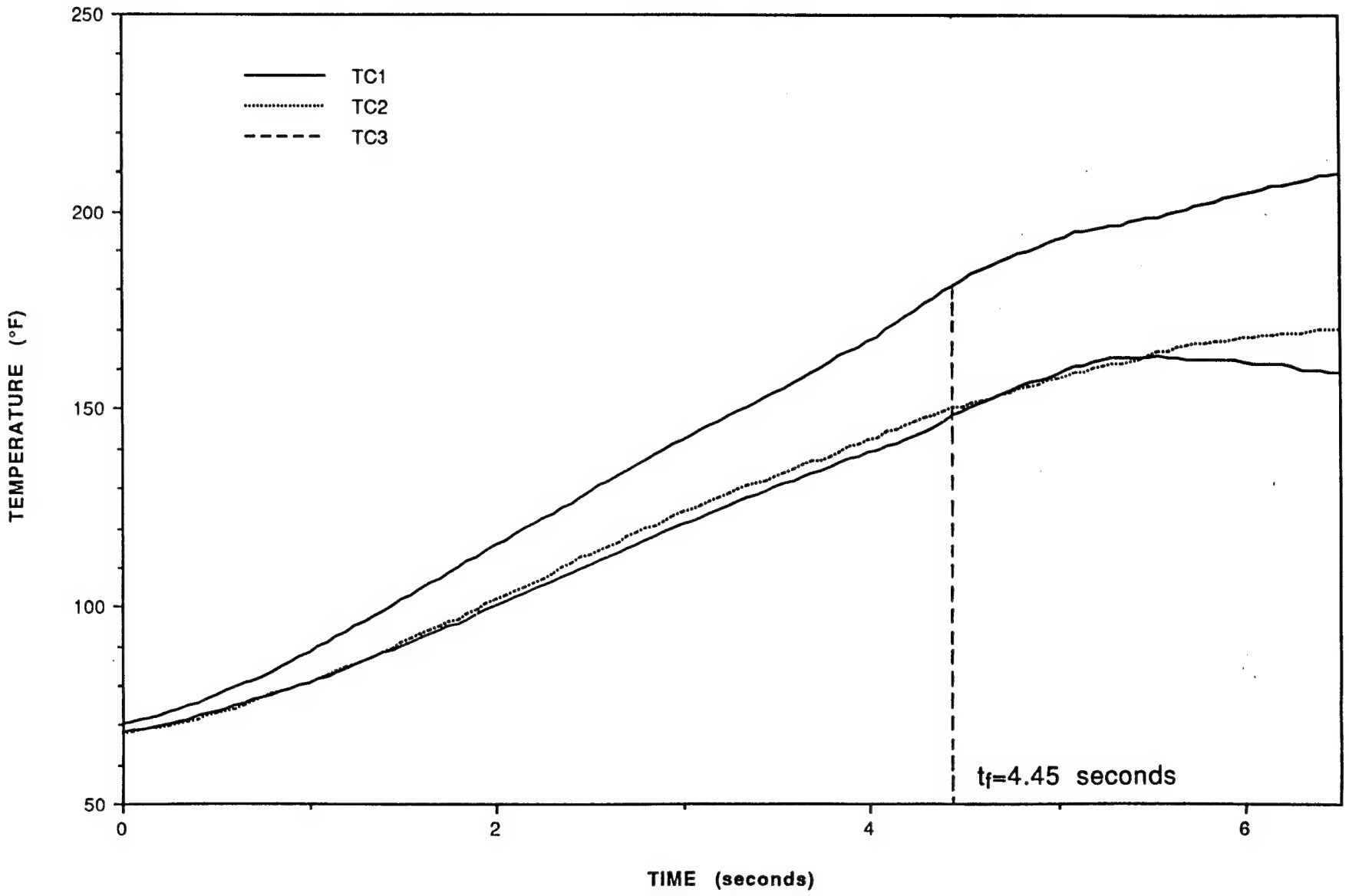

Figure D-41. Thermocouple response vs. time for TRAC sample #4.

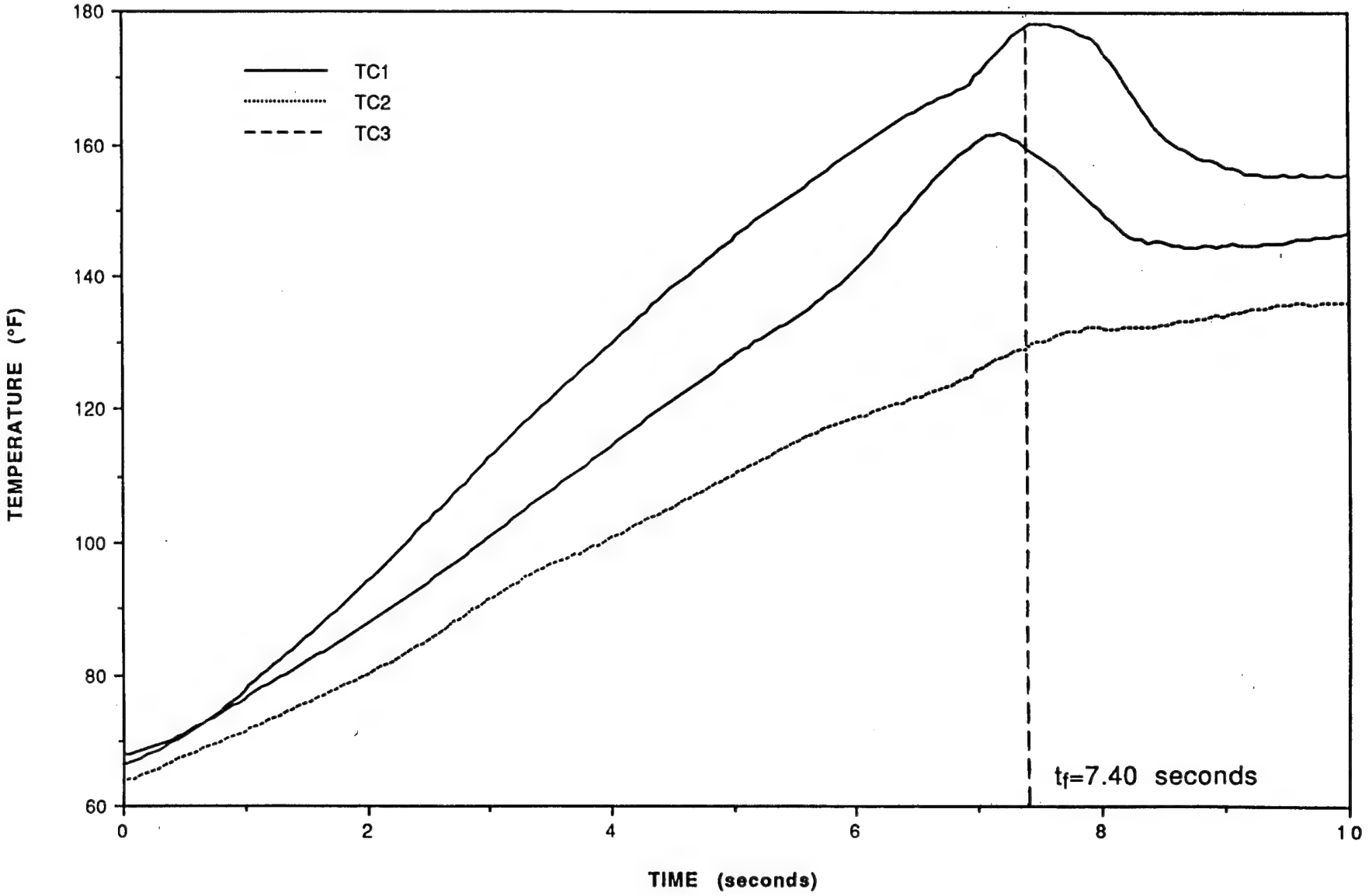

Figure D-42. Thermocouple response vs. time for TRAC sample #5.

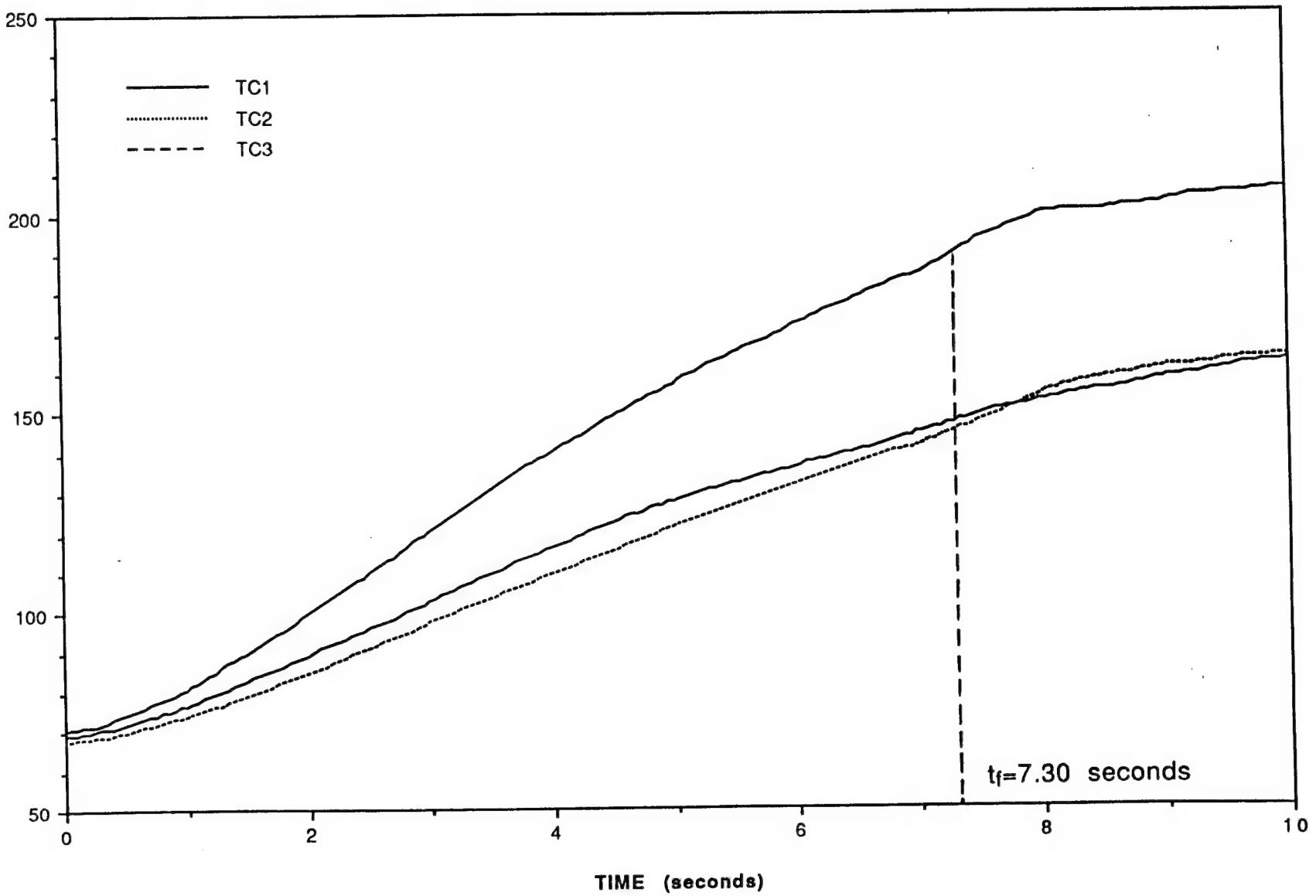

Figure D-43. Thermocouple response vs. time for TRAC sample #6.

APPENDIX E

TEST SAMPLE RESPONSE PLOTS AND PHOTOGRAPHS FROM TESTS WITH SIMULTANEOUS THERMAL FLUX AND 10% MECHANICAL PRELOAD

The following data was generated from combined thermal-mechanical testing of composite beams conducted at the National Renewable Energy Laboratory High Flux Solar Furnace during the week of September 27 - October 1, 1993. Results from these tests are described in Section 5.4.4.3.1.

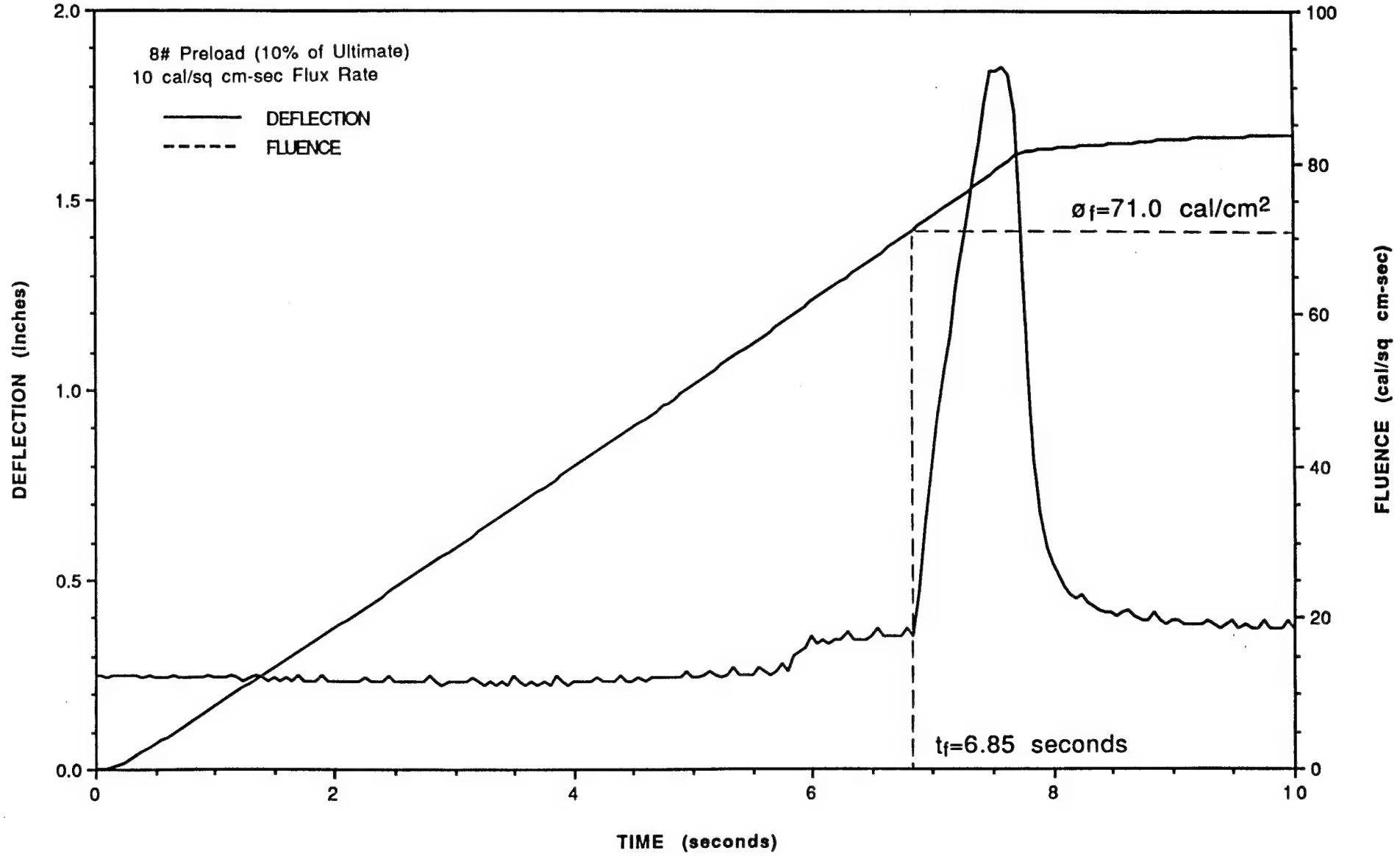

Figure E-1. Deflection and fluence vs. time for white sample #4.

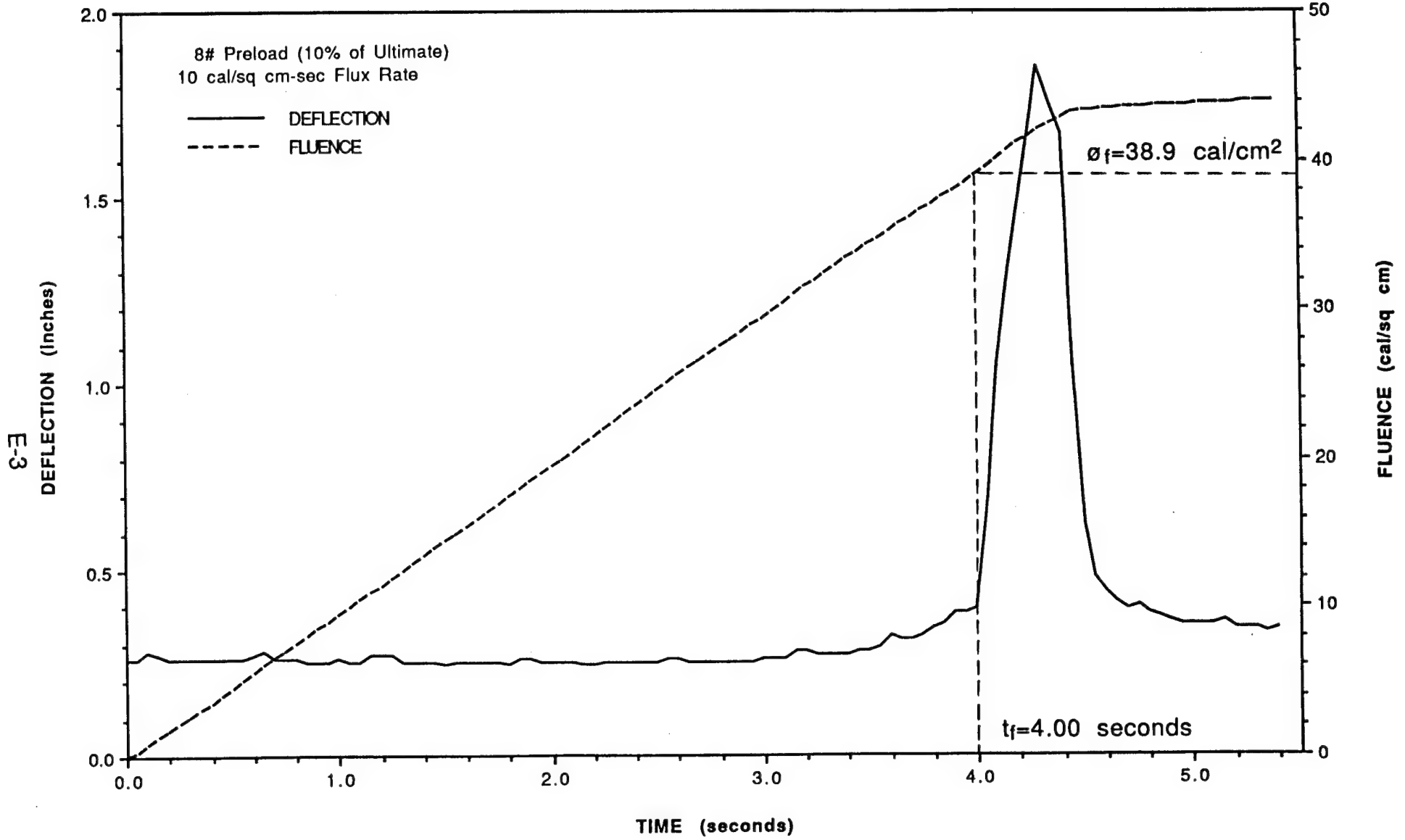

Figure E-2. Deflection and fluence vs. time for white sample #5.

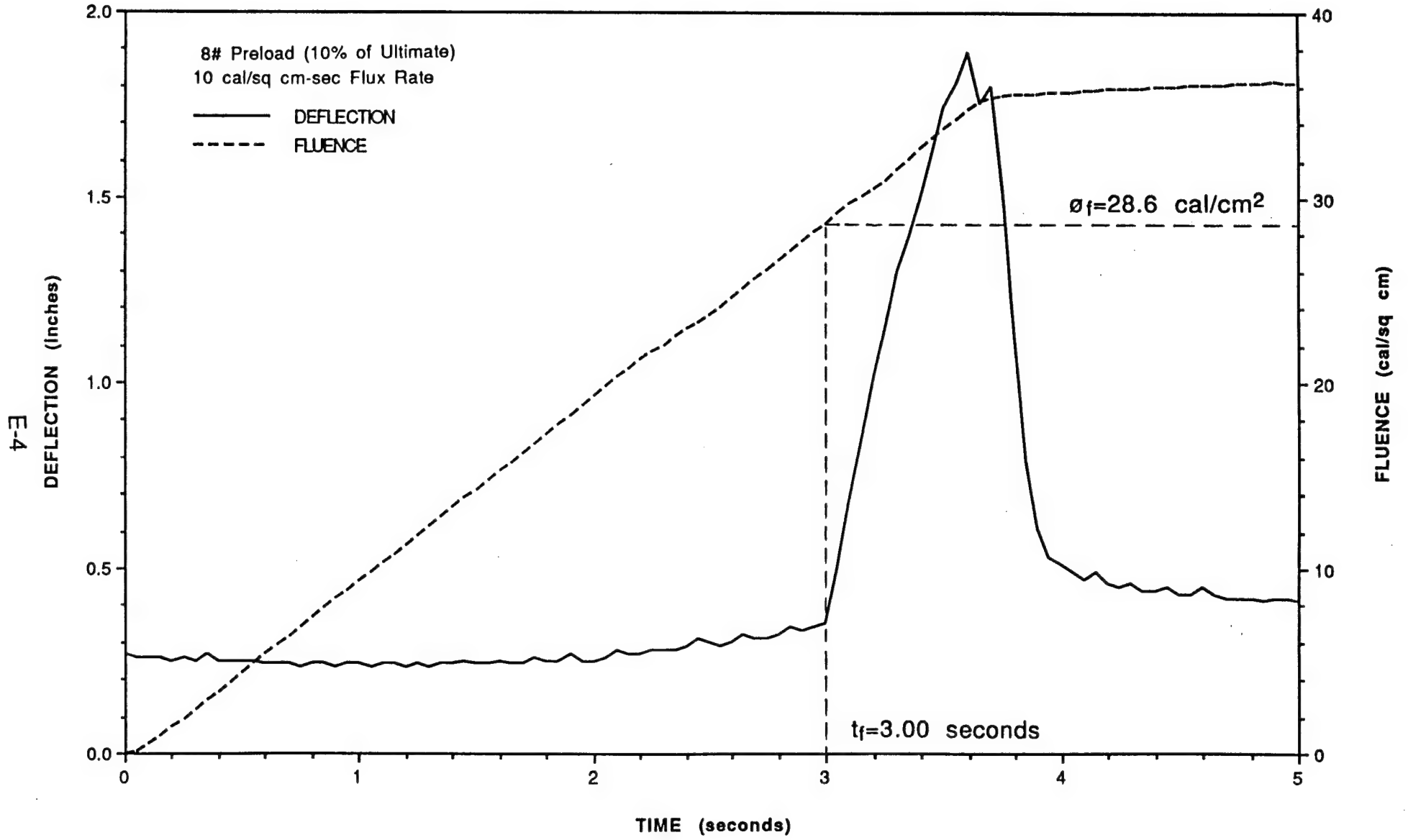

Figure E-3. Deflection and fluence vs. time for grey sample #9.

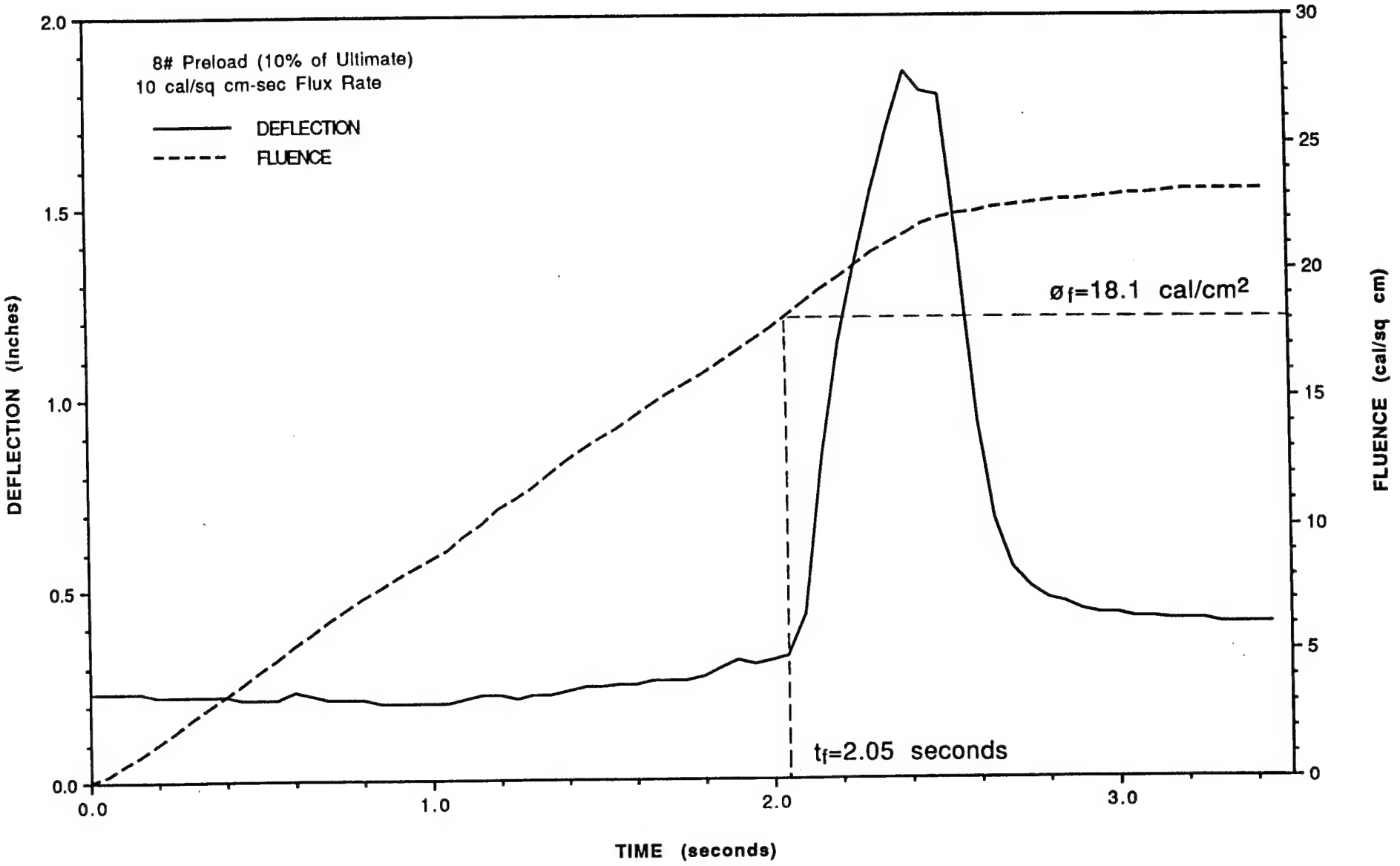

Figure E-4. Deflection and fluence vs. time for grey sample #10.

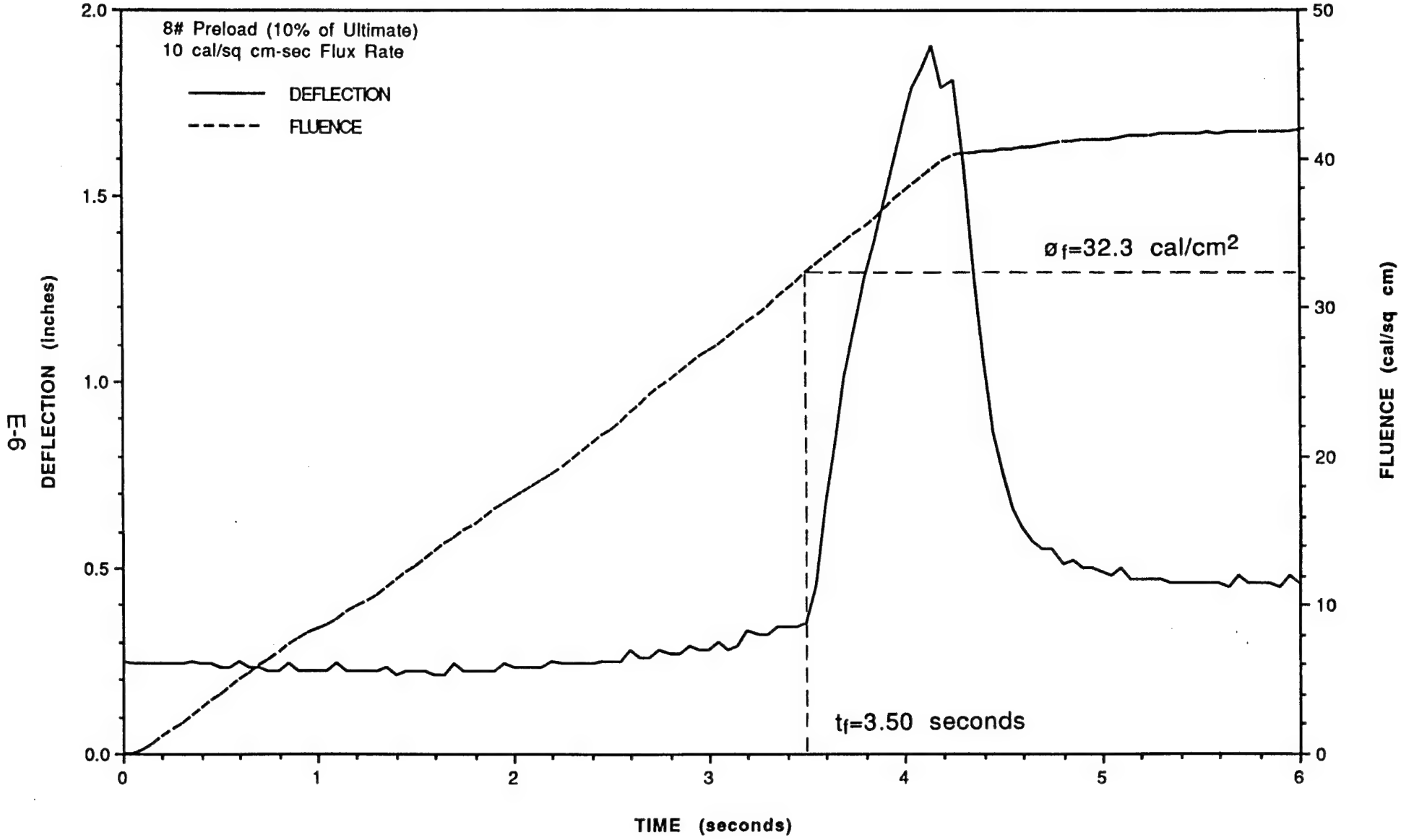

Figure E-5. Deflection and fluence vs. time for black sample #4.

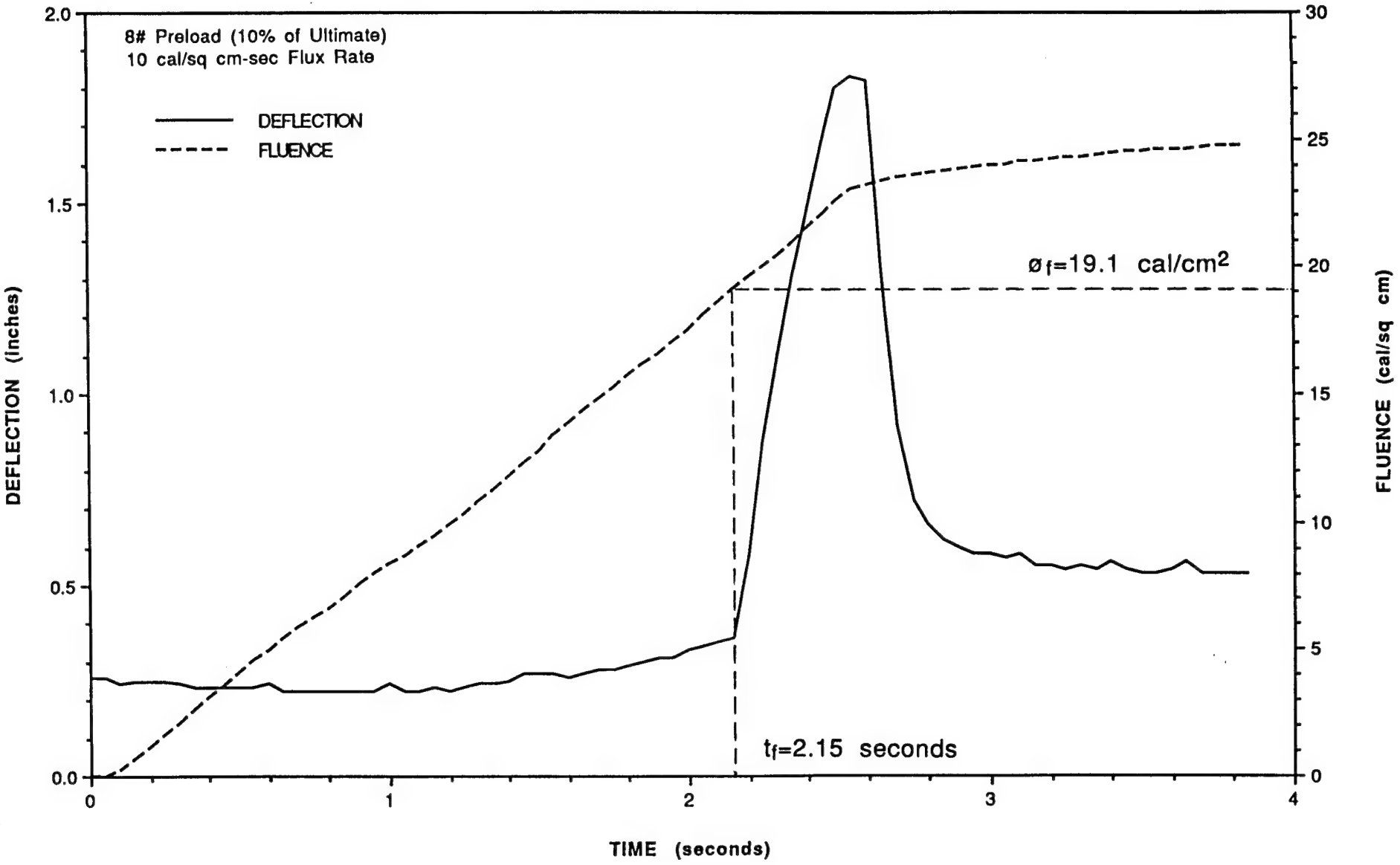

Figure E-6. Deflection and fluence vs. time for black sample #5.

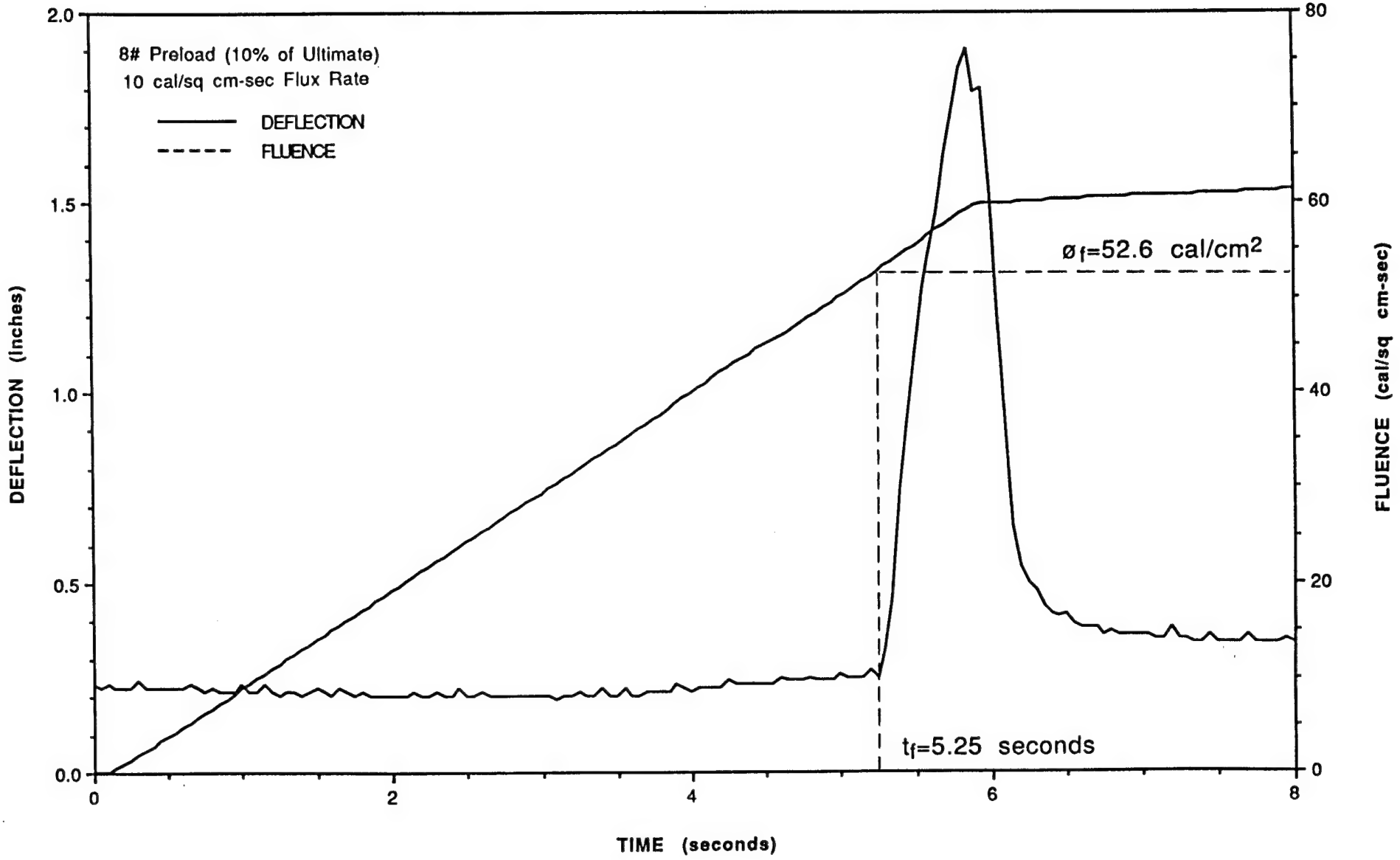

Figure E-7. Deflection and fluence vs. time for TRAC sample #17.

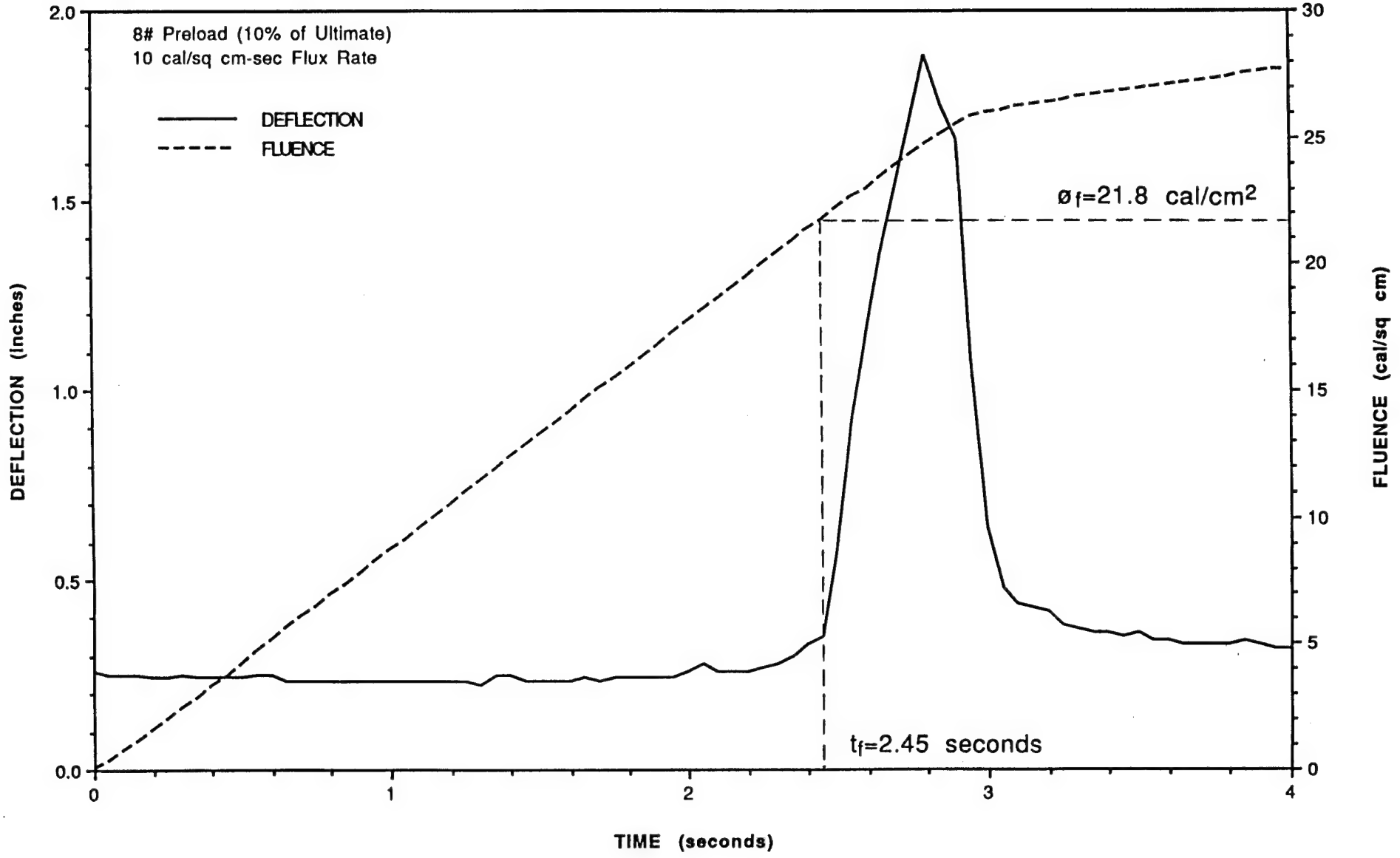

Figure E-8. Deflection and fluence vs. time for TRAC sample #18.

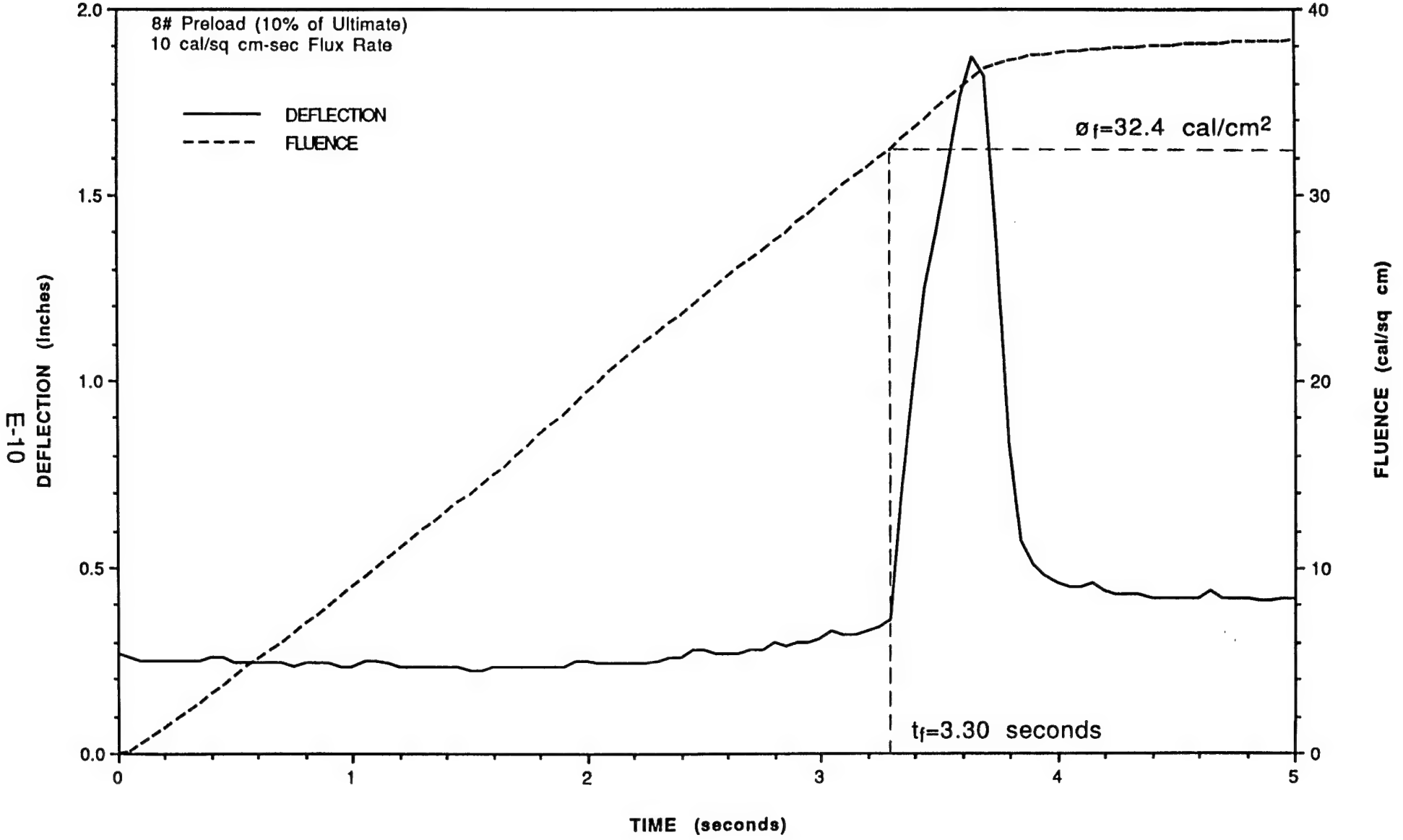

Figure E-9. Deflection and fluence vs. time for TRAC sample #19.

WHITE SAMPLE #4

INCIDENT FLUX LEVEL = 10.4 cal/cm^2-sec
STATIC LOAD = 8 lbs (10% of ultimate)
TIME TO FAILURE t_f = 6.85 seconds
FLUENCE TO FAILURE σ_f = 71.0 cal/cm^2

WHITE SAMPLE #5

INCIDENT FLUX LEVEL = 9.7 cal/cm^2-sec
STATIC LOAD = 8 lbs (10% of ultimate)
TIME TO FAILURE t_f = 4.00 seconds
FLUENCE TO FAILURE σ_f = 38.9 cal/cm^2

Figure E-10. Post test photograph of white samples #4 and #5.

GREY SAMPLE #9

INCIDENT FLUX LEVEL = 9.5 cal/cm^2-sec
STATIC LOAD = 8 lbs (10% of ultimate)
TIME TO FAILURE t_f = 3.00 seconds
FLUENCE TO FAILURE σ_f = 28.6 cal/cm^2

GREY SAMPLE #10

INCIDENT FLUX LEVEL = 8.8 cal/cm^2-sec
STATIC LOAD = 8 lbs (10% of ultimate)
TIME TO FAILURE t_f = 2.05 seconds
FLUENCE TO FAILURE σ_f = 18.1 cal/cm^2

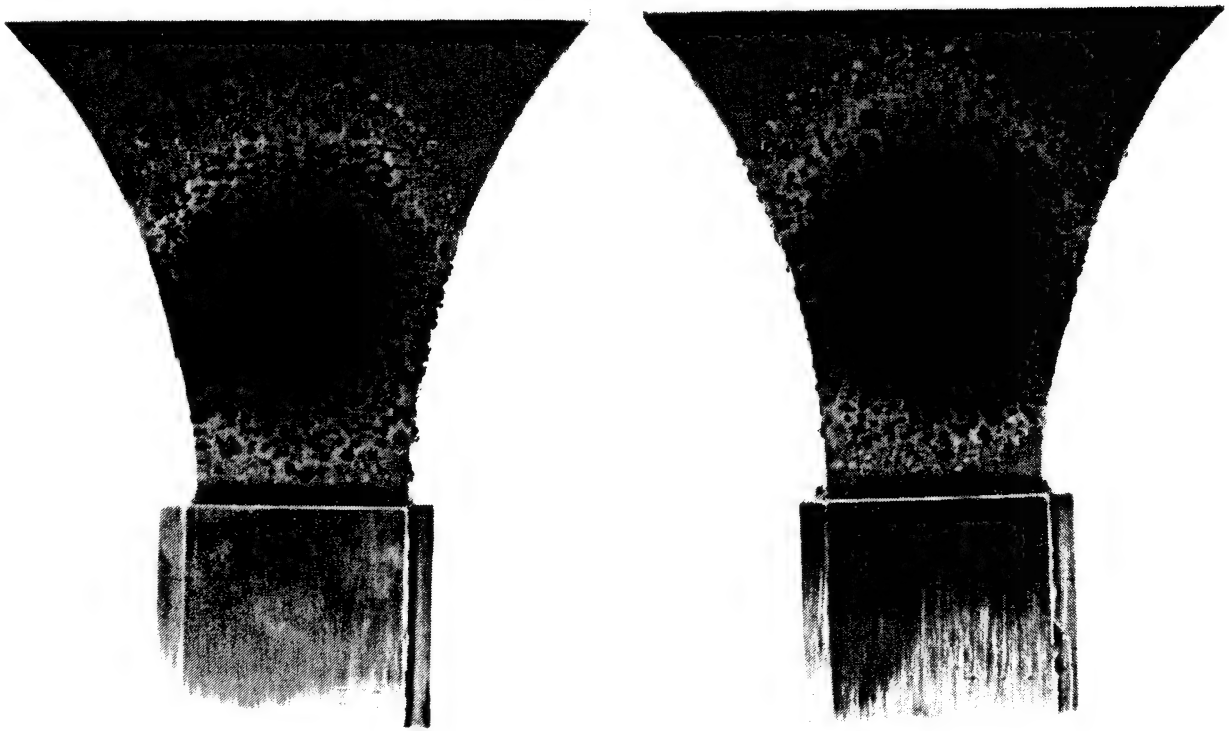

Figure E-11. Post test photograph of grey samples #9 and #10.

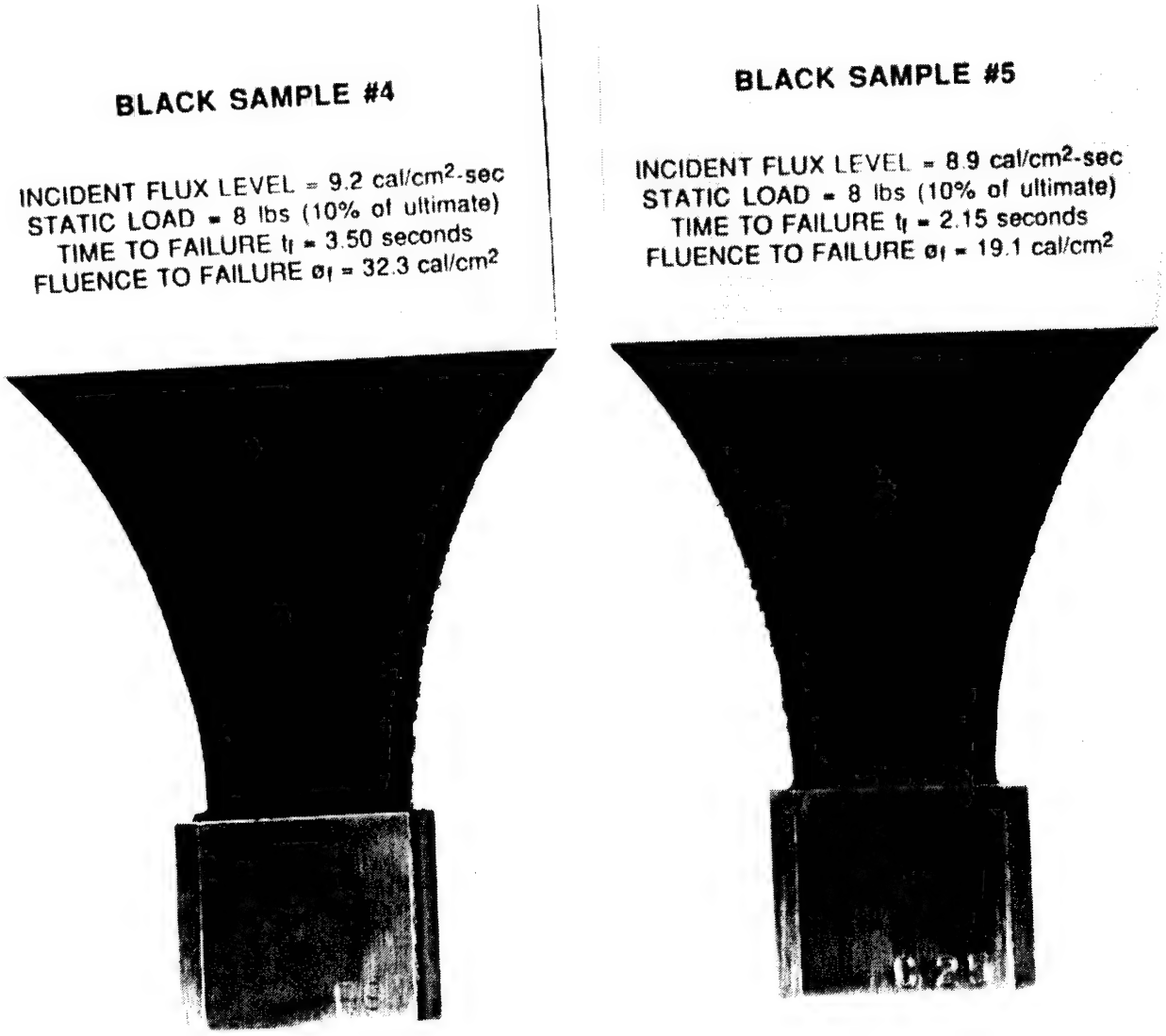

Figure E-12. Post test photograph of black samples #4 and #5.

TRAC SAMPLE #17

INCIDENT FLUX LEVEL = 10.0 cal/cm^2-sec
STATIC LOAD = 8 lbs (10% of ultimate)
TIME TO FAILURE t_f = 5.25 seconds
FLUENCE TO FAILURE ϕ_f = 52.6 cal/cm^2

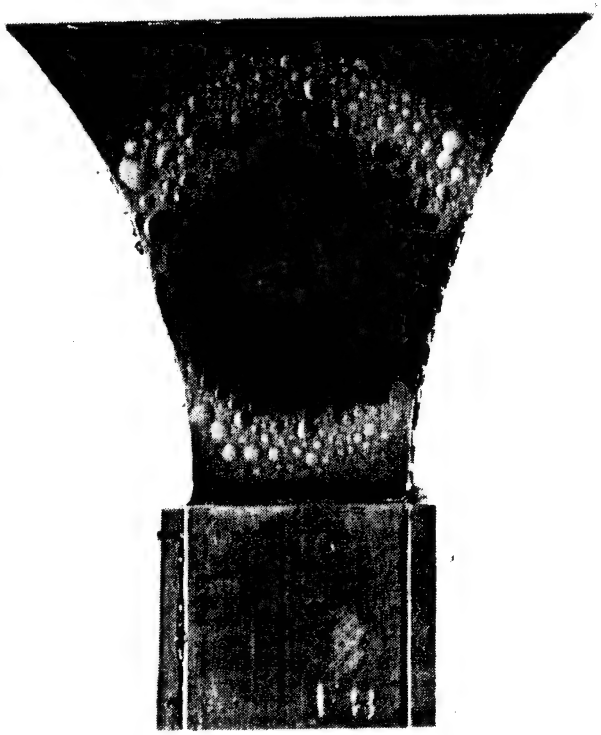

TRAC SAMPLE #18

INCIDENT FLUX LEVEL = 8.9 cal/cm^2-sec
STATIC LOAD = 8 lbs (10% of ultimate)
TIME TO FAILURE t_f = 2.45 seconds
FLUENCE TO FAILURE ϕ_f = 21.8 cal/cm^2

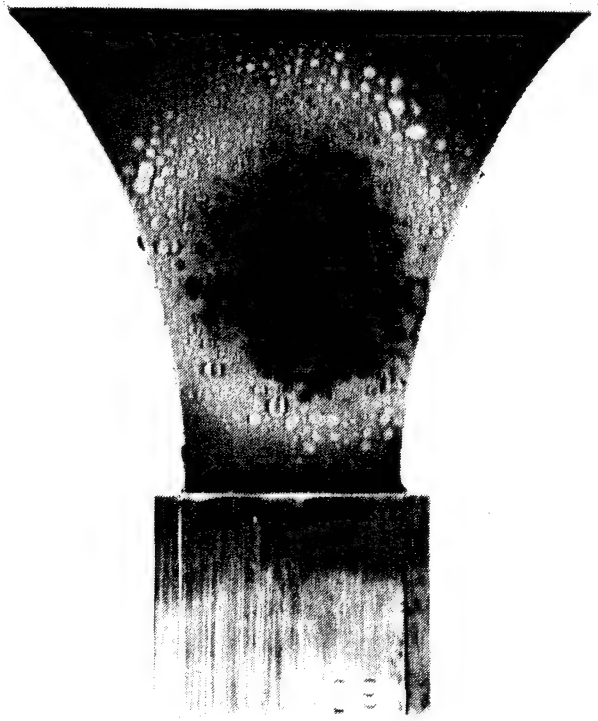

TRAC SAMPLE #19

INCIDENT FLUX LEVEL = 9.8 cal/cm^2-sec
STATIC LOAD = 8 lbs (10% of ultimate)
TIME TO FAILURE t_f = 3.30 seconds
FLUENCE TO FAILURE ϕ_f = 32.4 cal/cm^2

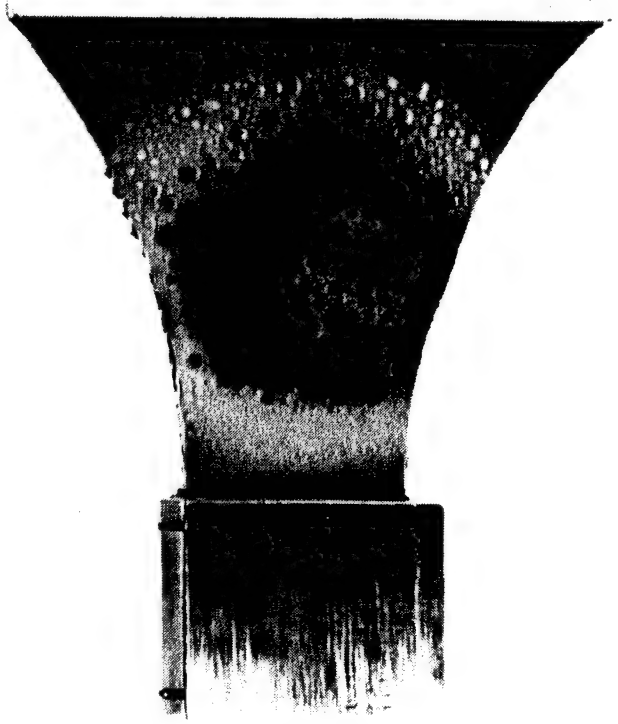

Figure E-13. Post test photograph of TRAC samples #17, 18 and 19.

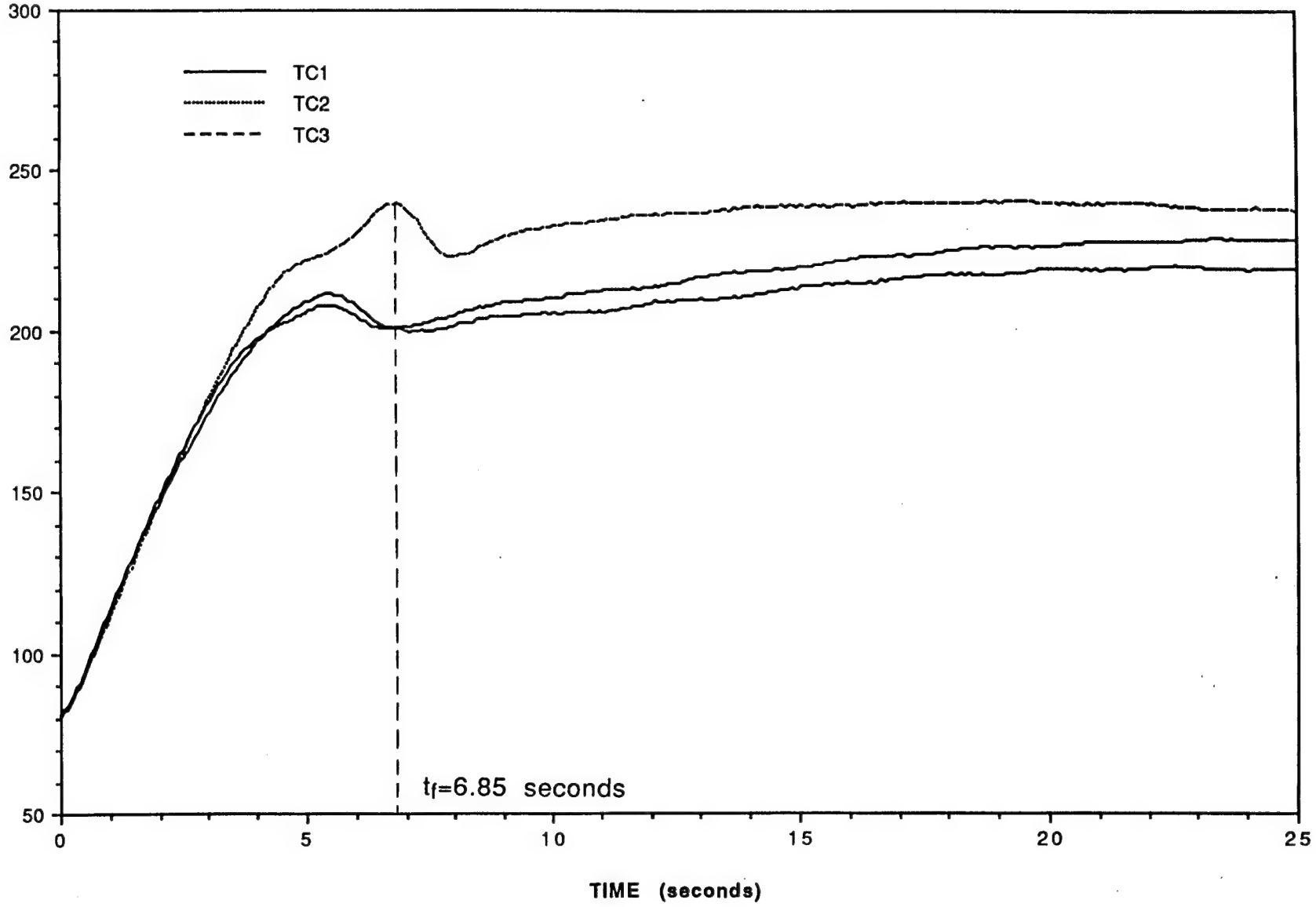

Figure E-14. Thermocouple response vs. time for white sample #4.

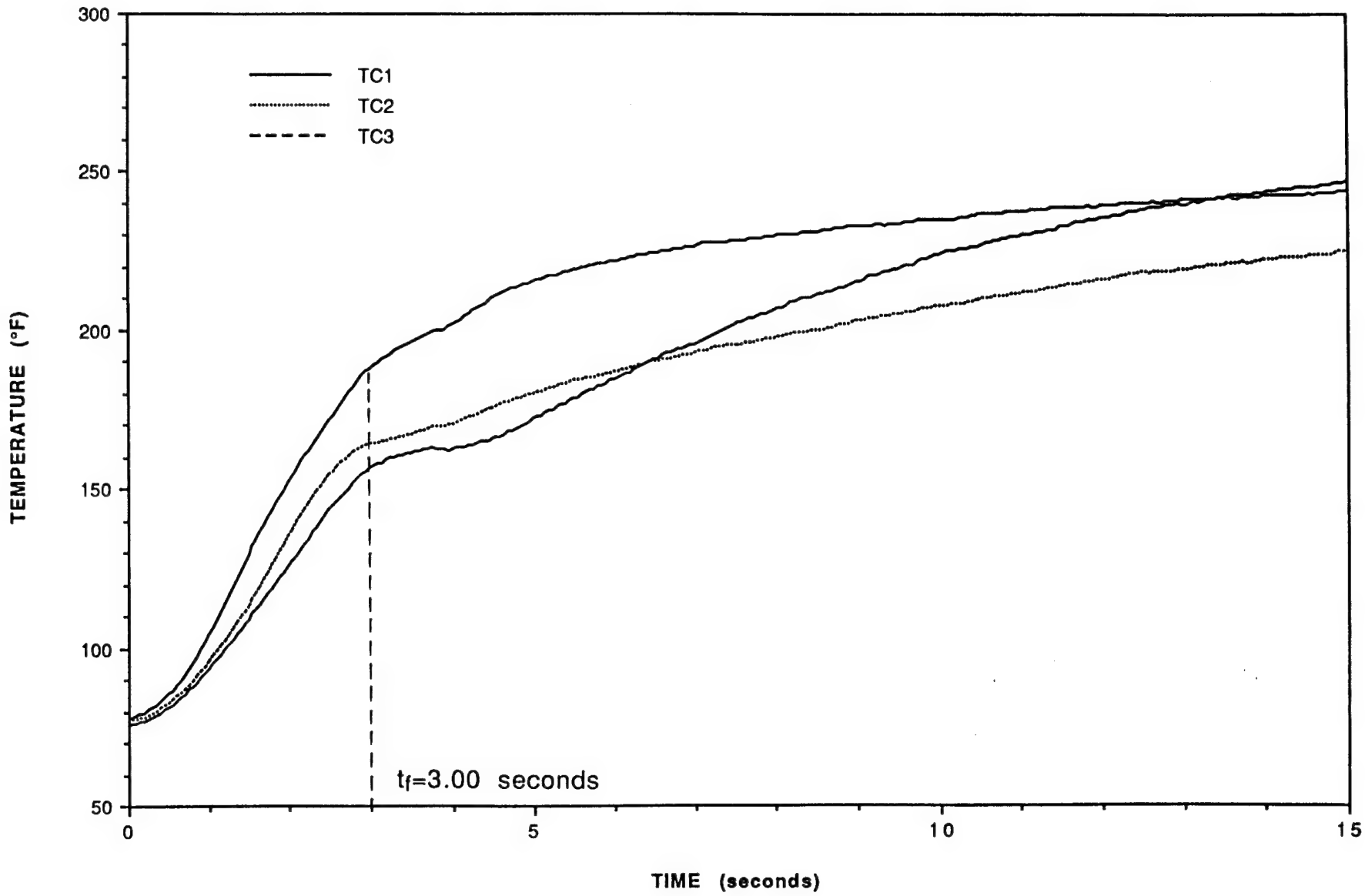

Figure E-15. Thermocouple response vs. time for grey sample #9.

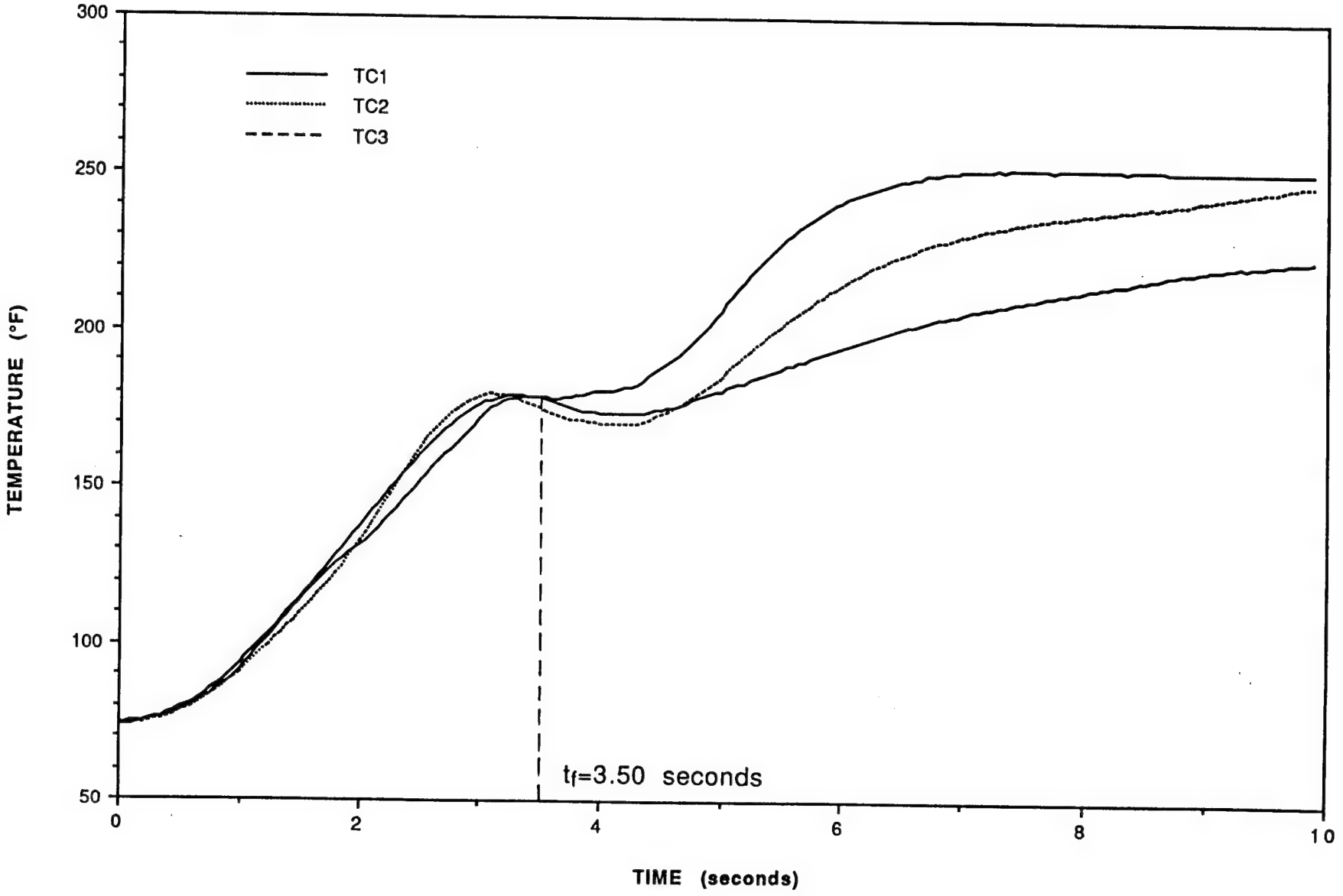

Figure E-16. Thermocouple response vs. time for black sample #4.

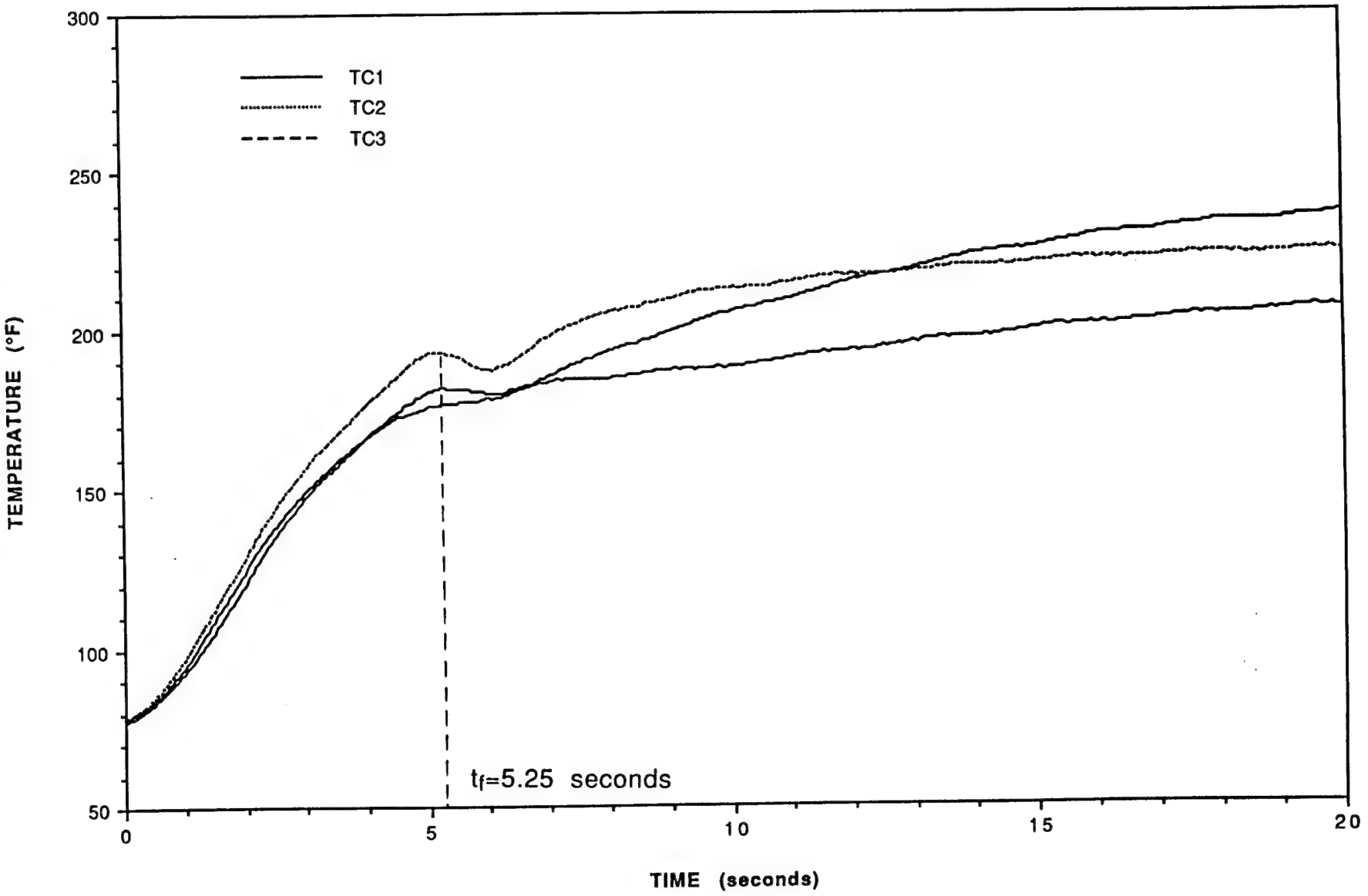

Figure E-17. Thermocouple response vs. time for TRAC sample #17.

APPENDIX F

TEST SAMPLE RESPONSE PLOTS AND PHOTOGRAPHS FROM TESTS WITH SHAPED THERMAL PULSES AND NO MECHANICAL PRELOAD

The following data was generated from combined thermal-mechanical testing of composite beams conducted at the National Renewable Energy Laboratory High Flux Solar Furnace during the week of September 27 - October 1, 1993. Results from these tests are described in Section 5.4.4.3.2.

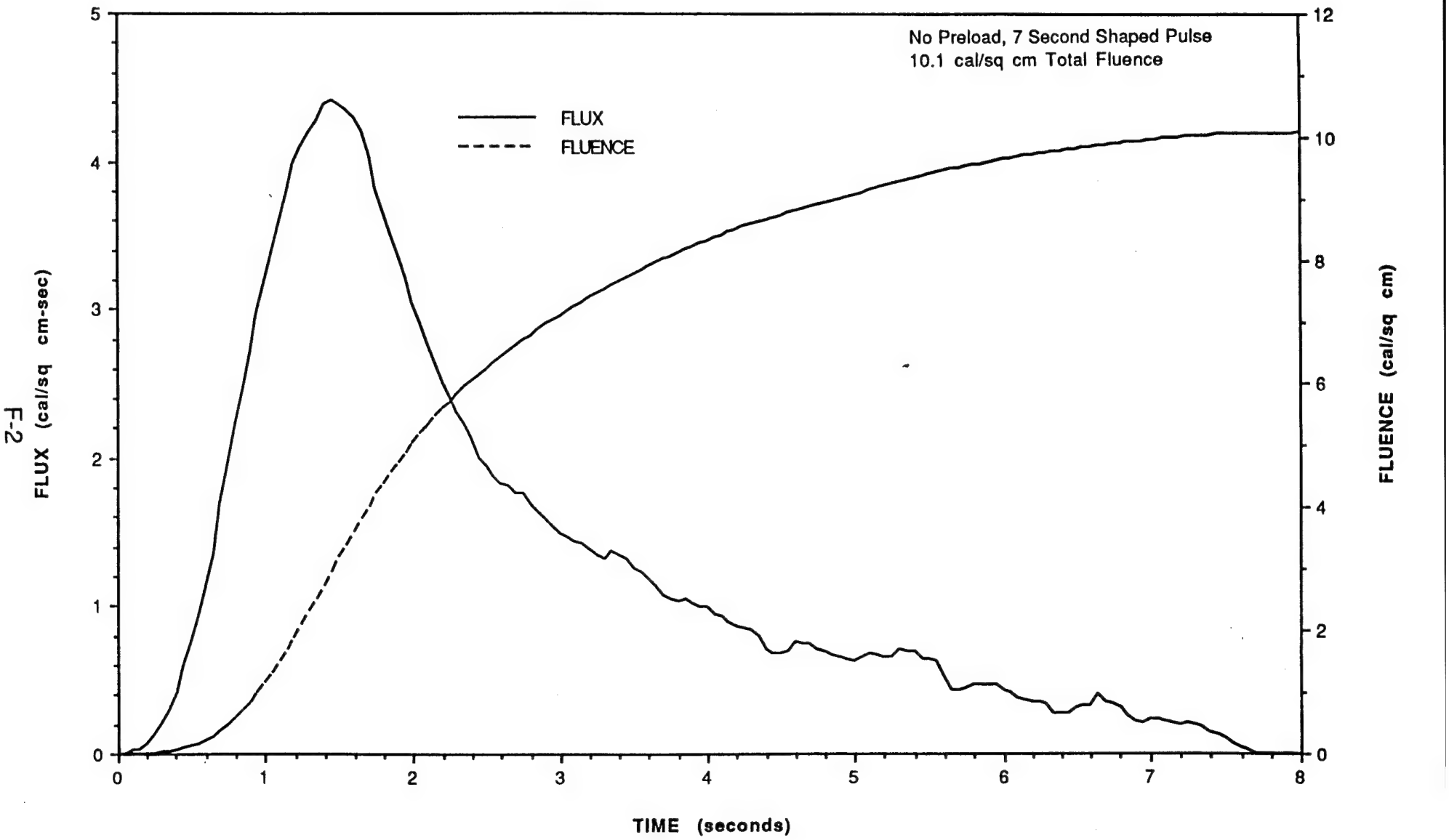

Figure F-1. Flux and fluence vs. time for grey sample #11.

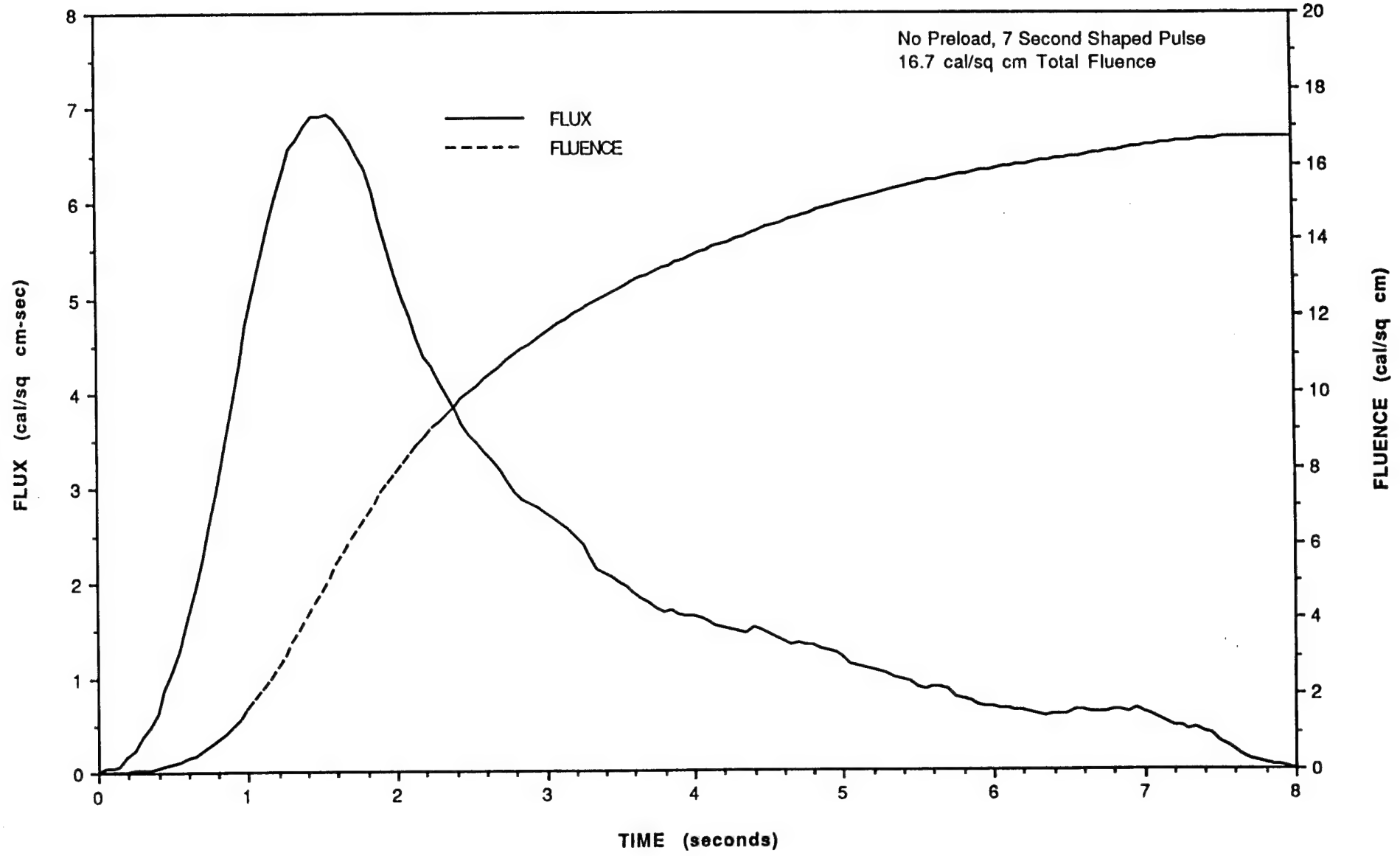

Figure F-2. Flux and fluence vs. time for grey sample #12.

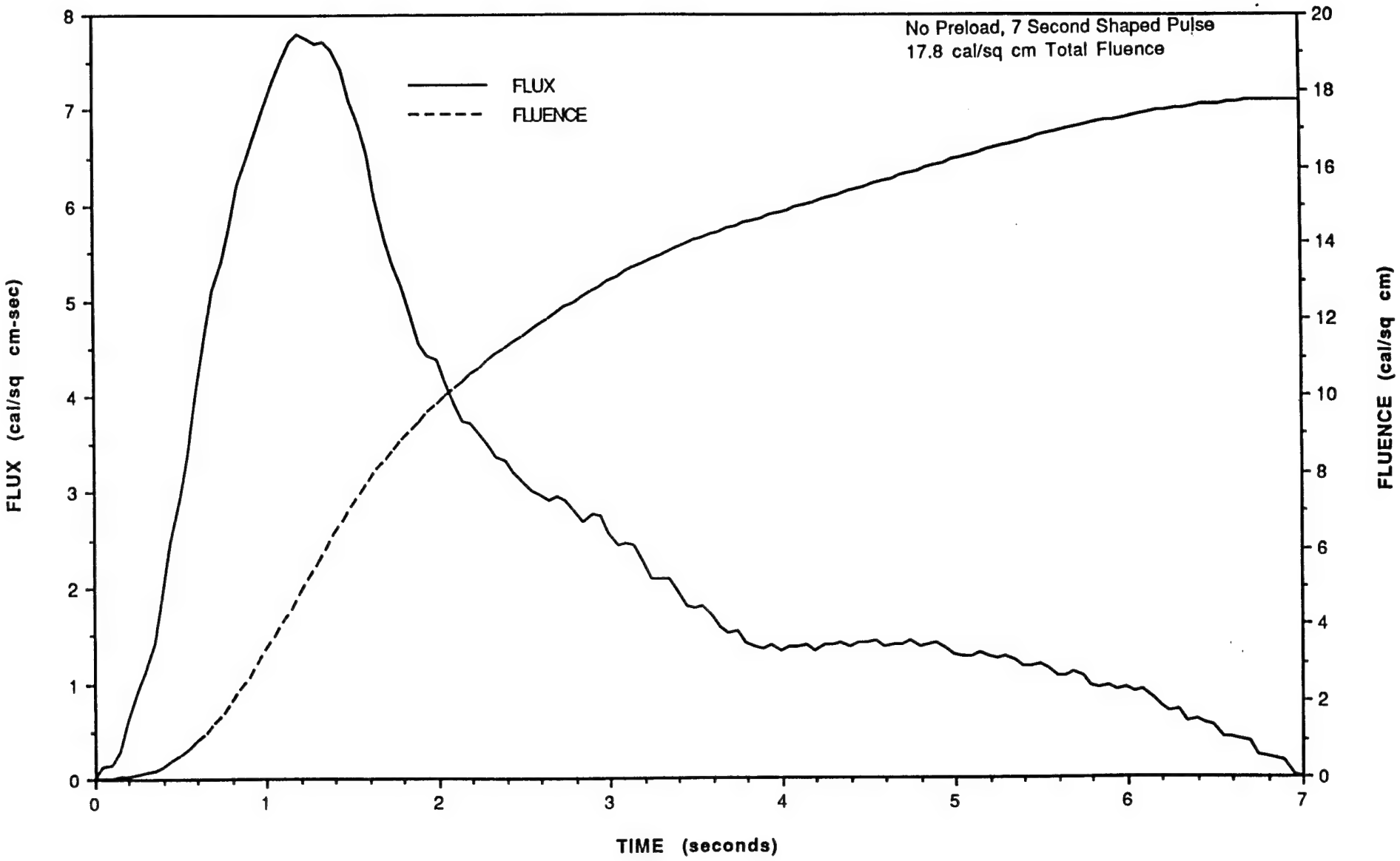

Figure F-3. Flux and fluence vs. time for grey sample #13.

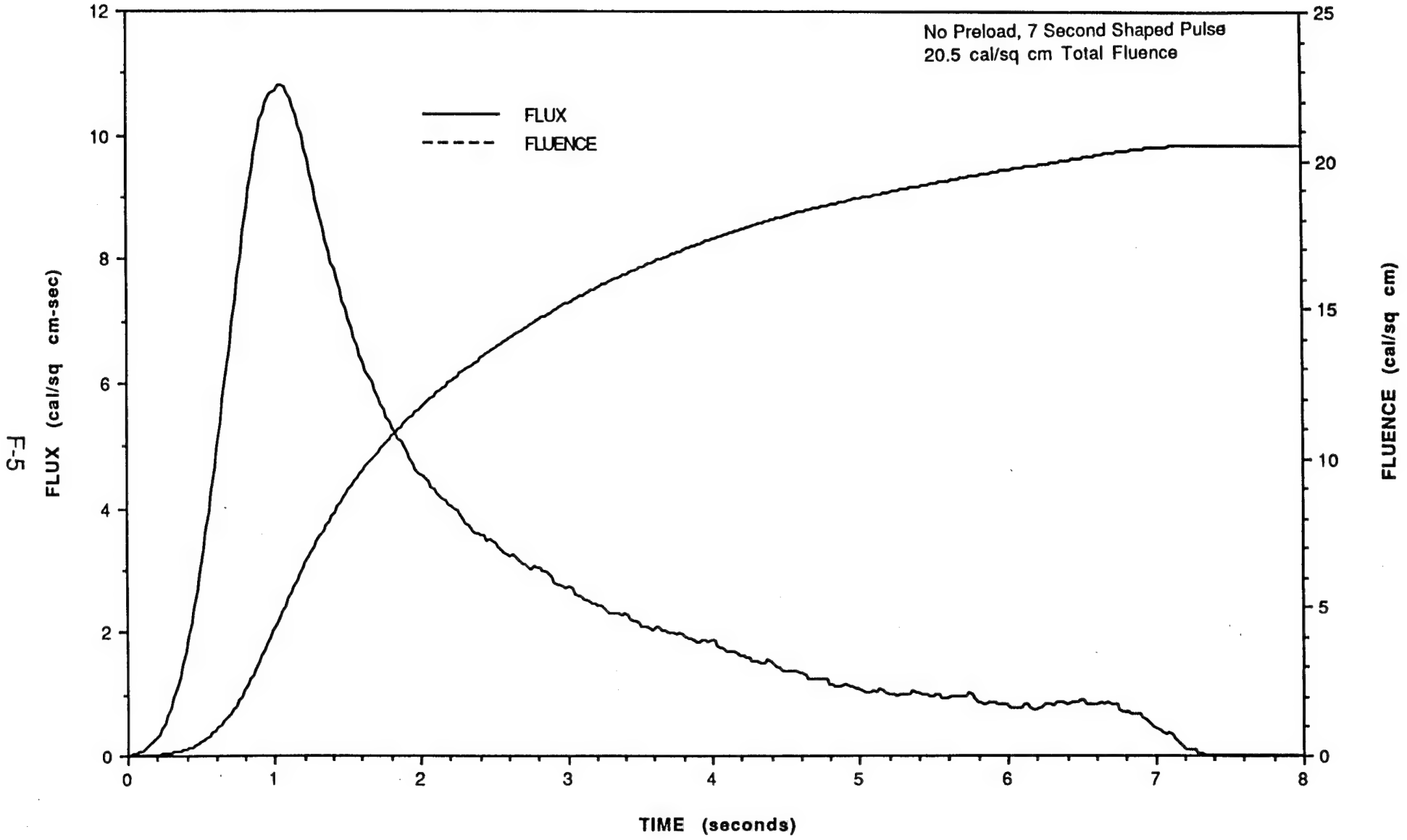

Figure F-4. Flux and fluence vs. time for TRAC sample #15.

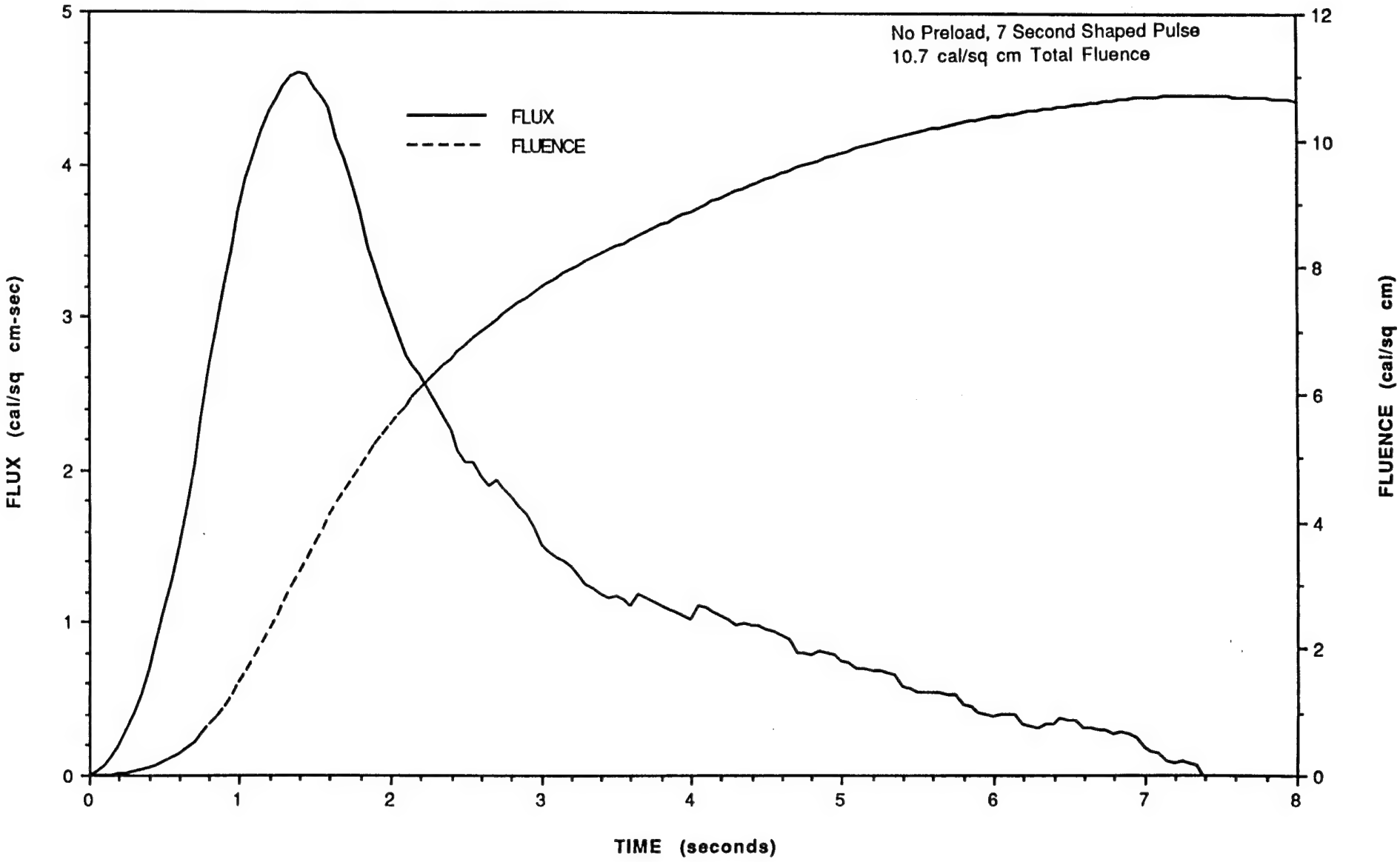

Figure F-5. Flux and fluence vs. time for TRAC sample #20.

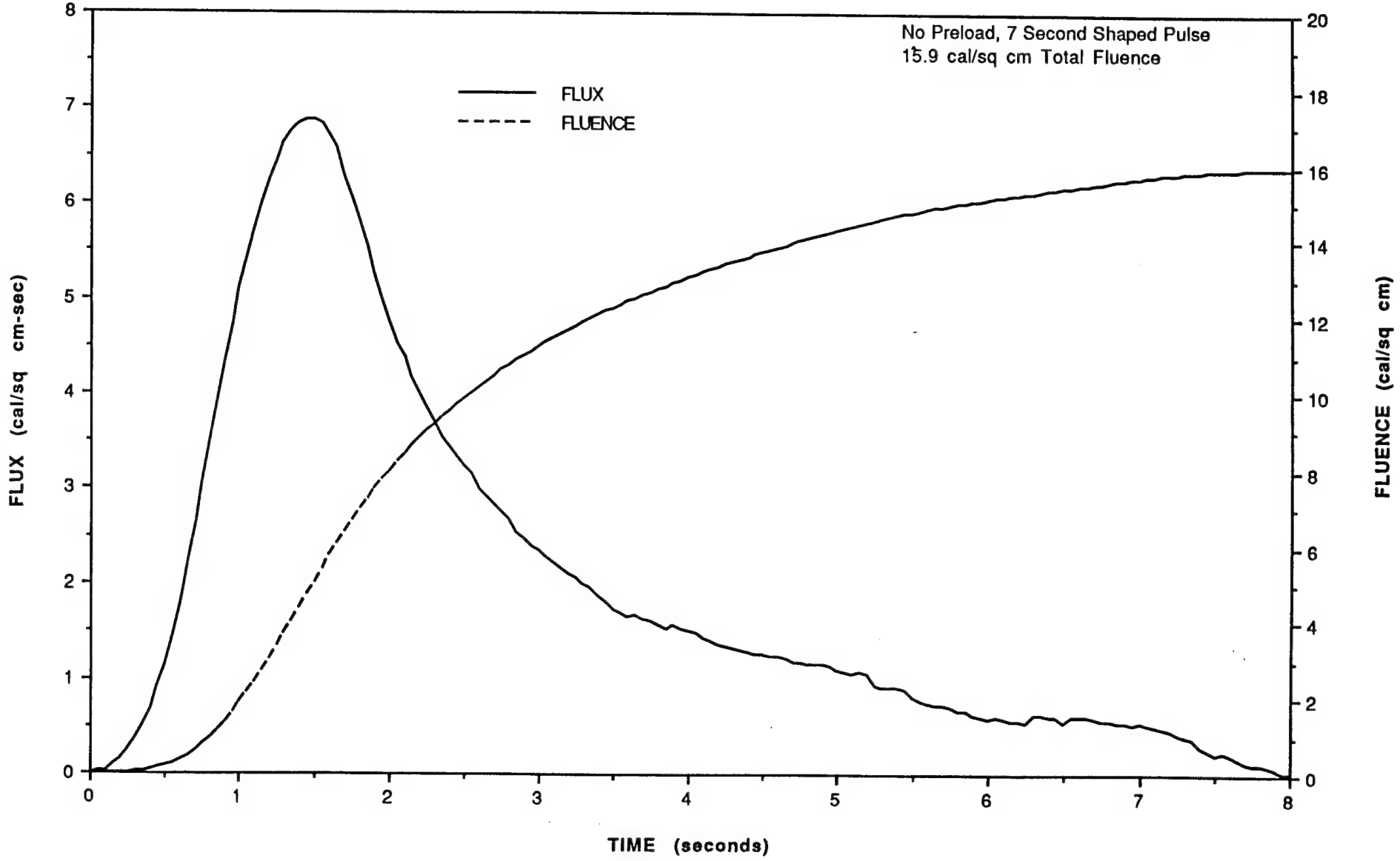

Figure F-6. Flux and fluence vs. time for TRAC sample #21.

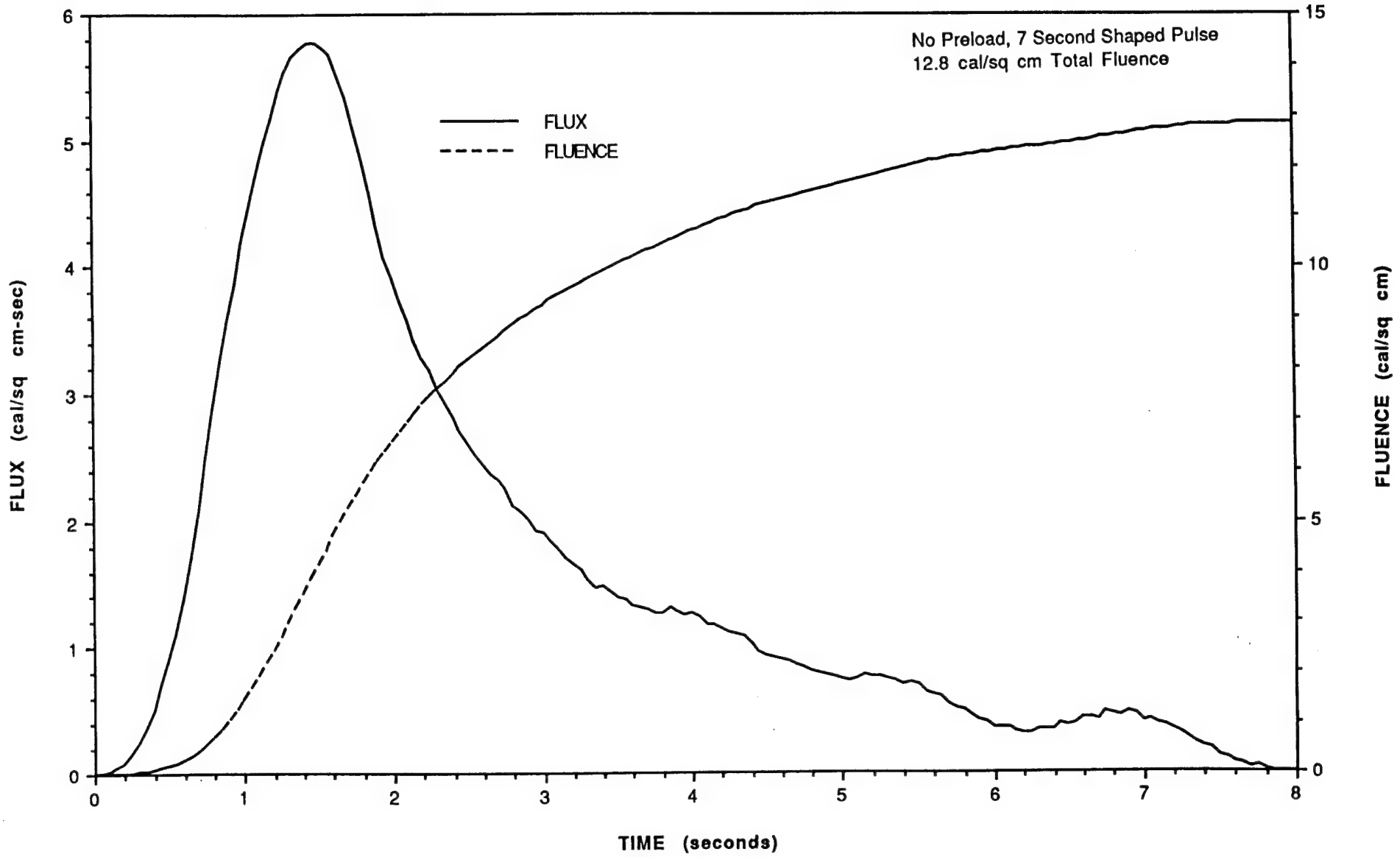

Figure F-7. Flux and fluence vs. time for TRAC sample #22.

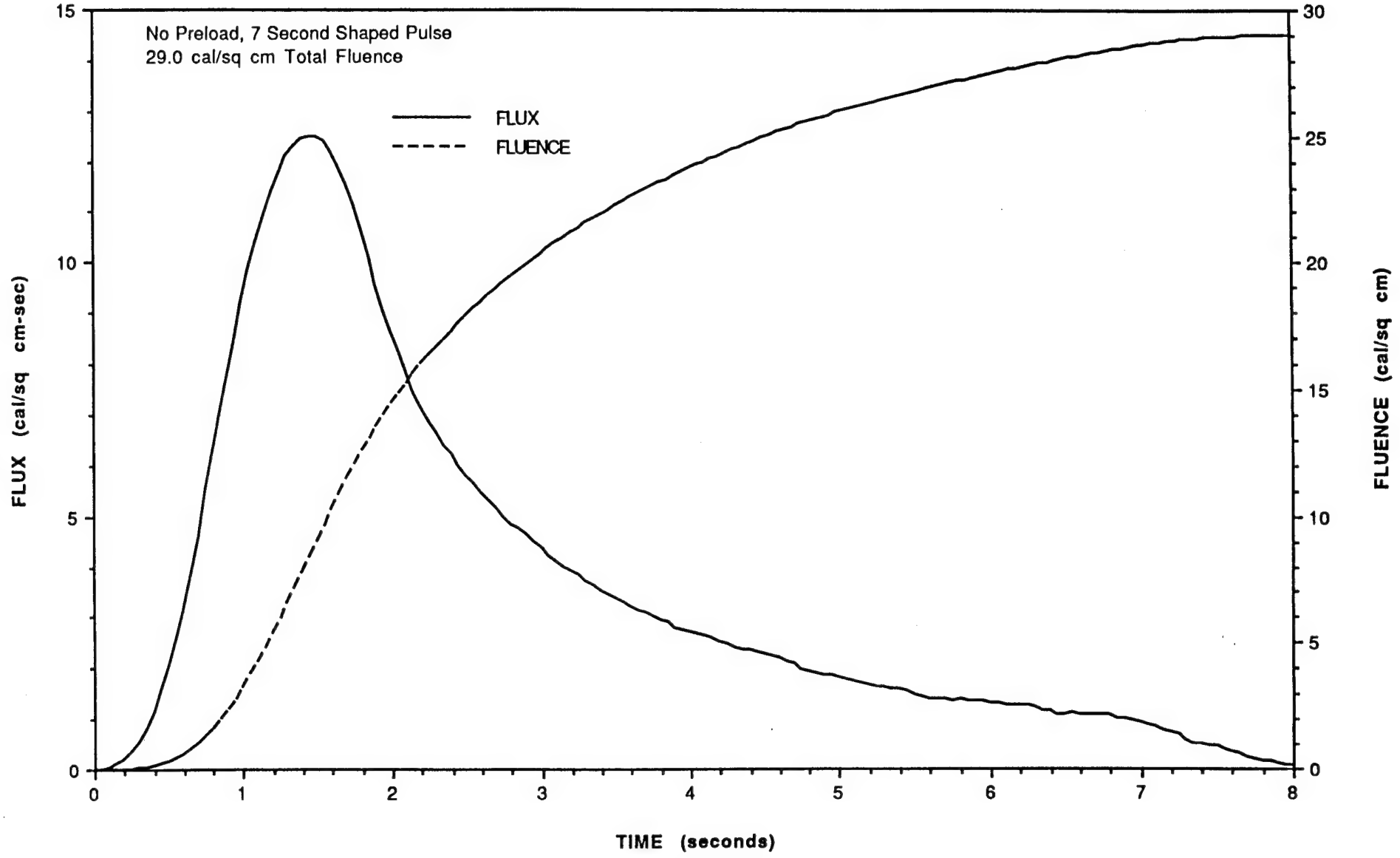

Figure F-8. Flux and fluence vs. time for TRAC sample #23.

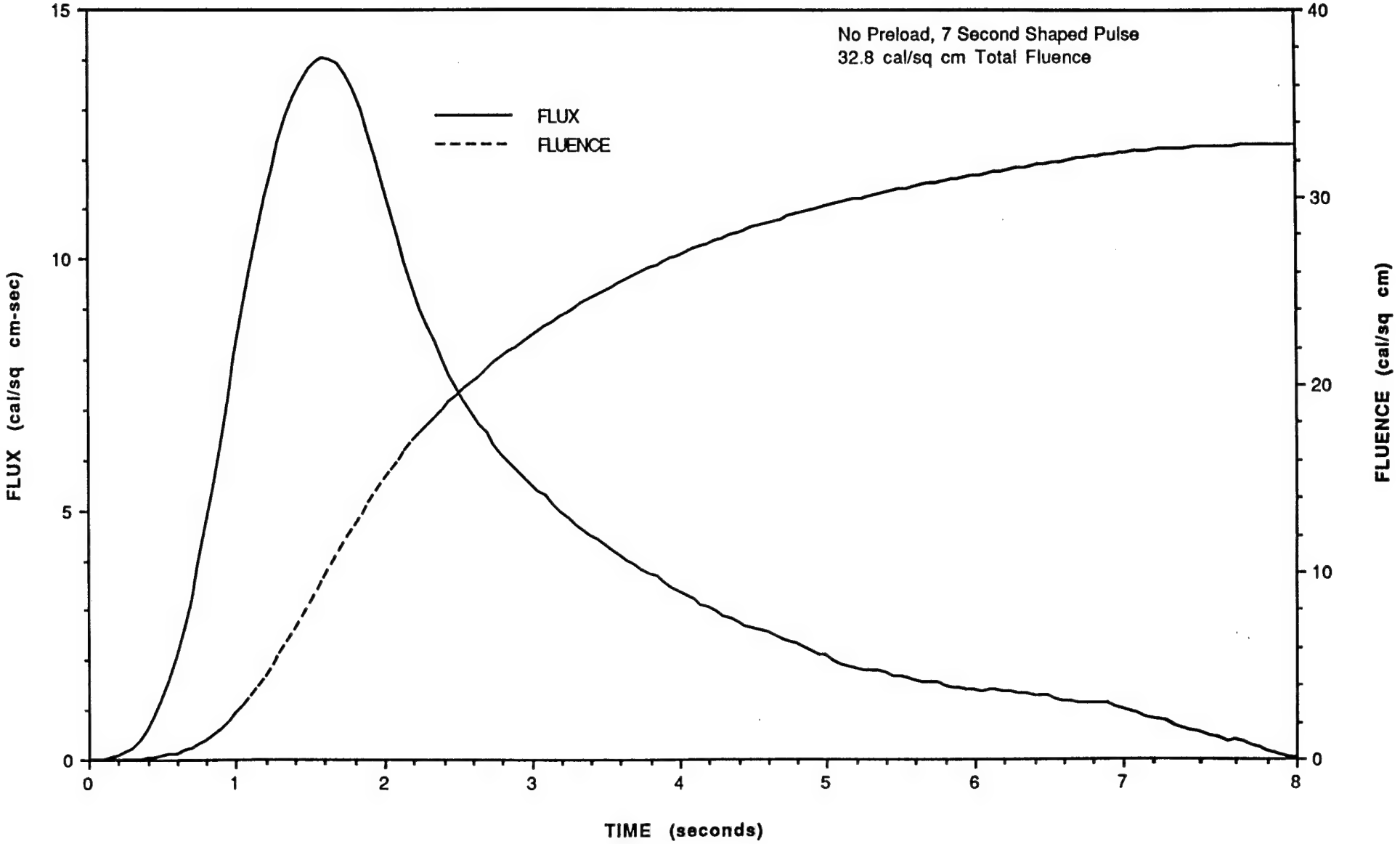

Figure F-9. Flux and fluence vs. time for TRAC sample #24.

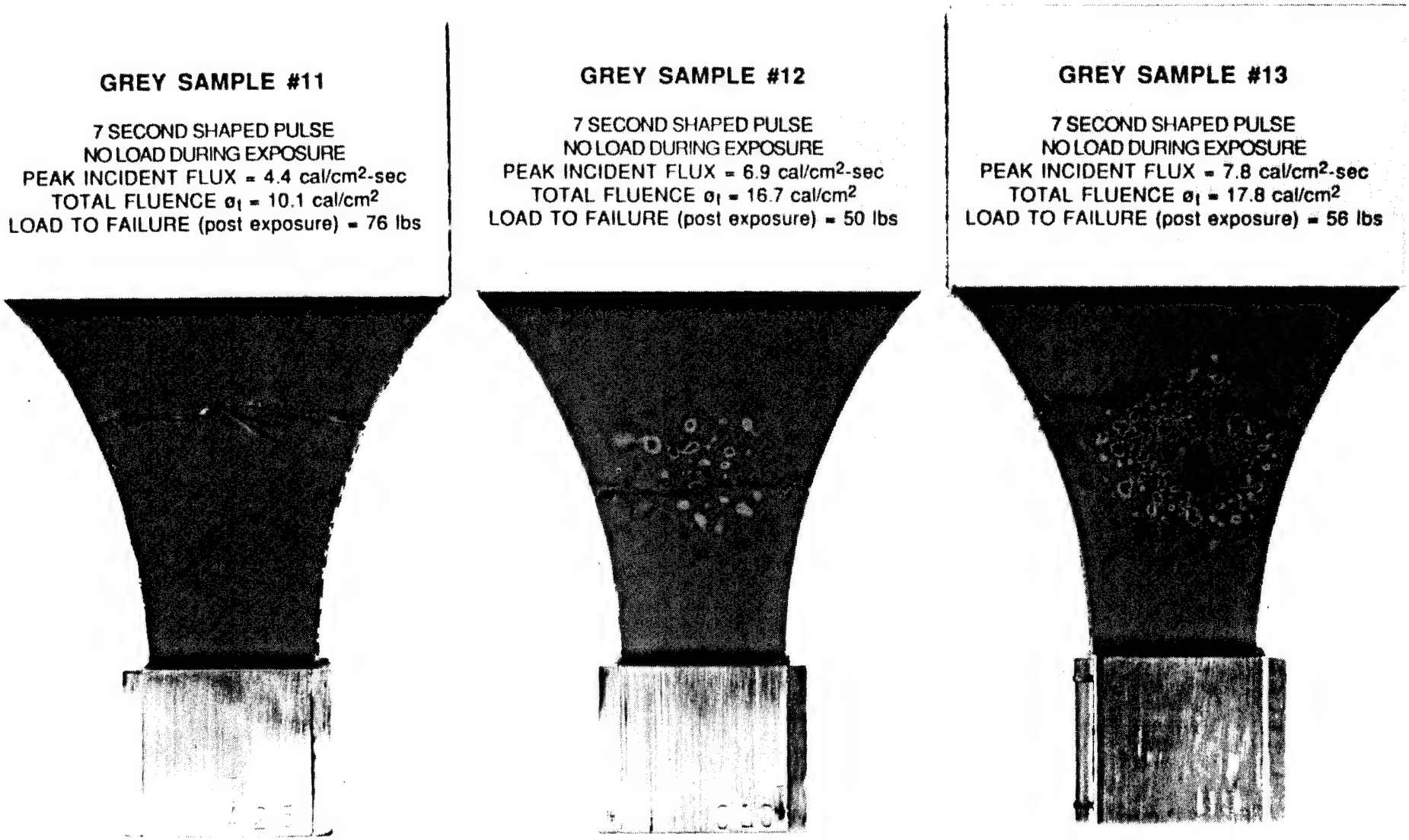

Figure F-10. Post test photograph of grey samples #11, 12 and 13.

TRAC SAMPLE #20

7 SECOND SHAPED PULSE
NO LOAD DURING EXPOSURE
PEAK INCIDENT FLUX = 4.6 cal/cm^2-sec
TOTAL FLUENCE σ_t = 10.7 cal/cm^2
LOAD TO FAILURE (post exposure) = 85 lbs

TRAC SAMPLE #22

7 SECOND SHAPED PULSE
NO LOAD DURING EXPOSURE
PEAK INCIDENT FLUX = 5.8 cal/cm^2-sec
TOTAL FLUENCE σ_t = 12.8 cal/cm^2
LOAD TO FAILURE (post exposure) = 82 lbs

TRAC SAMPLE #21

7 SECOND SHAPED PULSE
NO LOAD DURING EXPOSURE
PEAK INCIDENT FLUX = 6.9 cal/cm^2-sec
TOTAL FLUENCE σ_t = 15.9 cal/cm^2
LOAD TO FAILURE (post exposure) = 86 lbs

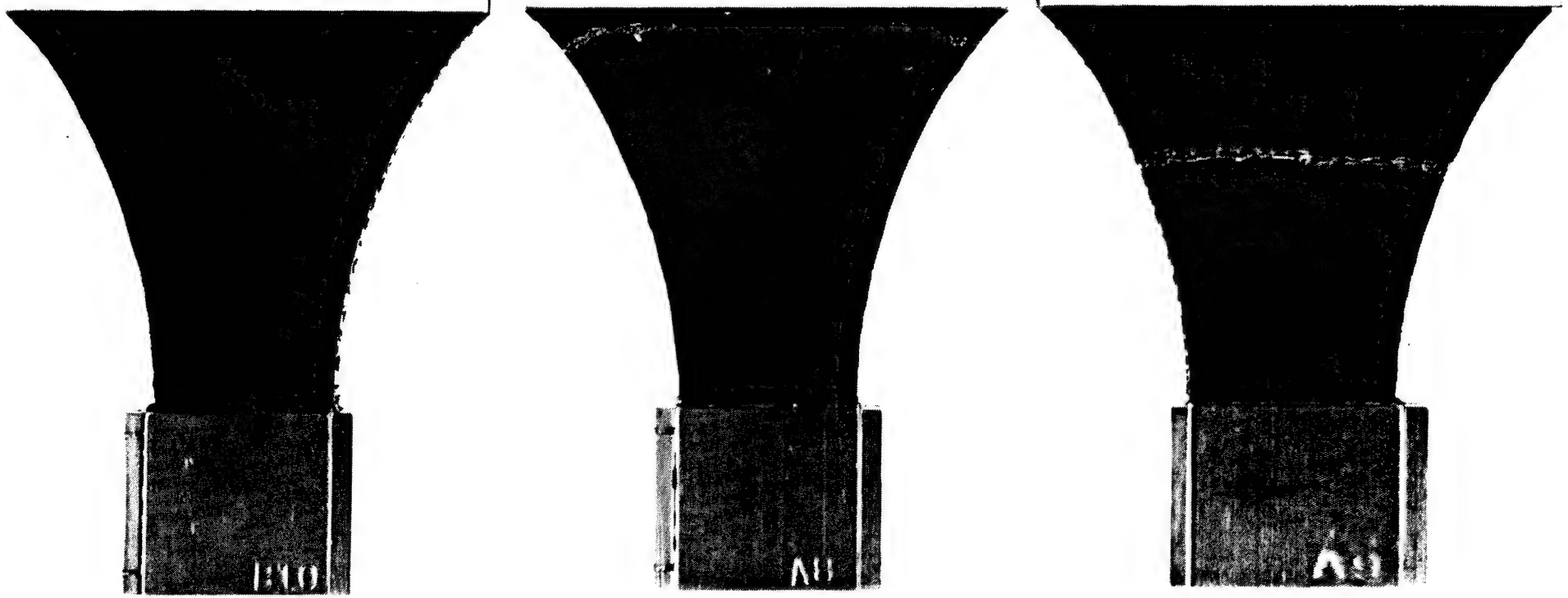

Figure. F-11. Post Test Photograph of TRAC Samples #20, 21 and 22.

TRAC SAMPLE #15

7 SECOND SHAPED PULSE
NO LOAD DURING EXPOSURE
PEAK INCIDENT FLUX = 10.8 cal/cm^2-sec
TOTAL FLUENCE ϕ_t = 20.5 cal/cm^2
LOAD TO FAILURE (post exposure) = 90 lbs

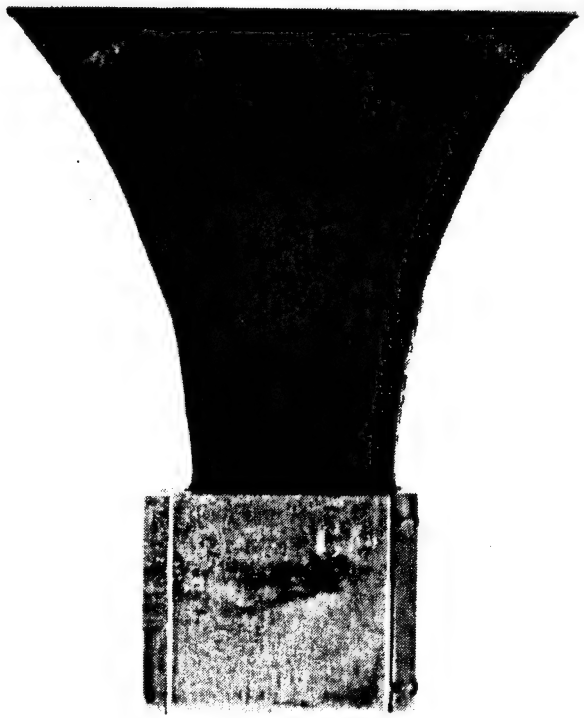

TRAC SAMPLE #23

7 SECOND SHAPED PULSE
NO LOAD DURING EXPOSURE
PEAK INCIDENT FLUX = 12.5 cal/cm^2-sec
TOTAL FLUENCE ϕ_t = 29.0 cal/cm^2
LOAD TO FAILURE (post exposure) = 71 lbs

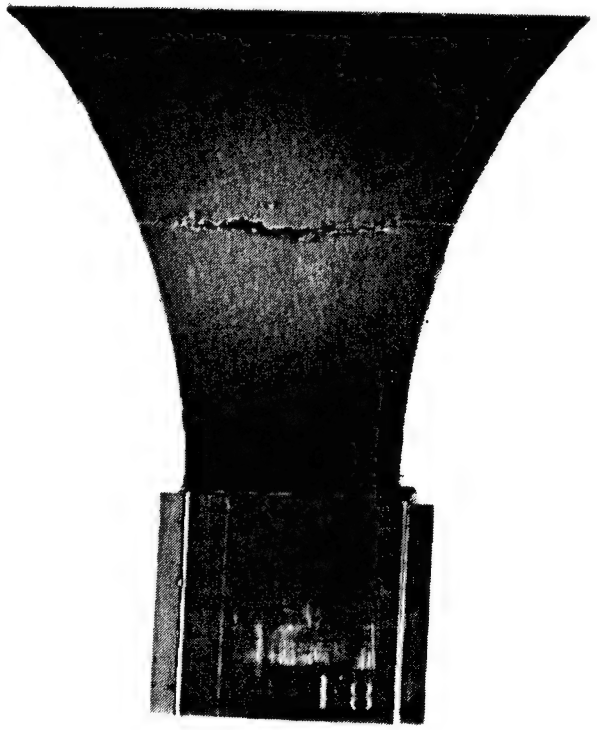

TRAC SAMPLE #24

7 SECOND SHAPED PULSE
NO LOAD DURING EXPOSURE
PEAK INCIDENT FLUX = 14.0 cal/cm^2-sec
TOTAL FLUENCE ϕ_t = 32.8 cal/cm^2
LOAD TO FAILURE (post exposure) = 62 lbs

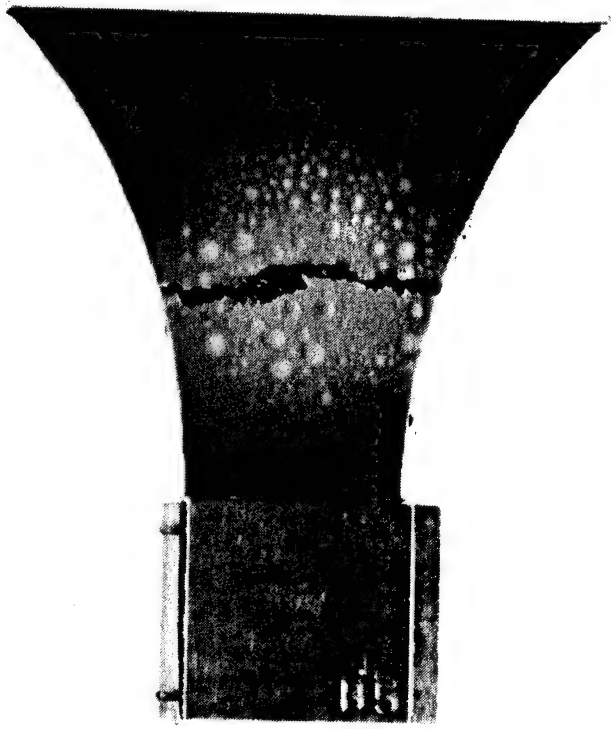

Figure F-12. Post test photograph of TRAC Samples #15, 23 and 24.

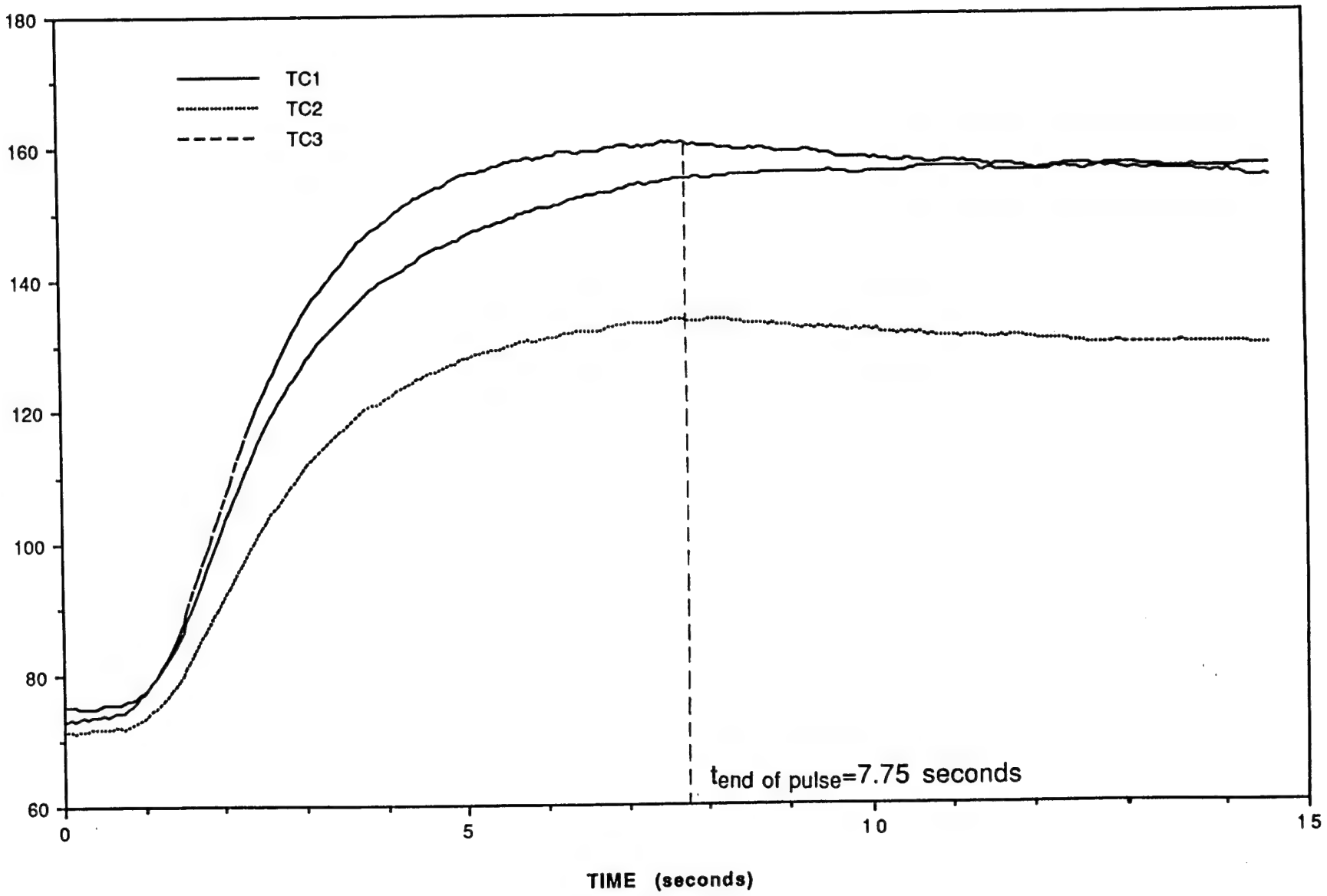

Figure F-13. Thermocouple response vs. time for grey sample #11.

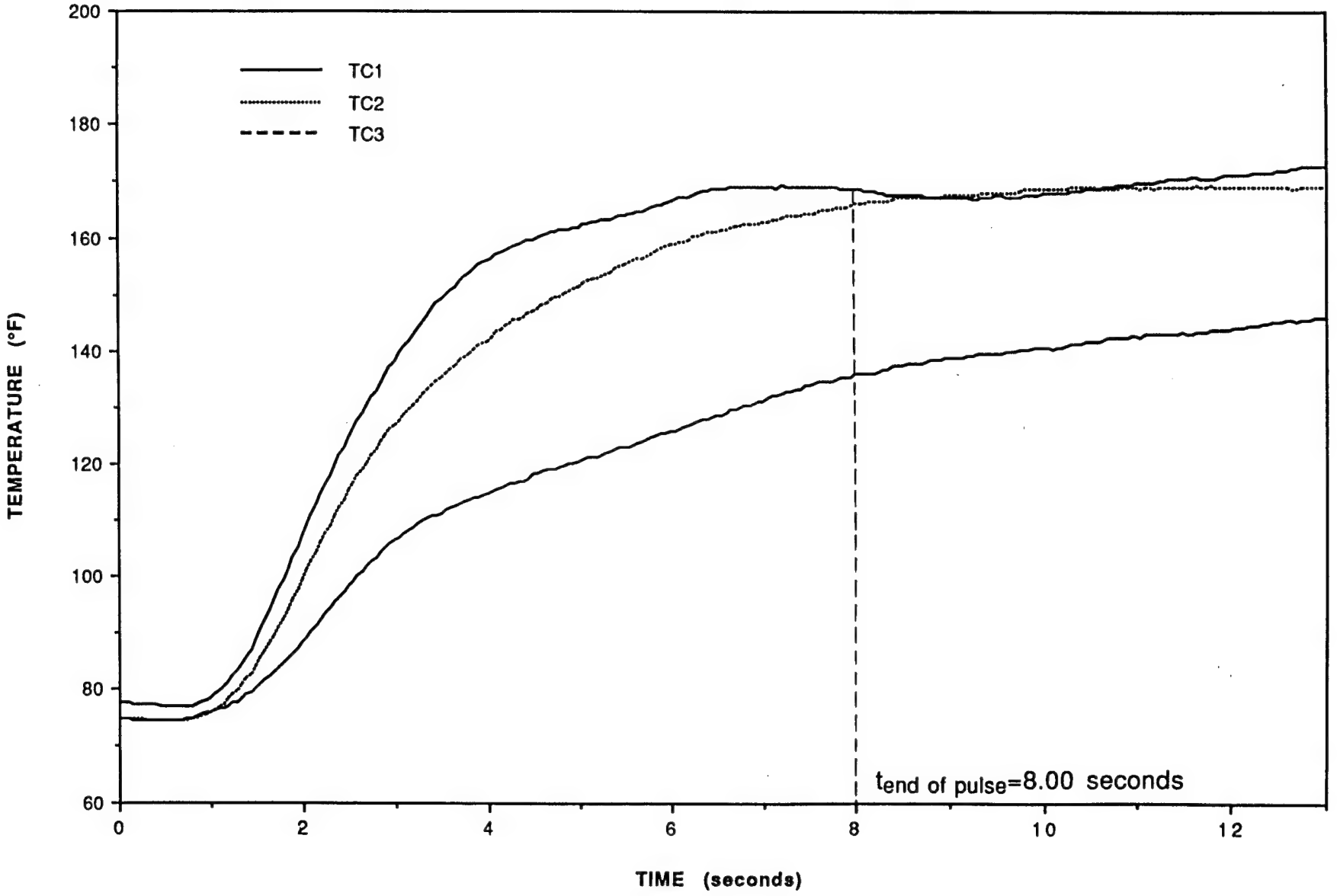

Figure F-14. Thermocouple response vs. time for grey sample #12.

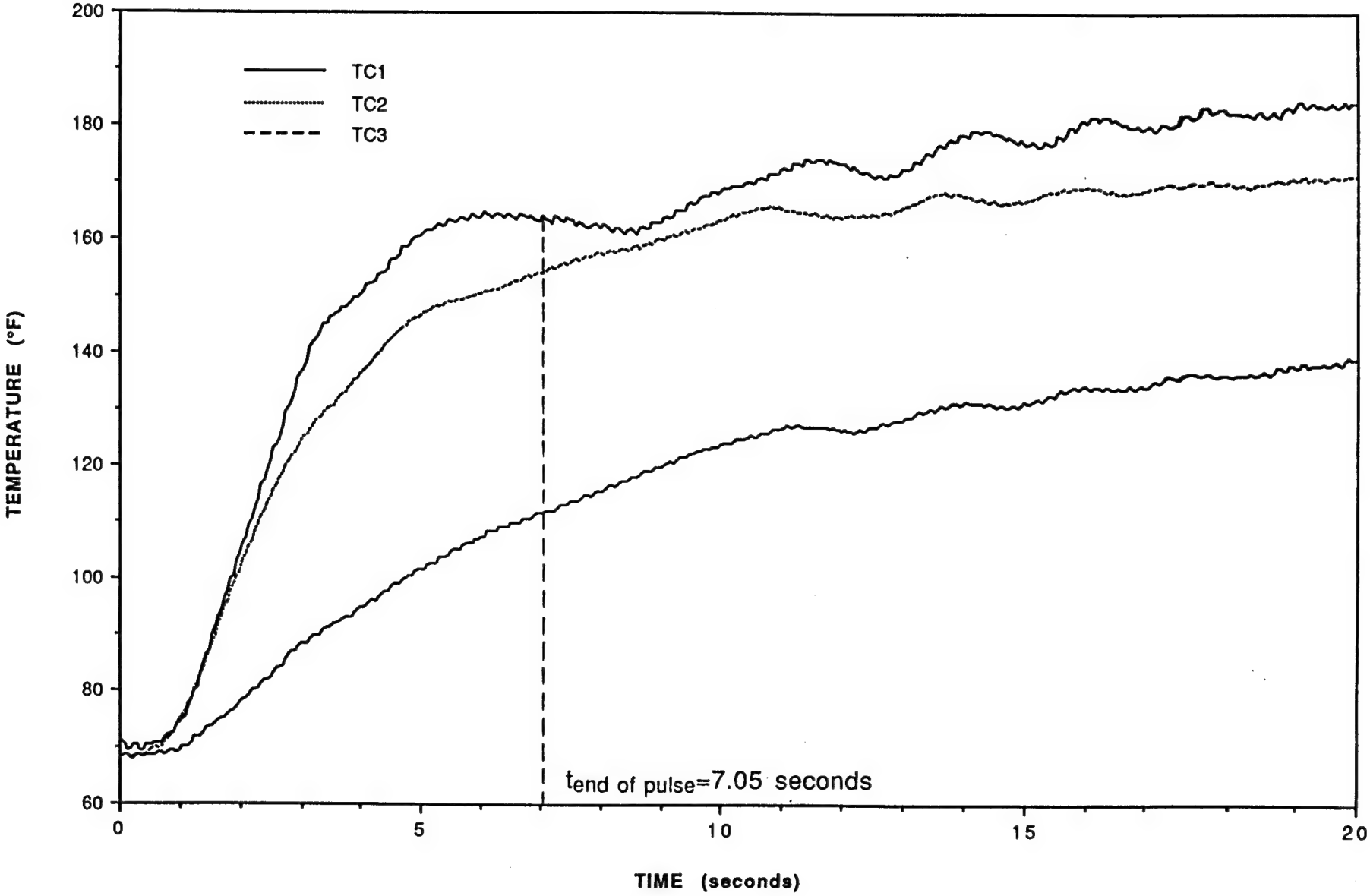

Figure F-15. Thermocouple response vs. time for grey sample #13.

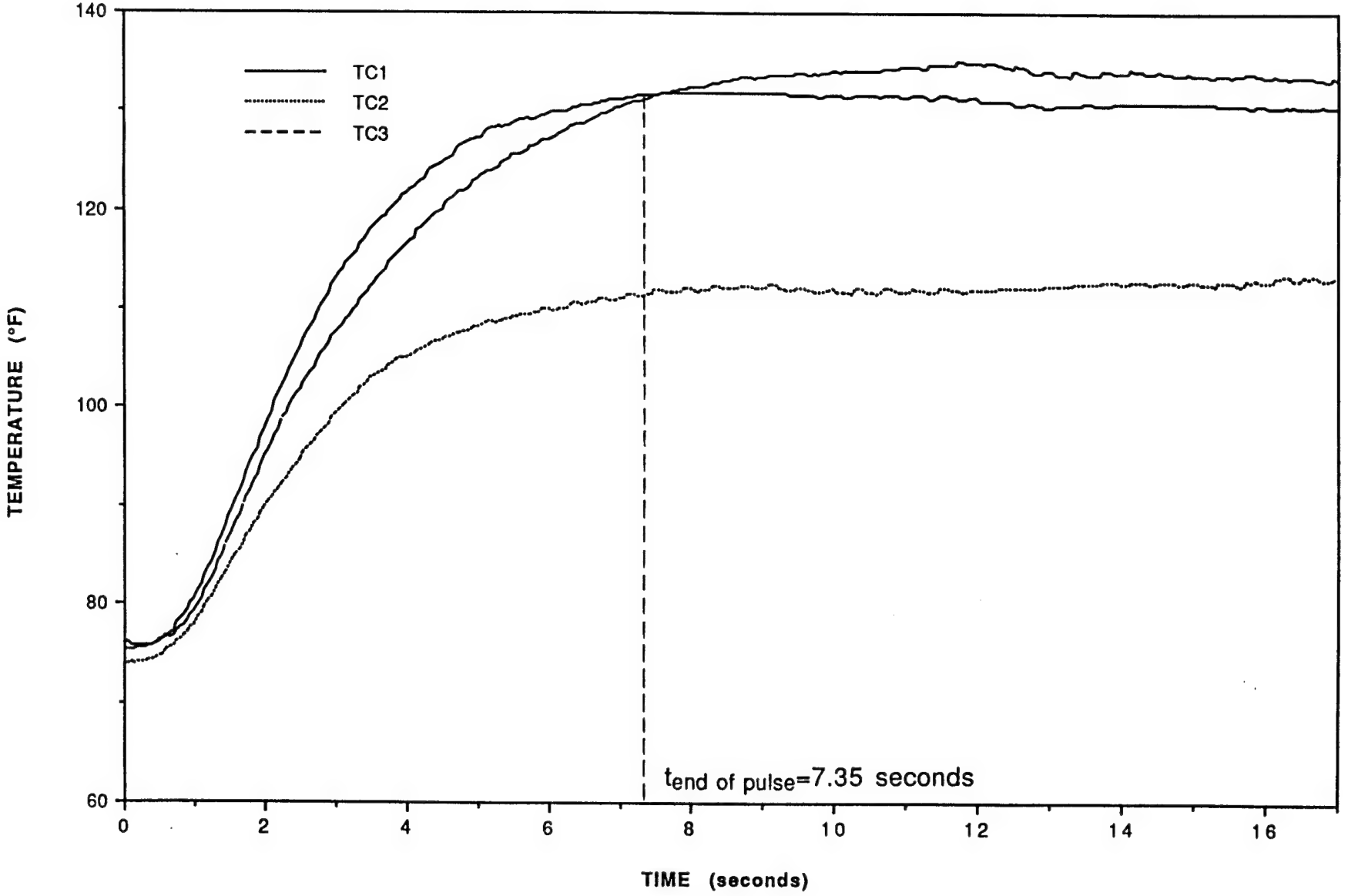

Figure F-16. Thermocouple response vs. time for TRAC sample #20.

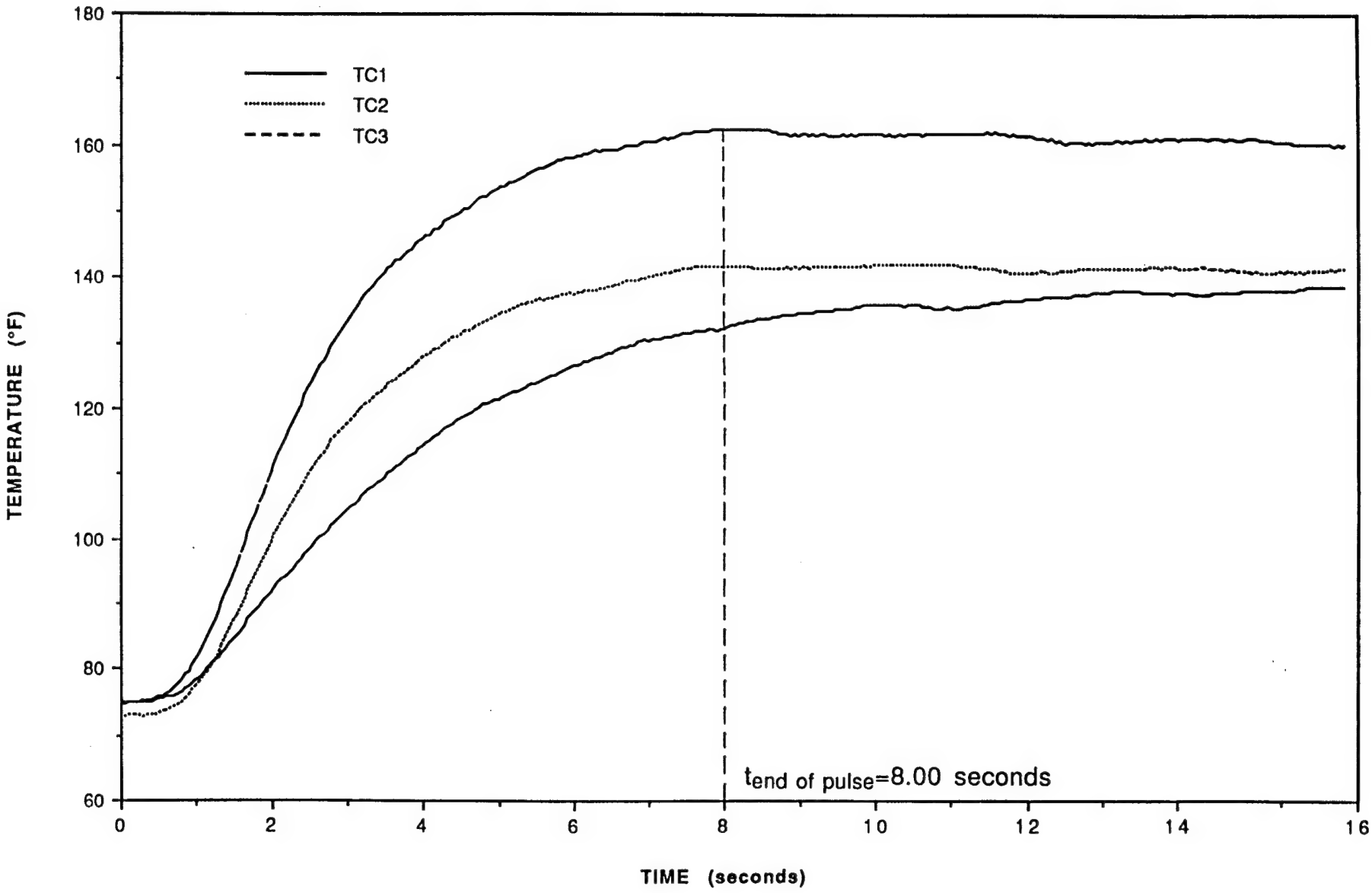

Figure F-17. Thermocouple response vs. time for TRAC sample #21.

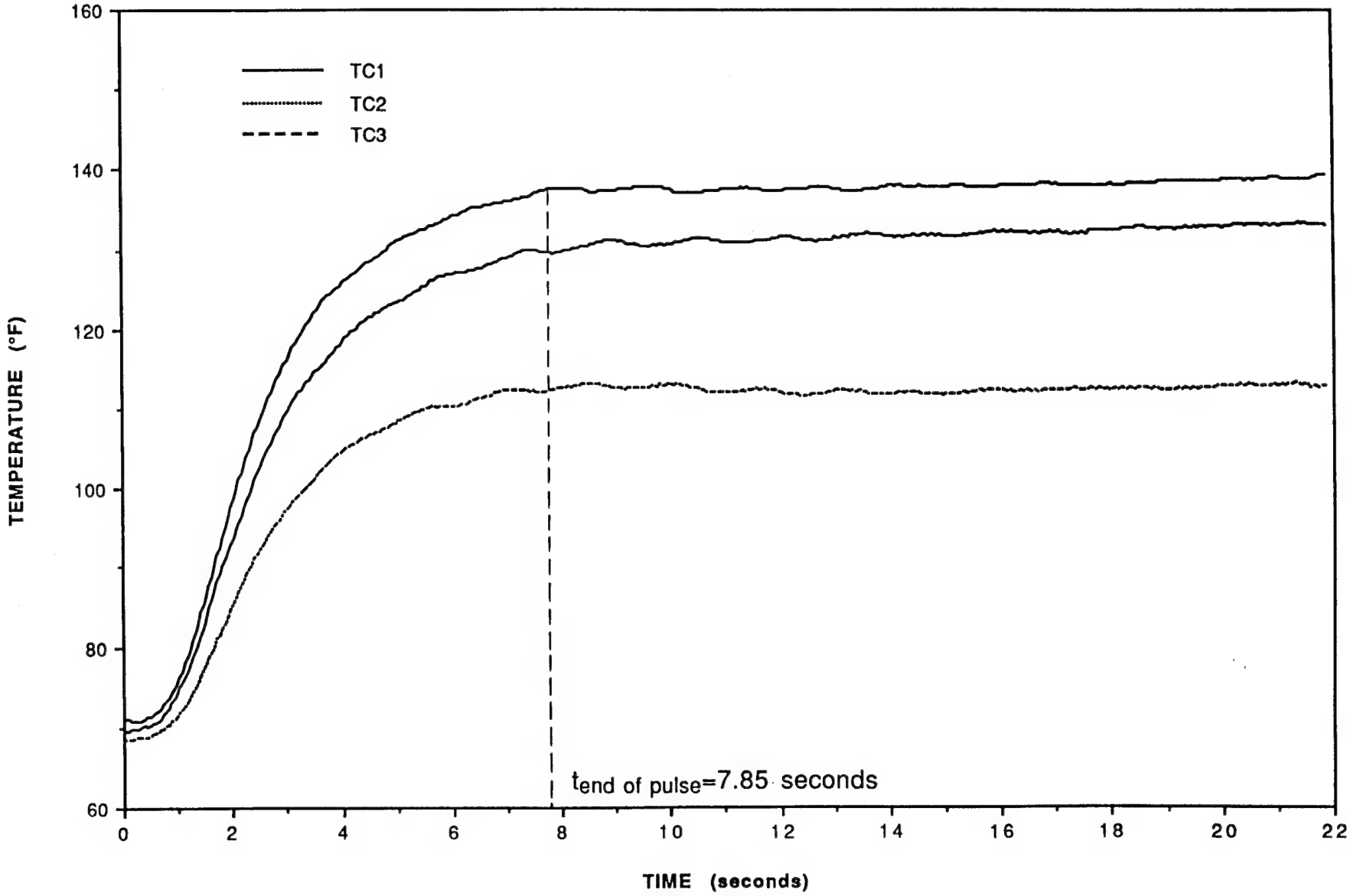

Figure F-18. Thermocouple response vs. time for TRAC sample #22.

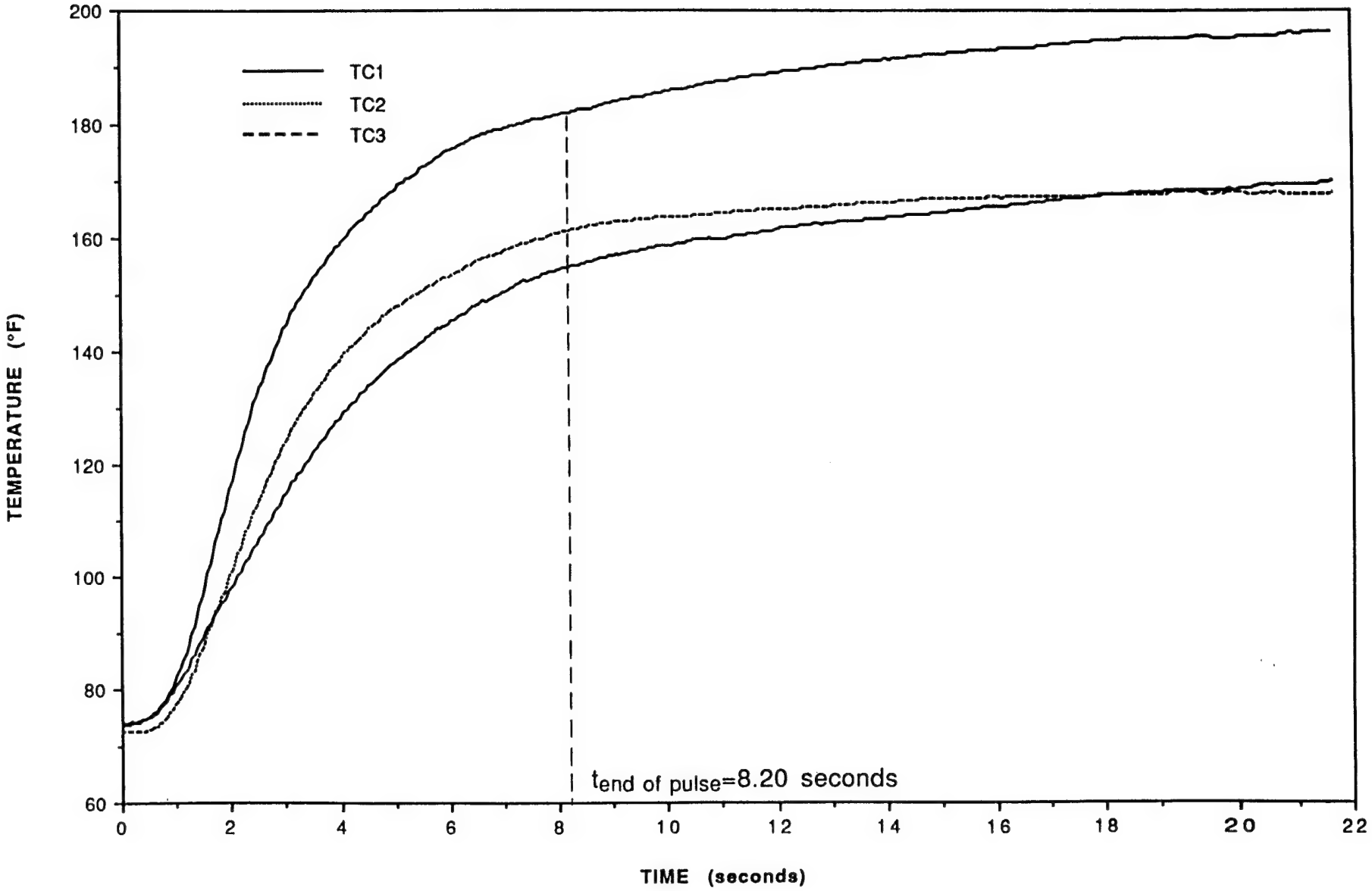

Figure F-19. Thermocouple response vs. time for TRAC sample #23.

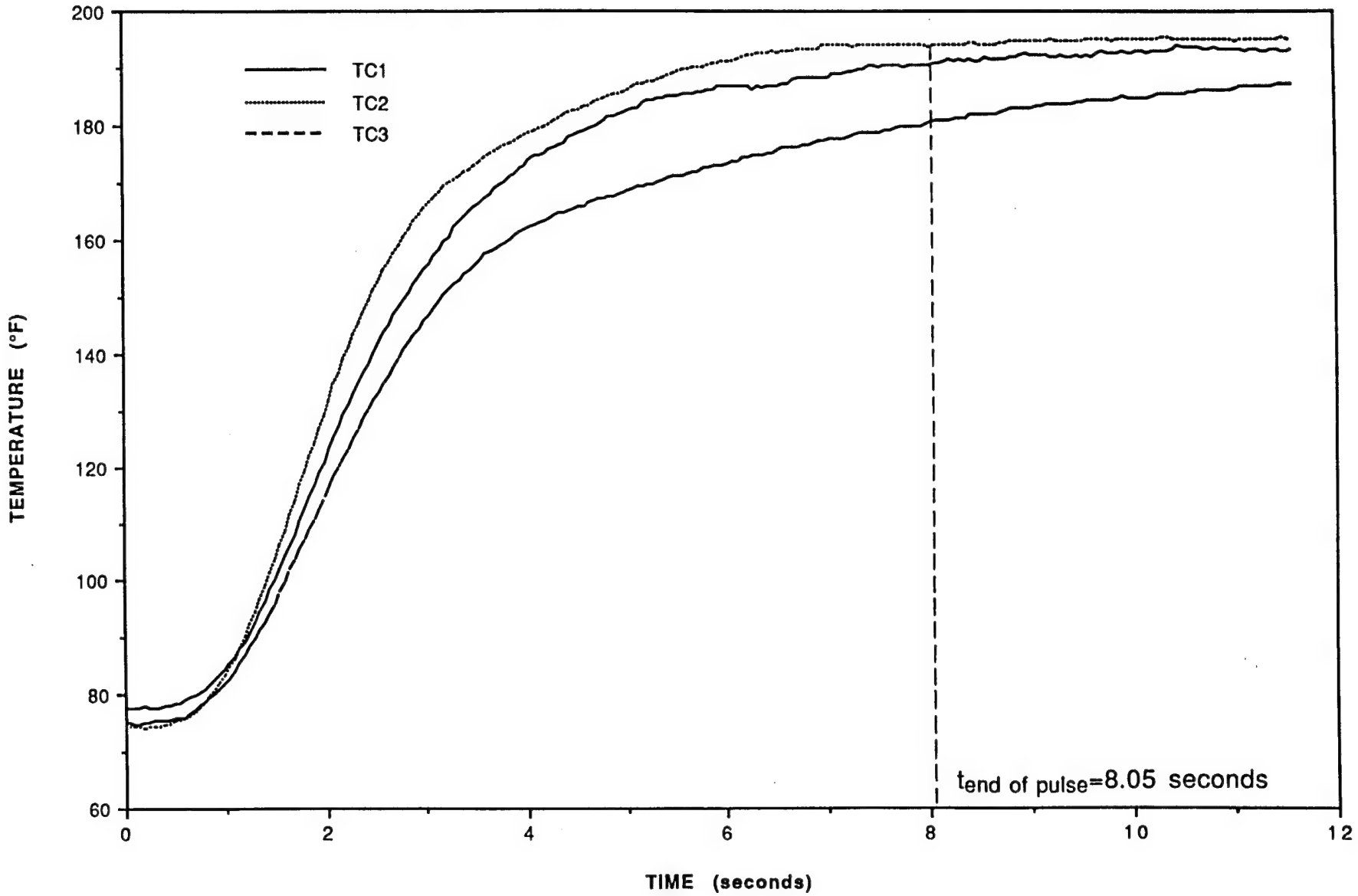

Figure F-20. Thermocouple response vs. time for TRAC sample #24.

APPENDIX G

TEST SAMPLE RESPONSE PLOTS AND PHOTOGRAPHS FROM TESTS WITH SHAPED THERMAL PULSES AND 25% MECHANICAL PRELOAD

The following data was generated from combined thermal-mechanical testing of composite beams conducted at the National Renewable Energy Laboratory High Flux Solar Furnace during the week of September 27 - October 1, 1993. Results from these tests are described in Section 5.4.4.3.3.

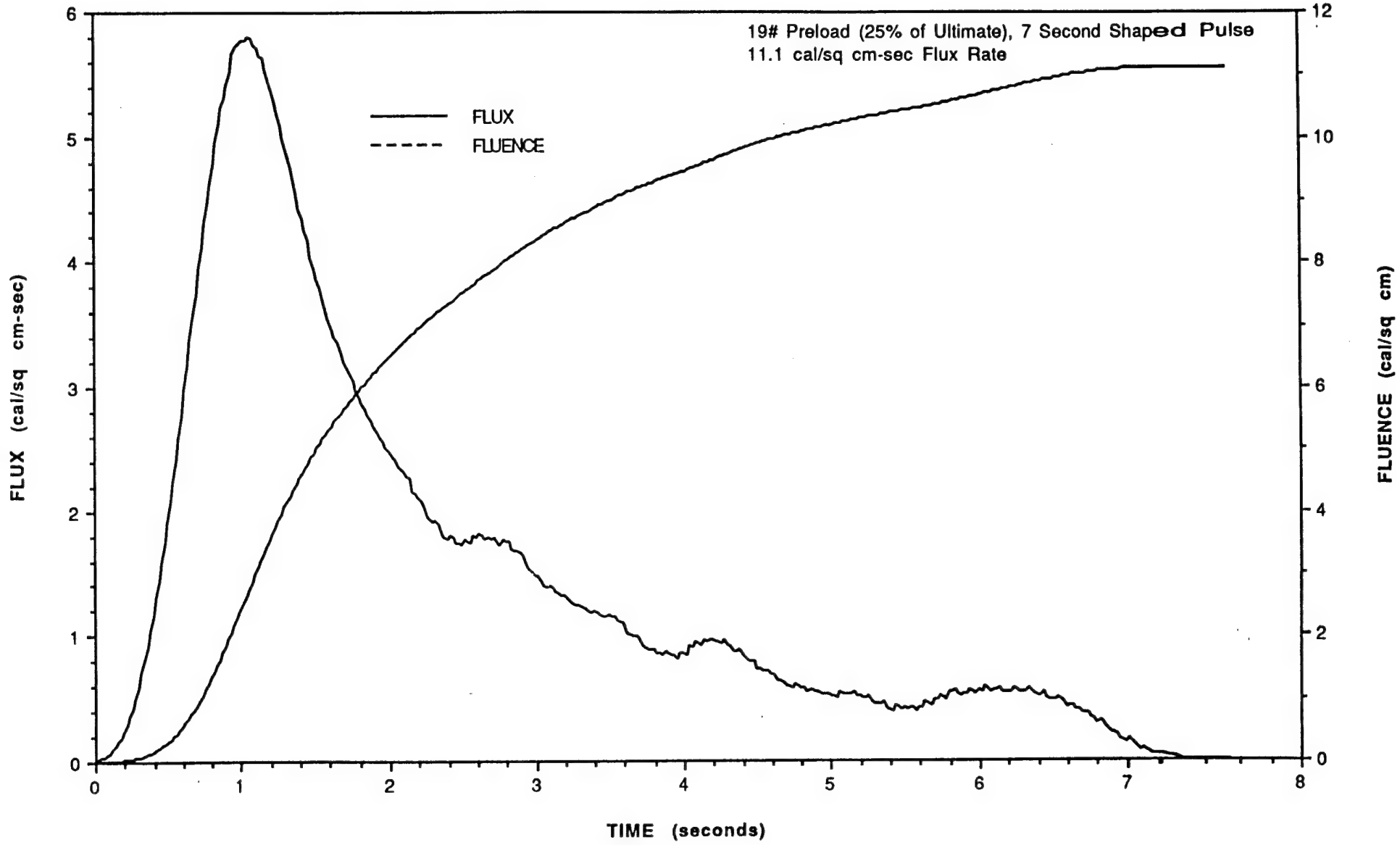

Figure G-1. Flux and fluence vs. time for grey sample #14.

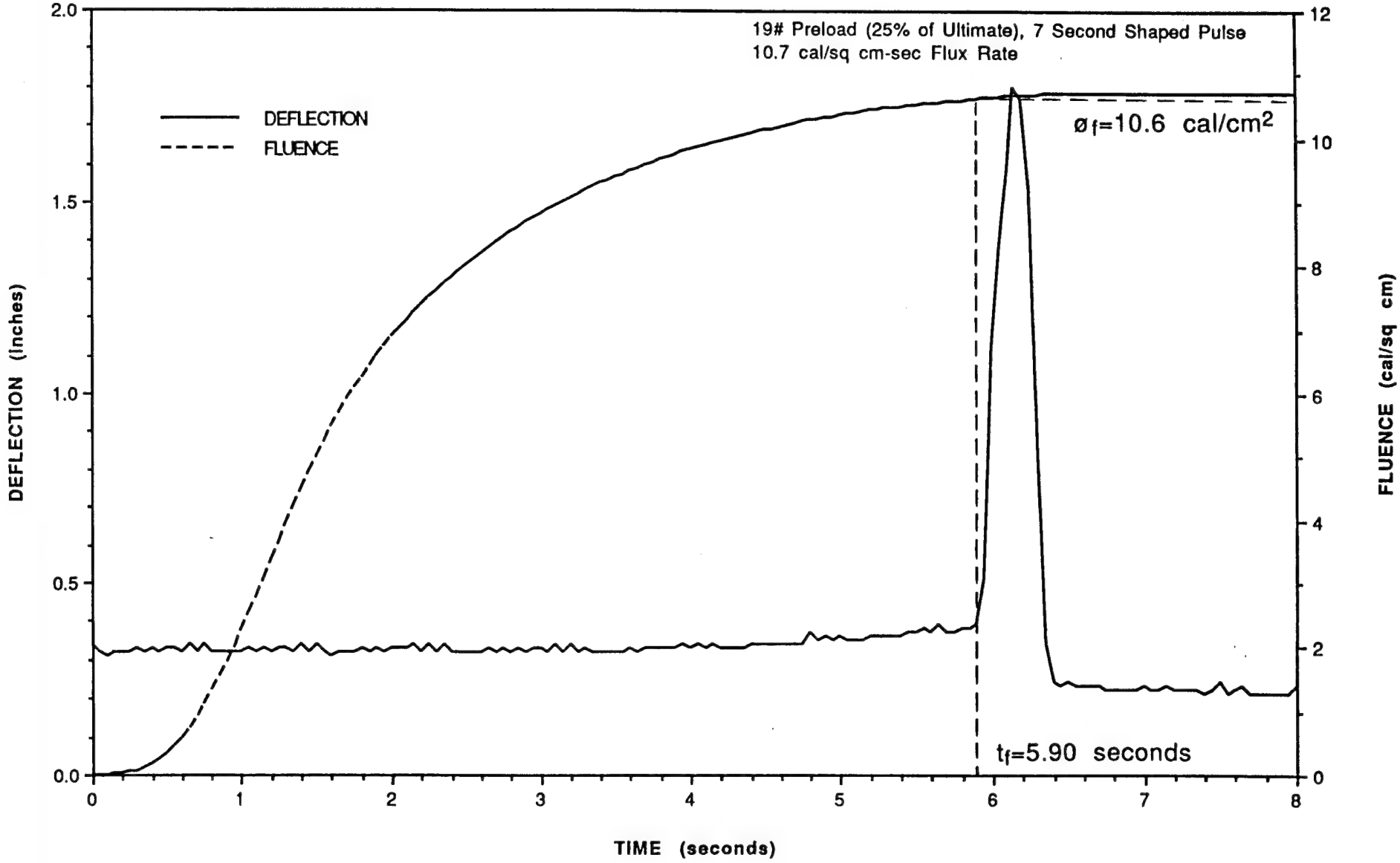

Figure G-2. Deflection and fluence vs. time for grey sample #15.

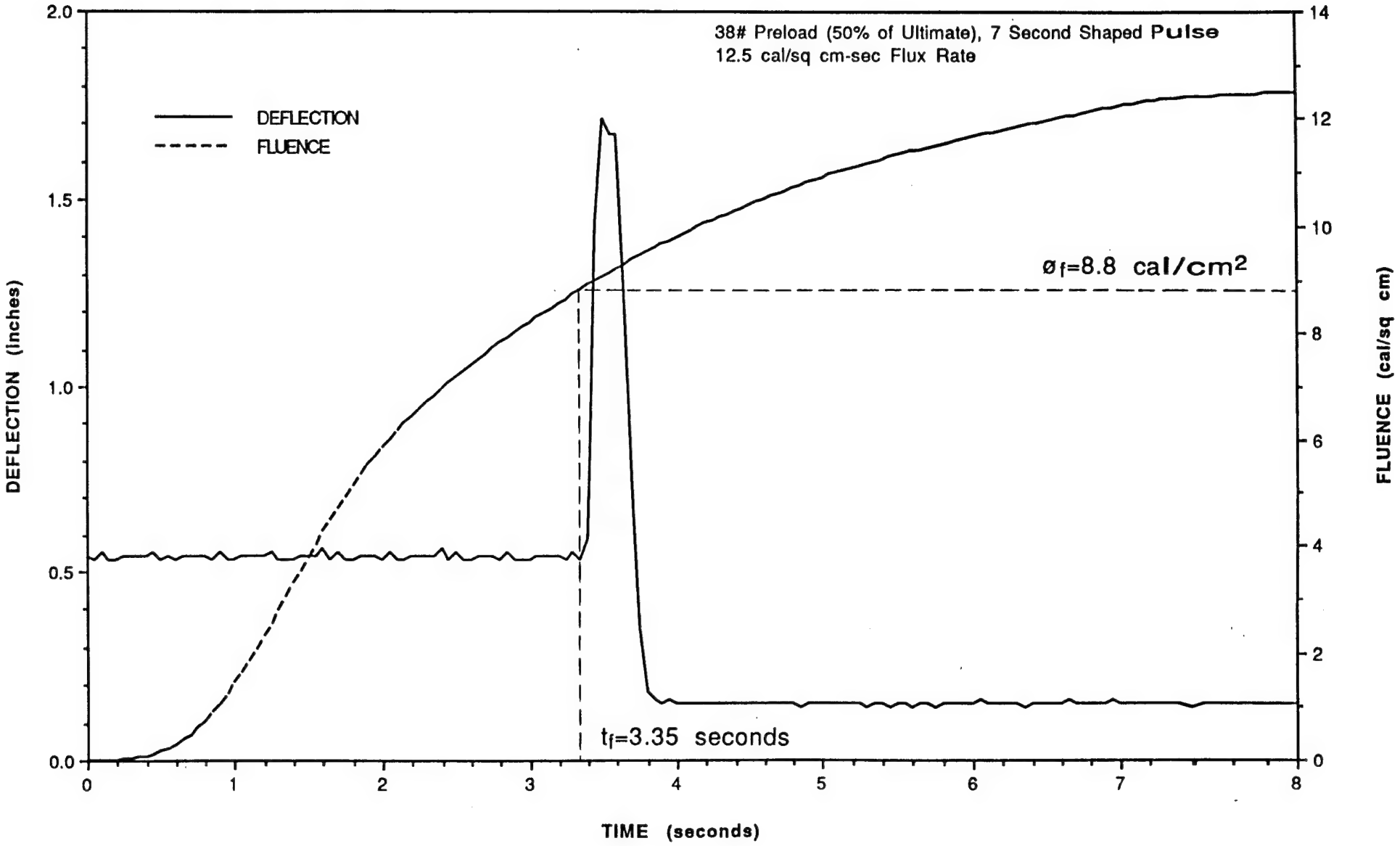

Figure G-3. Deflection and fluence vs. time for grey sample #16.

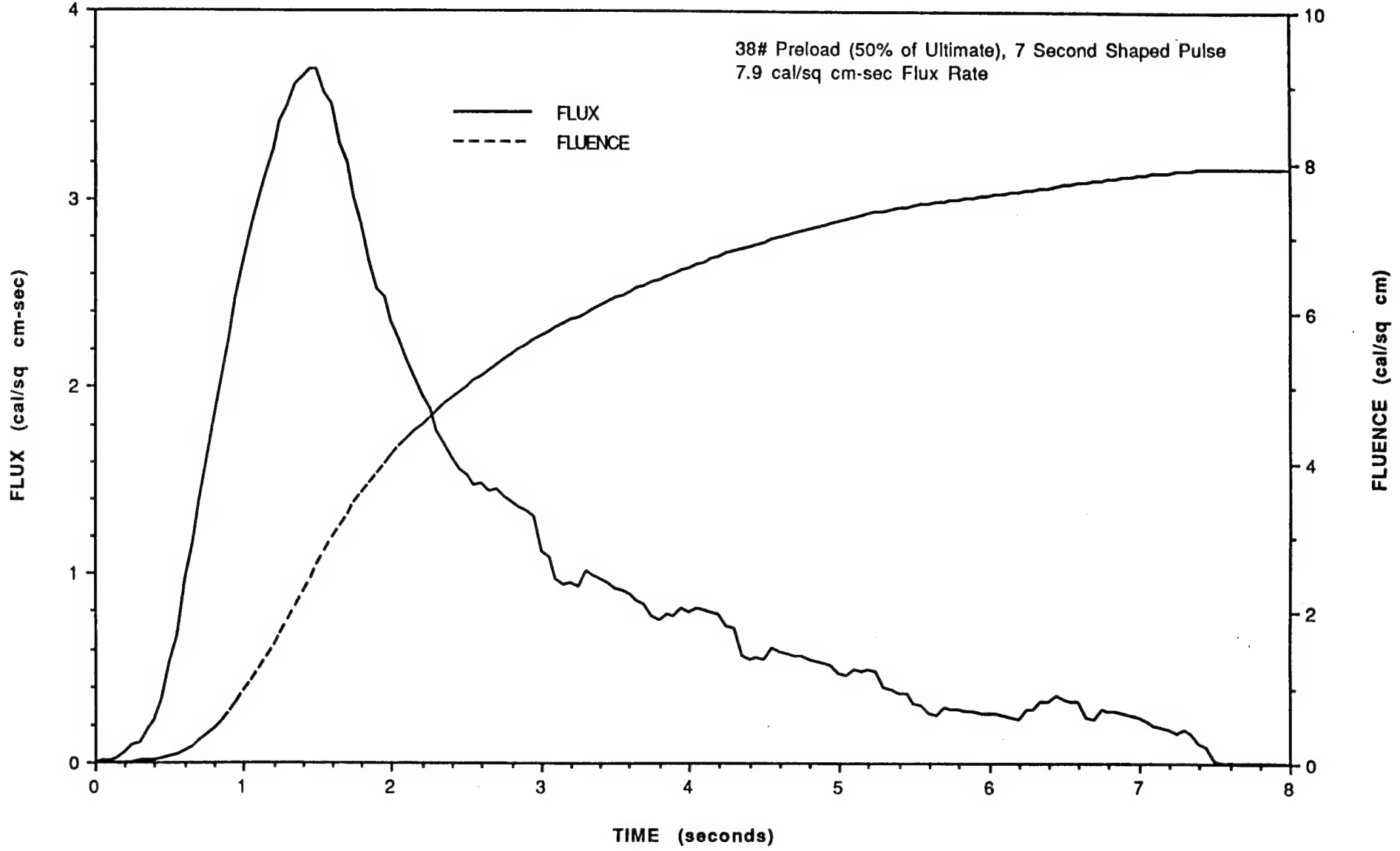

Figure G-4. Flux and fluence vs. time for grey sample #17.

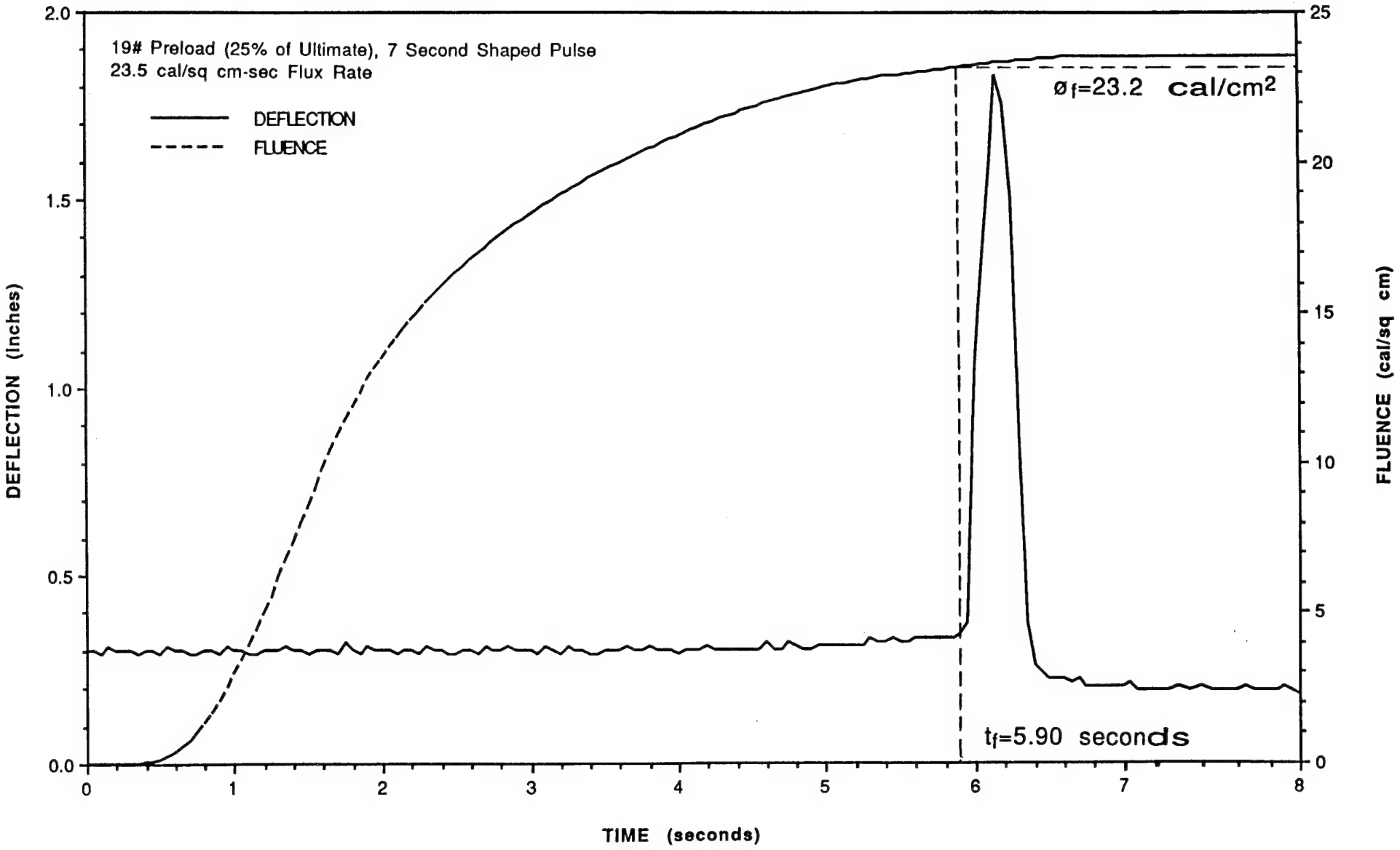

Figure G-5. Deflection and fluence vs. time for TRAC sample #16.

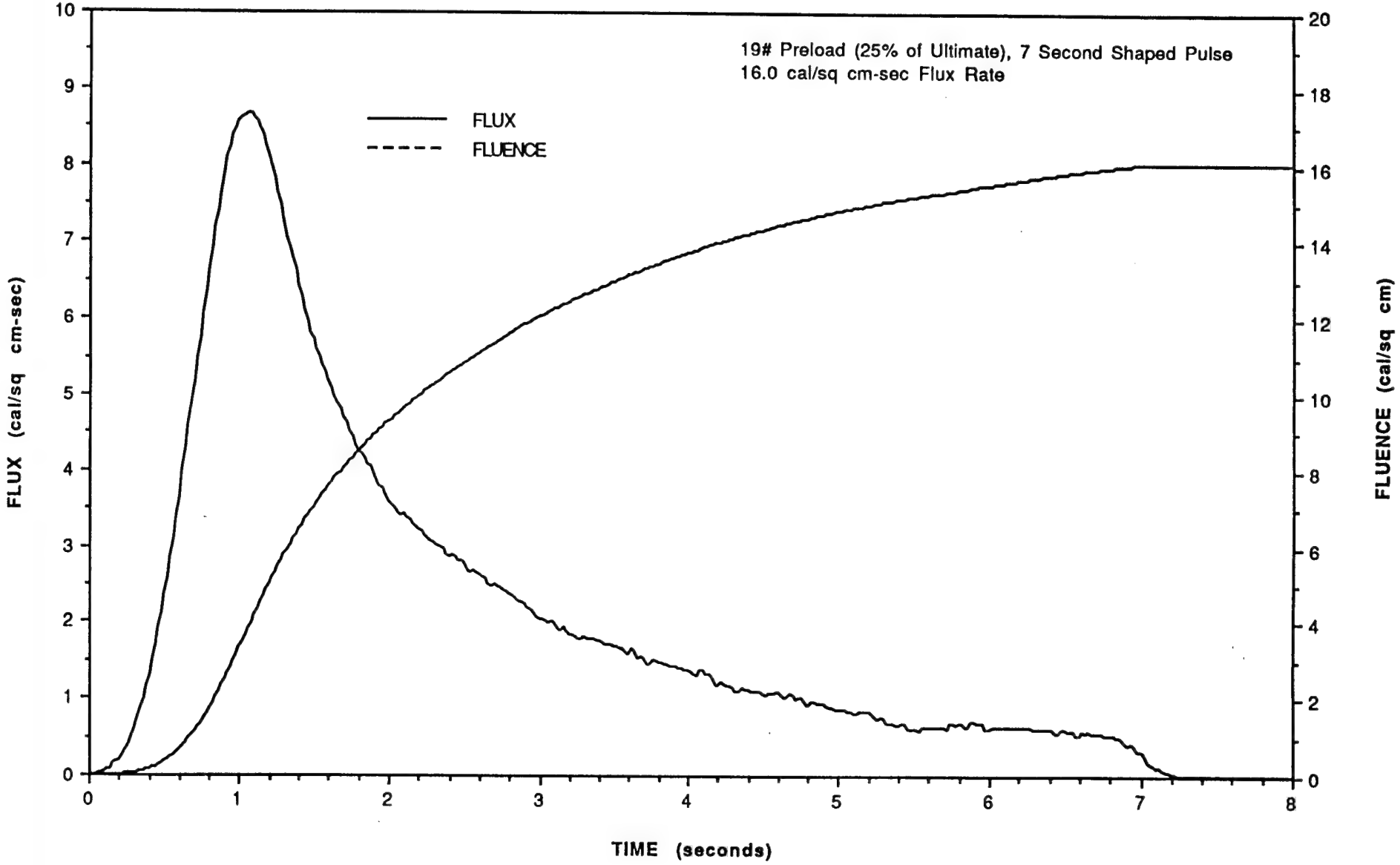

Figure G-6. Flux and fluence vs. time for TRAC sample #25.

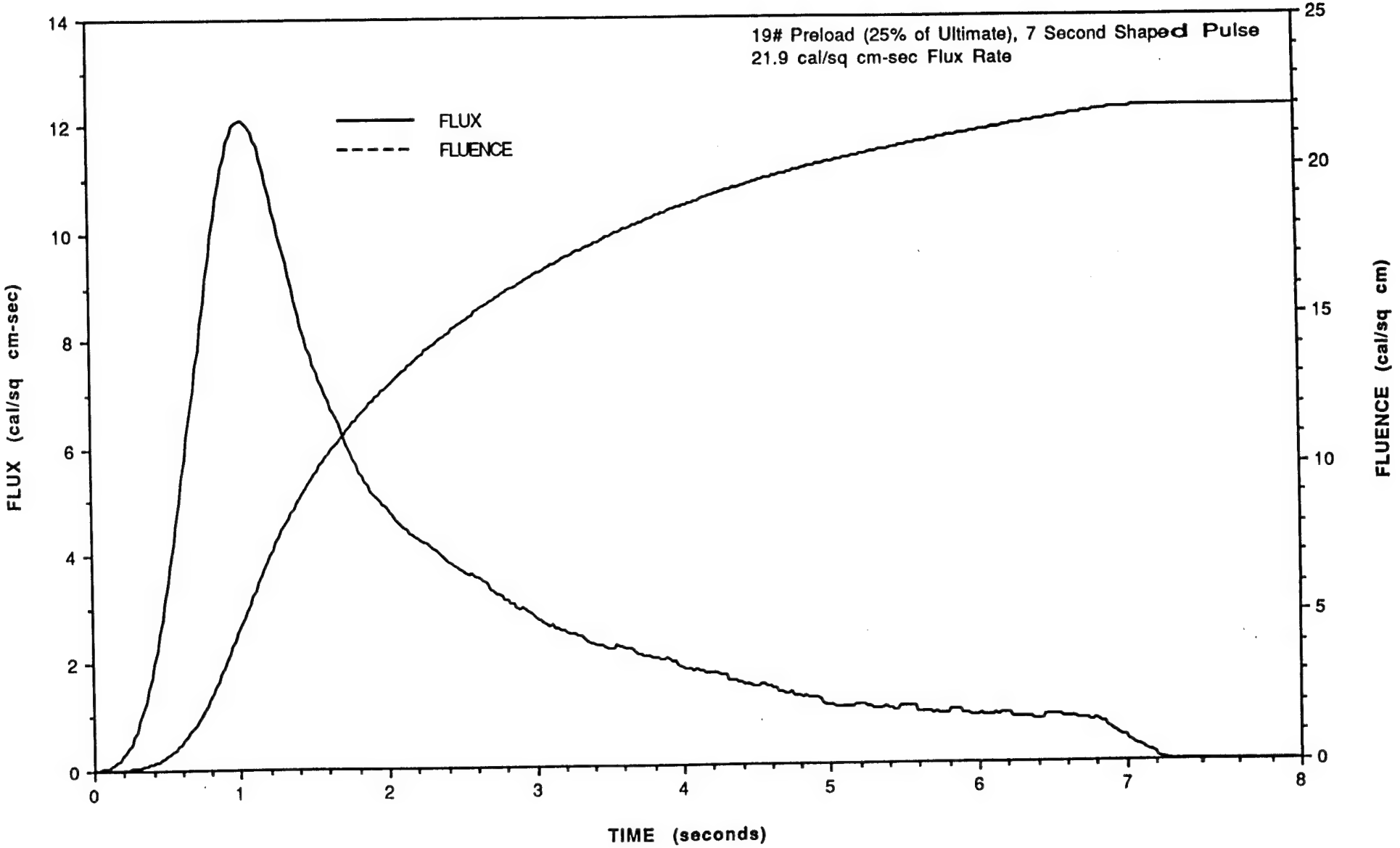

Figure G-7. Flux and fluence vs. time for TRAC sample #26.

GREY SAMPLE #14

7 SECOND SHAPED PULSE
STATIC LOAD DURING EXPOSURE = 19 lbs
PEAK INCIDENT FLUX = 5.8 cal/cm^2-sec
TOTAL FLUENCE ϕ_t = 11.1 cal/cm^2
LOAD TO FAILURE (post exposure) = 90 lbs

GREY SAMPLE #15

7 SECOND SHAPED PULSE
STATIC LOAD DURING EXPOSURE = 19 lbs
PEAK INCIDENT FLUX = 5.7 cal/cm^2-sec
TOTAL FLUENCE ϕ_t = 10.7 cal/cm^2
FAILED DURING EXPOSURE @ t_f = 5.90 seconds
FLUENCE TO FAILURE ϕ_f = 10.6 cal/cm^2

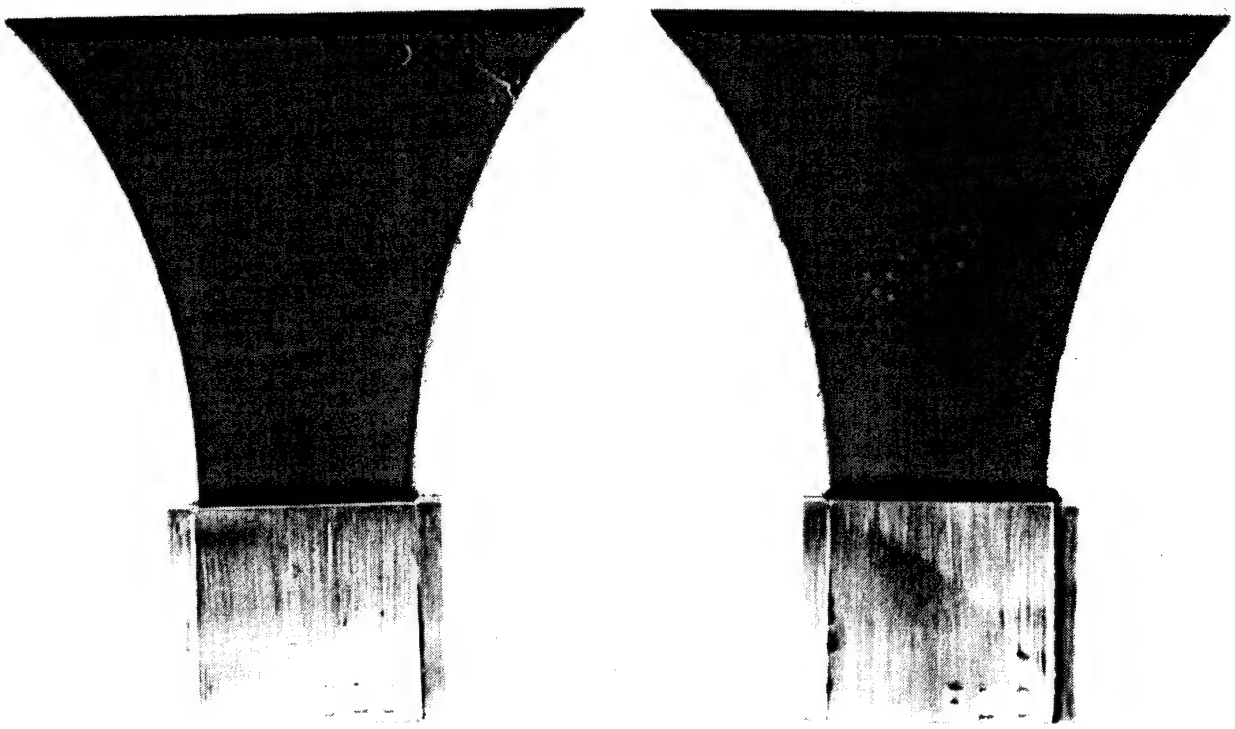

Figure G-8. Post test photograph of grey samples #14 and 15.

GREY SAMPLE #17

7 SECOND SHAPED PULSE
STATIC LOAD DURING EXPOSURE = 38 lbs
PEAK INCIDENT FLUX = 3.7 cal/cm^2-sec
TOTAL FLUENCE ϕ_I = 7.9 cal/cm^2
LOAD TO FAILURE (post exposure) = 93 lbs

GREY SAMPLE #16

7 SECOND SHAPED PULSE
STATIC LOAD DURING EXPOSURE = 38 lbs
PEAK INCIDENT FLUX = 4.9 cal/cm^2-sec
TOTAL FLUENCE ϕ_I = 12.5 cal/cm^2
FAILED DURING EXPOSURE @ t_f = 3.35 seconds
FLUENCE TO FAILURE ϕ_I = 8.8 cal/cm^2

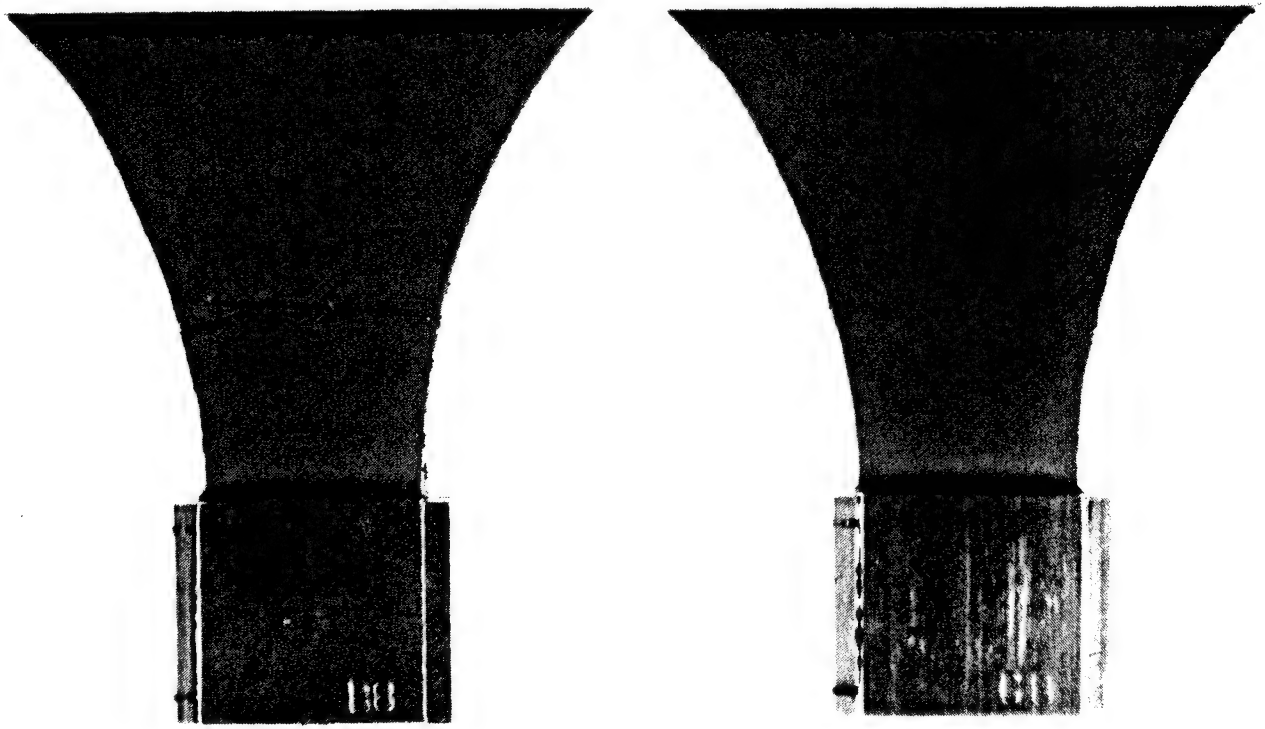

Figure G-9. Post test photograph of grey samples #17 and 16.

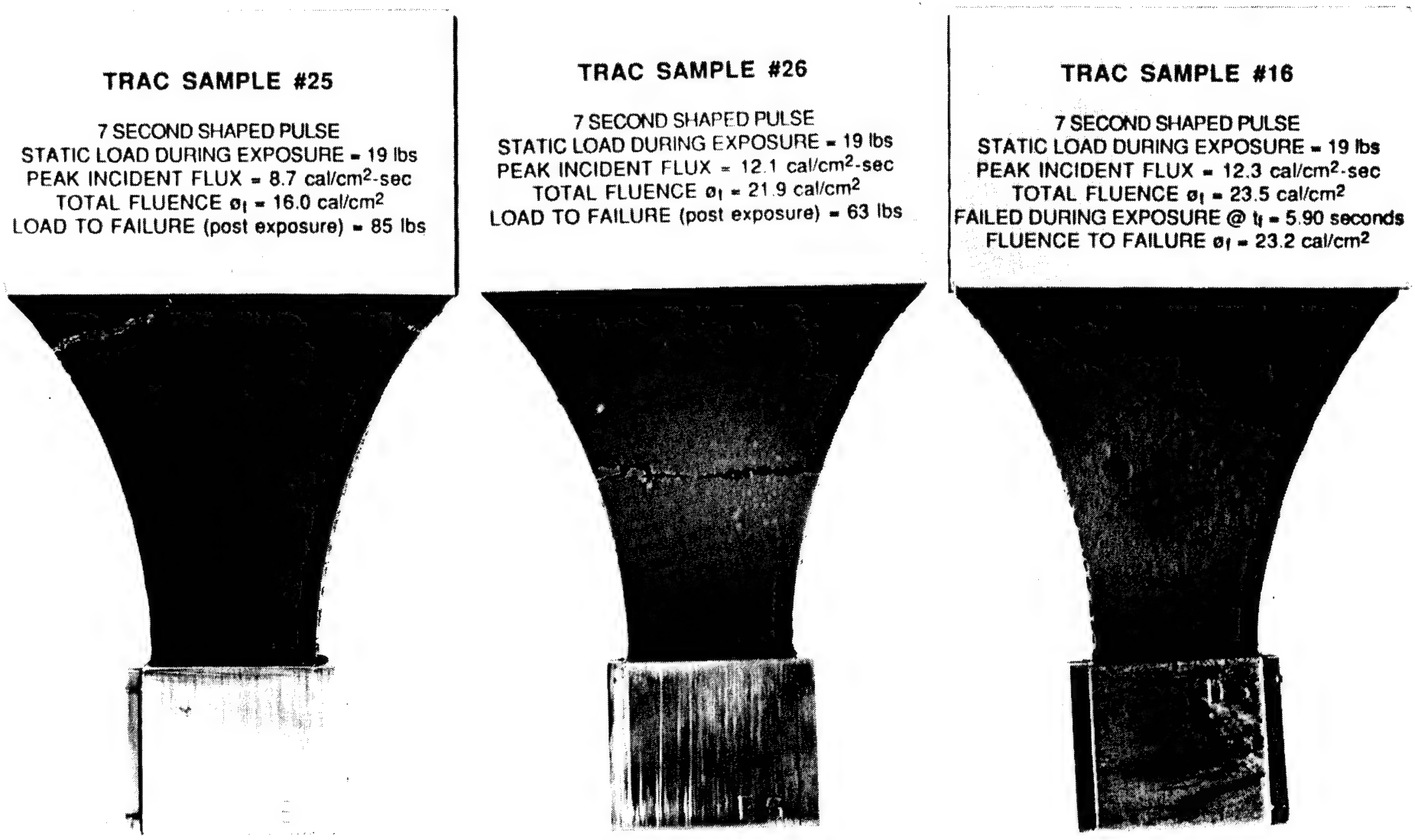

Figure G-10. Post test photograph of TRAC samples #25, 26 and 16.

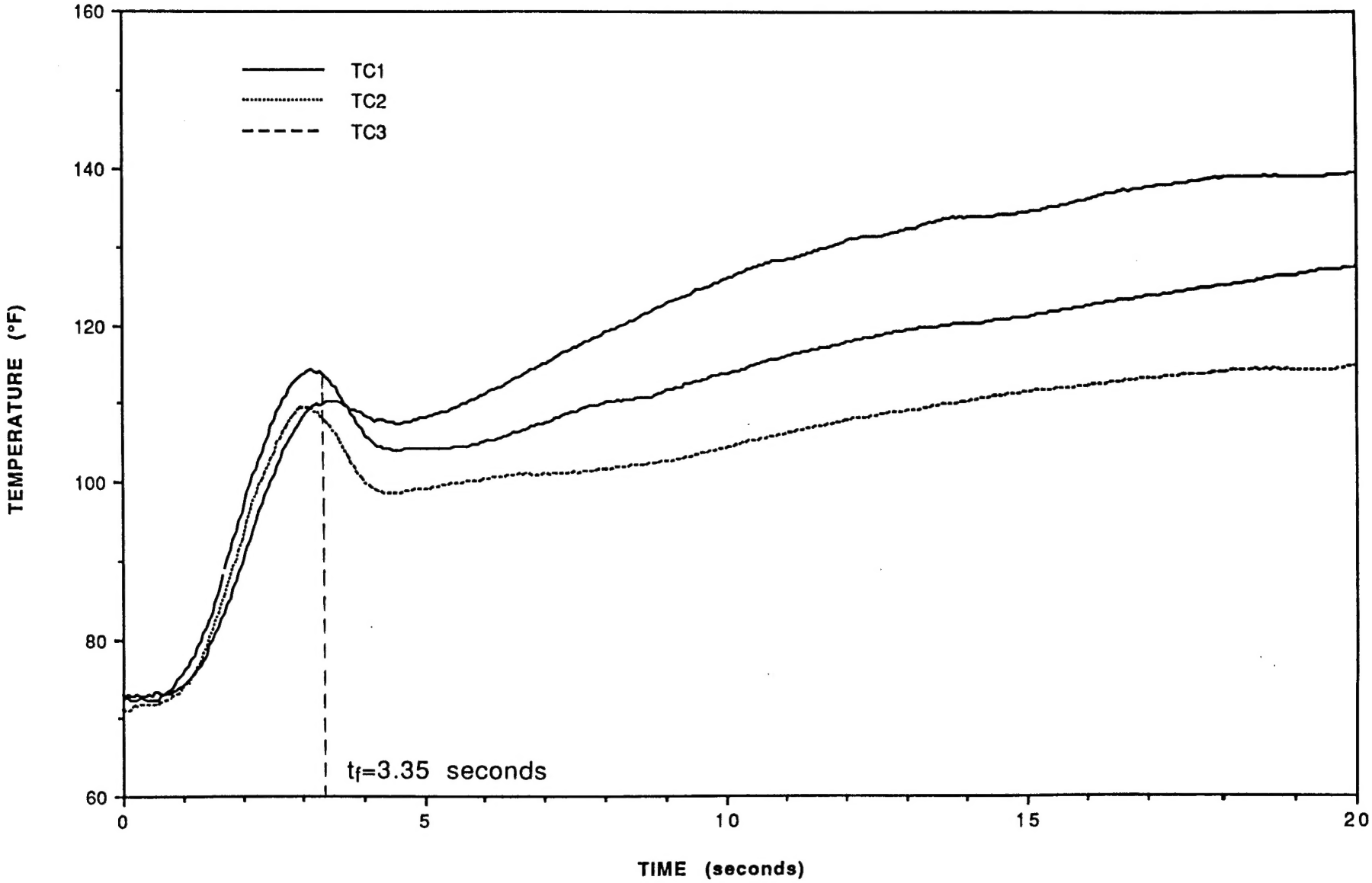

Figure G-11. Thermocouple response vs. time for grey sample #16.

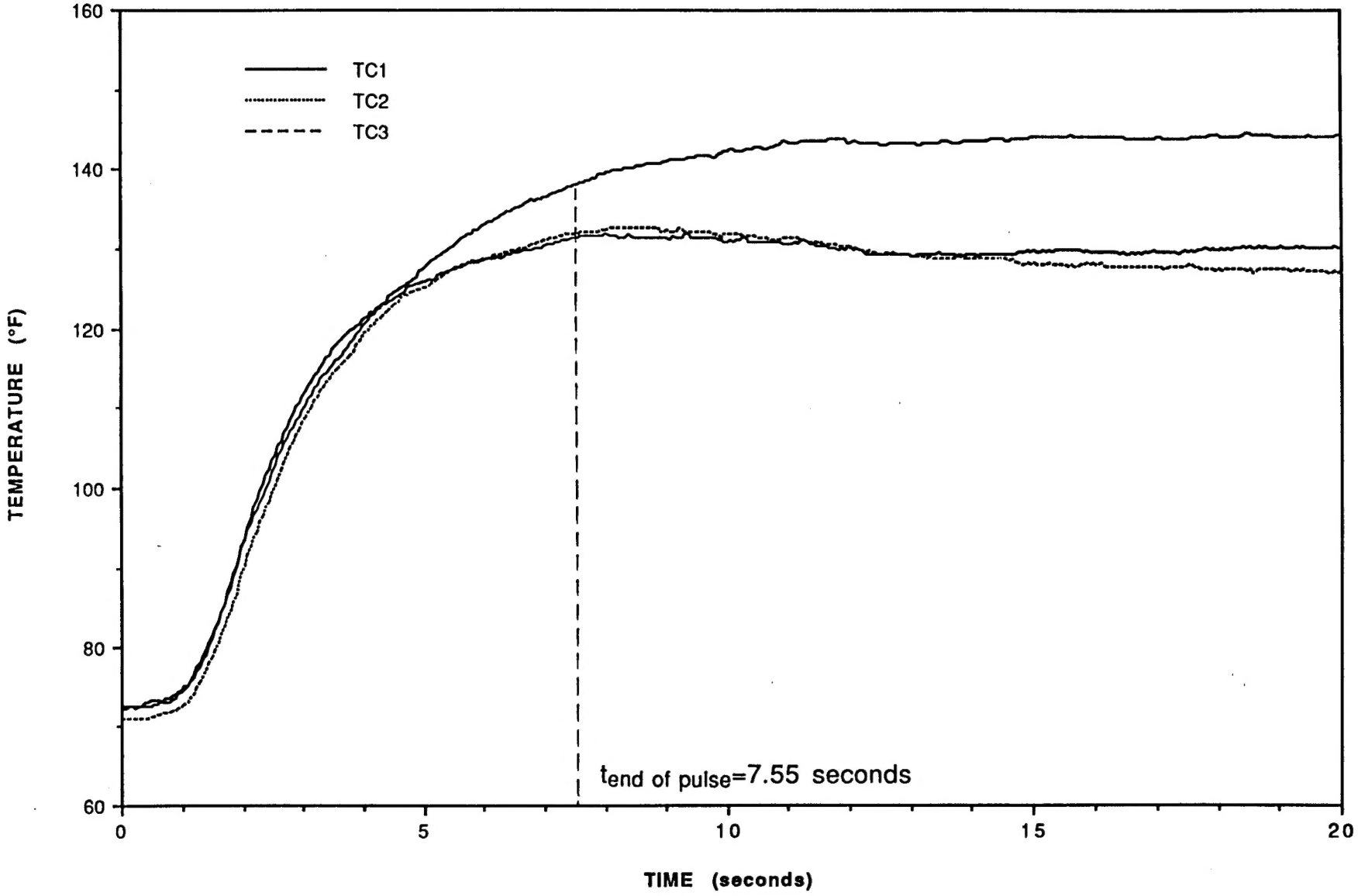

Figure G-12. Thermocouple response vs. time for grey sample #17.

DISTRIBUTION LIST

DNA-TR-94-59

DEPARTMENT OF DEFENSE

ASSISTANT TO THE SECRETARY OF DEFENSE
ATTN: EXECUTIVE ASSISTANT

DEFENSE INTELLIGENCE AGENCY
ATTN: PGI-4

DEFENSE NUCLEAR AGENCY
2 CY ATTN: IMTS
ATTN: RAEM
ATTN: SPWE LCDR DINOVA
2 CY ATTN: SPWE

DEFENSE TECHNICAL INFORMATION CENTER
2 CY ATTN: DTIC/OC

DEPARTMENT OF THE ARMY

ARMY RESEARCH LABORATORIES
ATTN: SLCSM-SE

US ARMY CHEMICAL SCHOOL
ATTN: COMMANDING OFFICER

USA CML & BIOLOGICAL DEFENSE AGENCY
ATTN: AMSCB-BDL J CANNALIATO

DEPARTMENT OF THE NAVY

NAVAL AIR SYSTEMS COMMAND
ATTN: E ECK

NAVAL RESEARCH LABORATORY
ATTN: CODE 7920

NAVAL SURFACE WARFARE CENTER
ATTN: CODE K42 L VALGE

OFFICE OF CHIEF NAVAL OPERATIONS
ATTN: NUC AFFAIRS & INT'L NEGOT BR

STRATEGIC SYSTEMS PROGRAM
ATTN: SP0272 R G STANTON

DEPARTMENT OF THE AIR FORCE

AIR COMBAT COMMAND
ATTN: LT COL R EASTERLIN

AIR FORCE STUDIES AND ANALYSIS
ATTN: AFSAA/SAS

AIR UNIVERSITY LIBRARY
ATTN: AUL-LSE

HQ USAF/XOFS
ATTN: XOFN

OKLAHOMA CITY AIR LOGISTICS CTR
ATTN: OCALC/LPAAM S GARDNER

WRIGHT RESEARCH & DEVELOPMENT CENTER
ATTN: D RICHMOND

412 TW/ LGLXP4
ATTN: P PAUGH

DEPARTMENT OF ENERGY

LAWRENCE LIVERMORE NATIONAL LAB
ATTN: ALLEN KUHL

OTHER GOVERNMENT

CENTRAL INTELLIGENCE AGENCY
ATTN: OSWR/NED 5S09 NHB

DEPARTMENT OF DEFENSE CONTRACTORS

AEROSPACE CORP
ATTN: D LYNCH

APPLIED RESEARCH INC
ATTN: J BOSCHMA

INTERNATIONAL DEVELOPMENT & RESOURCES
ATTN: HERBERT HEAD
ATTN: WILLIAM SCHILLING

JAYCOR
2 CY ATTN: CYRUS P KNOWLES

KAMAN SCIENCES CORP
ATTN: D COYNE

KAMAN SCIENCES CORP
ATTN: J HESS

KAMAN SCIENCES CORP
ATTN: DASIAC

KAMAN SCIENCES CORPORATION
ATTN: DASIAC

LOGICON R & D ASSOCIATES
ATTN: J DRAKE
ATTN: LIBRARY
ATTN: R ROSS

LOGICON R & D ASSOCIATES
ATTN: E FURBEE
ATTN: J WEBSTER
ATTN: R POPE

LOGICON R & D ASSOCIATES
ATTN: G GANONG

MCDONNELL DOUGLAS CORPORATION
ATTN: L COHEN

NORTHROP CORP
ATTN: G CURRY

PACIFIC-SIERRA RESEARCH CORP
ATTN: R LUTOMIRSKI
ATTN: S FUGIMURA

PACIFIC-SIERRA RESEARCH CORP
ATTN: M ALLERDING

PDA ENGINEERING
2 CY ATTN: D E BIELECKA
2 CY ATTN: K E JECHEL

PHYSITRON INC
ATTN: M PRICE

S-CUBED
ATTN: C NEEDHAM

SCIENCE APPLICATIONS INTL CORP
ATTN: D BACON
ATTN: J COCKAYNE
ATTN: P VERSTEEGEN

SRI INTERNATIONAL
ATTN: E UTHE
ATTN: J PRAUSA
ATTN: M SANAI

SRI INTERNATIONAL
ATTN: J MIATECH

TOYON RESEARCH CORP
ATTN: J CUNNINGHAM
ATTN: T W GEYER

W J SCHAFER ASSOCIATES, INC
ATTN: D YOUMANS
ATTN: W BUITENHUYS

W J SCHAFER ASSOCIATES, INC
ATTN: S HOWIE

WILLIAMS INTERNATIONAL CORP
ATTN: D FISHER